KELLY STAM

A NOVEL PRECLINICAL MODEL FOR CHRONIC THROMBO-EMBOLIC PULMONARY HYPERTENSION

DEVELOPMENT, VALIDATION AND CHARACTERIZATION

A Novel Preclinical Model for Chronic Thrombo-Embolic Pulmonary Hypertension

Development, Validation and Characterization

Kelly Stam

A Novel Preclinical Model for Chronic Thrombo-Embolic Pulmonary Hypertension

development, validation and characterization

Cover design: Davy Casteleins

Thesis Erasmus Medical Center, Rotterdam

ISBN 978-94-6380-443-1

Printed by ProefschriftMaken

A Novel Preclinical Model for Chronic Thrombo-Embolic Pulmonary Hypertension

development, validation and characterization

Een nieuw preklinisch model voor chronische trombo-embolische pulmonale hypertensie

ontwikkeling, validatie en karakterisatie

Proefschrift

ter verkrijging van de graad van doctor aan

de Erasmus Universiteit Rotterdam

op gezag van de rector magnificus

Prof. Dr. R.C.M.E. Engels

en volgens besluit van het College van Promoties.

De openbare verdediging zal plaatsvinden op

dinsdag 24 september 2019 om 11:30 uur

door

Kelly Stam

geboren te Enkhuizen

Erasmus University Rotterdam

Promotiecomissie

Promotoren:	Prof. Dr. D.J.G.M. Duncker
	Prof. Dr. D. Merkus
Overige leden:	Dr. B. Bartelds
	Prof. Dr. H.J Bogaard
	Prof. Dr. A.H.J. Danser

The studies in this thesis have been conducted at the Laboratory of Experimental Cardiology,Thorax Center, Erasmus Medical Center, Rotterdam, The Netherlands.

The studies described in this thesis were supported by Netherlands Cardiovascular Research Initiative; the Dutch Heart Foundation, the Dutch Federation of University Medical Centers, the Netherlands Organization for Health Research and Development and the Royal Netherlands Academy of Science. CVON (2012-08), PHAEDRA.

Financial support by the Dutch Heart Foundation for the publication of this thesis is gratefully acknowledged.

Contents

Chapter 1

General introduction and outline of this thesis

Pulmonary hypertension

Pulmonary hypertension (PH) is a chronic pathophysiological disorder of the pulmonary vasculature and is defined as a chronic pulmonary artery pressure (PAP) ≥ 25mmHg at rest (26). Pulmonary hypertension is a collective name for different types of PH. The world health organization (WHO) distinguishes 5 different subgroups of PH, based on etiology: type 1, pulmonary arterial hypertension; type 2, pulmonary hypertension due to left heart disease; type 3, pulmonary hypertension due to lung diseases and/or hypoxia; type 4, chronic thromboembolic pulmonary hypertension and other pulmonary artery obstructions; and type 5, pulmonary hypertension with unclear and/or multifactorial mechanisms (14) (Figure 1).

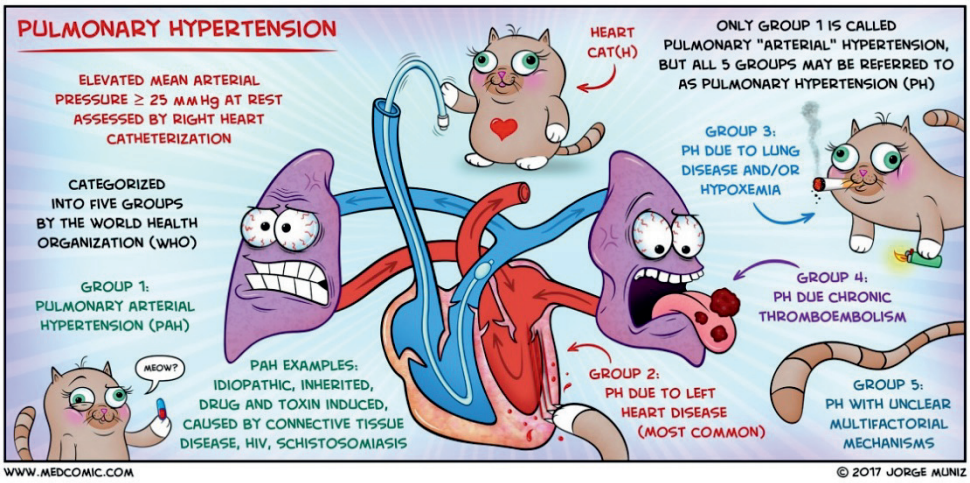

Figure 1. Pulmonary Hypertension definition and subtypes.
Indicated is the definition, and the subtypes, of pulmonary hypertension as an elevated mean arterial pressure ≥ 25 mmHg measured by right heart catheterization. Image provided by, and used with permission of Jorge Muniz (www.medcomic.com).

Symptoms of PH are very non-specific and include shortness of breath, fatigue, syncope, chest pain, palpitations, angina, weakness, dry cough and a reduced exercise capacity. All these symptoms contribute to a decreased quality

of life for the pulmonary hypertension patients (66). Due to the unspecific nature of the symptoms, PH is often diagnosed late in the process, or in some cases even remains undiagnosed. The true incidence and prevalence of PH in the general population are unknown and since it is even suggested that a group of patients is undiagnosed, all reported numbers are probably an underestimation (49).

Currently, treatment modalities for PH are still very limited and, even when treated, the disease often progresses to right heart failure and death. Heart failure means that the heart is not capable of pumping enough blood to the body to meet the oxygen demand of the body.

General cardiovascular physiology

In patients with PH, the work load of the right ventricle is increased, and the pump capacity of the right ventricle ultimately falls short. In order to understand the problems that may arise in PH, this section will first describe the healthy cardiopulmonary system.

Cells require oxygen and nutrients to be able to function and essentially keep the human body alive. In tissue, oxygen and nutrients are metabolized and, in this process, carbon dioxide (CO_2) is produced. Oxygen is taken up by the lungs, where CO_2 is released. The medium to transport these substances through the body is blood. Blood is transported though the body using blood vessels, called the circulatory system (Figure 2).This circulatory system is divided into two circulations, the pulmonary circulation and the systemic circulation. The movement (flow) of blood through these circulations is actively driven by the heart. The heart functions as a pump which contracts about 60 times each minute and ejects about 5 liters of blood per minute at rest. Heart rate can increase to 200 times each minute, circulating 20 liters of blood per minute during exercise (34, 35). The heart consists of two collecting compartments, called the atria, and

two ejecting compartments, called the ventricles. In short, deoxygenated blood from the body is collected in the right atrium, then goes in to the right ventricle, which subsequently pumps it in to the pulmonary circulation. Blood is oxygenated in the lungs where after it is collected in the left atrium. The left atrium pumps the oxygen rich blood to the left ventricle which subsequently pumps it to the various organs in the body via the aorta. The pressure in the aorta is what is commonly called “the blood pressure” as measured by the general practitioner. This mean systemic blood pressure is approximately 90mmHg in health. In the organs oxygen is absorbed and deoxygenated blood returns to the right atrium where the cycle starts again (69).

Pulmonary circulation

The pulmonary circulation is the part of the cardiovascular system which is affected in pulmonary hypertension. In the pulmonary circulation, the right ventricle pumps deoxygenated blood into the pulmonary artery (PA), from which it flows into the pulmonary vasculature for oxygenation and removal of carbon dioxide. The oxygen is supplied by the airways (bronchi) which subdivide into bronchioles and ultimately branches into the smallest air sacs (alveoli) which are in contact with the pulmonary capillaries for the diffusion of oxygen and carbon dioxide.

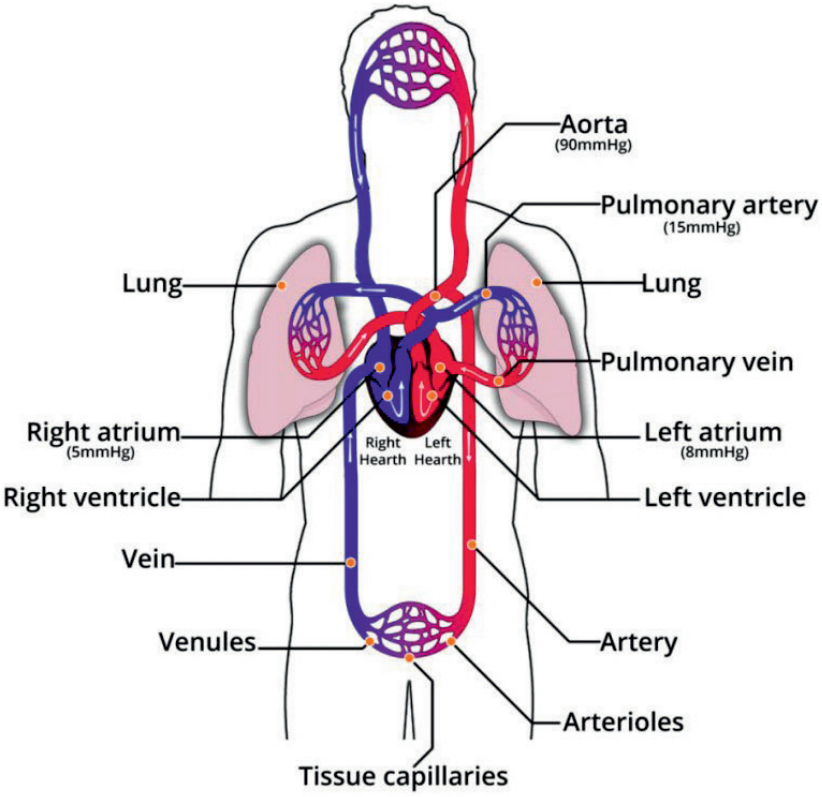

Figure 2. Schematic representation of the cardiovascular system.
Oxygen rich blood is depicted in red and oxygen deprived blood is depicted in blue. The arrows indicate the direction of flow.

Following oxygenation, blood is transported to the left side of the heart via the pulmonary veins. To optimize gas exchange in the pulmonary circulation, the blood-gas barrier needs to be thin, which results in a low-pressure, high-flow circulation. The pulmonary blood flow is equal to the systemic cardiac output while the mean pulmonary artery pressure is approximately 15mmHg in health (>25mmHg in PH patients). Since the pressure drop over the pulmonary vasculature from the PA to the left atrium (LA) is very low (approximately 7 mmHg) to enable blood to flow through the lungs, the pulmonary vascular resistance (PVR) is also very low (approximately one tenth of the systemic

resistance) in healthy individuals (69). In PH patients, this PVR is substantially increased due to constriction, remodeling and rarefaction of the pulmonary blood vessels, resulting in a higher pressure to maintain blood flow through the pulmonary vascular bed.

CTEPH

The World Health Organization differentiates 5 groups of PH based on their etiology. Chronic thromboembolic pulmonary hypertension (CTEPH), categorized as group 4 PH, is pulmonary hypertension caused by thrombo-emboli in the pulmonary vasculature. These thrombo-emboli can be, for instance, originating from a deep vein thrombosis, from which the emboli are released and travel through the body. The first small vascular bed these emboli travel through is the pulmonary vascular bed, in which these emboli get stuck. This is called acute pulmonary embolism and can be treated by anticoagulation and thrombolysis (30, 31). However, in a subgroup of these patients, not all the emboli will resolve. When these emboli remain in the pulmonary vasculature, most likely in combination with other risk factors, CTEPH can develop. Some of the risk factors that are linked and hypothesized to play a role in the development of CTEPH are genetics, ineffective endogenous fibrinolysis, hypercoagulability, deficient angiogenesis, inflammation and platelet endothelial cell adhesion molecule-1 deficiency (37, 59). In these patients the pressure and resistance in the pulmonary vasculature will rise and eventually result in chronic PH. CTEPH develops in about 3-4% of patients after acute pulmonary embolism and up to 10% of patients with recurrent pulmonary embolism (11, 65, 70). The definition of CTEPH is therefore defined as a persistent PAP above 25mmHg at rest for at least 3 months, despite therapeutic anticoagulation (14, 26, 27, 33), although pulmonary artery pressures ≥ 19mmHg at rest following embolism are already associated with increased mortality at long term (63). The prevalence of CTEPH is still largely unknown. The

reported annual incidence of acute pulmonary embolism ranges from 750 to 2700 per million adults (30, 50, 68) of which 3-4% of the survivors develop CTEPH (11, 65). According to these numbers, the expected incidence of CTEPH would be 22.5 to 108 per million adults, while the reported numbers of diagnosed patients with CTEPH are substantially smaller. Three countries assessed the CTEPH incidence through nationwide registries. In the United Kingdom the CTEPH incidence was 1.75 per million (6), in Spain it was 0.9 per million adults (12) and in Germany it was 5.7 per million adults (32). Between approximately 300 and 400 patients were newly diagnosed with CTEPH per year in France and Germany (32, 58), while the disease is still incompletely understood and therapeutic interventions are still limited, showing the importance of research into this disease.

The symptoms of CTEPH are the same as of other forms of PH, such as shortness of breath, fatigue, syncope, chest pain, palpitations and reduced exercise capacity, which (together with physician unawareness) contribute to the late diagnosis in a large number of patients. This delayed diagnosis in turn impacts the prognosis negatively (29). Unfortunately, to this day, treatment options for CTEPH patients are also not optimal. The main treatment options for CTEPH are surgical interventions to remove proximal obstructions such as pulmonary endarterectomy or balloon angioplasty (10, 16, 23) although these can only be performed in eligible patients. Therapeutic agents to modulate the pulmonary vascular tone are limited to date. Riociguat, which is a soluble guanylyl cyclase stimulator, that activates the nitric oxide (NO) pathway without endogenous NO, thus acting as a vasodilator, inhibiting pulmonary smooth muscle cell growth and antagonizes platelet inhibition (i.e. preventing clot formation) is the only approved therapeutic agent in CTEPH (2, 10, 21, 46). Nevertheless, treatment modalities for CTEPH are very limited and, even when treated, the disease often progresses to right heart failure and even death.

Changes in the control of vascular tone and remodeling of the pulmonary vasculature

The pathogenesis of CTEPH encompasses a combination of endothelial dysfunction, pulmonary vascular structural remodeling, thrombophilia, inflammation, vasoconstriction and impaired vasodilation (39). In the healthy pulmonary vasculature, endothelin and nitric oxide are key players in regulating pulmonary vascular resistance. In PH, pulmonary vascular resistance increases due to endothelial dysfunction resulting in a shift towards vasoconstriction and remodeling.

The vessel diameter is set by the contractile state (tone) of the smooth muscle cells in the vascular wall. Smooth muscle cells are lined underneath the endothelial cells of which the inner lining of the arterial wall is composed. Vascular tone is determined by many competing constricting (vasoconstrictor) and relaxing (vasodilator) influences acting on the muscular layer of the blood vessel. These influences can be divided into metabolic, mechanic, neurohumoral, endocrine, paracrine and endothelial influences. The endothelium plays a very important role in the regulation and excretion of vasodilators such as the key factor nitric oxide (NO), and vasoconstrictors, such as the key factor endothelin-1 (ET-1), which are the key regulators of vascular tone in the pulmonary circulation (55).

Nitric oxide is a vasoactive agent synthesized from L-arginine by endothelial NO synthase (eNOS) in the endothelium. NO diffuses from the endothelial cell to the adjacent vascular smooth muscle cell where it binds to, and thereby activates, soluble guanylyl cyclase (sGC). This enzyme increases the conversion rate of guanosine triphosphate (GTP) to cyclic guanosine monophosphate (cGMP). cGMP in turn leads to relaxation of the vascular smooth

muscle cells via reduction of Ca^{2+}release from the sarcoplasmic reticulum and activation of K^+ channels (55). Via this pathway, NO acts as a potent vasodilator (Figure 3), inhibits pulmonary smooth muscle cell growth and inhibits clot formations.

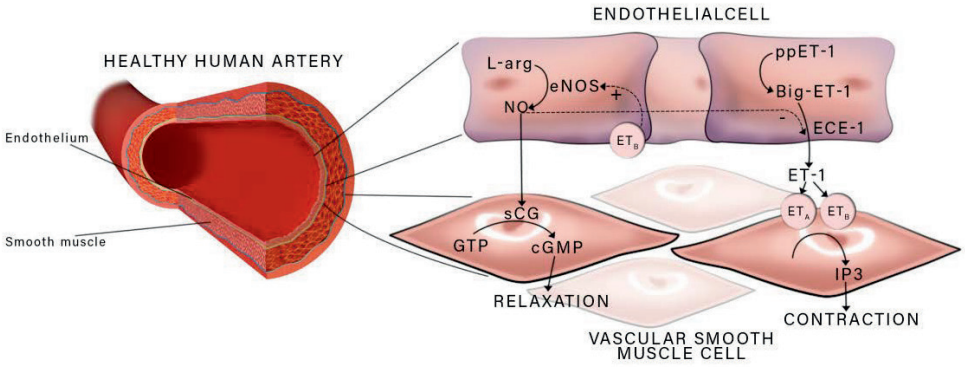

Figure 3. Vascular anatomy with the NO and ET-1 pathways.
Healthy human artery with endothelium and smooth muscle cell layers depicted on the left. The interplay of nitric oxide (NO) and endothelin-1 (ET-1) in the regulation of vascular tone in the right. L-arg, L-arginine; eNOS, endothelial nitric oxide synthase; sGC, soluble guanylyl cyclase; GTP, guanosine triphosphate; cGMP, cyclic guanosine monophosphate; ppET-1, preproendothelin-1; Big-ET-1, Big endothelin-1; ECE-1, endothelin converting enzyme-1; ET_A, endothelin receptor A; ET_B, endothelin receptor B; IP3, inositol triphosphate.

Endothelin-1 is a peptide which is synthesized from big ET (produced from preproendothelin by furin-like enzymes) by the endothelin converting enzyme (ECE)-1, which is found on the endothelial cell membrane (38). Upon release, ET-1 binds to its receptors on either the endothelium (ET_B receptor) or the vascular smooth muscle cell (ET_A or ET_B receptor). NO is one of the substances that is able to inhibit this ET-1 release which shows the delicate balance between these regulatory substances. Activation of the ET_B receptor on the endothelium leads to vasodilation by releasing prostacyclin and NO. In healthy conditions, ET-1 predominantly binds to the ET_A or ET_B receptor on the vascular wall, leading to

increases of inositol triphosphate (IP3) concentrations which in turn release Ca^{2+} from the sarcoplasmic reticulum. This Ca^{2+} release subsequently leads to contraction of the vascular smooth muscle cells (55). Via this pathway, ET-1 acts as a potent vasoconstrictor (Figure 3).

The obstructions in the pulmonary vascular bed in CTEPH cause a direct increase in pulmonary vascular resistance, and a redistribution of flow through the unobstructed parts of the pulmonary vasculature, which result in an increase in PAP. Both the increase in pressure and the local increase in flow are thought to contribute to remodeling of the unobstructed pulmonary vascular bed (15, 43). This remodeling encompasses structural remodeling of both the pulmonary small arteries (diameter >50μm) as well as the microvasculature (diameter <50μm). The structural remodeling presents predominantly with an increase in pulmonary vascular wall thickness which encroaches on the vascular lumen thereby increasing the resistance. In addition, the prolonged endothelial dysfunction, either as a cause or a consequence of the increased PAP, results in a shift towards vasoconstriction, even further increasing the vascular resistance, leading to a vicious cycle.

It is well known that both dysfunction of the endothelin and the nitric oxide pathway play important roles in the dysregulation of pulmonary vascular tone as well as microvascular remodeling in pulmonary arterial hypertension (PAH)(13, 60). However, how alterations in these pathways affect pathogenesis of microvascular structural and functional remodeling in CTEPH remains incompletely understood. Plasma markers of oxidative stress and the endogenous endothelial NO synthase (eNOS) inhibitor asymmetric dimethyl arginine (ADMA) are increased in patients with CTEPH (71). Moreover, circulating ET-1 levels are elevated in patients with CTEPH and correlate with clinical severity of the disease as well as with hemodynamic outcome after pulmonary endarterectomy (51).

However, there is some controversy as to whether therapeutic agents that interfere with the NO and the ET-1 systems, such as phosphodiesterase 5 (PDE5)-inhibitors and ET-receptor antagonists, that are the cornerstones of PAH therapy, are equally effective in CTEPH (10, 21, 46). The only approved therapy for CTEPH is the sGC stimulator Riociguat (10, 21, 46), suggesting that the NO-pathway is compromised in CTEPH.

Remodeling of the heart

The high pressure and resistance in the pulmonary vasculature impose an increased afterload on the right ventricle. As contractile reserve of the RV is limited (22), initially, subacute RV dilation and dysfunction present (59). With sustained PH, the increased pressure subsequently produces an augmentation of wall thickness by increasing the muscle mass resulting in right ventricular hypertrophy (59), in order to normalize RV wall stress. Although RV remodeling is initially beneficial and aims to normalize wall stress, the RV is not capable of sustaining a long-term progressive pressure overload. The dilation increases wall stress which requires a higher oxygen demand and thus decreases the perfusion of the RV leading to a vicious circle of compromised contractility of the cardiomyocytes and dilation which eventually leads to the development of RV failure.

V/Q mismatch in CTEPH

Obstructions in the pulmonary vasculature as observed in CTEPH patients impair ventilation (V) and perfusion (Q) matching. In the embolized lungs, there are areas that are overventilated and underperfused and areas that are underventilated and overperfused. This heterogeneity can be explained by the fact that some areas are not perfused due to the obstructions and some areas are overperfused due to redirection of the blood flow. Ventilation-perfusion inequality hampers

(i.e. reduces) the arterial oxygen uptake and carbon dioxide clearance, and leads to compensatory hyperventilation in an attempt to increase the carbon dioxide clearance but inadvertently leads to increased dead space ventilation of the lungs. Moreover, this hyperventilation of the lungs is insufficient to increase oxygen uptake (40). This decreased oxygenation of blood and increased lung ventilation contribute to the shortness of breath experienced by patients.

Exercise intolerance in CTEPH

Exercise intolerance is one of the symptoms of CTEPH and evaluation of RV function during stress testing has been shown to be of prognostic value in patients (24, 25, 52). RV dysfunction is exacerbated during exercise, when cardiac demand increases and the RV is required to pump more blood against an even more elevated afterload. Therefore, RV functional measurements during stress enable the evaluation of the capacity of the RV to cope with an elevated afterload and can facilitate early detection of RV dysfunction (56). Although the main cause of exercise intolerance in CTEPH is cardiac, the V/Q mismatch is thought to also play a role in the exercise intolerance observed in patients with CTEPH (4, 5, 52). To date, however studies describing animal models of CTEPH have not evaluated the pathophysiology during exercise.

Table 1. Comparison between large animal studies utilizing embolization techniques to create chronic thromboembolic pulmonary hypertension models.

1st author Year of publication	Species	Gender	Embolic material	Emboli zations (N)	N	Anesthesia during RHC	Recovery period	PAP (mmHg)	PVR (WU)	RVW/ LVW+S W	RV function assessment
Shelub 1984(57)	Canine	Female	Sephadex G50	Variable (16-30 weeks)	5	None	>7 days	29±4	8.3 ±2.3	0.54[e]	None
Perckett 1988(47)	Sheep	NR	Air (continuous)	12 days	5	None	1.5 hour	23[f] ±2	5.2[f]	0.38±0.0 6	None
Moser 1991(44)	Canine	NR	3-4 venousthrom	2	10	Halothane	32 days	20.3±2	4.2[a]	NR	None
Weimann 1999(67)	Swine	Male	Sephadex G50 (15mg/kg)	3	8	Ketamine	7 days	18±3	4.3[a,b]	NR	None
Kim 2000(28)	Canine	NR	Ceramicbeads (3 mm)	4	5	Halothane	6 months	17±2	4.3[a]	NR	None
Zhou 2011(72)	Sheep	Female	Air (continuous)	8 weeks	4	None	7 days	34±2.6	4.5 ±0.9	0.36±0.0 1	None
Sage 2012(54)	Swine	NR	Right PA ligation	1	10	Pento barbital	5 weeks	16.2±1.3	10.05[c] ±0.69	NR	None
Pohlmann 2012(48)	Sheep	NR	Sephadex G50 (~21.1±0.5g)	60	9	none	1 day	35±3	1.7 ±0.2	0.42±0.0 1	None
Garcia-Alvarez 2013(17)	Swine	Male	Sephadex G50	4 (3-6)	9	Midazolam	2 months	27±3	2.2[d] ±1.1	NR	CMR
Mercier 2013(41)	Swine	NR	Histoacryl + Left PA	5	5	NR	7 days	28.5±1.7	9.8[a]	NR	Echo, CT

Guihaire 2014(19)	Swine	NR	Histoacryl + Left PA	5	5	Isoflurane	6 weeks	41±4	10.0[a,c]	NR	Echo, PV-loop
Guihaire 2015(20)	Swine	NR	Histoacryl + Left PA	5	13	Isoflurane	7 days	34±9	12.4[a,c]	NR	Echo, Dobutamine, PV-loop
Boulate 2015(3)	Swine	Male	Histoacryl + Left PA	5	5	NR	7 weeks	27±1.1	7.9 ±0.6	NR	None
Aguero 2015(1)	Swine	Female	Sephadex G50 (20 mg/kg)	6	6	Propofol	14 days	16±2	1.5[b]	0.41±0.02	Echo
Aguero 2015(1)	Swine	Female	Sephadex G50 (20 mg/kg) + coiling	4	6	Propofol	1 month	23±4	1.6[b]	0.47±0.06	Echo
Tang 2015(62)	Canine	NR	Autologous thrombi (0.3*1cm)	NR	13	Propofol	14 days	25.2±3.6	NR	NR	Dual-energy CT
Rothman 2017(53)	Swine	Female	Ceramicbeads (0.6-0.9mm)	21-40	3	Isoflurane	NR	36.6[g]±0.9	NR	NR	None
Rothman 2017(53)	Canine	Female	Ceramicbeads (0.6-0.9mm)	9-12	3	Isoflurane	20 months[h]	47[g]	7.8	NR	None
Mulchrone 2019(45)	Canine	Male	Sephadex G50 (~51250±8189 spheres)	Every 3-4 days (4-8	4	Propofol	14-84 days	34.3±6.0	27.6 ±5.0	NR	Echo, CMR

a) Calculated from dynes·sec^{-1}·cm^{-5}; b) Calculated from indexed PVRi; c) Total pulmonary vascular resistance; d) Median (interquartile range) reported; e) Only reported 2/5 cases; f) Calculated from cmH_2O or cmH_2O·L^{-1}·min; g) systolic PAP; h) only reported of one animal. CMR, cardiovascular magnetic resonance; CPET, cardiopulmonary exercise testing; CT, computed tomography; LVW, left ventricular weight; NR, not reported; PA, pulmonary artery; PAP, mean pulmonary artery pressure; PV loop, pressure-volume loop; PVR, pulmonary vascular resistance; RHC, right heart catheterization; RVW, right ventricular weight; SW, septum weight; WU, wood units.

CTEPH Animal models

Dating back to 1984, many investigators have attempted to establish a large animal model to study the pathophysiology of CTEPH using different embolization frequencies and embolization materials including air, autologous blood clots, sephadex beads and glue (Table 1). Although the PAP increases acutely upon embolization in these models, most studies were unsuccessful in establishing a sustained level of elevated PAP during prolonged follow-up (7, 9, 18, 35, 42, 61, 64, 73, 74). Those studies that did report CTEPH during prolonged follow-up (8, 36, 45, 64, 73) have in common that they used repeated (between 4 and 40 times) embolization procedures, thereby obstructing a significant fraction of the pulmonary vasculature. In these studies, PAP also decreased in between embolization procedures, but gradual increase in PAP occurred over time. However, most studies did not determine whether this gradual increase in PAP was solely due to the progressive embolization of pulmonary vessels or that distal pulmonary microvasculopathy also developed. Recent findings by Boulate et al. suggest that distal vasculopathy was present in their model of left pulmonary artery ligation in combination with glue-embolizations (74). However, in the latter study, as in most of the aforementioned studies, hemodynamic measurements were performed under anesthesia, which may have influenced cardiac function and pulmonary hemodynamics (7, 36, 74). Moreover, and in most cases due to the use of anesthetic agents, pulmonary hemodynamics were not assessed during exercise. This shows the need for a large CTEPH animal model without all the previous limitations.

Outline of this thesis

The general aim of this thesis is to characterize and study the complex mechanisms involved in the development and progression of CTEPH. For this purpose, we developed and utilized a novel large animal model for CTEPH and studied the effects of cardiopulmonary exercise testing. In addition, we investigated the role of pulmonary endothelial (dys)function in the development and progression of CTEPH and characterize (molecular) pathways involved in cardiac remodeling with the emphasis on hypertrophy, contractility, inflammation, oxidative stress, apoptosis and angiogenesis

Part I Development and Validation

In order to study hemodynamic changes in a large animal model in the awake state, we developed a model of chronic instrumentation of swine as described in **Chapter 2**. The chronic instrumentation of swine allows for serial examination of hemodynamic parameters as well as blood samples in the awake state, and facilitates the infusion of embolizing material. In addition, treadmill exercise is possible with these catheterized animals, allowing cardiopulmonary exercise testing in health and disease in the experimental setting.

To investigate the development and pathophysiology of CTEPH, we aimed to develop a novel CTEPH large animal model to overcome the shortcomings, as described above, of previous animal models. We therefore developed a chronically instrumented, double-hit CTEPH swine model, by using the instrumentation method of **Chapter 2** and a combination of inducing endothelial dysfunction and emboli. We investigated the development of the disease and utilized cardiopulmonary exercise testing to allow for earlier detection of the disease in **Chapter 3** of this thesis. In **Chapter 4**, we present a state of the art

imaging modality, 4D flow MRI. The goal of this study was to validate this imaging modality against the established 2D MRI and the in vivo flow measurement, enabled by the catheterization described in **Chapter 2**. In addition, we investigated potential differences in pulmonary and aorta flow profiles in the CTEPH swine, as developed in **Chapter 3**, compared to healthy swine.

Part II Characterization

Since the pathophysiology of CTEPH is incompletely understood, we studied changes in both pulmonary microvascular (**Chapter 5**) and cardiac (**Chapter 6**) remodeling. We aimed to elucidate some of the mechanisms involved in this remodeling to better understand the pathophysiology of the disease. The pressing importance to elucidate this pathophysiology are all the patients for which no clear therapy is present to date. We believe that endothelial dysfunction plays a key role in the progression of the disease, and therefore focus on investigating pulmonary vascular remodeling and the role of the NO and endothelin pathways. Other factors involved in the development and progression of disease such as pulmonary and cardiac inflammation and angiogenesis were investigated as well. In addition, the influence of exercise on the pulmonary ventilation/perfusion and cardiac function was investigated for both contributions to exercise limitations and role for disease detection in patients.

A summary of the study protocol and the chapters in which we investigate what parts are depicted in Figure 4.

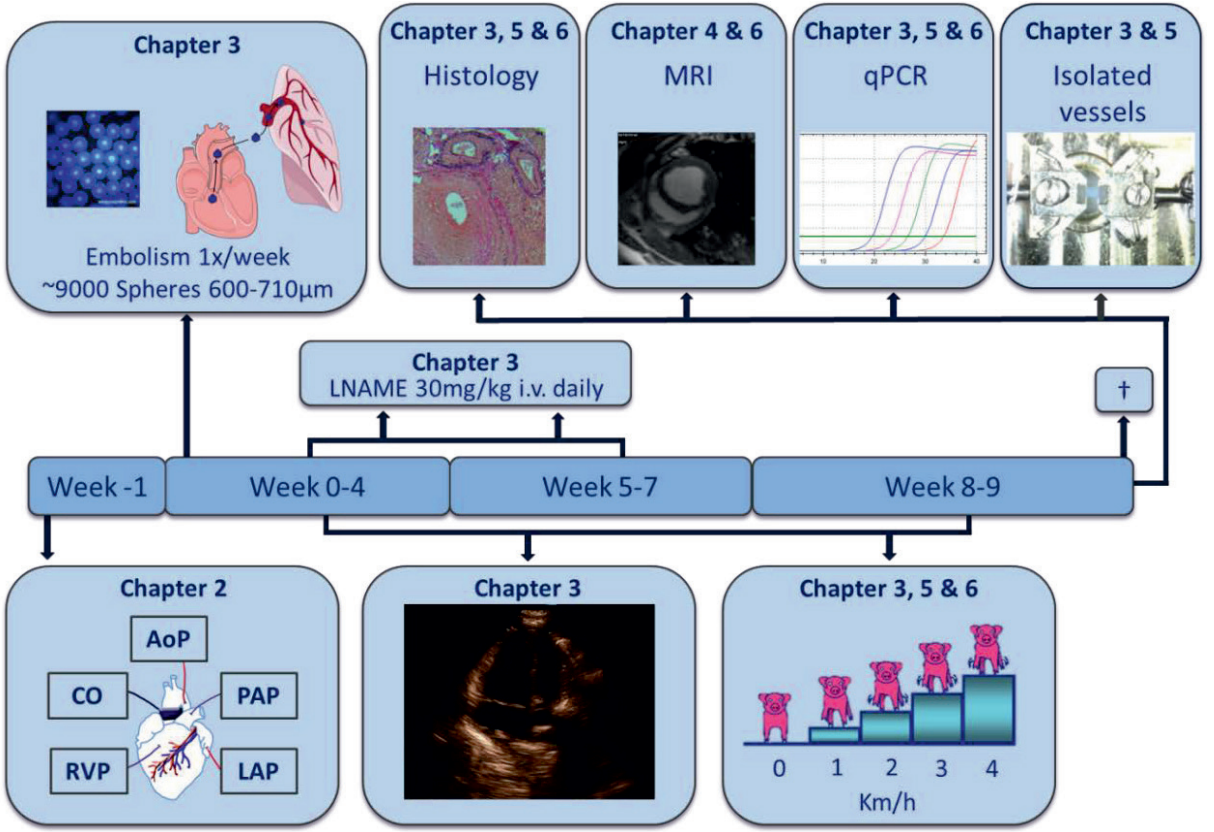

Figure 4. Study protocol.

Presented is the study protocol, and the corresponding chapters, for the developed CTEPH swine model. Chronic instrumentation is described in Chapter 2, development of the animal model by combined emboli and endothelial dysfunction (LNAME) in Chapter 3, echocardiography in Chapter 3 and cardiopulmonary exercise testing in Chapter 3, 5 and 6.

References

1. **Aguero J, Ishikawa K, Fish KM, Hammoudi N, Hadri L, Garcia-Alvarez A, Ibanez B, Fuster V, Hajjar RJ, and Leopold JA**. Combination proximal pulmonary artery coiling and distal embolization induces chronic elevations in pulmonary artery pressure in Swine. *PLoS One* 10: e0124526, 2015.

2. **Albani S, Biondi F, Stolfo D, Lo Giudice F, and Sinagra G**. Chronic thromboembolic pulmonary hypertension (CTEPH): what do we know about it? A comprehensive review of the literature. *J Cardiovasc Med (Hagerstown)* 2019.

3. **Boulate D, Perros F, Dorfmuller P, Arthur-Ataam J, Guihaire J, Lamrani L, Decante B, Humbert M, Eddahibi S, Dartevelle P, Fadel E, and Mercier O**. Pulmonary microvascular lesions regress in reperfused chronic thromboembolic pulmonary hypertension. *J Heart Lung Transplant* 34: 457-467, 2015.

4. **Claessen G, La Gerche A, Dymarkowski S, Claus P, Delcroix M, and Heidbuchel H**. Pulmonary vascular and right ventricular reserve in patients with normalized resting hemodynamics after pulmonary endarterectomy. *J Am Heart Assoc* 4: e001602, 2015.

5. **Claessen G, La Gerche A, Wielandts JY, Bogaert J, Van Cleemput J, Wuyts W, Claus P, Delcroix M, and Heidbuchel H**. Exercise pathophysiology and sildenafil effects in chronic thromboembolic pulmonary hypertension. *Heart* 101: 637-644, 2015.

6. **Condliffe R, Kiely DG, Gibbs JS, Corris PA, Peacock AJ, Jenkins DP, Hodgkins D, Goldsmith K, Hughes RJ, Sheares K, Tsui SS, Armstrong IJ, Torpy C, Crackett R, Carlin CM, Das C, Coghlan JG, and Pepke-Zaba J**. Improved outcomes in medically and surgically treated chronic thromboembolic pulmonary hypertension. *Am J Respir Crit Care Med* 177: 1122-1127, 2008.

7. **de Beer VJ, de Graaff HJ, Hoekstra M, Duncker DJ, and Merkus D**. Integrated control of pulmonary vascular tone by endothelin and angiotensin II in exercising swine depends on gender. *American journal of physiology Heart and circulatory physiology* 298: H1976-1985, 2010.

8. **Duncker DJ, and Bache RJ**. Regulation of coronary blood flow during exercise. *Physiological reviews* 88: 1009-1086, 2008.

9. **Duncker DJ, Stubenitsky R, and Verdouw PD**. Autonomic control of vasomotion in the porcine coronary circulation during treadmill exercise: evidence for feed-forward beta-adrenergic control. *Circulation research* 82: 1312-1322, 1998.

10. **Edward JA, and Mandras S**. An Update on the Management of Chronic Thromboembolic Pulmonary Hypertension. *Curr Probl Cardiol* 42: 7-38, 2017.

11. **Ende-Verhaar YM, Cannegieter SC, Vonk Noordegraaf A, Delcroix M, Pruszczyk P, Mairuhu AT, Huisman MV, and Klok FA**. Incidence of chronic thromboembolic pulmonary hypertension after acute pulmonary embolism: a contemporary view of the published literature. *Eur Respir J* 49: 2017.

12. **Escribano-Subias P, Blanco I, Lopez-Meseguer M, Lopez-Guarch CJ, Roman A, Morales P, Castillo-Palma MJ, Segovia J, Gomez-Sanchez MA, Barbera JA, and investigators R**. Survival in pulmonary hypertension in Spain: insights from the Spanish registry. *Eur Respir J* 40: 596-603, 2012.

13. **Fuji S, Matsushita S, Hyodo K, Osaka M, Sakamoto H, Tanioka K, Miyakawa K, Kubota M, Hiramatsu Y, and Tokunaga C**. Association between endothelial function and micro-vascular remodeling measured by synchrotron radiation pulmonary micro-angiography in pulmonary arterial hypertension. *Gen Thorac Cardiovasc Surg* 64: 597-603, 2016.

14. **Galie N, Humbert M, Vachiery JL, Gibbs S, Lang I, Torbicki A, Simonneau G, Peacock A, Vonk Noordegraaf A, Beghetti M, Ghofrani A, Gomez Sanchez MA, Hansmann G, Klepetko W, Lancellotti P, Matucci M, McDonagh T, Pierard LA, Trindade PT, Zompatori M, Hoeper M, and Group ESCSD**. 2015 ESC/ERS Guidelines for the diagnosis and treatment of pulmonary hypertension: The Joint Task Force for the Diagnosis and Treatment of Pulmonary Hypertension of the European Society of Cardiology (ESC) and the European Respiratory Society (ERS): Endorsed by: Association for European Paediatric and Congenital Cardiology (AEPC), International Society for Heart and Lung Transplantation (ISHLT). *Eur Heart J* 37: 67-119, 2016.

15. **Galie N, and Kim NH**. Pulmonary microvascular disease in chronic thromboembolic pulmonary hypertension. *Proc Am Thorac Soc* 3: 571-576, 2006.

16. **Gall H, Preston IR, Hinzmann B, Heinz S, Jenkins D, Kim NH, and Lang I**. An international physician survey of chronic thromboembolic pulmonary hypertension management. *Pulm Circ* 6: 472-482, 2016.

17. **Garcia-Alvarez A, Fernandez-Friera L, Garcia-Ruiz JM, Nuno-Ayala M, Pereda D, Fernandez-Jimenez R, Guzman G, Sanchez-Quintana D, Alberich-Bayarri A, Pastor-Escuredo D, Sanz-Rosa D, Garcia-Prieto J, Gonzalez-Mirelis JG, Pizarro G, Jimenez-Borreguero LJ, Fuster V, Sanz J, and Ibanez B**. Noninvasive monitoring of serial changes in pulmonary vascular resistance and acute

vasodilator testing using cardiac magnetic resonance. *J Am Coll Cardiol* 62: 1621-1631, 2013.

18. **Gross DR**. *Animal Models in Cardiovascular Research*. Springer, 2009.

19. **Guihaire J, Haddad F, Boulate D, Capderou A, Decante B, Flecher E, Eddahibi S, Dorfmuller P, Herve P, Humbert M, Verhoye JP, Dartevelle P, Mercier O, and Fadel E**. Right ventricular plasticity in a porcine model of chronic pressure overload. *J Heart Lung Transplant* 33: 194-202, 2014.

20. **Guihaire J, Haddad F, Noly PE, Boulate D, Decante B, Dartevelle P, Humbert M, Verhoye JP, Mercier O, and Fadel E**. Right ventricular reserve in a piglet model of chronic pulmonary hypertension. *Eur Respir J* 45: 709-717, 2015.

21. **Halank M, Hoeper MM, Ghofrani HA, Meyer FJ, Stahler G, Behr J, Ewert R, Fletcher M, Colorado P, Nikkho S, and Grimminger F**. Riociguat for pulmonary arterial hypertension and chronic thromboembolic pulmonary hypertension: Results from a phase II long-term extension study. *Respir Med* 128: 50-56, 2017.

22. **Hasler ED, Muller-Mottet S, Furian M, Saxer S, Huber LC, Maggiorini M, Speich R, Bloch KE, and Ulrich S**. Pressure-Flow During Exercise Catheterization Predicts Survival in Pulmonary Hypertension. *Chest* 150: 57-67, 2016.

23. **Haythe J**. Chronic thromboembolic pulmonary hypertension: a review of current practice. *Prog Cardiovasc Dis* 55: 134-143, 2012.

24. **Held M, Grun M, Holl R, Hubner G, Kaiser R, Karl S, Kolb M, Schafers HJ, Wilkens H, and Jany B**. Cardiopulmonary exercise testing to detect chronic thromboembolic pulmonary hypertension in patients with normal echocardiography. *Respiration* 87: 379-387, 2014.

25. **Held M, Hesse A, Gott F, Holl R, Hubner G, Kolb P, Langen HJ, Romen T, Walter F, Schafers HJ, Wilkens H, and Jany B**. A symptom-related monitoring program following pulmonary embolism for the early detection of CTEPH: a prospective observational registry study. *BMC Pulm Med* 14: 141, 2014.

26. **Hoeper MM, Bogaard HJ, Condliffe R, Frantz R, Khanna D, Kurzyna M, Langleben D, Manes A, Satoh T, Torres F, Wilkins MR, and Badesch DB**. Definitions and diagnosis of pulmonary hypertension. *J Am Coll Cardiol* 62: D42-50, 2013.

27. **Hoeper MM, Madani MM, Nakanishi N, Meyer B, Cebotari S, and Rubin LJ**. Chronic thromboembolic pulmonary hypertension. *Lancet Respir Med* 2: 573-582, 2014.

28. **Kim H, Yung GL, Marsh JJ, Konopka RG, Pedersen CA, Chiles PG, Morris TA, and Channick RN**. Endothelin mediates pulmonary vascular remodelling in a canine model of chronic embolic pulmonary hypertension. *Eur Respir J* 15: 640-648, 2000.

29. **Klok FA, Barco S, Konstantinides SV, Dartevelle P, Fadel E, Jenkins D, Kim NH, Madani M, Matsubara H, Mayer E, Pepke-Zaba J, Delcroix M, and Lang IM**. Determinants of diagnostic delay in Chronic Thromboembolic Pulmonary Hypertension: results from the European CTEPH registry. *Eur Respir J* 2018.

30. **Konstantinides SV, Barco S, Lankeit M, and Meyer G**. Management of Pulmonary Embolism: An Update. *J Am Coll Cardiol* 67: 976-990, 2016.

31. **Konstantinides SV, Torbicki A, Agnelli G, Danchin N, Fitzmaurice D, Galie N, Gibbs JS, Huisman MV, Humbert M, Kucher N, Lang I, Lankeit M, Lekakis J, Maack C, Mayer E, Meneveau N, Perrier A, Pruszczyk P, Rasmussen LH, Schindler TH, Svitil P, Vonk Noordegraaf A, Zamorano JL, Zompatori M, Task Force for the D, and Management of Acute Pulmonary Embolism of the European Society of C**. 2014 ESC guidelines on the diagnosis and management of acute pulmonary embolism. *Eur Heart J* 35: 3033-3069, 3069a-3069k, 2014.

32. **Kramm T, Wilkens H, Fuge J, Schafers HJ, Guth S, Wiedenroth CB, Weingard B, Huscher D, Pittrow D, Cebotari S, Hoeper MM, Mayer E, and Olsson KM**. Incidence and characteristics of chronic thromboembolic pulmonary hypertension in Germany. *Clin Res Cardiol* 107: 548-553, 2018.

33. **Lang IM, and Madani M**. Update on chronic thromboembolic pulmonary hypertension. *Circulation* 130: 508-518, 2014.

34. **Laughlin MH**. Cardiovascular response to exercise. *Am J Physiol* 277: S244-259, 1999.

35. **Laughlin MH, Davis MJ, Secher NH, van Lieshout JJ, Arce-Esquivel AA, Simmons GH, Bender SB, Padilla J, Bache RJ, Merkus D, and Duncker DJ**. Peripheral circulation. *Comprehensive Physiology* 2: 321-447, 2012.

36. **Lautt WW**. Resistance or conductance for expression of arterial vascular tone. *Microvascular research* 37: 230-236, 1989.

37. **Mahmud E, Madani MM, Kim NH, Poch D, Ang L, Behnamfar O, Patel MP, and Auger WR**. Chronic Thromboembolic Pulmonary Hypertension: Evolving Therapeutic Approaches for Operable and Inoperable Disease. *J Am Coll Cardiol* 71: 2468-2486, 2018.

38. **Masaki T**. Historical review: Endothelin. *Trends Pharmacol Sci* 25: 219-224, 2004.

39. **Matthews DT, and Hemnes AR**. Current concepts in the pathogenesis of chronic thromboembolic pulmonary hypertension. *Pulm Circ* 6: 145-154, 2016.

40. **Melot C, and Naeije R**. Pulmonary vascular diseases. *Comprehensive Physiology* 1: 593-619, 2011.

41. **Mercier O, Tivane A, Dorfmuller P, de Perrot M, Raoux F, Decante B, Eddahibi S, Dartevelle P, and Fadel E**. Piglet model of chronic pulmonary hypertension. *Pulm Circ* 3: 908-915, 2013.

42. **Merkus D, and Duncker DJ**. Perspectives: Coronary microvascular dysfunction in post-infarct remodelled myocardium. *European Heart Journal Supplements* 16: A74-A79, 2014.

43. **Moser KM, and Bloor CM**. Pulmonary vascular lesions occurring in patients with chronic major vessel thromboembolic pulmonary hypertension. *Chest* 103: 685-692, 1993.

44. **Moser KM, Cantor JP, Olman M, Villespin I, Graif JL, Konopka R, Marsh JJ, and Pedersen C**. Chronic pulmonary thromboembolism in dogs treated with tranexamic acid. *Circulation* 83: 1371-1379, 1991.

45. **Mulchrone A, Kellihan HB, Forouzan O, Hacker TA, Bates ML, Francois CJ, and Chesler NC**. A Large Animal Model of Right Ventricular Failure due to Chronic Thromboembolic Pulmonary Hypertension: A Focus on Function. *Frontiers in Cardiovascular Medicine* 5: 2019.

46. **Pepke-Zaba J, Ghofrani HA, and Hoeper MM**. Medical management of chronic thromboembolic pulmonary hypertension. *Eur Respir Rev* 26: 2017.

47. **Perkett EA, Brigham KL, and Meyrick B**. Continuous air embolization into sheep causes sustained pulmonary hypertension and increased pulmonary vasoreactivity. *Am J Pathol* 132: 444-454, 1988.

48. **Pohlmann JR, Akay B, Camboni D, Koch KL, Mervak BM, and Cook KE**. A low mortality model of chronic pulmonary hypertension in sheep. *J Surg Res* 175: 44-48, 2012.

49. **Prins KW, and Thenappan T**. World Health Organization Group I Pulmonary Hypertension: Epidemiology and Pathophysiology. *Cardiol Clin* 34: 363-374, 2016.

50. **Raskob GE, Angchaisuksiri P, Blanco AN, Buller H, Gallus A, Hunt BJ, Hylek EM, Kakkar A, Konstantinides SV, McCumber M, Ozaki Y, Wendelboe A, Weitz JI,**

and Day ISCfWT. Thrombosis: a major contributor to global disease burden. *Arterioscler Thromb Vasc Biol* 34: 2363-2371, 2014.

51. **Reesink HJ, Meijer RC, Lutter R, Boomsma F, Jansen HM, Kloek JJ, and Bresser P**. Hemodynamic and clinical correlates of endothelin-1 in chronic thromboembolic pulmonary hypertension. *Circ J* 70: 1058-1063, 2006.

52. **Richter MJ, Pader P, Gall H, Reichenberger F, Seeger W, Mayer E, Guth S, Kramm T, Grimminger F, Ghofrani HA, and Voswinckel R**. The prognostic relevance of oxygen uptake in inoperable chronic thromboembolic pulmonary hypertension. *Clin Respir J* 2015.

53. **Rothman A, Wiencek RG, Davidson S, Evans WN, Restrepo H, Sarukhanov V, and Mann D**. Challenges in the development of chronic pulmonary hypertension models in large animals. *Pulm Circ* 7: 156-166, 2017.

54. **Sage E, Mercier O, Herve P, Tu L, Dartevelle P, Eddahibi S, and Fadel E**. Right lung ischemia induces contralateral pulmonary vasculopathy in an animal model. *The Journal of thoracic and cardiovascular surgery* 143: 967-973, 2012.

55. **Sandoo A, van Zanten JJ, Metsios GS, Carroll D, and Kitas GD**. The endothelium and its role in regulating vascular tone. *Open Cardiovasc Med J* 4: 302-312, 2010.

56. **Sharma T, Lau EM, Choudhary P, Torzillo PJ, Munoz PA, Simmons LR, Naeije R, and Celermajer DS**. Dobutamine stress for evaluation of right ventricular reserve in pulmonary arterial hypertension. *Eur Respir J* 45: 700-708, 2015.

57. **Shelub I, van Grondelle A, McCullough R, Hofmeister S, and Reeves JT**. A model of embolic chronic pulmonary hypertension in the dog. *J Appl Physiol Respir Environ Exerc Physiol* 56: 810-815, 1984.

58. **Simonneau G, and Hoeper MM**. Evaluation of the incidence of rare diseases: difficulties and uncertainties, the example of chronic thromboembolic pulmonary hypertension. *Eur Respir J* 49: 2017.

59. **Simonneau G, Torbicki A, Dorfmuller P, and Kim N**. The pathophysiology of chronic thromboembolic pulmonary hypertension. *Eur Respir Rev* 26: 2017.

60. **Sitbon O, and Gaine S**. Beyond a single pathway: combination therapy in pulmonary arterial hypertension. *Eur Respir Rev* 25: 408-417, 2016.

61. **Stubenitsky R, Verdouw PD, and Duncker DJ**. Autonomic control of cardiovascular performance and whole body O2 delivery and utilization in swine during treadmill exercise. *Cardiovasc Res* 39: 459-474, 1998.

62. **Tang CX, Yang GF, Schoepf UJ, Han ZH, Qi L, Zhao YE, Wu J, Zhou CS, Zhu H, Stubenrauch AC, Mangold S, Zhang LJ, and Lu GM**. Chronic thromboembolic pulmonary hypertension: Comparison of dual-energy computed tomography and single photon emission computed tomography in canines. *Eur J Radiol* 85: 498-506, 2016.

63. **Torbicki A**. Hypertension: Definition of pulmonary hypertension challenged? *Nat Rev Cardiol* 13: 250-251, 2016.

64. **Tune JD, Gorman MW, and Feigl EO**. Matching coronary blood flow to myocardial oxygen consumption. *Journal of applied physiology* 97: 404-415, 2004.

65. **Vavera Z, Vojacek J, Pudil R, Maly J, and Elias P**. Chronic thromboembolic pulmonary hypertension after the first episode of pulmonary embolism? How often? *Biomed Pap Med Fac Univ Palacky Olomouc Czech Repub* 160: 125-129, 2016.

66. **Vonk Noordegraaf A, Boonstra A, Konings TC, Marques KM, and Bogaard HJ**. [Diagnosis and treatment of pulmonary hypertension]

Diagnostiek en behandeling van pulmonale hypertensie. *Ned Tijdschr Geneeskd* 158: A7315, 2014.

67. **Weimann J, Zink W, Schnabel PA, Jakob H, Gebhard MM, Martin E, and Motsch J**. Selective vasodilation by nitric oxide inhalation during sustained pulmonary hypertension following recurrent microembolism in pigs. *J Crit Care* 14: 133-140, 1999.

68. **White RH**. The epidemiology of venous thromboembolism. *Circulation* 107: I4-8, 2003.

69. **Widmaier EP, Raff H, and Strang KT**. *Vander's Human Physiology*. New York, NY: McGraw-Hill, 2008, p. 770.

70. **Yang S, Yang Y, Zhai Z, Kuang T, Gong J, Zhang S, Zhu J, Liang L, Shen YH, and Wang C**. Incidence and risk factors of chronic thromboembolic pulmonary hypertension in patients after acute pulmonary embolism. *J Thorac Dis* 7: 1927-1938, 2015.

71. **Zhang S, Yang T, Xu X, Wang M, Zhong L, Yang Y, Zhai Z, Xiao F, and Wang C**. Oxidative stress and nitric oxide signaling related biomarkers in patients with pulmonary hypertension: a case control study. *BMC Pulm Med* 15: 50, 2015.

72. **Zhou X, Wang D, Castro CY, Hawkins H, Lynch JE, Liu X, and Zwischenberger JB**. A pulmonary hypertension model induced by continuous pulmonary air embolization. *J Surg Res* 170: e11-16, 2011.

73. **Zhou Z, de Beer VJ, Bender SB, Jan Danser AH, Merkus D, Laughlin MH, and Duncker DJ**. Phosphodiesterase-5 activity exerts a coronary vasoconstrictor influence in awake swine that is mediated in part via an increase in endothelin production. *American journal of physiology Heart and circulatory physiology* 306: H918-927, 2014.

74. **Zhou Z, de Beer VJ, de Wijs-Meijler D, Bender SB, Hoekstra M, Laughlin MH, Duncker DJ, and Merkus D**. Pulmonary vasoconstrictor influence of endothelin in exercising swine depends critically on phosphodiesterase 5 activity. *Am J Physiol Lung Cell Mol Physiol* 306: L442-452, 2014.

Part I

Development and Validation

Chapter 2

Surgical Placement of Catheters for Long-term Cardiovascular Exercise Testing in Swine

Kelly Stam, Daphne P M De Wijs-Meijler*, Richard W B van Duin, Annemarie Verzijl, Irwin K Reiss, Dirk J Duncker, Daphne Merkus*

* Both authors contributed equally

J Vis Exp. 2016 Feb 9;(108):e53772

Abstract

This protocol describes the surgical procedure to chronically instrument swine and the procedure to exercise swine on a motor-driven treadmill. Early cardiopulmonary dysfunction is difficult to diagnose, particularly in animal models, as cardiopulmonary function is often measured invasively, requiring anesthesia. As many anesthetic agents are cardiodepressive, subtle changes in cardiovascular function may be masked. In contrast, chronic instrumentation allows for measurement of cardiopulmonary function in the awake state, so that measurements can be obtained under quiet resting conditions, without the effects of anesthesia and acute surgical trauma. Furthermore, when animals are properly trained, measurements can also be obtained during graded treadmill exercise.

Flow probes are placed around the aorta or pulmonary artery for measurement of cardiac output and around the left anterior descending coronary artery for measurement of coronary blood flow. Fluid-filled catheters are implanted in the aorta, pulmonary artery, left atrium, left ventricle and right ventricle for pressure measurement and blood sampling. In addition, a 20 G catheter is positioned in the anterior interventricular vein to allow coronary venous blood sampling.

After a week of recovery, swine are placed on a motor-driven treadmill, the catheters are connected to pressure and flow meters, and swine are subjected to a five-stage progressive exercise protocol, with each stage lasting 3 min. Hemodynamic signals are continuously recorded and blood samples are taken during the last 30 sec of each exercise stage.

The major advantage of studying chronically instrumented animals is that it allows serial assessment of cardiopulmonary function, not only at rest but also during

physical stress such as exercise. Moreover, cardiopulmonary function can be assessed repeatedly during disease development and during chronic treatment, thereby increasing statistical power and hence limiting the number of animals required for a study.

Introduction

Adequate cardiopulmonary function is essential to supply the body with oxygen and nutrients, particularly during conditions of increased metabolic demand such as during exercise (9). The cardiopulmonary response to exercise is characterized by a number of adaptations in cardiac function, i.e., an increase in heart rate, contractility and stroke volume, and microvascular function, i.e., vasodilation in the vascular beds supplying exercising muscles as well as in the pulmonary vasculature, and vasoconstriction in the vascular beds supplying the gastrointestinal system as well as inactive muscles (9). Impaired exercise capacity is an early hallmark of cardiopulmonary dysfunction, and cardiopulmonary exercise testing is used as an effective method to delineate between cardiac dysfunction, vascular dysfunction and/ or pulmonary dysfunction in patients with impaired exercise capacity (2). Early cardiopulmonary dysfunction is difficult to diagnose, particularly in animal models, as cardiopulmonary function is often measured invasively, requiring anesthesia, with many anesthetic agents possessing cardiodepressive properties (20). Chronic instrumentation allows for measurement of cardiopulmonary function in the awake state, and when the animals are fully adjusted to the laboratory conditions measurements can be obtained under quiet resting conditions without the effects of anesthesia and acute surgical trauma. Furthermore, when the animals are appropriately trained, measurements can also be obtained during graded treadmill exercise (4, 18). More specifically, left and right ventricular function can be assessed and related to myocardial perfusion, while regulation of vasomotor tone in the coronary, systemic and pulmonary microcirculation can be determined. The use of fluid-filled catheters allows measurement of pressure as well as taking blood samples without imposing additional stress on the animals. Another advantage of studying chronically instrumented animals is that cardiopulmonary exercise testing can be

repeated allowing the use of an animal as its own control, either during disease development or during chronic treatment, thereby increasing statistical power and hence limiting the number of animals required for a study. Cardiopulmonary anatomy of swine closely resembles that of humans and it is possible to induce various forms of cardiopulmonary disease, such as diabetes (19), myocardial infarction (23), pulmonary hypertension (11, 15) and pacing-induced heart failure (16, 21). Moreover, the size of swine allows chronic instrumentation, and repeated blood sampling of sufficient quantity to analyze not only blood gases, but also to perform neurohumoral measurements and/or to search for biomarkers of disease. This protocol describes the surgery used to chronically instrument swine as well as the protocol for exercising the swine on a motor-driven treadmill.

Protocol

Procedures involving animal subjects have been approved by the Animal Care Committee at Erasmus Medical Center Rotterdam (NL). Swine with weights between 6 and 80 kg have been successfully instrumented using this protocol.

1. Adaptation of the Animals to Human Handling

1. After arrival in the facility, house the animals solitarily but enable them to interact with each other.

2. Accustomize swine to human handling and transportation from the animal facility to the experimental laboratory, by handling the animal at least once a day for one week.

3. Train the animals appropriately for exercise experiments on a motor-driven treadmill by exercising them on the treadmill for a minimum of three times before surgery.

4. Animals should be fasted O/N before surgery to prevent nausea, vomiting and thereby potential aspiration of stomach fluids.

2. Preparation for Surgery

1. Sedation

1. Prepare medication for sedation in a 10 ml syringe. Premedication consists of tiletamine/zolazepam (5 mg/kg), xylazine, (2.25 mg/kg) and atropine (1 mg).

2. Inject the medication intramuscularly in the trapezius muscle with a 19 G 1.5'' needle to sedate the pig.

3. Wait for approximately 10 min and check for muscle relaxation and unconsciousness to confirm appropriate and stable level of sedation.

4. Place a 20 G peripheral safety catheter in an ear vein for subsequent intravenous administration of anesthesia and/or fluids.

2. Intubation and Ventilation

1. Place the animal on a table and/or trolley in supine position.

2. Open the mouth of the animal with an oral spreader.

3. In case of insufficient relaxation of the jaws or presence of swallowing reflexes, which hinder intubation, administer thiopental (10 mg/ kg)

intravenously via the ear vein catheter. Alternatively, the pig could be masked with isoflurane to induce sedation.

4. Use a conventional laryngoscope with a light and a Miller blade to allow the laryngoscopist to directly view the larynx. If there is laryngospasm, apply 2% lidocaine to the cords and larynx to reduce the spasm and allow intubation.

5. Insert an intubating stylet into the endotracheal tube to make the tube conform better to the upper airway anatomy and pass the tube through the mouth and between the vocal cords into the trachea.

6. Inflate the balloon cuff with a 10 ml syringe to help secure it in place, to prevent leakage of respiratory gases, and to protect the airways from possible aspiration of stomach fluid.

7. Connect the tube to a breathing filter (heat and moisture exchanger) and to the mechanical ventilator.

8. Place the animal on its right side on the surgical table.

9. To achieve pO2 levels of 100-120 mmHg, ventilate the animal with a mixture of oxygen and nitrogen (1:2 v/v), using the following ventilator settings: Pressure control mode: positive end-expiratory pressure (PEEP) 4 cmH2O; peak inspiratory pressure 16 - 18 cmH2O; breathing frequency depending on the size of the animal (for a 20 kg animal, decrease frequency with increasing body weight) this should result in a tidal volume of ~10 ml/kg, monitor ventilation with capnography.

10. Monitor temperature using a rectal thermometer and maintain temperature between 37 - 39 ºC using a heat lamp or heat mat. Moreover, monitor heart rate with electrocardiography.

3. Anesthesia

1. Induce and maintain anesthesia preferably by adding 2.0% of isoflurane (v/v) to the ventilation gas-mixture or alternatively by intravenous administration of fentanyl (10 µg/kg/h) via the ear vein catheter.

2. Check adequate depth of anesthesia by testing pain reflexes with a hind leg toe pinch before starting surgery. When necessary, add additional anesthesia or wait for a few minutes. Check pain reflexes regularly throughout the surgery.

4. Fluids and Antibiotics

1. Administer the first dose of amoxicillin (25 mg/kg) intravenously via the ear vein catheter. 2. Connect a transfusion system to the ear vein catheter to enable slow infusion of glucose 10% (500 ml) during surgery.

5. Sterilization of Surgical Site

1. Shave and clean the skin of the animal over an area of approximately 25 cm width from the vertebral column all the way to the left axilla.

2. Scrub the moisturized skin with povidone-iodine scrub (75 mg/ml) for approximately 5 min.

3. Remove the povidone-iodine soap from the skin with wet sterile gauzes, before sterilizing the skin with povidone-iodine lotion (100 mg/ ml).

4. Cover the animal with sterile surgical drapes to reduce bacterial transfer and subsequent contamination of the surgical site.

3. Surgery

1. Opening the Thorax (Thoracotomy)

1. Make an incision in the skin, starting 1 cm caudal to the left inferior angle of the scapula down to the left axilla (Figure 1). Use diathermy to cauterize blood vessels in the skin to prevent excessive bleeding.

2. Cut through the serratus muscle and pectoralis major muscle, using the cutting modality of the diathermy. Also use diathermy to cauterize blood vessels in the muscle layer to prevent excessive bleeding.

3. Use blunt dissection to carefully divide the intercostal muscle of the fourth left intercostal space with a mosquito clamp. Now the costal surface of the left lung covered with visceral and parietal pleura should be exposed.

4. To enter the pleural cavity, carefully pierce both layers of the pleura and tear them open.

5. Use a thoracic retractor to separate the edges of the wound and the ribs and to forcefully drive tissues apart to obtain good exposure of the pleural cavity.

6. Push away the left lung in the caudal direction and keep it in place with a wet gauze. Now the heart and great vessels should be clearly exposed.

2. Placement of Catheters and Flow Probes (Figure 1)

1. Use blunt dissection to remove ~2 cm2 of the surrounding connective tissue of the descending thoracic aorta.

2. Perform a purse-string suture, consisting of three stitches, in the aortic wall with a non-absorbable USP3-0 braided silk suture (Ø0.2 mm).

3. Penetrate the aortic vessel wall with a stainless steel 16 G needle in the middle of the purse-string suture.

4. Insert the tip of the fluid-filled catheter (until the ring) into the aorta, pull the purse-string suture firmly together and tie the two strings of the suture.

5. To keep the catheter in place, wind the suture 3 times around the catheter above the ring and again tie the two strings of the suture. Further secure the catheter with a new stitch approximately 1 cm cranial from the insertion place.

6. Connect the fluid-filled catheter to the calibrated pressure transducer, which is connected to the computer, to monitor the mean arterial pressure during the surgery. Obtain an arterial blood gas to verify or adjust for correct ventilation settings.

7. Open the pericardium with a crossed cut. Be aware to keep the phrenic nerve that runs over the pericardium intact.

8. Identify the pulmonary artery and pull it slightly in the caudal direction with a Farabeuf retractor. Now the ascending aorta and aortic arch should

be exposed. Monitor mean arterial pressure while retracting the pulmonary artery.

9. Make a small cut (~1 cm) in the connective tissue between the ascending aorta and the pulmonary artery using Metzenbaum scissors, to be able to dissect either the ascending aorta or the pulmonary artery with a large curved mosquito clamp to place the flow probe.

10. Place the rubber band of the flow probe around the vessel. To make this easier, place a suture through one end of the rubber band, place this suture around the vessel and pull it until the rubber band surrounds the vessel.

11. Fix the flow probe measurement device on the rubber band. Connect the flow probe to the computer and check the cardiac output signal on the computer to confirm a correct placement of the flow probe.

12. Place fluid-filled catheters in the pulmonary artery, right ventricle, left ventricle and left atrium at the same manner as described for the aortic fluid-filled catheter (3.2.2 - 3.2.5). Note that it is not necessary to remove connective tissue before performing a purse-string suture in these structures.

13. Expose and dissect the proximal part of the left anterior descending coronary artery by first lifting the tissue with a forceps and making a small (2 - 3 mm) cut with Metzenbaum scissors, followed by carefully teasing the tissue away from the artery with a cotton swab. Ensure complete dissection of the coronary artery by passing a small straight angled mosquito clamp underneath.

14. Make a stitch parallel to the anterior interventricular coronary vein with a suture, which is connected to the coronary venous catheter.

15. Puncture the coronary vein with the 20 G needle of the coronary venous catheter and insert the cannula of the catheter intravenously.

16. Remove the needle and secure the catheter with the already performed stitch (3.2.14). Further secure the catheter with a new stitch approximately 1cm from the place of initial puncture.

17. Place the coronary flow probe around the previously dissected left anterior descending coronary artery. When the artery is constricted and is hardly visible, use lidocaine 10% spray to relax the vessel to get a better exposure of the vessel. Check the signal of the coronary flow on the computer to confirm a correct placement of the flow probe (Figure 2).

3. Tunneling

1. Tunnel the flow probes individually through the third left intercostal space beneath the muscle and above the rib by using a large curved mosquito clamp.

2. Tunnel the fluid-filled catheters through either the third or the fifth left intercostal space by piercing the intercostal muscle. Clamp off the fluid-filled catheters and remove the three-way stopcock to minimize the piercing area and prevent leakage of the fluid-filled catheters during the tunneling.

3. Fix the flow probes and the fluid-filled catheters with non-absorbable USP2-0 braided silk (Ø0.3 mm) by means of a purse string suture on the

intercostal muscle. This suture also serves to prevent air leakage after re-instating negative intrathoracic pressure.

4. Make three incisions in the skin approximately 2 cm sinister and parallel to the vertebral column, approximately 3 cm in length 3 cm apart of each other.

5. Pierce a trochar beneath the left latissimus dorsi muscle from rostral incision site to the incisions on the back. Tunnel the flow probes and fluid catheters to the back within this trochar.

6. Place the stopcocks on the fluid-filled catheters and remove the clamp. Withdraw blood to remove clots and air bubbles and fill the fluid-filled catheters with 1,000 IU/ml heparin. Coronary venous catheters should be filled with 5,000 IU/ml heparin.

4. Closing the Thorax

1. Make an incision with a length of approximately 1.5 cm, 8 cm caudal and parallel to the first incision.

2. Lead the drain from the pleural cavity through the sixth intercostal muscles subcutaneously to this incision with a large curved mosquito clamp. Connect the drain to the suction device to remove any remaining fluid and reinstate negative pressure in the pleural cavity during the closing of the thorax.

3. Relieve and inflate the lung with an end-inspiratory hold. Ensure adequate filling of the lung by visual monitoring.

4. Close the thorax by pulling the ribs of the fourth intercostal space together at two separate sites with non-absorbable USP6 braided polyester (Ø0.8 mm).

5. Close the serratus muscle and pectoralis major muscle with a running stitch and the skin with a running subcuticular suture using nonabsorbable USP2-0 braided silk (Ø0.3 mm)

6. Suture the incisions on the dorsal side with non-absorbable USP2-0 braided polyester (Ø0.3 mm) between the catheters. First tie a knot directly onto the skin to close the incision, then fixate the catheters to the suture with a knot 1 cm from the skin. For the flow probes, use an absorbable USP2-0 braided polyglactin (Ø0.3 mm) suture to prevent cutting of the suture in the flow probe wire (Figure 1).

7. Carefully remove the drain while applying pressure on the cranial side of the incision to maintain negative pressure in the pleural cavity. Close the incision with a purse string suture using non-absorbable USP2-0 braided polyester (Ø0.3 mm) and seal the wound with petroleum jelly.

5. Termination of anesthesia and recovery from surgery

1. Stop anesthesia when all incision sites are closed.

2. Provide analgesia by administering buprenorphine (0.015 mg/kg) i.m. in the gracilis muscle.

3. Stop the ventilation when the animal is breathing independently and disconnect the tracheal tube from the ventilator. Check regularly if the animal is breathing sufficiently.

4. Place gauze pads between exteriorization sites of the catheters to absorb wound fluid.

5. To protect the external segments of the catheters, give the animal an elastic vest and package the catheters between two pieces of artificial sheepskin.

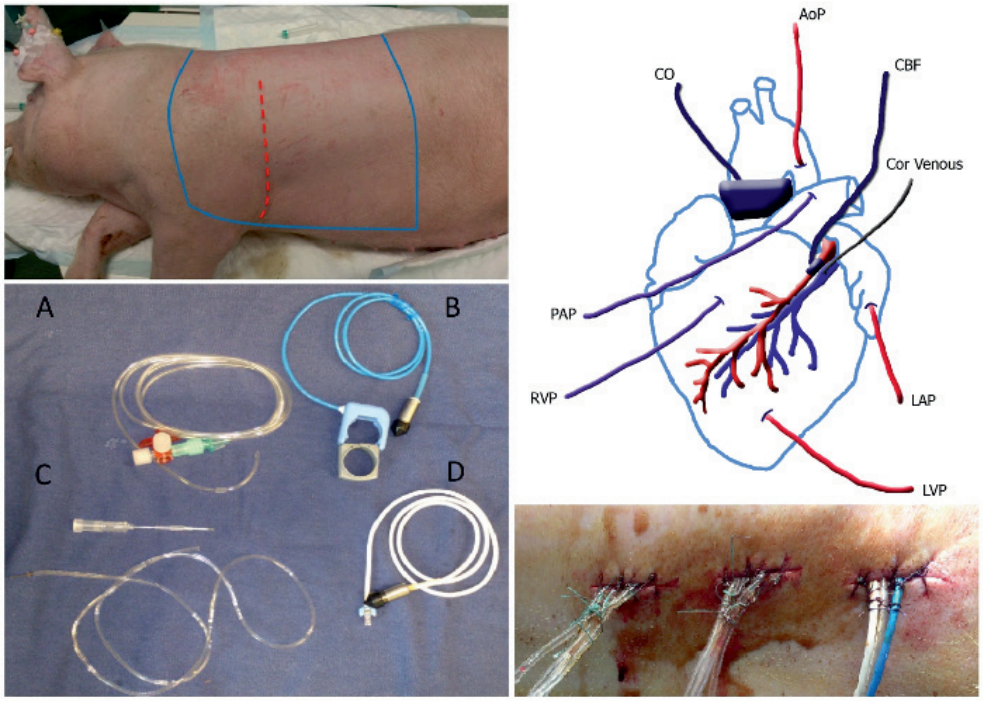

Figure 1. Overview of the Surgery.

Top left panel: The sterile area of the animal, which should be shaved and sterilized lies between the bleu lines. The incision site is depicted as the red dotted line. Bottom left panel: Picture of catheters and flow probes: fluid-filled catheter (A), aorta/ pulmonary flow probe including rubber band (B), coronary venous catheter including 20 G needle (C) and the coronary flow probe (D). Top right panel: Schematic overview of placement of the catheters and flow probes. MAP, mean arterial pressure; Cor venous, coronary venous catheter; LAP, left atrial pressure; LVP left ventricular pressure; RVP, right ventricular pressure; PAP, pulmonary artery pressure; CO, cardiac output; CBF, coronary blood flow. Bottom right panel: Tunneled catheters exiting the back secured with a stitch and a knot at approximately 1 cm distance along the suture.

6. Deflate the balloon of the tracheal tube and extubate when the animal regains its swallowing reflex.

7. Provide long-term analgesia by means of a Fentanyl slow-release patch (12 µg/hr for a 20 kg pig; adjust strength according to bodyweight). Place the patch on a thin part of the skin (such as the lower abdomen) to ensure adequate delivery of analgesia.

8. House the animal separately for the entire post-operative period. Provide a heating lamp for the first week after surgery to keep the animal warm.

9. Supply enough fluid i.v. if the animal is not drinking independently.

10. Flush the fluid-filled catheters daily, by first withdrawing blood to remove clots, then refilling with saline and finally with heparinized saline (1,000 - 5,000 IU/ml) to prevent blood clot formation. Take care not to infuse any air bubbles while flushing the catheters.

11. Administer amoxicillin (25 mg/kg) i.v. daily for 6 days after surgery to prevent post-surgical infections.

4. Treadmill Experiment (Figure 2)

1. Flush the fluid-filled catheters as described (3.5.10) and attach the flushed catheters to the pressure transducers. Measure the rectal temperature to be able to obtain temperature corrected blood gas values.

2. Flush the pressure transducers with saline to prevent damping of the signals due to air bubbles. Attach the pressure transducers to the elastic vest on the dorsal side.

3. Connect the pressure transducers and flow probes to the amplifier. Start measuring in the computer program and calibrate the pressure transducers and flow probes with 0 mmHg being open to the air (and closed to animal) and 100 mmHg using a manometer.

4. Switch the three-way stopcock in a way that the fluid catheters have an open connection with the pressure transducers. Note that the blood pressures can now be obtained. Check signals for shape and amplitude (Figure 2).

5. If required, connect an extension line to either of the fluid catheters for sampling of mixed venous and arterial blood.

6. Measure hemodynamics when the animal is lying as well as standing quietly on the treadmill. Average blood pressures are measured over a timeframe of 10 sec.

7. Obtain arterial and mixed venous blood samples by first withdrawing 5 ml of blood using a 10 ml syringe so that 1 ml of pure blood can be obtained using a heparinized 1 ml syringe. For the coronary venous blood samples, a 2 ml syringe is used instead of the 10 ml syringe and withdrawal of 1 ml is sufficient to obtain pure blood.

8. Keep the sealed 1 ml syringes on ice before processing the blood samples with a blood gas analyzer to determine the metabolic and ventilatory condition of the animal.

9. Subject the swine to a five-stage exercise protocol on the treadmill, 3 min per speed, 1 - 5 km/hr (~85% of maximal heart rate). Obtain

hemodynamics and blood gases after 1.5 - 2 min per speed on each speed as in the resting position.

Figure 2. Treadmill Experiment.

Left panels: Instrumented swine on the treadmill. Fluid-filled catheters are connected to the pressure transducers, placed on the back of the swine. Top right panel: Overview of the total experimental set-up, including treadmill, amplifier and recording computer. Bottom right panel: Typical example of recorded hemodynamic data. From top to bottom; aortic pressure (AoP, blue) and left ventricular pressure (LVP, red); left atrial pressure (LAP,blue) and left ventricular pressure (red); pulmonary artery pressure (PAP, blue) and right ventricular pressure (RVP, red); aortic flow/cardiac output (AoF, blue); coronary blood flow (CBF, red).

10. After the exercise protocol close the stopcocks and check if drift has occurred in the 0 mmHg calibration, make a note of this calibration. Remove the pressure transducers of the fluid-filled catheters and disconnect the flow probes.

11. Flush the fluid-filled catheters with saline and heparin (1,000 - 5,000 IU/ml). Protect the catheters and flow probes by putting them beneath the elastic vest between two pieces of artificial sheepskin. The animal can now be returned to its cage.

Representative results

Exercise up to 5 km/hr resulted in a doubling of cardiac output from 4.3 ± 0.3 to 8.5 ± 0.7 L/min which was principally accomplished by an increase in heart rate from 137 ± 7 to 256 ± 8 beats per min in combination with a small increase in stroke volume from 32 ± 2 to 36 ± 3 ml (Figure 3). The increase in stroke volume was facilitated by an increase in left ventricular contractility, as evidenced by an increase in the maximum of the first derivative of left ventricular pressure dP/dtmax together with an increased rate of relaxation of the left ventricle and an increase in left atrial pressure, being the filling pressure of the left ventricle (Figure 3). The increase in cardiac output together with an increase in hemoglobin concentration (from 8.5 ± 0.4 to 9.2 ± 0.4 g/dl) and an increase in body oxygen extraction from 45 ± 1 to 71 ± 1% allowed a tripling of body oxygen consumption (Figure 3). Systemic vasodilation occurred as evidenced by an increase in systemic vascular conductance and a decrease in systemic vascular resistance, which accommodated the increase in cardiac output almost completely, so that mean aortic pressure increased only slightly (Figure 3). Exercise also resulted in modest vasodilation in the pulmonary circulation, as evidenced by a 33 ± 8% increase in pulmonary vascular conductance. However, the 101 ± 8% increase in cardiac output, together with the increase in left atrial pressure (from 3 ± 1 to 10 ± 1 mmHg), resulted in an increase in pulmonary artery pressure and thereby in an increase in right ventricular afterload (Figure 3). The increase in heart rate, together with the slight increase in arterial pressure resulted in an increase in left

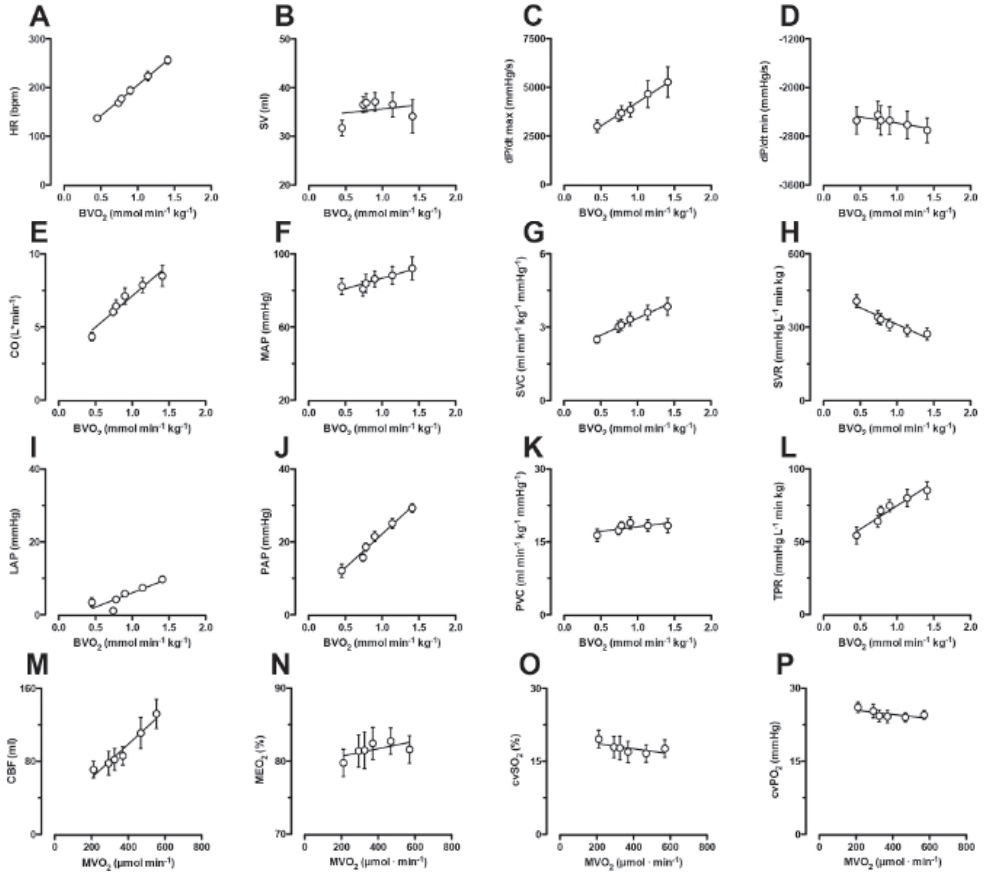

Figure 3. Typical Hemodynamic Response to Exercise.

Body oxygen consumption (BVO2) was used as an index for exercise intensity (x-axes of panel A-L). Shown are the responses of heart rate (HR, panel A), stroke volume (SV, panel B), maximum and minimum of the first derivative of left ventricular pressure (dP/dtmax, panel C and dP/dtmin, panel D resp) as indices of contractility and rate of relaxation, cardiac output (CO, panel E), mean arterial pressure (MAP, panel F), systemic vascular conductance (SVC, panel G), systemic vascular resistance (SVR, panel H), Pulmonary artery pressure (PAP, panel J), left atrial pressure (LAP, panel I), pulmonary vascular conductance (PVC, panel K). Total pulmonary resistance (TPR index for right ventricular afterload increased during exercise, Panel L). The increase in heart rate, together with the slight increase in arterial pressure resulted in an increase in left ventricular myocardial oxygen consumption (x-axes of panels M-P), which was principally met by an increase in coronary blood flow (CBF, panel M), as myocardial oxygen extraction (MEO2, panel N), coronary venous oxygen saturation (CVSO2, panel O) and coronary venous oxygen tension (cvPO2, panel P) were minimally affected. All data are presented as mean with standard error of the mean (SEM).

ventricular myocardial oxygen consumption, which was principally met by an increase in coronary blood flow which, in combination with the increase in hemoglobin concentration resulted in an increase in myocardial oxygen delivery (from 310 ± 37 to 738 ± 68 µmol/min). The increase in myocardial oxygen demand was commensurate with the increase in myocardial oxygen supply, as myocardial oxygen extraction (79.8 ± 1.9% at rest 81.6 ± 1.9% during maximal exercise) was essentially maintained constant, resulting in an unchanged coronary venous oxygen saturation and coronary venous oxygen tension (Figure 3).

Discussion

The present study describes the surgery for chronical instrumentation of swine as well as the protocol for exercising the instrumented swine on a motor-driven treadmill while measuring hemodynamics and taking blood samples for measurement of oxygen content in arterial, mixed venous and coronary venous blood.

Critical Steps within the Protocol

There are several critical steps within the protocol that start already during the intubation procedure. Thiopental (2.1.5) is a respiratory depressive agent, therefore requiring swift intubation upon administration. Also, it is important to carefully monitor ventilator settings during the procedure. Thus, when the thoracic cavity is opened (step 3.1.4), this results in a loss of the negative intrathoracic pressure. To compensate for this loss and to prevent alveolar collapse, ventilation requires positive end expiratory pressure (PEEP). Moreover, ventilator settings (peak inspiratory pressure) should be adjusted to maintain a tidal volume of ~10 ml/kg. Also note that when the left lung is pushed away

(3.1.6.) tidal volume is likely to be decreased because only part of the left lung is ventilated. Ventilator settings should be adjusted based on blood gasses.

Another important note with respect to hemodynamic measurements with fluid filled catheters is that there is a hydrostatic pressure difference between the pressure transducer and the insertion site of the fluid-filled catheter into the cardiovascular system. The height difference between the level of the pressure transducer pressure on the elastic vest (4.2), and the insertion point of the catheter should be estimated during surgery and at sacrifice of the animal and corrected for by interpolation either pre- or post- processing of the data.

Another important point to consider when using this technique is that blood loss, either during surgery or during repeated blood sampling should be minimized, despite the fact that swine are relatively large and consequently have a large blood volume (65 ml/kg). During surgery, blood loss during insertion of the catheters can be minimized by simply applying compression on the puncture wounds. According to animal experimentation guidelines, up to 10% of the circulating blood volume can be taken on a single occasion from normal, healthy animals with minimal adverse effects, but it will take an animal about 14 days to replenish this amount of blood (6). This means that the recovery from surgery is prolonged when a significant amount of blood is lost.

During the repeated blood sampling during the exercise experiments, a maximum of 1.0% of an animal's circulating blood volume, or 0.6 ml/ kg can be removed every 24 hr 15. This also means that the amount of blood that is sampled during treadmill exercise, should be well-planned and that, after removal of the initial clots that are invariably present in the lumen of the catheter near the tip at the interface with the blood, the remaining blood withdrawn to flush the lines should be given back to the animals.

Modifications and Troubleshooting

Implanted fluid-filled catheters should be flushed daily to prevent malfunctioning because of blood clot formation. Depending on the amount of blood clots in the fluid filled catheters, the amount of heparin in each line can be varied from 1,000 IU/ml to 5,000 IU/ml. The amount of heparin should be kept to a minimum in the first week after surgery to prevent bleeding from surgical incision wounds due to the presence of the anticoagulant heparin.

However, even when flushed daily, some fluid-filled catheters will get clogged. When this happens, try withdrawing blood with a smaller 2 ml syringe by applying minimal and/or pulsatile suction. It can take several minutes before the catheter will be unclogged. When this does not work, carefully flush a small amount of saline into the catheter and immediately try to withdraw blood. Be aware that infusion can result in a release of thrombus into the circulation and embolism of distal organs, depending on the site of the catheter. When careful flushing does not work, connect the clogged line to a pressure-transducer to check if there is still a hemodynamic signal. If there is no signal, the fluid filled line should be sealed by several knots and cut off.

Interpretation and Limitations

When all points as mentioned above are taken into account, the combination of hemodynamic measurements and blood samples allows for interpretation of the exercise response in terms of whole body and myocardial oxygen consumption, which are better measures for exercise intensity than treadmill speed alone (5, 17, 22, 23).

In order to meet the increased metabolic requirements of the body, exercise requires changes in cardiac function as well as changes in local perfusion.

Tissue perfusion is regulated by changes in diameter of the small arteries and arterioles of the vascular bed supplying the tissue. Myriad vasoactive factors, derived from neurohumoral systems, the endothelium and local metabolites interact to determine vascular tone and ensure adequate tissue perfusion (5, 9, 12, 18). Changes in systemic and pulmonary vascular resistance or the inverse, vascular conductance, can be calculated from the blood pressure and flow signals and interpreted in terms of changes in vasomotor tone in the systemic and pulmonary vasculature. Intuitively, vascular resistance is often used to assess changes in vascular tone. However, in our research group, we advocate the use of conductance although conductance and resistance are mathematically related, with conductance being flow normalized for pressure, and resistance equaling pressure divided by flow. Although conductance and resistance are interchangeable if one investigates the effect of only a single stimulus (i.e., exercise) (3, 23), interpretation of the two parameters can differ when combining exercise with pharmacological interventions, to investigate the contributions of various vasoactive systems to regulation of vascular tone (4, 10, 18, 22, 23).

During exercise, the systemic circulation transforms from a system at rest that is characterized by a low flow and a high resistance (i.e., low conductance) into a system with high flow and low resistance, (high conductance). As such, pharmacological vasodilation has different consequences for conductance and resistance during rest versus exercise. The decrease in resistance that is produced by a pharmacological vasodilator at rest is large while the increase in conductance is only small. In contrast, during exercise the same degree of vasodilation translates into a large increase in conductance, but only a small decrease in resistance. Thus, when conductance is used, a greater vasodilation seems to occur during exercise, while when looking at resistance vasodilation appears to be larger at rest. Interpretation of the data thus differs when using resistance or

conductance. Although the choice between resistance and conductance may seem rather arbitrary, in physics the variable that undergoes the primary change is designated as the numerator of the index for a response (3, 10, 23). Since during exercise aortic blood pressure remains fairly constant whereas cardiac output increases markedly, the most appropriate parameter to describe the systemic vascular response to exercise would appear to be systemic vascular conductance (cardiac output / aortic blood pressure), rather than resistance. Moreover, the systemic circulation consists of a multitude of vascular beds from a variety of organs that are principally perfused in a parallel manner. Since parallel resistors add up reciprocally, while parallel conductors add up in a linear manner, any change in conductance of a particular regional vascular bed translates into an identical (absolute) change of the total systemic vascular conductance. This consideration lends further support to the use of vascular conductance to describe the systemic vascular responses to exercise and pharmacological interventions.

The choice for either resistance or conductance to describe the vascular responses to exercise in the pulmonary bed appears to be less obvious, because exercise produced increases in cardiac output as well as pulmonary artery pressure (3, 23). A choice for either resistance or conductance is also less critical, in view of the relatively minor exercise-induced changes in PVR and PVC as compared to the degree of vasodilation produced by, for example, ET-receptor blockade (23). As a result, the use of either resistance or conductance to characterize the vascular effects of a pharmacological vasodilator in the pulmonary circulation will yield similar conclusions.

In the coronary circulation, interpretation of the data is even more complex as systemic administration of pharmacological antagonists of

endogenous vasoactive substances results not only in alterations in coronary resistance vessel tone, but often also produce pronounced changes in systemic hemodynamic variables (3, 14, 22, 23). These altered hemodynamics influence cardiac work, and thereby cause changes in coronary blood flow resulting from changes in metabolic requirements of the heart or from autoregulation, rather than as a direct effect of the intervention on coronary vascular tone. For example, blockade of an endogenous vasoconstrictor system decreases mean aortic pressure, as a consequence of systemic vasodilation, and elicits autoregulatory adjustments in coronary microvascular tone. Moreover, baroreceptor reflex activation acts to increase heart rate and myocardial contractility. Such changes in heart rate and/or blood pressure subsequently will result in alterations in myocardial metabolism, requiring an adjustment in myocardial oxygen supply and hence in coronary blood flow.

To take into account the effects of such drug-induced alterations in myocardial oxygen consumption, investigators examine the relation between coronary venous oxygen levels and myocardial oxygen consumption (MVO2) (4, 18), as this approach allows assessment of regulation of coronary resistance vessel tone independently of changes in myocardial oxygen demand. Administration of a vasodilator will increase myocardial oxygen delivery at a given level of MVO2. As this increase in oxygen delivery occurs without a change in oxygen consumption, myocardial oxygen extraction will decrease, thereby leading to increases in coronary venous oxygen content and hence in an upward shift of the relation between MVO2 and coronary venous oxygen levels. It is therefore imperative to measure both myocardial oxygen demand as well as myocardial oxygen supply in order to correctly study the regulation coronary resistance vessel tone (4, 18).

Notwithstanding its elegance and usefulness, some investigators have pointed out the limitations of this approach (8). Thus, plotting MVO2 versus coronary venous PO2 or coronary venous SO2 could be considered to be inappropriate because these variables are actually part of the equation to compute MVO2. Consequently, MVO2 is not a variable that is independent of coronary venous PO2 or SO2. Alternatively, investigators should consider using another index of myocardial work, the rate-pressure product (RPP), which is the product of heart rate and left ventricular systolic pressure. However, as RPP and MVO2 are almost linearly related, substituting RPP for MVO2 yields virtually identical results (22), and the relation between MVO2 and coronary venous oxygen levels is considered a sensitive way of studying alterations in coronary vasomotor tone.

Significance with Respect to Existing Methods

Another method commonly used to assess changes in regulation of vascular tone is the use of isolated coronary and pulmonary small arteries or arterioles in a pressure or wire myograph (13, 19, 22). The advantage of myograph studies is that vessels can be studied independent of surrounding tissue and without potentially confounding effect from circulating factors. These in vitro techniques are therefore complementary to the in vivo measurements. However, in vivo and in vitro techniques sometimes give opposing results. For example, the response to the potent vasoconstrictor endothelin was reduced in the intact coronary circulation after myocardial infarction, but was augmented in isolated coronary small arteries from swine with myocardial infarction as compared to healthy control swine (13). This difference between the in vivo and in vitro data was due to an increased suppression of the vasoconstrictor influence of endothelin by prostanoids in vivo (13).

Future Applications

Given the proposed role of changes in coronary microvascular function in both left and right ventricular dysfunction, assessment of these changes in relevant models of cardiovascular disease is required. The use of chronically instrumented animals allows correlations of the severity of the disease with microvascular (dys)function. Moreover, both coronary and pulmonary microvascular function may appear normal under basal resting conditions, while microvascular dysfunction may be revealed under cardiovascular stress, such as during exercise.

Several swine models of cardiopulmonary disease, such as diabetes (19), myocardial infarction (7), pulmonary hypertension (11, 15) and pacing induced heart failure (16) are available and could be combined with chronic instrumentation. A potential drawback is that, when commercially available swine breeds such as Yorkshire, Landrace, Large White etc, are used, adult swine are very large and may therefore be difficult to handle. Therefore, juvenile swine are often used. However, as juvenile swine grow rapidly, positioning and function of flow probes and pressure catheters and patency of fluid-filled catheters may become compromised, limiting the duration of serial measurements within individual animals to approximately 10 weeks. An alternative is the use of adult miniature swine, such as Yucatan or Gottingen swine, of which the adult weight is 40 - 60 kg (1).

In conclusion, the use of chronically instrumented animals allows serial assessment of cardiopulmonary function either during development of disease or evaluation of treatment, thereby increasing statistical power and limiting the number of animals required for a study.

References

1. **Bender SB, van Houwelingen MJ, Merkus D, Duncker DJ, and Laughlin MH**. Quantitative analysis of exercise-induced enhancement of early- and late-systolic retrograde coronary blood flow. *Journal of applied physiology* 108: 507-514, 2010.

2. **Datta D, Normandin E, and ZuWallack R**. Cardiopulmonary exercise testing in the assessment of exertional dyspnea. *Annals of thoracic medicine* 10: 77-86, 2015.

3. **de Beer VJ, de Graaff HJ, Hoekstra M, Duncker DJ, and Merkus D**. Integrated control of pulmonary vascular tone by endothelin and angiotensin II in exercising swine depends on gender. *American journal of physiology Heart and circulatory physiology* 298: H1976-1985, 2010.

4. **Duncker DJ, and Bache RJ**. Regulation of coronary blood flow during exercise. *Physiological reviews* 88: 1009-1086, 2008.

5. **Duncker DJ, Stubenitsky R, and Verdouw PD**. Autonomic control of vasomotion in the porcine coronary circulation during treadmill exercise: evidence for feed-forward beta-adrenergic control. *Circulation research* 82: 1312-1322, 1998.

6. **Gross DR**. *Animal Models in Cardiovascular Research*. Springer, 2009.

7. **Haitsma DB, Bac D, Raja N, Boomsma F, Verdouw PD, and Duncker DJ**. Minimal impairment of myocardial blood flow responses to exercise in the remodeled left ventricle early after myocardial infarction, despite significant hemodynamic and neurohumoral alterations. *Cardiovascular research* 52: 417-428, 2001.

8. **Heusch G**. The paradox of alpha-adrenergic coronary vasoconstriction revisited. *J Mol Cell Cardiol* 51: 16-23, 2011.

9. **Laughlin MH, Davis MJ, Secher NH, van Lieshout JJ, Arce-Esquivel AA, Simmons GH, Bender SB, Padilla J, Bache RJ, Merkus D, and Duncker DJ**. Peripheral circulation. *Comprehensive Physiology* 2: 321-447, 2012.

10. **Lautt WW**. Resistance or conductance for expression of arterial vascular tone. *Microvascular research* 37: 230-236, 1989.

11. **Mercier O, Sage E, Izziki M, Humbert M, Dartevelle P, Eddahibi S, and Fadel E**. Endothelin A receptor blockade improves regression of flow-induced pulmonary vasculopathy in piglets. *The Journal of thoracic and cardiovascular surgery* 140: 677-683, 2010.

12. **Merkus D, and Duncker DJ**. Perspectives: Coronary microvascular dysfunction in post-infarct remodelled myocardium. *European Heart Journal Supplements* 16: A74-A79, 2014.

13. **Merkus D, Houweling B, van den Meiracker AH, Boomsma F, and Duncker DJ**. Contribution of endothelin to coronary vasomotor tone is abolished after myocardial infarction. *American journal of physiology Heart and circulatory physiology* 288: H871-880, 2005.

14. **Merkus D, Visser M, Houweling B, Zhou Z, Nelson J, and Duncker DJ**. Phosphodiesterase 5 inhibition-induced coronary vasodilation is reduced after myocardial infarction. *American journal of physiology Heart and circulatory physiology* 304: H1370-1381, 2013.

15. **Pereda D, Garcia-Alvarez A, Sanchez-Quintana D, Nuno M, Fernandez-Friera L, Fernandez-Jimenez R, Garcia-Ruiz JM, Sandoval E, Aguero J, Castella M, Hajjar RJ, Fuster V, and Ibanez B**. Swine model of chronic postcapillary pulmonary hypertension with right ventricular remodeling: long-term characterization by cardiac catheterization, magnetic resonance, and pathology. *Journal of cardiovascular translational research* 7: 494-506, 2014.

16. **Spinale FG, Hendrick DA, Crawford FA, Smith AC, Hamada Y, and Carabello BA**. Chronic supraventricular tachycardia causes ventricular dysfunction and subendocardial injury in swine. *The American journal of physiology* 259: H218-229, 1990.

17. **Stubenitsky R, Verdouw PD, and Duncker DJ**. Autonomic control of cardiovascular performance and whole body O2 delivery and utilization in swine during treadmill exercise. *Cardiovascular research* 39: 459-474, 1998.

18. **Tune JD, Gorman MW, and Feigl EO**. Matching coronary blood flow to myocardial oxygen consumption. *Journal of applied physiology* 97: 404-415, 2004.

19. **van den Heuvel M, Sorop O, Koopmans SJ, Dekker R, de Vries R, van Beusekom HM, Eringa EC, Duncker DJ, Danser AH, and van der Giessen WJ**. Coronary microvascular dysfunction in a porcine model of early atherosclerosis and diabetes. *American journal of physiology Heart and circulatory physiology* 302: H85-94, 2012.

20. **Vatner SF, and Braunwald E**. Cardiovascular control mechanisms in the conscious state. *The New England journal of medicine* 293: 970-976, 1975.

21. **Yarbrough WM, and Spinale FG**. Large animal models of congestive heart failure: a critical step in translating basic observations into clinical applications.

Journal of nuclear cardiology : official publication of the American Society of Nuclear Cardiology 10: 77-86, 2003.

22. **Zhou Z, de Beer VJ, Bender SB, Jan Danser AH, Merkus D, Laughlin MH, and Duncker DJ**. Phosphodiesterase-5 activity exerts a coronary vasoconstrictor influence in awake swine that is mediated in part via an increase in endothelin production. *American journal of physiology Heart and circulatory physiology* 306: H918-927, 2014.

23. **Zhou Z, de Beer VJ, de Wijs-Meijler D, Bender SB, Hoekstra M, Laughlin MH, Duncker DJ, and Merkus D**. Pulmonary vasoconstrictor influence of endothelin in exercising swine depends critically on phosphodiesterase 5 activity. *American journal of physiology Lung cellular and molecular physiology* 306: L442-452, 2014.

Chapter 3

Exercise Facilitates Early Recognition of Cardiac and Vascular Remodeling in Chronic Thrombo-Embolic Pulmonary Hypertension in Swine

Kelly Stam, Richard W.B. van Duin, André Uitterdijk, Zongye Cai, Dirk J. Duncker, Daphne Merkus

Am J Physiol Heart Circ Physiol 2018 Mar 1; 314(3): H627-H642

Abstract

Chronic thrombo-embolic pulmonary hypertension (CTEPH) develops in 4% of patients after pulmonary embolism and is accompanied by an impaired exercise tolerance, which is ascribed to the increased right ventricular (RV) afterload and a ventilation/perfusion (V/Q) mismatch in the lungs. This study investigated changes in arterial PO_2 and hemodynamics in response to graded treadmill exercise during development and progression of CTEPH in a swine model.

Swine were chronically instrumented and received multiple pulmonary embolisms by *(i)* microsphere infusion (Spheres) over five weeks, *(ii)* endothelial dysfunction by administration of eNOS inhibitor L-N^{ω}-Nitroarginine methyl ester (LNAME) during seven weeks, *(iii)* combined pulmonary embolisms and endothelial dysfunction (LNAME+Spheres), or *(iv)* served as sham-operated controls (Sham).

After nine weeks follow-up, embolization combined with endothelial dysfunction resulted in CTEPH as evidenced by a mean pulmonary artery pressure of 39.5±5.1mmHg versus 19.1±1.5mmHg (Spheres, $p<0.001$), 22.7±2.0mmHg (LNAME, $p<0.001$) and 20.1±1.5mmHg (Sham, $p<0.001$), and a decrease in arterial PO_2 that was exacerbated during exercise, indicating a V/Q-mismatch. RV dysfunction was present after five weeks of embolization, both at rest (trend towards increased RV end systolic lumen area, $p=0.085$ and decreased SVi $p=0.042$) and during exercise (decreased SVi vs Control $p=0.040$). With sustained PH, RV hypertrophy (Fulton index $p=0.022$) improved RV function at rest and during exercise, but this improvement was insufficient in the CTEPH swine to result in an exercise-induced increase in cardiac index.

In conclusion, embolization in combination with endothelial dysfunction results in CTEPH in swine. Exercise increased RV afterload, exacerbated the V/Q mismatch and unmasked RV dysfunction.

Introduction

Pulmonary hypertension (PH) is a chronic pathophysiological disorder of the pulmonary vasculature and is defined as a chronic pulmonary artery pressure (PAP) ≥ 25mmHg at rest for a consecutive period of at least 6 weeks, although pulmonary artery pressures ≥ 19mmHg at rest are associated with increased mortality at long term (27). Treatment modalities for PH are very limited and, even when treated, the disease often progresses to right heart failure and death. The World Health Organization differentiates 5 groups of PH based on their etiology. Chronic thromboembolic PH (CTEPH), categorized as group 4, develops in about 4% of patients after acute pulmonary embolism and up to 10% of patients with recurrent pulmonary embolism (9, 59) and is defined as persistent PAP above 25mmHg for over 6 months (11). The obstructions in the pulmonary arteries increase pulmonary vascular resistance (PVR) and result in ventilation-perfusion (V/Q) mismatch in the lungs. The main treatment options for CTEPH are interventions to remove proximal obstructions in eligible patients such as pulmonary endarterectomy or balloon angioplasty (57, 58, 65). Moreover, it is increasingly being recognized that distal pulmonary vasculopathy, which is left untreated when only removing the proximal obstruction(s) contributes significantly to the increase in pulmonary vascular resistance (32, 40, 53, 62). It is currently unknown when these distal vascular lesions develop, and whether endothelial dysfunction promotes such development.

Dating back to 1984, many investigators have attempted to establish a solid large animal model to study the pathophysiology of CTEPH using different embolization frequencies and embolization materials including air, autologous blood cloths, sephadex beads and glue (Table 1). Although PAP increases acutely upon embolization in these models, most studies were unsuccessful in

establishing a sustained level of elevated PAP during prolonged follow-up (10, 12, 15, 27, 34, 54, 57, 64, 65). Those studies that did report CTEPH during prolonged follow-up (11, 28, 57, 64) have in common that they used repeated (between 4 and 40 times) embolization procedures, thereby obstructing a significant fraction of the pulmonary vasculature. In these studies, PAP also decreased in between embolization procedures, but gradual increase in PAP occurred over time. However, most studies did not determine whether this gradual increase in PAP was solely due to the progressive embolization of pulmonary vessels or that distal pulmonary microvasculopathy also developed. Recent findings by Boulate et al. suggest that distal vasculopathy was present in their model of left pulmonary artery ligation in combination with glue-embolizations (65). However, in the latter study, as in most of the aforementioned studies, hemodynamic measurements were performed under anesthesia, which may have influenced cardiac function and pulmonary hemodynamics (10, 28, 65). Moreover, and in most cases due to the use of anesthetic agents, pulmonary hemodynamics were not assessed during exercise.

The increased PVR imposes an increased afterload on the right ventricle (RV). As contractile reserve of the RV is limited (10), PH results in subacute RV dilation and dysfunction (65). With sustained PH, the right ventricle undergoes structural remodeling and hypertrophy (65). Although RV remodeling is initially beneficial and helps the RV to cope with the increased afterload, it poses a risk factor for the later development of RV failure. Evaluation of RV function during stress has been shown to be of prognostic value in patients (10, 36, 64). RV dysfunction is exacerbated during exercise, when cardiac demand increases and the RV is required to pump more blood against an increased afterload. Therefore, RV functional measurements during stress enable the evaluation of the capacity of the RV to cope with an increased afterload and facilitate early detection of RV

dysfunction (65). In addition to RV dysfunction, V/Q mismatch is thought to contribute to the exercise intolerance observed in patients with CTEPH (11, 57). To date, however studies describing animal models of CTEPH have not evaluated the occurrence of V/Q mismatch at rest and during exercise.

In light of these considerations, we developed and characterized a clinically relevant swine model of PH type 4, using a double hit (endothelial dysfunction in conjunction with repeated embolizations) approach, in which we applied treadmill exercise as a physiological stressor to evaluate the function of the right ventricle in the development and progression of CTEPH.

Table 1. Comparison between large animal studies utilizing embolization techniques to create chronic thromboembolic pulmonary hypertension models.

1st author Year of publication	Species	Gender	Embolic material	Emboli zations (N)	N	Anesthesia during RHC	Recovery period	PAP (mmHg)	PVR (WU)	RVW/ LVW +SW	RV function assessment
Shelub 1984(53)	Canine	Female	Sephadex G50	Variable (16-30 weeks)	5	None	>7 days	29 (4)	8.3 (2.3)	0.54[e]	None
Perckett 1988(42)	Sheep	NR	Air (continuous)	12 days	5	None	1.5 hour	23 (2)[f]	5.2[f]	0.38 (0.06)	None
Moser 1991(39)	Canine	NR	3-4 venous thrombi	2	10	Halothane	32 days	20.3 (2)	4.2[a]	NR	None
Weimann. 1999(63)	Swine	Male	Sephadex G50 (15mg/kg)	3	8	Ketamine	7 days	18 (3)	4.3[a,b]	NR	None
Kim 2000(31)	Canine	NR	Ceramic beads (3 mm)	4	5	Halothane	6 months	17 (2)	4.3[a]	NR	None
Zhou 2011(66)	Sheep	Female	Air (continuous)	8 weeks	4	None	7 days	34 (2.6)	4.5 (0.9)	0.36 (0.01)	None
Sage 2012(51)	Swine	NR	Right PA ligation	1	10	Pentobarbital	5 weeks	16.2 (1.3)	10.05[c] (0.69)	NR	None
Pohlmann 2012(43)	Sheep	NR	Sephadex G50 (~21.1±0.5g)	60	9	none	1 day	35 (3)	1.7 (0.2)	0.42 (0.01)	None
Garcia-Alvarez 2013(18)	Swine	Male	Sephadex G50	4 (3-6)	9	Midazolam	2 months	27 (3)	2.2[d] (1.1)	NR	CMR
Mercier 2013(37)	Swine	NR	Histoacryl + Left PA ligation	5	5	NR	7 days	28.5 (1.7)	9.8[a]	NR	Echo, CT
Guihaire 2014(20)	Swine	NR	Histoacryl + Left PA ligation	5	5	Isoflurane	6 weeks	41 (4)	10.0[a,c]	NR	Echo, PV loop

Guihaire 2015(21)	Swine	NR	Histoacryl + Left PA ligation	5	13	Isoflurane	7 days	34 (9)	12.4[a,c]	NR	Echo, Dobutamine, PV-loop
Boulate 2015(5)	Swine	Male	Histoacryl + Left PA ligation	5	5	NR	7 weeks	27 (1.1)	7.9 (0.6)	NR	None
Aguero 2015(1)	Swine	Female	Sephadex G50 (20 mg/kg)	6	6	Propofol	14 days	16 (2)	1.5[b]	0.41 (0.02)	Echo
Aguero 2015(1)	Swine	Female	Sephadex G50 (20 mg/kg) + coiling	4	6	Propofol	1 month	23 (4)	1.6[b]	0.47 (0.06)	Echo
Tang 2015(58)	Canine	NR	Autologous thrombi (0.3*1cm)	NR	13	Propofol	14 days	25.2 (3.6)	NR	NR	Dual-energy CT
Rothman 2017(50)	Swine	Female	Ceramic beads (0.6-0.9mm)	21-40	3	Isoflurane	NR	36.6 (0.9)[g]	NR	NR	None
Rothman 2017(50)	Canine	Female	Ceramic beads (0.6-0.9mm)	9-12	3	Isoflurane	20 months[h]	47[g]	7.8	NR	None
Stam 2017 (Current study)	Swine	Male + Female	Polyethylene spheres (600-710µm, ~9000 per embolization)	4 (2-5)	6	None	4-5 weeks	39.5 (5.1)	7.8 (3.4)	0.51 (0.03)	Echo, CPET

a) Calculated from dynes·sec^{-1}·cm^{-5}; b) Calculated from indexed PVRi; c) Total pulmonary vascular resistance; d) Median (interquartile range) reported; e) Only reported 2/5 cases; f) Calculated from cmH_2O or cmH_2O·L^{-1}·min; g) systolic PAP; h) only reported of one animal. CMR, cardiovascular magnetic resonance; CPET, cardiopulmonary exercise testing; CT, computed tomography; LVW, left ventricular weight; NR, not reported; PA, pulmonary artery; PAP, mean pulmonary artery pressure; PV loop, pressure-volume loop; PVR, pulmonary vascular resistance; RHC, right heart catheterization; RVW, right ventricular weight; SW, septum weight; WU, wood units.

Methods

Studies were performed in accordance with the "Guiding Principles in the Care and Use of Laboratory Animals" as approved by the Council of the American Physiological Society, and with approval of the Animal Care Committee of the Erasmus Medical Center Rotterdam (3158, 109-13-09). Twenty-four Yorkshire x Landrace swine (2-3 months old, 21.5 ± 0.9kg at the time of surgery) of either sex entered the study. Eighteen animals completed the protocol as six animals were excluded due to complications; 2 due to infections, 2 due to catheter failure and 2 animals due to acute cardiopulmonary failure after CTEPH induction. An overview of the experimental protocol is depicted in Figure 1.

Surgery

Surgical details have been extensively described previously (57). In short, swine were sedated with an intramuscular (i.m.) injection of tiletamine/zolazepam (5mg/kg, Virbac BV, Barneveld, The Netherlands), xylazine (2.25 mg/kg, AstFarma BV, Oudewater, The Netherlands) and atropine (1mg, Teva Nederland BV, Haarlem, The Netherlands), intubated and ventilated with a mixture of O_2 and N_2 (1:2v/v) to which 2% (v/v) isoflurane was added to maintain anesthesia. Under sterile conditions, the chest was opened via a left thoracotomy in the fourth intercostal space and fluid-filled polyvinylchloride catheters (B Braun Medical Inc., Bethlehem, PA, USA) were placed in the right ventricle, pulmonary artery, aorta and left atrium for blood sampling and measurement of pressures. A flow probe (Transonic Systems Inc., Ithaca, NY, USA) was positioned around the ascending aorta for measurement of cardiac output. The catheters were tunneled to the back and animals were allowed to recover for one week, receiving analgesia (0.015mg/kg buprenorphine i.m. and a slow-release transdermal fentanyl patch 12µg/h for 48 hours, Indivior, Slough, United Kingdom) on the day of the surgery

and daily antibiotic prophylaxis (25mg/kg amoxicillin intravenous (i.v.), Centrafarm B.V. Etten-Leur, The Netherlands) for 7 days.

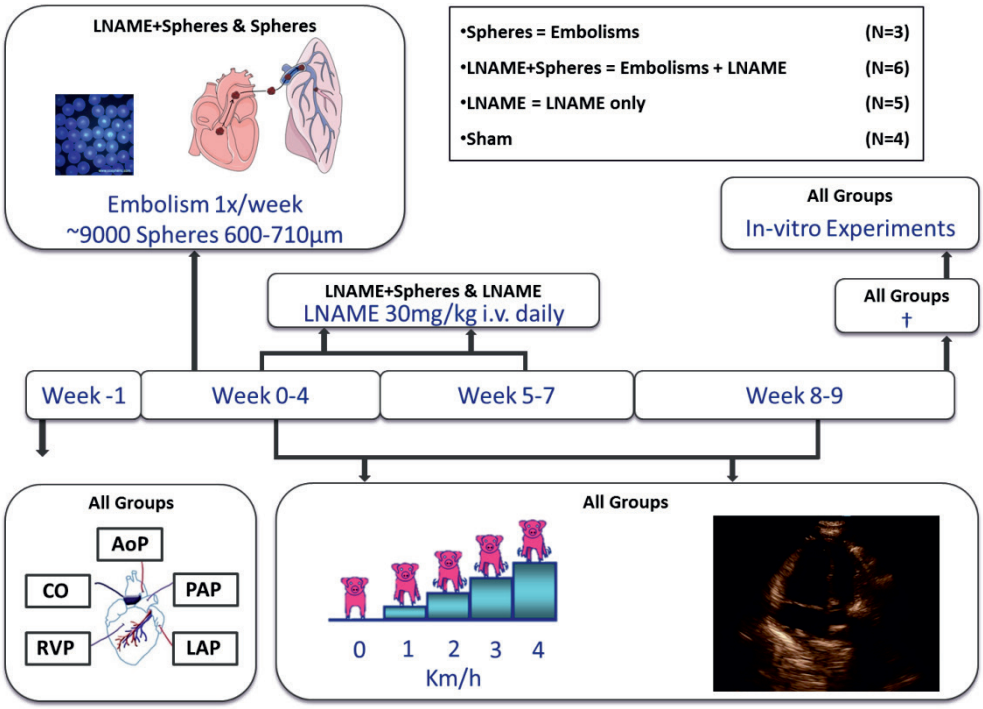

Figure 1. Experimental protocol.

Catheters were placed in the Aorta, Right Ventricle (RV), Pulmonary Artery (PA) and left atrium (LA) for blood sampling and measurement of pressures and a flow probe was positioned around the ascending aorta for measurement of cardiac output. The eNOS-inhibitor LNAME was administered intravenously in both the LNAME and LNAME+Spheres groups until 2 weeks before sacrifice. Embolization procedures were performed in awake state in the Spheres and LNAME+Spheres group from week 2 until week 5. All animals performed the treadmill exercise protocol and RV function was echocardiographically determined weekly in awake state. At the end of the follow-up (week 9-10) all the animals were sacrificed and in-vitro experiments were performed. AoP, aorta pressure; CO, cardiac output; RVP, right ventricular pressure; PAP, pulmonary artery pressure; LAP, left atrial pressure.

CTEPH induction

Four groups of animals were studied. In the first group (Spheres, N=3), multiple injections of fluorescent blue polyethylene microspheres (diameter 600-710µm (maximal microsphere size that did not cause clogging of the catheter); density 1.134g/mL, UVPMS-BB-1.13, Cospheric LLC, Santa Barbara, CA, USA) were given. Microspheres (500mg, being equal to ~2500 microspheres) were suspended in 50mL autologous blood with 0.5mL 5000 I.U. heparin added and slowly infused into the right ventricle while monitoring PAP. Microsphere infusions were repeated until the PAP reached ~60mmHg, or when arterial PO_2 (PO_{2art}) dropped below ~40mmHg, measured 30 min after infusion in resting condition or a maximum of 3 gram (~15000) microspheres were infused. In the subsequent four weeks, microsphere infusions were repeated. In the first animal, embolization procedures were performed multiple times per week, whereas in the subsequent two animals, embolization procedures were performed once per week. As no sustained PH was induced with this protocol, in the second group (N=6), multiple injections of microspheres were combined with a daily bolus infusion of the eNOS-inhibitor L-N^{ω}-Nitroarginine methyl ester (LNAME, Enzo Life Sciences International Inc, NY, USA) to mimic endothelial dysfunction often present in CTEPH patients. LNAME is converted to its active metabolite LNNA within 19 minutes, with the half-life of LNNA amounting to approximately 20 hours (22). On the first day, animals were given LNAME (10mg/kg i.v.) as a bolus infusion. On subsequent days, the dose of LNAME was increased by 10mg/kg per day up to 30mg/kg i.v., which was maintained until 2 weeks before the end of the study (35, 64). Four days after the first LNAME administration, hemodynamic measurements were performed as described above, then microspheres were infused into the right ventricle as described for group 1. In the subsequent four weeks, microsphere infusion was performed at weekly intervals if the PAP was <25mmHg and/or

PO_{2art}>70mmHg, as described above. During the final four weeks of follow-up, no microsphere infusions were performed.

The third group of sham animals did not receive LNAME or microspheres (Sham, N=4) and the fourth group was given chronic LNAME, but no microspheres were infused (LNAME, N=5).

Exercise protocol

Studies were performed 1-9 weeks after surgery. Catheters were connected to fluid-filled pressure transducers (Combitrans, B. Braun Medical, Oss, The Netherlands) positioned on the back of the animals and calibrated at mid-chest level. With swine standing quietly, resting hemodynamic measurements, consisting of cardiac output (CO), aorta pressure (MAP), pulmonary artery pressure (PAP), left atrial pressure (LAP) and right ventricular pressure (RVP), were obtained, and arterial and mixed venous blood samples were taken. Hemodynamic measurements and blood gas sampling were repeated during a graded exercise protocol, with swine running on a motor-driven treadmill (58, 64). During the embolization period, exercise was performed just prior to the weekly injection of microspheres and/or LNAME. Swine were subjected to a four-stage exercise protocol (1-4km/h). Hemodynamic variables were continuously recorded and blood samples were collected during the last 60sec of each 3min exercise stage, when hemodynamic steady-state was reached. Measurements of arterial and mixed venous PO_2 (mmHg), pCO_2 (mmHg), O_2 saturation (%), hemoglobin concentration (g/dL) and lactate (mmol/L) were immediately performed with a blood gas analyzer (ABL 800, Radiometer Medical ApS, Brønshøj, Denmark) (35).

Echocardiography

During the entire follow-up period, RV dimensions and tricuspid annular plane systolic excursion (TAPSE) were weekly assessed using echocardiography (ALOKA ProSound SSD-4000, Hitachi Aloka Medical, Ltd., Japan) in awake resting conditions. An apical four chamber view was obtained for the determination of RV end-diastolic cross-sectional lumen area (EDA) and end-systolic cross-sectional lumen area (ESA), whereas TAPSE was determined using M-mode in the four-chamber view.

Sacrifice

After completing the experimental protocols, the animals were sedated and intubated as described before. With the animals ventilated under deep anesthesia (pentobarbital sodium (6-12mg kg/h)), a sternotomy was performed. The heart was arrested and immediately excised together with the lungs. To assess relative RV hypertrophy, the heart was sectioned into RV and left ventricle including septum (LV), weighed, and RV hypertrophy was assessed using the Fulton index (RV/LV). Myograph experiments were performed on isolated pulmonary small arteries (diameter ~300µm) (18, 58). Pulmonary small arteries were dissected and stored overnight in cold, oxygenated (95% O_2/5% CO_2) Krebs bicarbonate solution (in mM: 118 NaCl, 4.7 KCl, 2.5 $CaCl_2$, 1.2 $MgSO_4$, 1.2 KH_2PO_4, 25 $NaHCO_3$, and glucose 8.3; pH 7.4). The next day, the dissected vessels were cut into segments of ~2mm length, mounted in microvascular myograph baths (Danish MyoTechnology, Aarhus, Denmark) containing 6mL Krebs bicarbonate solution aerated with 95% O_2-5% CO_2, maintained at 37°C and the internal diameter was set to a tension equivalent of 0.9 times the estimated diameter at 20mmHg effective transmural pressure. Changes in contractile force were recorded with a Harvard isometric transducer. The vessels were subsequently exposed to 30mM

KCl twice. Endothelial function was measured by observing dilation to 10nM substance P after preconstriction with 100nM of the stable thromboxane-A2 analog 9,11-dideoxy-11α,9α epoxymethanoprostaglandin $F_{2\alpha}$ (U46619).

Histology

The accessory lobe of the right lung was first flushed with physiologic saline (0.9% NaCl) through the main bronchus to flush the airways from sputum and surfactant at constant physiological pressure of 25cmH_2O. Subsequently, the lobe was fixed by tracheal installation of 3.5-4% buffered formaldehyde at constant physiological pressure of 25cmH_2O for a minimum of 24 hours with the lobe submerged in fixative (32). Transverse sections were obtained from the tip, middle and base of the fixed accessory lobe for histology. All sections were processed and embedded in paraffin wax. Paraffin sections of 4.5µm were cut and stained with Resorcin Fuchsin von Gieson (RF). These sections were evaluated by light microscopy using the Hamamatsu NDP slide scanner (Hamamatsu Nanozoomer 2.0HT, Hamamatsu Photonics K.K., Hamamatsu City, Japan). Morphometric measurements of pulmonary arteries were performed using NanoZoomer Digital Pathology (NDP) viewer (Hamamatsu Photonics K.K., Japan). To ensure that pulmonary veins were excluded for analysis, vessels in close proximity to the septae were excluded from analysis. Only transversely cut vessels of predetermined diameters (<50µm) were analysed. Assuming circularity of the vessels, inner and outer radius were calculated as r = perimeter/2*π. Wall thickness was calculated as outer radius – inner radius.

A section of the RV was processed and embedded in paraffin wax. Paraffin sections of 4.5µm were cut and stained with a Gomori staining. Only transversely cut cardiomyocytes were analyzed for cross sectional area (CSA) using NDP viewer.

Quantitative PCR

For detection of IL-6, TNF-α, TGF-β1, Ang-1, Ang-2, TIE-2, VEGF-A, FLT-1 and KDR mRNA, lung tissue was snap frozen in liquid nitrogen after excision. Small pieces of tissue (<30mg) were homogenized by adding RLT lysisbuffer (Qiagen, Venlo, The Netherlands) and 2-mercaptoethanol (Sigma-Aldrich, Zwijndrecht, The Netherlands) using a homogenizer. After a proteinase K (Invitrogen, Breda, The Netherlands) treatment at 55°C for 10 min, total RNA was isolated using the RNeasy Fibrous Tissue Mini Kit (Qiagen, Venlo, The Netherlands). RNA was eluted in RNase-free water and the concentration was determined using a NanoDrop (NanoDrop1000, Thermo Fisher Scientific, Bleiswijk, The Netherlands). RNA integrity was confirmed with a Bioanalyzer (2100 Bioanalyzer, Agilent, Santa Clara, California, USA). cDNA was synthesized from 500ng of total RNA with SensiFAST cDNA Synthesis Kit (Bioline, London, UK). Quantitative PCR (qPCR) (CFX-96, Bio-Rad, Hercules, California, USA) was performed with SensiFAST SYBR & Fluorescein Kit (Bioline, London, UK). Target gene mRNA levels were normalized against β-actin, glyceraldehyde-3-phosphate dehydrogenase (GADPH), and Cyclophilin using the CFX manager software (Bio-Rad, Hercules, California, USA). Relative gene expression data were calculated using the ΔΔCt method. All primer sequences are presented in Table 2.

Table 2. Primer sequences used for the quantitative PCR.

	Sequence	
Genes	**Forward**	**Reverse**
IL-6	CTCCAGAAAGAGTATGAGAGC	AGCAGGCCGGCATTTGTGGTG
TNF-α	TGCACTTCGAGGTTATCGGCC	CCACTCTGCCATTGGAGCTG
TGF-β1	GTGGAAAGCGGCAACCAAAT	CACTGAGGCGAAAACCCTCT
Ang-1	AATGGACTGGGAAGGAAACCG	TCTGTTTTCCTGCTGTCCCAC
Ang-2	AGGCAACGAGGCTTACTCAC	TCGTTGTCTGCGTCCTTTGT
TIE-2	GTCCCGAGGTCAAGAAGTGT	AAGGGGTGCCACCTAAGCTA
VEGF-A	ACTGAGGAGTTCAACATCGCC	CATTTACACGTCTGCGGATCTT
FLT-1	AAGGAGGGCGTGAGGATGAGG	GGCTTGCAGCAGGTCGCCTAG
KDR	TTCTCCGAGCTGGTGGAGCAC	AGGTAGGCAGAGAGAGTCCGG

IL-6, interleukin 6; TNF-α, tumor necrosis factor α; TGF-β1, transforming growth factor β1; Ang-1, angiopoietin 1; Ang-2, angiopoietin 2; TIE-2, angiopoietin 1 receptor; VEGF-A, vascular endothelial growth factor A; FLT-1, vascular endothelial growth factor receptor 1; KDR, kinase insert domain receptor (vascular endothelial growth factor receptor 2).

Data analysis and statistics

Echocardiography data were analyzed using DICOM viewer (Rubo Medical Imaging BV, Aerdenhout, The Netherlands) and SigmaScan Pro (Systat Software Inc, San Jose, CA, USA). Three images of end-diastole, three images of end-systole and three TAPSE recordings per echo were selected in DICOM viewer. RV lumen area and TAPSE length were manually drawn per image, automatically calculated in SigmaScan and then averaged per animal per time point.

Digital recording and offline analysis of hemodynamic data were performed with MatLab (MathWorks, Natick, MA, USA) and have been described in detail elsewhere (4, 40).To accommodate for growth, cardiac output was corrected for bodyweight, resulting in cardiac index (CI). Total pulmonary vascular resistance index (tPVRi) and systemic vascular resistance (SVRi) were calculated as PAP divided by CI and mean aortic pressure divided by CI, respectively. Body

oxygen consumption index (BVO_2i) was calculated as the product of CI and the difference between arterial and mixed venous oxygen content of the blood.

Statistical analysis was performed using SPSS version 21.0 (IBM, Armonk, NY, USA). Differences between Spheres, LNAME+Spheres, LNAME and Sham over time at rest were analyzed with a two-way MANOVA with PAP, tPVRi, CI and stroke volume index (SVi) as dependent variables and time and group as fixed factors. As no differences were observed in hemodynamics, oxygenation, histology, inflammation and angiogenesis between Sham, LNAME and the Spheres groups, these groups were pooled into a single Control group (Control) for the subsequent analyses. Echocardiography data and Fulton index were analyzed by a one-way MANOVA with the RVESA, RVEDA, right ventricular fractional area change (RVFAC), TAPSE, CSA, RVW/LVW and RVW/BW as dependent variables and group as fixed factor. The difference in effect of exercise on the hemodynamic parameters between LNAME+Spheres and Control at the same time point were assessed by two-way repeated measures (RM)-ANOVA with exercise as within-subject factor and group as between-subject factor. The difference in effect of exercise on hemodynamic parameters compared to baseline within the individual groups, a two-way RM-ANOVA with exercise as within-subject factor and time as between-subject factor. Statistical significance was accepted when $p \leq 0.05$. Data are presented as mean ± SEM.

Results

Induction and progression of CTEPH

To induce CTEPH, microspheres (600-710µm) were infused slowly into the right ventricle. In the Spheres group, one animal received twenty-five embolizations with an average of 2700 microspheres per embolization procedure. The two other animals underwent five embolization procedures with an average of 9200 microspheres per embolization procedure. Each microsphere has a cross-sectional area of 2.5-4.7 · $10^{-14}m^2$, a volume 1.1-1.8 · $10^{-10}m^3$ and a total surface area of 1.0-1.9 · $10^{-13}m^2$. With an average of 36000 spheres per animal. This results in a total cross-sectional area of 9.1-17.0 · $10^{-10}m^2$, a total volume of 4.1-6.5 · $10^{-6}m^3$ and a total surface area of 3.7-6.8 · $10^{-9}m^2$. Although immediately following injection a substantial increase in PAP was observed, this increase waned over the course of the next few days, such that with weekly measurements, resting PAP and tPVRi did not increase significantly over time in these animals (PAP being 21.0±1.8mmHg and tPVRi being 100±4mmHg·min/L/kg at baseline and 19.1±1.5mmHg and 147±22mmHg·min/L/kg respectively at week 9).

In the second group (LNAME+Spheres), an average of four embolization procedures (range between two and five), were required to induce chronic PH. The number of microspheres infused per embolization procedure did not change over time, being 9000±400.

In these animals, resting PAP increased gradually over time (from 21.8±1.1mmHg at baseline before LNAME to 32.2±3.1at week 5 and 39.5±5.1mmHg at week 9) as a result of a progressive increase in pulmonary vascular resistance (Figure 2). The increase in tPVRi in the LNAME+Spheres animals was due to a combination of vascular obstruction by the injected spheres

in combination with remodeling and dysfunction of the pulmonary microvessels. The latter was reflected by an increased wall-thickness (Figure 4) and impaired vasorelaxation in response to Substance P in isolated pulmonary small arteries (86±3%, 82±3%, 90% and 62±8% in Sham, LNAME, Spheres and LNAME+Spheres respectively). Histologically, microspheres in the lungs were surrounded by fibrous tissue, however, qPCR analysis revealed no changes in the inflammatory markers IL-6, TNF-α and TGF-β1 (Figure 5). Moreover, expression of the angiogenic factors VEGF-A, Flt-1, KDR as well as Ang-1, Ang-2 and Tie-2 were also not different between groups (Figure 5).

Although acute LNAME administration did result in a small increase in PAP and tPVRi within the first 30 minutes, both at baseline (BL) (17.3±0.9 to 21.0±2.1mmHg and 101±14 to 137±17mmHg·min/L/kg) and after 5 weeks of LNAME administration (17.6±1.8 to 21.9±2.2 mmHg and 120±6 to 150±18mmHg·min/L/kg), PAP and tPVRi normalized before the next injection. Thus, in the LNAME group, PAP did not significantly increase over time being 18.0±1.4mmHg at week 1 and 22.7±2.0mmHg at week 9, which was not significantly different from PAP in the Sham group (17.5±1.2mmHg at BL and 20.1±1.5mmHg at week 9) (Figure 2). As there were no sustained differences in hemodynamics, oxygenation, histology, inflammation and angiogenic markers between the Spheres, LNAME and Sham groups (Figure 2-5), these groups were pooled into one Control group (Control) for the remainder of the analyses.

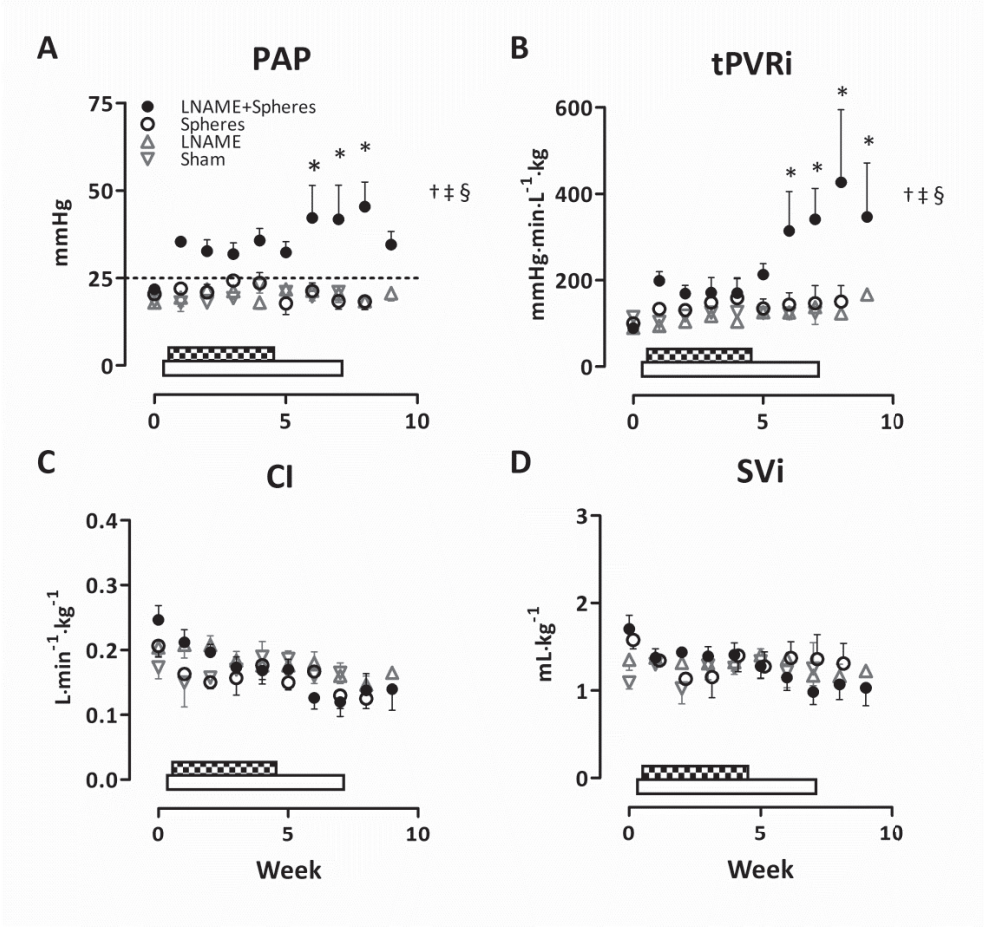

Figure 2. Changes in pulmonary hemodynamics over time.

*Dotted bar indicates period of weekly embolizations with microspheres and white bar indicates administration time of LNAME. Please note that all baseline measurements were taken prior to administration of LNAME and/or Spheres. A) Mean pulmonary artery pressure (PAP); B) total pulmonary vascular resistance index (tPVRi); C) cardiac index (CI) and D) stroke volume index (SVi). Data are means ± SEM. Sham N=4; LNAME N=5; Spheres N=3; LNAME+Spheres N=6, N=5 from week 7 due to death of one animal caused by acute cardiopulmonary failure. * P < 0.05 vs baseline (prior to start of LNAME and/or Spheres; † P < 0.05 LNAME+Spheres vs Sham; ‡ P < 0.05 LNAME+Spheres vs LNAME; § P < 0.05 LNAME+Spheres vs Spheres; Sham vs LNAME vs Spheres NS.*

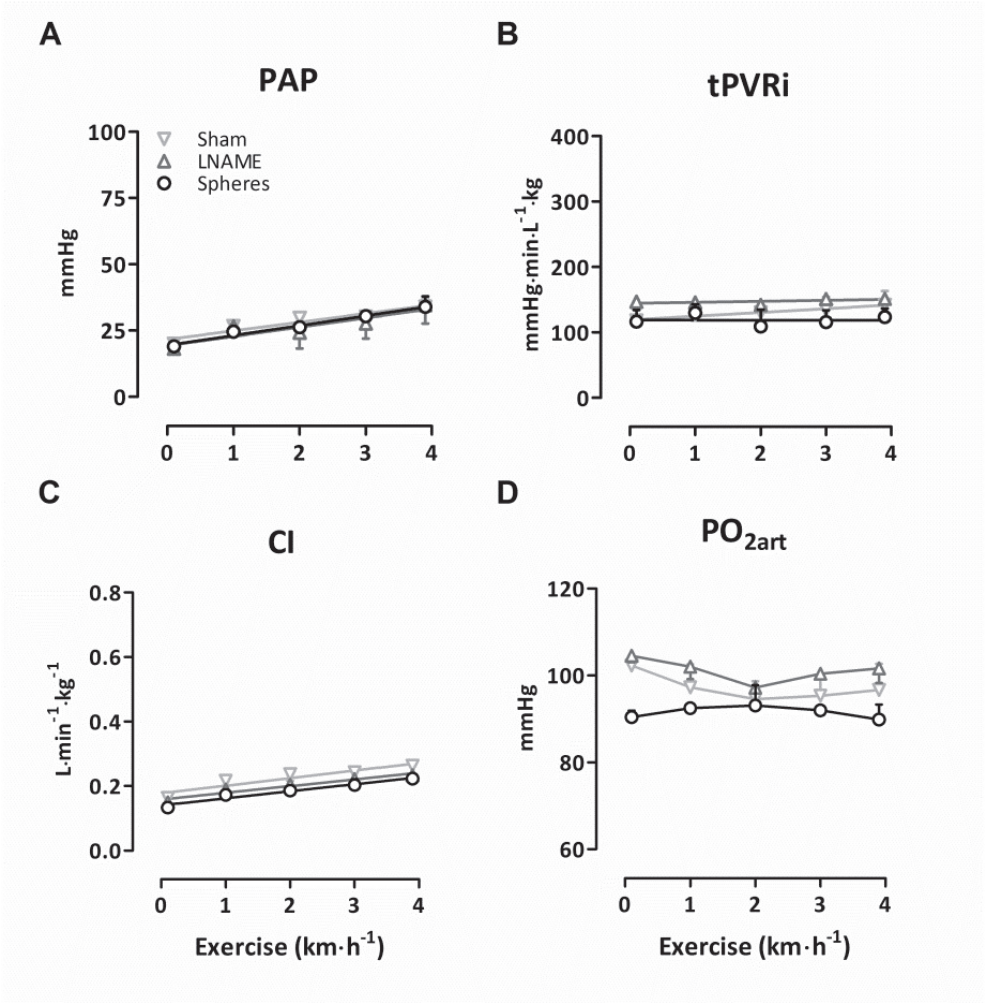

Figure 3. Changes in pulmonary and cardiac hemodynamics with incremental levels of exercise at the end of follow-up of different control groups.

Presented is the effect of exercise on A) mean pulmonary artery pressure (PAP); B) total pulmonary vascular resistance index (tPVRi); C) cardiac index (CI) and D) arterial oxygen pressure (PO_{2art}). Data are means ± SEM. Sham N=4; LNAME N=5; Spheres N=3. No significant differences were observed.

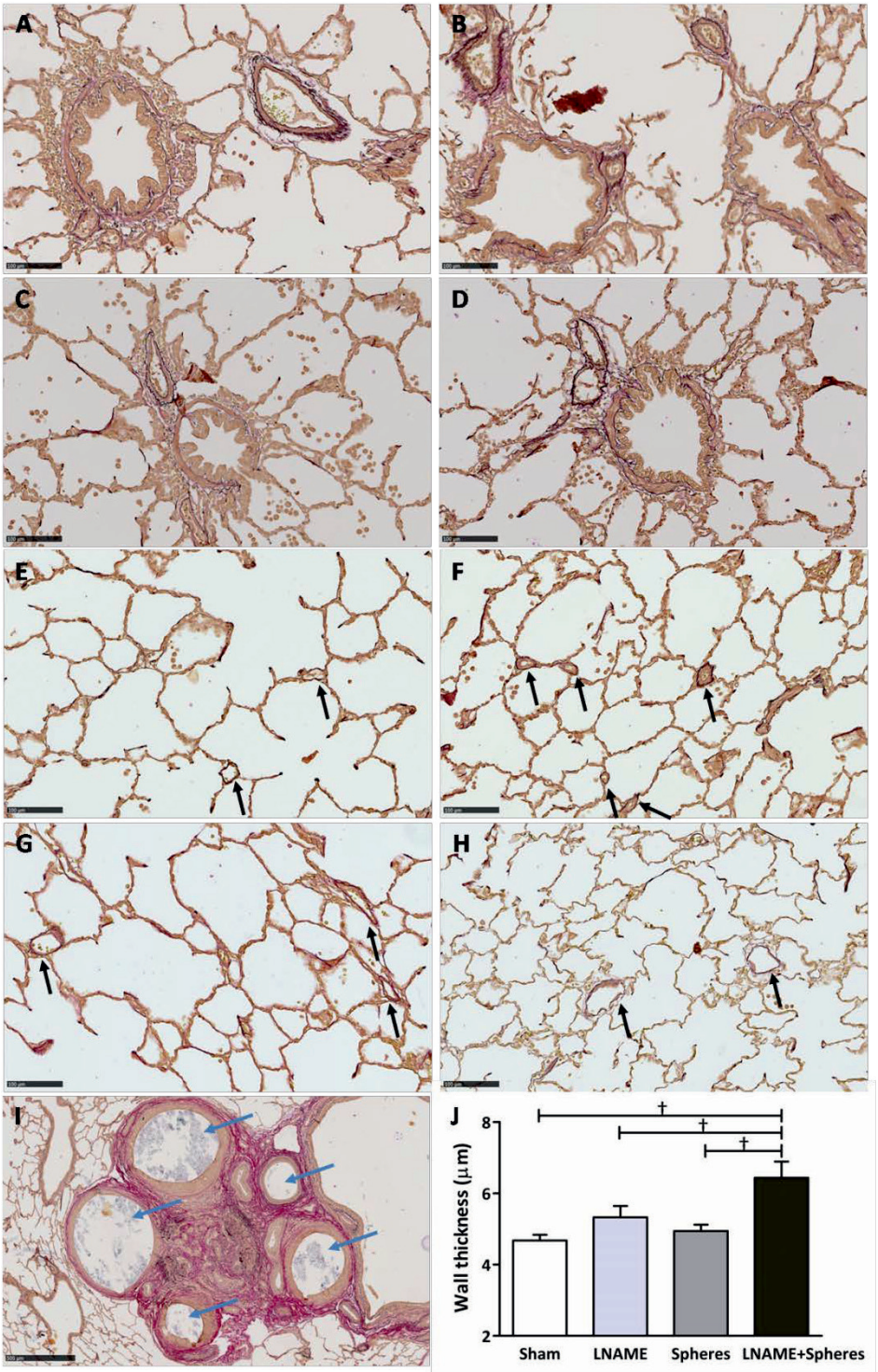
A
B
C
D
E
F
G
H
I
J
Wall thickness (µm)
8
6
4
2
†
†
†
Sham
LNAME
Spheres
LNAME+Spheres

Figure 4. Histological overview of lung tissue stained with Resorcin Fuchsin von Gieson.
Typical examples of bronchi with arteries of animals with A) Spheres; B) LNAME+Spheres; C) LNAME and D) sham at 20x magnification. Panels E-H are pulmonary microvessels adjacent to alveoli at 20x magnification in swine from different groups E) Spheres; F) LNAME+Spheres; G) LNAME and H) Sham. In the LNAME+Spheres lung tissue, microvessels presented with a thickened/muscularized wall (black arrows). Panel I shows an example of the occluded vessels due to the microspheres (blue arrows) surrounded by remodeled small unobstructed vessels in swine that received LNAME+Spheres. Panel J is a quantitative presentation of the microvascular remodeling. The wall of microvessels (diameter <50µm) of the LNAME+Spheres were thickened compared to all other groups.Data are means ± SEM.Sham N=4; Spheres N=3; LNAME N=5; LNAME+Spheres N=6. † P < 0.05 vs LNAME+Spheres.

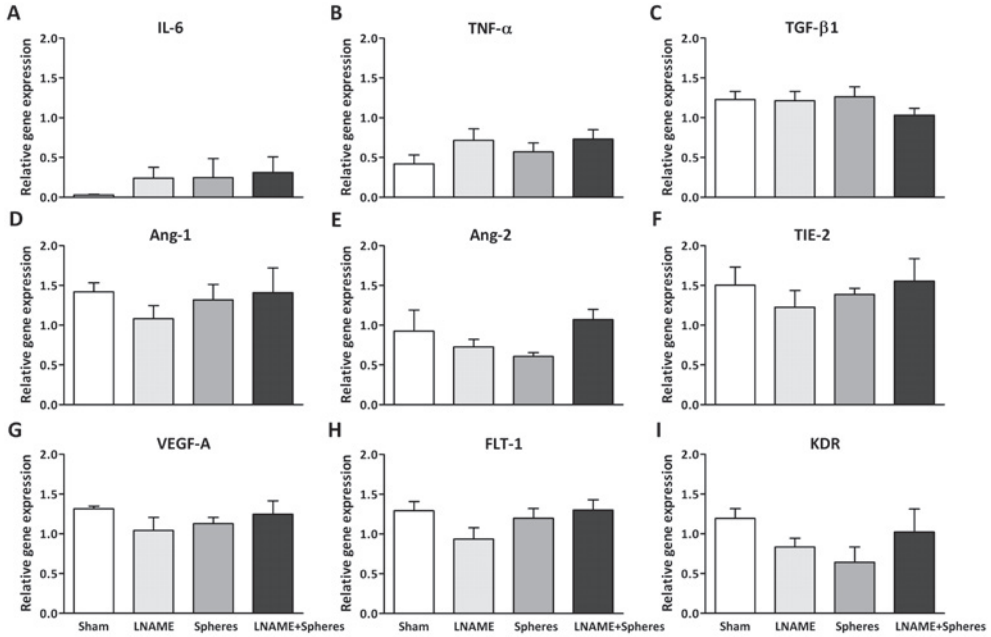

Figure 5. Quantitative PCR.
Inflammatory (panel A-C) and angiogenic (panel D-I) gene expression in lung tissue of all experimental groups at the end time-point of A) Interleukin 6 (IL-6); B) tumor necrosis factor α (TNF-α); C) transforming growth factor β1 (TGF-β1); D) Angiopoietin 1 (Ang-1); E) Angiopoietin 2 (Ang-2); F) Angiopoietin 1 receptor (TIE-2); G) vascular endothelial growth factor A (VEGF-A); H) vascular endothelial growth factor receptor 1 (FLT-1) and I) vascular endothelial growth factor receptor 2 (KDR). Data are means ± SEM. Sham N=4; Spheres N=3; LNAME N=5; LNAME+Spheres N=6. No significant differences between groups were observed.

RV function and hypertrophy

Echocardiography showed that RV diastolic and systolic lumen area increased over time, while TAPSE tended to increase and RVFAC remained constant in the Control group, reflecting growth of the RV over time (Figure 6). Repeated microsphere injections over 5 weeks in the LNAME+Spheres group resulted in a trend towards higher end-systolic (P=0.085) but not end-diastolic right ventricular lumen area (P=0.15), indicating mild RV contractile dysfunction. This was associated with a slight decrease in SVi as compared to BL, while RVFAC and TAPSE did not change. With sustained PH, SVi was reduced as compared to BL, but neither SVi, nor RV diastolic and systolic lumen area and RVFAC were significantly different from Control, although TAPSE showed a trend towards a reduction, indicating that resting RV function recovered. The Fulton index (RVW/LVW) and RVW/bodyweight (BW), measured at sacrifice after sustained PH, were significantly higher in LNAME+Spheres compared to Control swine, implying right ventricular hypertrophy due to chronic PH (Figure 6).

Exercise response

As CTEPH is accompanied by exercise intolerance due to both the increase in RV afterload and V/Q mismatch in the lungs, the response to exercise was examined in the initial phase after embolization (at 5 weeks, referred to as 'after microspheres' (AM) in the figures and at the end of follow-up (8-9 weeks after the first microsphere injection), referred to as 'End' in the figures, and compared to the pooled Control group at the corresponding time-points. Graded treadmill exercise resulted in an increase in PAP at all time-points in both LNAME+Spheres and Control animals (Figure 7).

In the LNAME+Spheres animals, PAP was increased compared to its BL measurement as well as to the Control at the corresponding time-point in the initial phase after embolization (week 5), and the exercise-induced increase in PAP was exacerbated due to the significant elevation in tPVRi (Figure 7). This increase in tPVRi was also reflected in the significantly higher slope of the relation between CI and PAP (Figure 8). The exercise-induced increase in CI was attenuated in the LNAME+Spheres group, which was due to a significant decrease in SVi during exercise (Figure 7), as the exercise-induced increase in heart rate was not different between LNAME+Spheres and Control (Table 3). These observations indicate that the right ventricle could not cope with the increased afterload during exercise in the initial phase after embolizations.

At the end of the follow-up period, PAP was still elevated compared to both BL and Control. Moreover, the exercise-induced increase in CI was attenuated while the exercise-induced increase in PAP was exacerbated at the end of the follow-up period in the Spheres+LNAME group compared to Control (Figure 7). This translated into a persistent elevation of the slope of the relation between CI and PAP compared with Control (Figure 8), reflecting the sustained increase in tPVRi (Figure 7). Interestingly, although SVi was still depressed at the End of follow-up, the exercise-induced decrease in SVi that was observed at AM, was no longer present at the End of follow-up. The significant RV hypertrophy and recovery of RV-function as assessed with echo, in conjunction with the blunted exercise-induced decrease of SVi as compared to the initial phase after embolization, could be interpreted to suggest that RV-hypertrophy served to restore RV function in the face of an increase in afterload.

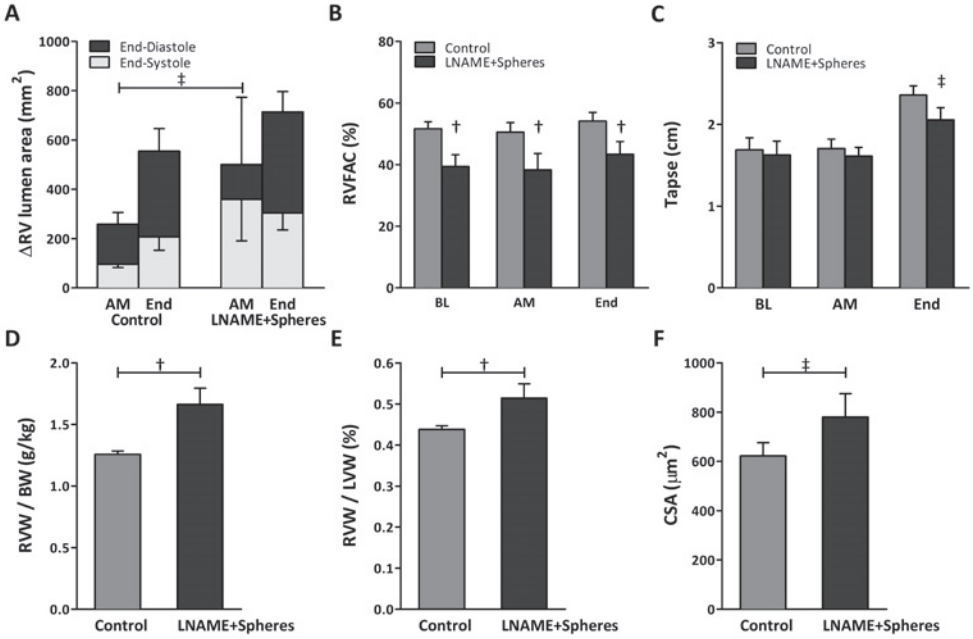

Figure 6. Right ventricular remodeling.

A) End-diastolic and end-systolic lumen area changes over time as measured with echocardiography compared to baseline (week 0, prior to injection of LNAME and Spheres). End-systolic RV lumen area tended to be increased in LNAME+Spheres compared to Control at the end of the embolization period (AM), but not at the time-point prior to sacrifice (End). B) RVFAC was decreased at all time-points in LNAME+Spheres compared to Control. C) TAPSE tended to be increased in LNAME+Spheres at the end time-point compared to Control. D) Right ventricular weight (RVW) over bodyweight (BW) was increased at sacrifice. E) Fulton index (RVW over left ventricular weight (LVW)) was increased in LNAME+Spheres vs Control. F) RV cardiomyocyte CSA tended to be increased in LNAME+Spheres compared to Control at sacrifice. AM, after microspheres; end, end of follow-up; RVFAC, right ventricular fractional area change; TAPSE, tricuspid annular plane systolic excursion; CSA, cross sectional area. Data are means ± SEM. A) Control AM N=6, End N=9; LNAME+Spheres AM N=5, End N=7. B-C) Control N=9; LNAME+Spheres N=5. D-F) Control N=9; LNAME+Spheres N=6. ‡ P < 0.1 End-Systole LNAME+Spheres vs Control; † P < 0.05 LNAME+Spheres vs Control.

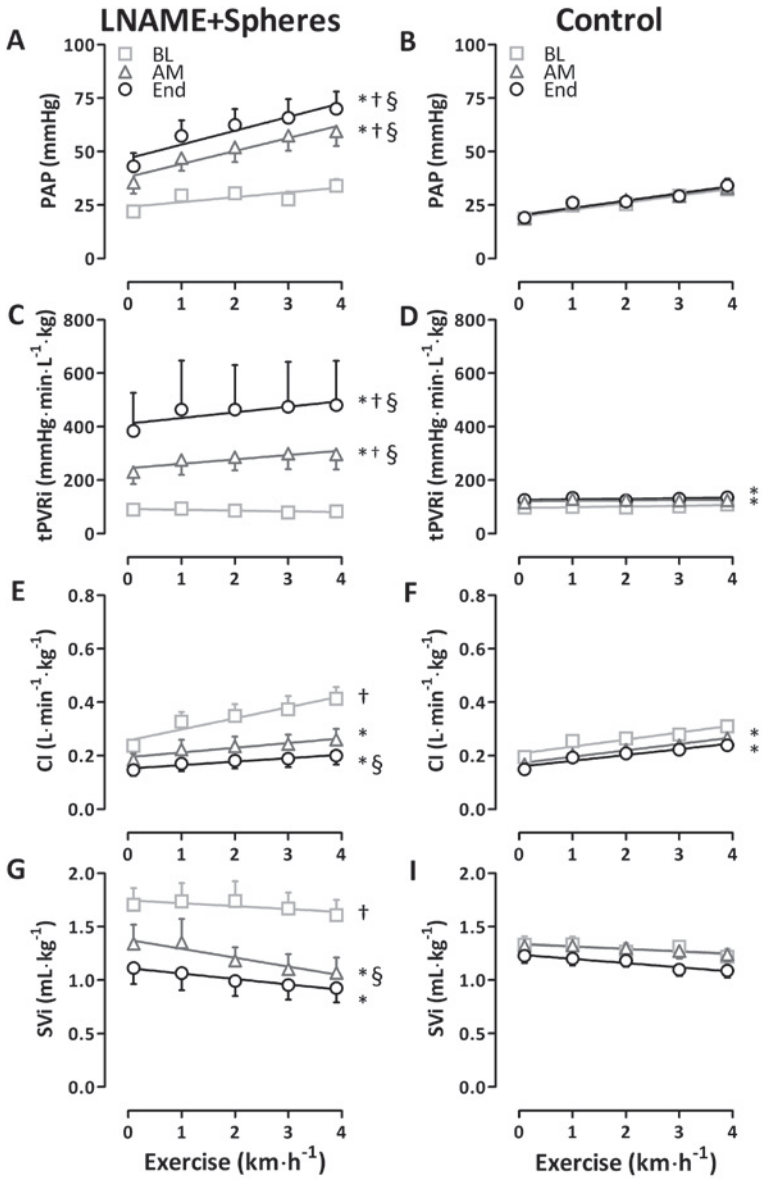

Figure 7. Changes in pulmonary and cardiac hemodynamics during incremental levels of exercise at baseline (BL), after completion of embolization (AM) and at the end of follow-up (End).

*Presented is the effect of exercise on: mean pulmonary artery pressure (PAP), panels A&B; total pulmonary vascular resistance index (tPVRi), panels C&D; cardiac index (CI), panels E&F; and stroke volume index (SVi) in panels G&H. Data are means ± SEM. Control N=12; LNAME+Spheres N=6. * P < 0.05 vs BL; † P < 0.05 vs corresponding Control; § P < 0.05 vs effect of exercise in Control.*

PO_{2art} was lower in the LNAME+Spheres swine compared to Control after the embolization phase and at the end of follow-up. Moreover, PO_{2art} decreased more during exercise in LNAME+Spheres compared to Control at both time-points. After the embolization phase, body O_2 extraction at rest was increased in the LNAME+Spheres group compared to both BL and Control group. The increased O_2 extraction compensated for the decreases in CI and arterial oxygenation, so that body O_2 consumption was unaltered. At the end of follow-up, the increase in body O_2 extraction was insufficient to compensate for the decrease in PO_{2art} and the O_2 consumption was lower at rest (Figure 9). Although there was no difference in the exercise-induced increase in O_2 extraction, the exercise-induced increase in O_2 consumption was significantly attenuated both after the initial embolization phase (AM) and at the end of follow-up (End) in LNAME+Spheres compared to Control animals, reflecting the attenuated increase in CI.

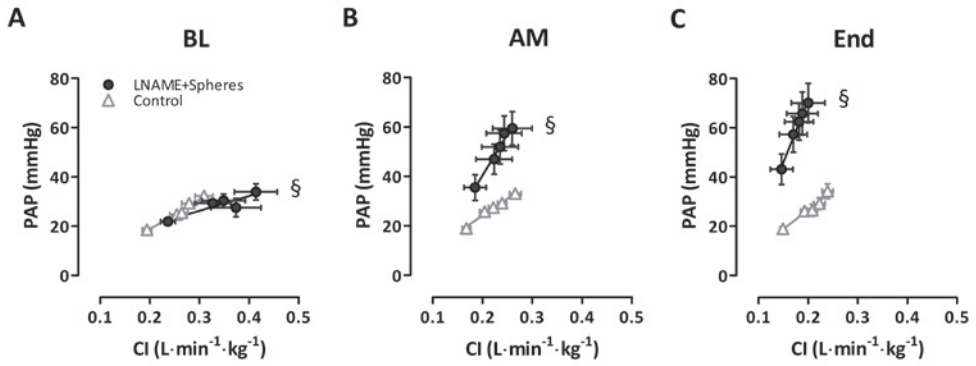

Figure 8. Pulmonary vascular reserve.

Presented is the relationship between pulmonary artery pressure (PAP) and cardiac index (CI) during incremental exercise at A) baseline (BL); B) after completion of embolization (AM) and C) at the end of follow-up (End). Data are means ± SEM. Control N=12; LNAME+Spheres N=6. § P < 0.05 Effect of exercise in LNAME+Spheres vs Control (slope).

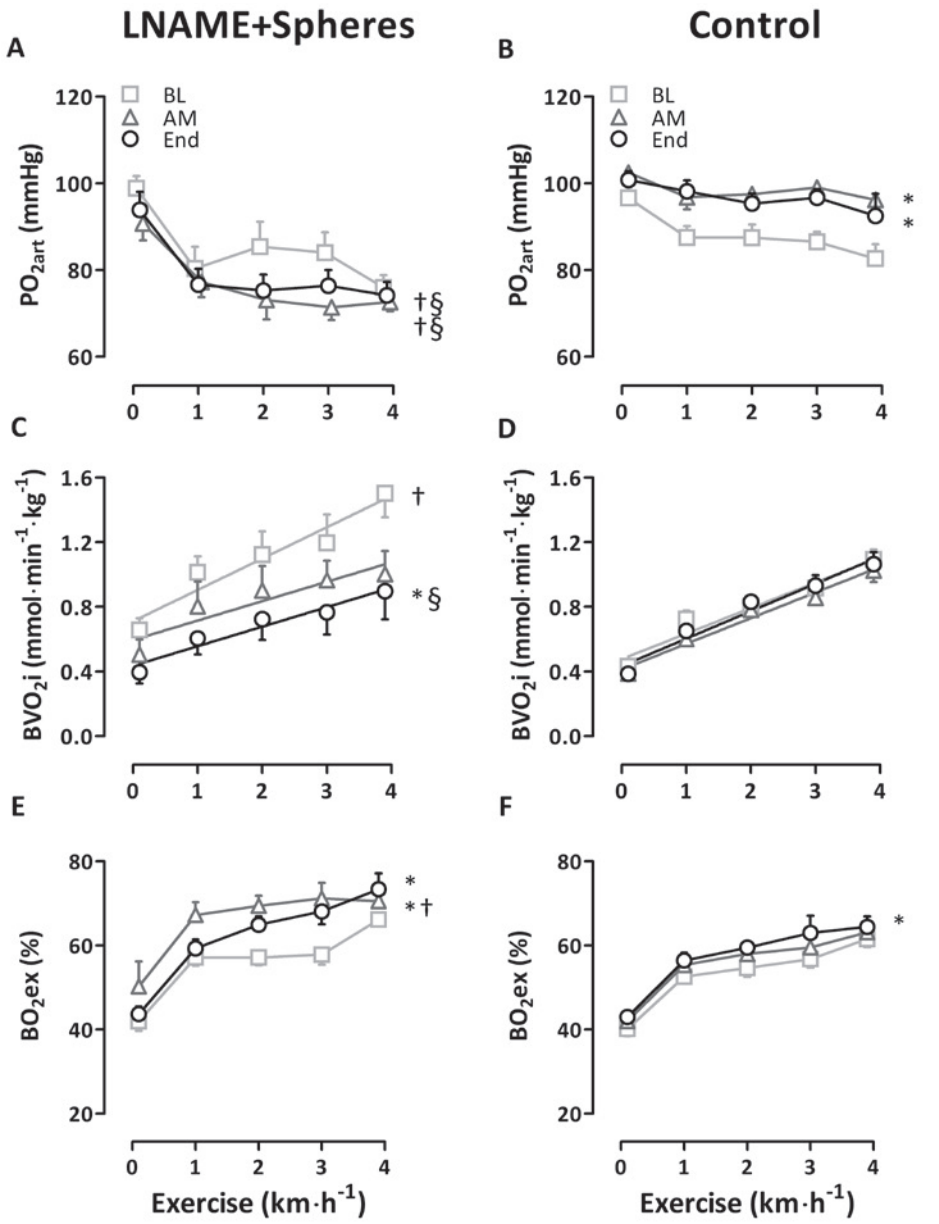

Figure 9. Systemic oxygenation and body oxygen consumption during incremental levels of exercise at baseline (BL), after microspheres (AM) and at the end of follow-up (End).
*Presented is the effect of exercise on: Arterial oxygen pressure (PO_{2art}), panels A&B; Body oxygen consumption index (BVO_2i), panels C&D; and body oxygen extraction (BVO_2ex), panels E&F. Data are means ± SEM. Control N=12; LNAME+Spheres N=6. * P < 0.05 vs BL; † P < 0.05 vs corresponding Control; § P < 0.05 vs effect of exercise in Control.*

Discussion

The main findings of this present study are that *i)* induction of CTEPH with a sustained increase in PAP and tPVRi over time required a combination of endothelial dysfunction (LNAME) and repeated embolization procedures, as either stimulus alone did not result in a sustained increase in PAP or tPVRi; *ii)* PAP and tPVRi were still increased up to 5 weeks after the last embolization and 2 weeks after the last LNAME injection, consistent with sustained pulmonary hypertension; *iii)* development of CTEPH is accompanied by a decrease in arterial oxygen tension during exercise both in the early phase following embolizations as well as at the end of follow-up; *iv)* impaired oxygenation of the arterial blood was compensated by a small increase in systemic oxygen extraction; *v)* repeated embolizations initially resulted in RV dysfunction at rest, as assessed with echocardiography, and by a decrease in SVi during exercise. However, at the end of follow-up, the presence of RV hypertrophy was associated with a maintained SVi during exercise.

Induction of CTEPH requires both repeated embolizations and endothelial dysfunction

As summarized in Table 1, over the past decades several research groups have attempted to develop a large animal model of CTEPH, using different embolization materials, particle sizes and embolization frequencies. Many of these attempts have failed to show a sustained (>2 weeks after the last embolization) increase in PAP (1, 17, 26, 33, 38, 41, 42, 48, 55, 60). The studies that did show a sustained increase in PAP (5, 16, 47, 49, 63), have in common that they embolized a large part of the pulmonary vasculature, with multiple embolization procedures. It has been suggested that 40-60% of the lung vasculature needs to be obstructed for CTEPH to develop (3, 13). Indeed, Mercier and co-workers performed ligation of

the left pulmonary artery in combination with progressive embolization of the segmental arteries of the right lower lobe (5), leaving the right upper and possibly right middle lobe unaffected.

Estimation of the relative magnitude of the obstructed part of the pulmonary vasculature requires comparison of the number of microspheres infused with the number of vascular branches of corresponding size present in the pulmonary vascular bed. The pulmonary vasculature can be morphometrically described with diameter defined Strahler orders, starting at the capillaries and ending at the main pulmonary artery (24). The pulmonary vascular tree of swine is less well described than that of humans, in which a total of 15 orders was observed (24). In swine, pulmonary vascular morphometry of pulmonary arteries larger than 160µm in diameter was analyzed using multidetector-row computed tomography, resulting in 10 branching orders (29). This number of branching orders corresponds well with the human study, in which vessels of the 5^{th} order had an average diameter of 150µm. In the present study, CTEPH was induced with embolizations using microspheres of 600-710µm in diameter. This size of microspheres corresponds with order 3 (diameter 430µm, range 380-570µm) and order 4 (diameter 760µm, range 660-990µm), of which approximately 2100 and 590 are present in the porcine pulmonary vasculature (29). It has to be taken into account that supernumerary vessels were not measured because of the computational model used. These supernumerary vessels are estimated to be present in a ratio of 1.6 (45) or 2.8 (6) to conventional arteries. Adding these vessels to the number of vessels results in an estimated total of 5460-7980 arteries of order 3, and 1530-2240 arteries of order 4. Assuming that the pulmonary vascular tree of a 20kg pig is 3-fold smaller than that of a 70kg human, these numbers correspond well with the estimated 22000 (order 8, diameter 510±40µm) and 6225 (order 9, diameter 770±70µm) pulmonary small arteries

present per lung in humans (24). To ensure full coverage of the pulmonary vasculature, microspheres were slowly injected into the RV, assuming that microspheres flow to perfused, non-embolized vessels. The presence of microspheres in all lung lobes was visually confirmed upon sacrifice, and no microspheres were observed in systemic organs. Histologically, microspheres in the lungs were surrounded by fibrous tissue, however, qPCR analyses revealed no changes in the expression of inflammatory markers IL-6, TNF-α and TGF-β1. Although some microspheres clustered, with an approximate total of 36000 microspheres per animal, it is likely that 60% of these pulmonary small arteries were obstructed. Nevertheless, with microspheres alone, no sustained CTEPH developed.

Since CTEPH patients present with dysfunctional endothelium as evidenced by alterations in coagulation, inflammation, angiogenesis and vasoregulation (2, 30, 43, 51, 52), endothelial dysfunction was used as a second hit to induce CTEPH. Nitric oxide is an important endothelium-derived anti-coagulatory, anti-inflammatory, pro-angiogenic, vasodilator. Therefore, endothelial dysfunction was induced by inhibiting eNOS by chronic LNAME administration, which in combination with multiple microsphere infusions resulted in a sustained increase in PAP and tPVRi. This increase in PAP above 25mmHg for a prolonged period of time after embolizations and in the awake state is evidence for successful induction of chronic PH (1, 17, 26, 33, 38, 41, 42, 48, 49, 60, 63). Our findings are in accordance with a recent study in rats, that show that sustained CTEPH developed when combining embolizations with endothelial dysfunction produced by VEGF-inhibition (39). Importantly, in the present study CTEPH persisted when eNOS inhibition was discontinued, which together with the reduced endothelium-dependent vasodilator response to Substance P in isolated pulmonary small arteries, indicates that CTEPH in itself

was sufficient to maintain a state of endothelial dysfunction. It is well established that secondary to pulmonary embolisms, worsening of PH results from progressive microvascular remodeling of the non-obstructed pulmonary small arteries (23, 37). Indeed, we also observed microvascular remodeling as evidenced by an increased wall thickness of the non-obstructed pulmonary small arteries and exaggerated vasoconstriction to both KCl and the thromboxane analogue U46619. Contrary to results in lungs of patients with CTEPH, in which a reduction in VEGF-expression and an elevation of the anti-angiogenic factor angiopoietin-1 were observed (51), microvascular remodeling in our model was not accompanied by changes in expression of angiogenic factors as measured with qPCR in tissues obtained at sacrifice. The exact time-course of microvascular remodeling cannot be determined from our data, as the increase in resistance due to embolization cannot be distinguished from the increase in resistance due to microvascular remodeling during the embolization period. However, tPVRi continued to increase after cessation of the embolization procedures, which is consistent with remodeling of the distal vasculature, although an increase in microvascular tone secondary to endothelial dysfunction may also have contributed.

Cardiopulmonary stress testing and RV function

Exercise testing after pulmonary embolism is predictive of development of PH and/or patient outcome in established CTEPH (19-21, 46). Swine were exercised on a motor driven treadmill up to 4km/h prior to induction of CTEPH and on a weekly basis during and after the embolization period to investigate the influence of cardiopulmonary stress on hemodynamic variables and blood oxygenation. Swine reached heart rates of approximately 255bpm at the beginning of the study and 210bpm at the final exercise trial (Table 3), whereas maximal heart rates of

272 bpm have been reported in literature in swine of similar size (61). Nevertheless, the significant lactate production during exercise at the beginning of the study as well as at the final exercise trial in the CTEPH swine suggests that near maximal levels were reached at those time points.

In accordance with Claessen et al. 2015 (7, 8), we observed that the right ventricle was not able to cope with the increased afterload during exercise evidenced by a decreased SVi, particularly early after embolization. Furthermore, whereas RV EDA was unchanged but RV ESA tended to be increased, suggestive of systolic contractile dysfunction, although TAPSE was not different. The decreased SVi was not compensated by an increase in heart rate, and hence cardiac index was lower in swine with CTEPH. Despite the blunted exercise-induced increase in cardiac index, the increase in PAP and tPVRi were exacerbated during exercise. Moreover, the ventilation-perfusion mismatch was exacerbated during exercise, resulting in a further decrease in PO_{2art} during exercise.

At the end of follow-up, the time-point which resembles the time where most patients present in the hospital with symptoms, PAP and tPVRi were still elevated at rest and, similar to patients with CTEPH the increase in PAP was exacerbated during exercise (7, 8). However, as a result of the chronically elevated RV afterload, the RV underwent hypertrophy reflected by increases in RVW/BW, Fulton index and cardiomyocyte cross-sectional area. Although TAPSE showed a trend towards a decrease in LNAME+Spheres, RV hypertrophy blunted the systolic dysfunction of the heart as observed using echocardiography at rest, as well as the decrease in SVi during exercise. Nevertheless, CI was persistently decreased at rest and did not increase significantly during exercise. In addition, patients presenting with a V/Q mismatch in the lungs suffer a further decrease in ventilatory efficiency during exercise. Although this V/Q mismatch correlates to

RV function in other types of PH, there is no correlation in either CTEPH patients or in the LNAME+Spheres animals in the present study (data not shown) (14, 44, 56). The reduction in O_2 uptake was exacerbated during exercise as evidenced by a decrease in PO_{2art}, which in combination with the decreased CI resulted in a reduced VO_2max (25, 31, 46). Similarly, in our swine model, the V/Q mismatch increased in severity with incremental exercise intensity, as evidenced by a further decrease in arterial PO_2. This V/Q mismatch remained present during the entire follow-up period. However, given the relatively mild reduction in PO_{2art}, the capability of the body to increase O_2 extraction, and the more severe reduction in SVi during exercise, it is likely that the main cause of the exercise limitations in CTEPH is cardiac insufficiency. These data in our porcine model are consistent with the observations by Claessen et al. (7, 8) that exercise intolerance in CTEPH patients is principally determined by a disproportional increase in RV afterload.

Conclusions

A combination of repeated embolization procedures and endothelial dysfunction was required to successfully develop a large animal model for chronic embolic pulmonary hypertension. To the best of our knowledge the present study is the first to investigate the role of both cardiac dysfunction and V/Q mismatch in exercise intolerance in an animal model of CTEPH. This model emulates critical features of patients with CTEPH, including V/Q mismatch and early RV dysfunction. The latter likely contributed to the reduced SVi that was present at rest. Both the V/Q mismatch and the cardiac dysfunction were aggravated by exercise. Prolonged increases in RV afterload were associated with adaptive RV hypertrophy, while the V/Q mismatch remained present. This animal model can be further utilized to investigate disease development, early diagnostic markers and interventions that interfere with microvascular remodeling in the field of

CTEPH research. Finally, this model may also be used to delineate sex-differences that are known to exist in development and progression of CTEPH (50).

Acknowledgements

The authors would like to acknowledge the technical support of Annemarie Verzijl, Ilona Krabbendam-Peters, Esther van de Kamp, Dylan van der Vusse, Brechje de Rapper and Paula Krul.

Table 3. Hemodynamics and blood gas values of swine at rest and during exercise at baseline (BL), after microspheres (AM) and at the end of follow-up (End).

			Rest				Exercise (km/h)											
							1			2			3			4		
HR	Control	BL	149	±	7		200	±	10	219	±	15	224	±	11	255	±	10
		AM	128	±	6		156	±	6 *	172	±	6 *	191	±	7	219	±	8 *
(beats/min)		End	128	±	6	*	153	±	7 *	169	±	7 *	195	±	12	211	±	12
	LNAME+	BL	158	±	7		191	±	11	200	±	10	221	±	12	253	±	9
	Spheres	AM	134	±	8		162	±	10	197	±	14	218	±	10	237	±	10
		End	129	±	7	*	157	±	7 *	175	±	10	187	±	15	209	±	5 *
MAP	Control	BL	88	±	2		94	±	2	92	±	3	92	±	3	92	±	2
		AM	90	±	4		97	±	3	101	±	4 *	102	±	4	105	±	4 *
(mmHg)		End	94	±	4		98	±	4	99	±	4 *	101	±	5 *	104	±	5 *
	LNAME+	BL	88	±	3		94	±	2	90	±	2	90	±	3	92	±	3
	Spheres	AM	103	±	4	*	109	±	6	113	±	6 *	115	±	5 *	113	±	5 *
		End	96	±	7		104	±	7	107	±	9	107	±	9	112	±	10
SVRi	Control	BL	463	±	22		368	±	17	357	±	13	325	±	14	320	±	26
		AM	550	±	31	*	485	±	29 *	456	±	24 *	425	±	21 *	395	±	20 *
(mmHg×		End	624	±	29	*	552	±	43 *	517	±	41 *	497	±	36 *	482	±	41 *
min/L/kg)	LNAME+	BL	340	±	29	†	299	±	25 †	272	±	24 †	257	±	24 †	246	±	14 †
	Spheres	AM	590	±	79	*	494	±	81	474	±	72 *	462	±	65 *	440	±	68 *
		End	892	±	283		917	±	357	890	±	340	562	±	79 *	554	±	79 *
LAP	Control	BL	6	±	1		8	±	1	8	±	1	9	±	2	12	±	2
		AM	4	±	1		7	±	1	7	±	1	7	±	1	9	±	1
(mmHg)		End	8	±	1		10	±	1	10	±	1	11	±	1	12	±	1

	LNAME+	BL	10	±	2	†	12	±	1	†	11	±	1		12	±	1		12	±	1	
	Spheres	AM	8	±	2		10	±	0		10	±	2		9	±	2		15	±	3	†
		End	9	±	2		10	±	3		10	±	3		13	±	3		17	±	4	
Hb	Control	BL	9.4	±	0.3		10.0	±	0.3		9.5	±	0.3		10.0	±	0.3		9.7	±	0.3	
		AM	9.5	±	0.3		9.8	±	0.3		10.2	±	0.3		10.1	±	0.4		10.5	±	0.4	
(g/dL)		End	10.0	±	0.4		10.2	±	0.4		10.8	±	0.4	*	10.9	±	0.4	*	11.1	±	0.4	*
	LNAME+	BL	9.1	±	0.4		9.2	±	0.3		9.5	±	0.3		9.3	±	0.3		9.6	±	0.3	
	Spheres	AM	8.9	±	0.3		9.2	±	0.3		9.7	±	0.4		10.0	±	0.5		10.1	±	0.6	
		End	9.2	±	0.3		9.8	±	0.2		9.8	±	0.2	*	10.3	±	0.3	*	10.6	±	0.4	
Lactate	Control	BL	0.7	±	0.0		0.9	±	0.1		0.9	±	0.2		1.2	±	0.3		1.9	±	0.3	
		AM	0.8	±	0.1		0.7	±	0.1		0.8	±	0.1		0.9	±	0.1		1.5	±	0.2	
(mmol/L)		End	0.7	±	0.1		0.7	±	0.1		0.7	±	0.1		0.7	±	0.1		1.4	±	0.3	
	LNAME+	BL	0.9	±	0.1		1.1	±	0.1		1.0	±	0.1		1.1	±	0.2		1.8	±	0.3	
	Spheres	AM	0.9	±	0.1		0.9	±	0.1		1.2	±	0.2		1.6	±	0.2	†	2.8	±	0.5	†
		End	0.7	±	0.1		0.9	±	0.1		0.9	±	0.1		1.2	±	0.2		2.4	±	1.0	
SO_{2art}	Control	BL	96	±	1		94	±	1		94	±	1		94	±	1		93	±	1	
		AM	98	±	0		97	±	0		97	±	1		97	±	0		97	±	1	
(%)		End	97	±	0		97	±	1		96	±	0		97	±	0		96	±	1	
	LNAME+	BL	97	±	1		93	±	1		94	±	2		94	±	2		93	±	1	
	Spheres	AM	95	±	1	†	91	±	2	†	89	±	2	†	91	±	2	†	91	±	1	†
		End	96	±	1		91	±	2	†	92	±	3		92	±	2		92	±	2	†

Data are presented as mean ± SEM. Control N = 12; LNAME+Spheres N = 6. † P < 0.05 vs corresponding Control; * P < 0.05 vs corresponding BL. HR, heart rate; MAP, mean arterial pressure; SVRi, systemic vascular resistance index; LAP, left atrial pressure; Hb, hemoglobin; SO_{2art}, arterial oxygen saturation.

References

1. **Aguero J, Ishikawa K, Fish KM, Hammoudi N, Hadri L, Garcia-Alvarez A, Ibanez B, Fuster V, Hajjar RJ, and Leopold JA**. Combination proximal pulmonary artery coiling and distal embolization induces chronic elevations in pulmonary artery pressure in Swine. *PLoS One* 10: e0124526, 2015.

2. **Alias S, Redwan B, Panzenbock A, Winter MP, Schubert U, Voswinckel R, Frey MK, Jakowitsch J, Alimohammadi A, Hobohm L, Mangold A, Bergmeister H, Sibilia M, Wagner EF, Mayer E, Klepetko W, Holzenbein TJ, Preissner KT, and Lang IM**. Defective angiogenesis delays thrombus resolution: a potential pathogenetic mechanism underlying chronic thromboembolic pulmonary hypertension. *Arterioscler Thromb Vasc Biol* 34: 810-819, 2014.

3. **Azarian R, Wartski M, Collignon MA, Parent F, Herve P, Sors H, and Simonneau G**. Lung perfusion scans and hemodynamics in acute and chronic pulmonary embolism. *J Nucl Med* 38: 980-983, 1997.

4. **Bender SB, van Houwelingen MJ, Merkus D, Duncker DJ, and Laughlin MH**. Quantitative analysis of exercise-induced enhancement of early- and late-systolic retrograde coronary blood flow. *Journal of applied physiology* 108: 507-514, 2010.

5. **Boulate D, Perros F, Dorfmuller P, Arthur-Ataam J, Guihaire J, Lamrani L, Decante B, Humbert M, Eddahibi S, Dartevelle P, Fadel E, and Mercier O**. Pulmonary microvascular lesions regress in reperfused chronic thromboembolic pulmonary hypertension. *J Heart Lung Transplant* 34: 457-467, 2015.

6. **Burrowes KS, Hunter PJ, and Tawhai MH**. Anatomically based finite element models of the human pulmonary arterial and venous trees including supernumerary vessels. *J Appl Physiol (1985)* 99: 731-738, 2005.

7. **Claessen G, La Gerche A, Dymarkowski S, Claus P, Delcroix M, and Heidbuchel H**. Pulmonary vascular and right ventricular reserve in patients with normalized resting hemodynamics after pulmonary endarterectomy. *J Am Heart Assoc* 4: e001602, 2015.

8. **Claessen G, La Gerche A, Wielandts JY, Bogaert J, Van Cleemput J, Wuyts W, Claus P, Delcroix M, and Heidbuchel H**. Exercise pathophysiology and sildenafil effects in chronic thromboembolic pulmonary hypertension. *Heart* 101: 637-644, 2015.

9. **Datta D, Normandin E, and ZuWallack R**. Cardiopulmonary exercise testing in the assessment of exertional dyspnea. *Annals of thoracic medicine* 10: 77-86, 2015.

10. **de Beer VJ, de Graaff HJ, Hoekstra M, Duncker DJ, and Merkus D**. Integrated control of pulmonary vascular tone by endothelin and angiotensin II in exercising swine depends on gender. *American journal of physiology Heart and circulatory physiology* 298: H1976-1985, 2010.

11. **Duncker DJ, and Bache RJ**. Regulation of coronary blood flow during exercise. *Physiological reviews* 88: 1009-1086, 2008.

12. **Duncker DJ, Stubenitsky R, and Verdouw PD**. Autonomic control of vasomotion in the porcine coronary circulation during treadmill exercise: evidence for feed-forward beta-adrenergic control. *Circulation research* 82: 1312-1322, 1998.

13. **Fedullo PF, Auger WR, Kerr KM, and Rubin LJ**. Chronic thromboembolic pulmonary hypertension. *N Engl J Med* 345: 1465-1472, 2001.

14. **Gopalan D, Delcroix M, and Held M**. Diagnosis of chronic thromboembolic pulmonary hypertension. *Eur Respir Rev* 26: 2017.

15. **Gross DR**. *Animal Models in Cardiovascular Research*. Springer, 2009.

16. **Guihaire J, Haddad F, Boulate D, Capderou A, Decante B, Flecher E, Eddahibi S, Dorfmuller P, Herve P, Humbert M, Verhoye JP, Dartevelle P, Mercier O, and Fadel E**. Right ventricular plasticity in a porcine model of chronic pressure overload. *J Heart Lung Transplant* 33: 194-202, 2014.

17. **Guihaire J, Haddad F, Noly PE, Boulate D, Decante B, Dartevelle P, Humbert M, Verhoye JP, Mercier O, and Fadel E**. Right ventricular reserve in a piglet model of chronic pulmonary hypertension. *Eur Respir J* 45: 709-717, 2015.

18. **Haitsma DB, Bac D, Raja N, Boomsma F, Verdouw PD, and Duncker DJ**. Minimal impairment of myocardial blood flow responses to exercise in the remodeled left ventricle early after myocardial infarction, despite significant hemodynamic and neurohumoral alterations. *Cardiovascular research* 52: 417-428, 2001.

19. **Hasler ED, Muller-Mottet S, Furian M, Saxer S, Huber LC, Maggiorini M, Speich R, Bloch KE, and Ulrich S**. Pressure-Flow During Exercise Catheterization Predicts Survival in Pulmonary Hypertension. *Chest* 150: 57-67, 2016.

20. **Held M, Grun M, Holl R, Hubner G, Kaiser R, Karl S, Kolb M, Schafers HJ, Wilkens H, and Jany B**. Cardiopulmonary exercise testing to detect chronic thromboembolic pulmonary hypertension in patients with normal echocardiography. *Respiration* 87: 379-387, 2014.

21. **Held M, Hesse A, Gott F, Holl R, Hubner G, Kolb P, Langen HJ, Romen T, Walter F, Schafers HJ, Wilkens H, and Jany B**. A symptom-related monitoring program following pulmonary embolism for the early detection of CTEPH: a prospective observational registry study. *BMC Pulm Med* 14: 141, 2014.

22. **Heusch G**. The paradox of alpha-adrenergic coronary vasoconstriction revisited. *J Mol Cell Cardiol* 51: 16-23, 2011.

23. **Hoeper MM, Mayer E, Simonneau G, and Rubin LJ**. Chronic thromboembolic pulmonary hypertension. *Circulation* 113: 2011-2020, 2006.

24. **Huang W, Yen RT, McLaurine M, and Bledsoe G**. Morphometry of the human pulmonary vasculature. *Journal of applied physiology* 81: 2123-2133, 1996.

25. **Iwase T, Nagaya N, Ando M, Satoh T, Sakamaki F, Kyotani S, Takaki H, Goto Y, Ohkita Y, Uematsu M, Nakanishi N, and Miyatake K**. Acute and chronic effects of surgical thromboendarterectomy on exercise capacity and ventilatory efficiency in patients with chronic thromboembolic pulmonary hypertension. *Heart* 86: 188-192, 2001.

26. **Kim H, Yung GL, Marsh JJ, Konopka RG, Pedersen CA, Chiles PG, Morris TA, and Channick RN**. Endothelin mediates pulmonary vascular remodelling in a canine model of chronic embolic pulmonary hypertension. *Eur Respir J* 15: 640-648, 2000.

27. **Laughlin MH, Davis MJ, Secher NH, van Lieshout JJ, Arce-Esquivel AA, Simmons GH, Bender SB, Padilla J, Bache RJ, Merkus D, and Duncker DJ**. Peripheral circulation. *Comprehensive Physiology* 2: 321-447, 2012.

28. **Lautt WW**. Resistance or conductance for expression of arterial vascular tone. *Microvascular research* 37: 230-236, 1989.

29. **Lee YC, Clark AR, Fuld MK, Haynes S, Divekar AA, Hoffman EA, and Tawhai MH**. MDCT-based quantification of porcine pulmonary arterial morphometry and self-similarity of arterial branching geometry. *J Appl Physiol (1985)* 114: 1191-1201, 2013.

30. **Matthews DT, and Hemnes AR**. Current concepts in the pathogenesis of chronic thromboembolic pulmonary hypertension. *Pulm Circ* 6: 145-154, 2016.

31. **McCabe C, Deboeck G, Harvey I, Ross RM, Gopalan D, Screaton N, and Pepke-Zaba J**. Inefficient exercise gas exchange identifies pulmonary hypertension in chronic thromboembolic obstruction following pulmonary embolism. *Thromb Res* 132: 659-665, 2013.

32. **Mercier O, Sage E, Izziki M, Humbert M, Dartevelle P, Eddahibi S, and Fadel E**. Endothelin A receptor blockade improves regression of flow-induced pulmonary vasculopathy in piglets. *The Journal of thoracic and cardiovascular surgery* 140: 677-683, 2010.

33. **Mercier O, Tivane A, Dorfmuller P, de Perrot M, Raoux F, Decante B, Eddahibi S, Dartevelle P, and Fadel E**. Piglet model of chronic pulmonary hypertension. *Pulm Circ* 3: 908-915, 2013.

34. **Merkus D, and Duncker DJ**. Perspectives: Coronary microvascular dysfunction in post-infarct remodelled myocardium. *European Heart Journal Supplements* 16: A74-A79, 2014.

35. **Merkus D, Houweling B, van den Meiracker AH, Boomsma F, and Duncker DJ**. Contribution of endothelin to coronary vasomotor tone is abolished after myocardial infarction. *American journal of physiology Heart and circulatory physiology* 288: H871-880, 2005.

36. **Merkus D, Visser M, Houweling B, Zhou Z, Nelson J, and Duncker DJ**. Phosphodiesterase 5 inhibition-induced coronary vasodilation is reduced after myocardial infarction. *American journal of physiology Heart and circulatory physiology* 304: H1370-1381, 2013.

37. **Moser KM, and Bloor CM**. Pulmonary vascular lesions occurring in patients with chronic major vessel thromboembolic pulmonary hypertension. *Chest* 103: 685-692, 1993.

38. **Moser KM, Cantor JP, Olman M, Villespin I, Graif JL, Konopka R, Marsh JJ, and Pedersen C**. Chronic pulmonary thromboembolism in dogs treated with tranexamic acid. *Circulation* 83: 1371-1379, 1991.

39. **Neto-Neves EM, Brown MB, Zaretskaia MV, Rezania S, Goodwill AG, McCarthy BP, Persohn SA, Territo PR, and Kline JA**. Chronic Embolic Pulmonary Hypertension Caused by Pulmonary Embolism and Vascular Endothelial Growth Factor Inhibition. *Am J Pathol* 187: 700-712, 2017.

40. **Pereda D, Garcia-Alvarez A, Sanchez-Quintana D, Nuno M, Fernandez-Friera L, Fernandez-Jimenez R, Garcia-Ruiz JM, Sandoval E, Aguero J, Castella M, Hajjar RJ, Fuster V, and Ibanez B**. Swine model of chronic postcapillary pulmonary hypertension with right ventricular remodeling: long-term characterization by cardiac catheterization, magnetic resonance, and pathology. *Journal of cardiovascular translational research* 7: 494-506, 2014.

41. **Perkett EA, Brigham KL, and Meyrick B**. Continuous air embolization into sheep causes sustained pulmonary hypertension and increased pulmonary vasoreactivity. *Am J Pathol* 132: 444-454, 1988.

42. **Pohlmann JR, Akay B, Camboni D, Koch KL, Mervak BM, and Cook KE**. A low mortality model of chronic pulmonary hypertension in sheep. *J Surg Res* 175: 44-48, 2012.

43. **Quarck R, Wynants M, Ronisz A, Sepulveda MR, Wuytack F, Van Raemdonck D, Meyns B, and Delcroix M**. Characterization of proximal pulmonary arterial cells from chronic thromboembolic pulmonary hypertension patients. *Respir Res* 13: 27, 2012.

44. **Rehman MB, Howard LS, Christiaens LP, Gill D, Gibbs JS, and Nihoyannopoulos P**. Resting right ventricular function is associated with exercise performance in PAH, but not in CTEPH. *Eur Heart J Cardiovasc Imaging* 2017.

45. **Rendas A, Branthwaite M, and Reid L**. Growth of pulmonary circulation in normal pig--structural analysis and cardiopulmonary function. *J Appl Physiol Respir Environ Exerc Physiol* 45: 806-817, 1978.

46. **Richter MJ, Pader P, Gall H, Reichenberger F, Seeger W, Mayer E, Guth S, Kramm T, Grimminger F, Ghofrani HA, and Voswinckel R**. The prognostic relevance of oxygen uptake in inoperable chronic thromboembolic pulmonary hypertension. *Clin Respir J* 2015.

47. **Rothman A, Wiencek RG, Davidson S, Evans WN, Restrepo H, Sarukhanov V, and Mann D**. Challenges in the development of chronic pulmonary hypertension models in large animals. *Pulm Circ* 7: 156-166, 2017.

48. **Sage E, Mercier O, Herve P, Tu L, Dartevelle P, Eddahibi S, and Fadel E**. Right lung ischemia induces contralateral pulmonary vasculopathy in an animal model. *J Thorac Cardiovasc Surg* 143: 967-973, 2012.

49. **Shelub I, van Grondelle A, McCullough R, Hofmeister S, and Reeves JT**. A model of embolic chronic pulmonary hypertension in the dog. *J Appl Physiol Respir Environ Exerc Physiol* 56: 810-815, 1984.

50. **Shigeta A, Tanabe N, Shimizu H, Hoshino S, Maruoka M, Sakao S, Tada Y, Kasahara Y, Takiguchi Y, Tatsumi K, Masuda M, and Kuriyama T**. Gender differences in chronic thromboembolic pulmonary hypertension in Japan. *Circ J* 72: 2069-2074, 2008.

51. **Simonneau G, Torbicki A, Dorfmuller P, and Kim N**. The pathophysiology of chronic thromboembolic pulmonary hypertension. *Eur Respir Rev* 26: 2017.

52. **Skoro-Sajer N, Mittermayer F, Panzenboeck A, Bonderman D, Sadushi R, Hitsch R, Jakowitsch J, Klepetko W, Kneussl MP, Wolzt M, and Lang IM**. Asymmetric dimethylarginine is increased in chronic thromboembolic pulmonary hypertension. *Am J Respir Crit Care Med* 176: 1154-1160, 2007.

53. **Spinale FG, Hendrick DA, Crawford FA, Smith AC, Hamada Y, and Carabello BA**. Chronic supraventricular tachycardia causes ventricular dysfunction and subendocardial injury in swine. *The American journal of physiology* 259: H218-229, 1990.

54. **Stubenitsky R, Verdouw PD, and Duncker DJ**. Autonomic control of cardiovascular performance and whole body O2 delivery and utilization in swine during treadmill exercise. *Cardiovasc Res* 39: 459-474, 1998.

55. **Tang CX, Yang GF, Schoepf UJ, Han ZH, Qi L, Zhao YE, Wu J, Zhou CS, Zhu H, Stubenrauch AC, Mangold S, Zhang LJ, and Lu GM**. Chronic thromboembolic pulmonary hypertension: Comparison of dual-energy computed tomography and single photon emission computed tomography in canines. *Eur J Radiol* 85: 498-506, 2016.

56. **Tsuboi Y, Tanaka H, Nishio R, Sawa T, Terashita D, Nakayama K, Satomi-Kobayashi S, Sakai Y, Emoto N, and Hirata KI**. Associations of Exercise Tolerance With Hemodynamic Parameters for Pulmonary Arterial Hypertension and for Chronic Thromboembolic Pulmonary Hypertension. *J Cardiopulm Rehabil Prev* 37: 341-346, 2017.

57. **Tune JD, Gorman MW, and Feigl EO**. Matching coronary blood flow to myocardial oxygen consumption. *Journal of applied physiology* 97: 404-415, 2004.

58. **van den Heuvel M, Sorop O, Koopmans SJ, Dekker R, de Vries R, van Beusekom HM, Eringa EC, Duncker DJ, Danser AH, and van der Giessen WJ**. Coronary microvascular dysfunction in a porcine model of early atherosclerosis and diabetes. *American journal of physiology Heart and circulatory physiology* 302: H85-94, 2012.

59. **Vatner SF, and Braunwald E**. Cardiovascular control mechanisms in the conscious state. *The New England journal of medicine* 293: 970-976, 1975.

60. **Weimann J, Zink W, Schnabel PA, Jakob H, Gebhard MM, Martin E, and Motsch J**. Selective vasodilation by nitric oxide inhalation during sustained pulmonary hypertension following recurrent microembolism in pigs. *J Crit Care* 14: 133-140, 1999.

61. **White FC, McKirnan MD, Breisch EA, Guth BD, Liu YM, and Bloor CM**. Adaptation of the left ventricle to exercise-induced hypertrophy. *J Appl Physiol (1985)* 62: 1097-1110, 1987.

62. **Yarbrough WM, and Spinale FG**. Large animal models of congestive heart failure: a critical step in translating basic observations into clinical applications. *Journal of nuclear cardiology : official publication of the American Society of Nuclear Cardiology* 10: 77-86, 2003.

63. **Zhou X, Wang D, Castro CY, Hawkins H, Lynch JE, Liu X, and Zwischenberger JB**. A pulmonary hypertension model induced by continuous pulmonary air embolization. *J Surg Res* 170: e11-16, 2011.

64. **Zhou Z, de Beer VJ, Bender SB, Jan Danser AH, Merkus D, Laughlin MH, and Duncker DJ**. Phosphodiesterase-5 activity exerts a coronary vasoconstrictor influence in awake swine that is mediated in part via an increase in endothelin production. *American journal of physiology Heart and circulatory physiology* 306: H918-927, 2014.

65. **Zhou Z, de Beer VJ, de Wijs-Meijler D, Bender SB, Hoekstra M, Laughlin MH, Duncker DJ, and Merkus D**. Pulmonary vasoconstrictor influence of endothelin in exercising swine depends critically on phosphodiesterase 5 activity. *Am J Physiol Lung Cell Mol Physiol* 306: L442-452, 2014.

Chapter 4

Validation of 4D flow MRI against invasive measurements – a swine study

Kelly Stam, Raluca G Chelu, Nikki van der Velde, Richard van Duin, Piotr Wielopolski, Koen Nieman, Daphne Merkus, Alexander Hirsch

Int J Cardiovasc Imaging 2019 Apr 8

Abstract

Purpose

The purpose of this study was to compare invasively measured aorta flow with 2D phase contrast flow and 4D flow measurements by cardiovascular magnetic resonance (CMR) imaging in a large animal model.

Methods

Nine swine (mean weight 63±4 kilograms) were included in the study. 4D flow CMR exams were performed on a 1.5T MRI scanner. Flow measurements were performed on 4D flow images at the aortic valve level, in the ascending aorta, and main pulmonary artery. Simultaneously, flow was measured using an invasive flow probe, placed around the ascending aorta. Additionally, standard 2D phase contrast flow and 2D left ventricular (LV) volumetric data were used for comparison.

Results

The correlations of cardiac output (CO) between the invasive flow probe, and CMR modalities were strong to very strong. CO measured by 4D flow CMR correlated better with the CO measured by the invasive flow probe than 2D flow CMR flow and volumetric LV data (4D flow CMR: Spearman's rho 0.86 at the aortic valve level and 0.90 at the ascending aorta level; 2D flow CMR: 0.67 at aortic valve level; LV measurements: 0.77). In addition, there tended to be a correlation between mean pulmonary artery flow and aorta flow with 4D flow (Spearman's rho=0.65, P=0.07), which was absent in measurements obtained with 2D flow CMR (Spearman's rho=0.40, P=0.33).

Conclusion

This study shows that aorta flow can be accurately measured by 4D flow CMR compared to simultaneously measured invasive flow. This helps to further validate the quantitative reliability of this technique.

Introduction

Cardiovascular magnetic resonance (CMR) imaging has been used for flow visualization and quantification in daily clinical practice for several decades. (15, 21) CMR is the gold standard for non-invasive quantification of left and especially right heart function and shunt fraction. (20, 22) Nowadays, standard imaging protocols consists of the acquisition of cine imaging and 2D phase contrast flow measurements in multiple planes using numerous breath-holds. Especially, in complex congenital heart disease patients this can be challenging and time consuming.

A promising and rapidly evolving CMR technique is 4D flow imaging: a volumetric, free-breathing acquisition technique of flow velocity data with simultaneous assessment of anatomic structures. (24) 4D flow CMR allows flow quantification at any level within the acquired field of view and calculation of cardiac volumes and biventricular function. (10, 13) Until now, several studies have evaluated the use of 4D flow CMR for visualization and quantification of cardiac shunts. (4, 11, 14, 23) 4D flow CMR was previously validated against echocardiography (5) and standard 2D flow CMR in humans (6, 12). In addition, the 4D flow determined pulmonary vascular resistance was validated against in vivo measurements in a canine study. (16)

In this study, we sought to validate this promising 4D flow CMR technique by direct, simultaneous comparison with 2D flow CMR and invasive flow measurements using a validated flow probe positioned around the ascending aorta in a large animal model.

Methods

Study design

Studies were performed in accordance with the "Guiding Principles in the Care and Use of Laboratory Animals" as approved by the Council of the American Physiological Society, and with approval of the Animal Care Committee of the Erasmus Medical Center Rotterdam (3158, 109-13-09). Nine Yorkshire x Landrace swine (5-6 months old, 21 ± 1 kg at the time of surgery, 63 ± 4 kg at the time of the CMR scan) of either sex were included in the study. The swine included in this study were part of previously published studies. (17, 18)

Chronic instrumentation of the swine

The swine were chronically catheterized for hemodynamic monitoring approximately two to three months prior to the scanning procedure. Surgical details have been extensively described previously. (7) In short, swine were sedated with an intramuscular injection of tiletamine/zolazepam (5 mg/kg), xylazine (2.25 mg/kg) and atropine (1 mg), intubated and ventilated with a mixture of O2 and N2 (1:2 v/v) to which 2% (v/v) isoflurane was added to maintain anesthesia. Under sterile conditions, the chest was opened via a left thoracotomy in the fourth intercostal space and fluid-filled polyvinylchloride catheters (B Braun Medical Inc., Bethlehem, PA, USA) were placed in the right ventricle, pulmonary artery, aorta and left atrium. A flow probe (Transonic Systems Inc., Ithaca, NY, USA) was positioned around the ascending aorta for measurement of aorta flow. The catheters were tunneled to the back and animals received analgesia (0.015 mg/kg buprenorphine i.m. and a slow-release fentanyl patch 12 µg/h for 48 hours) on the day of the surgery and daily antibiotic prophylaxis (25 mg/kg amoxicillin i.v.) for 7 days.

CTEPH induction

CTEPH was induced in awake state as describe previously (17). In short, following the recovery week, on the first day, the CTEPH animals (n=6), were given the eNOS-inhibitor L-N^{ω}-Nitroarginine methyl ester (LNAME) (10 mg/kg i.v., Enzo Life Sciences International Inc, NY, USA) as a bolus infusion which was increased by 10 mg/kg per day up to 30 mg/kg i.v., which was maintained until 2 weeks before the end of the study. Four days after the start of LNAME administration, microsphere infusions were started. Polyethylene microspheres (diameter 600-710 µm, density 1.13 g/cm^3, 500 mg, corresponding to ~2500 microspheres, Cospheric LLC, Santa Barbara, California, US) were suspended in 50 mL autologous blood with 2500 I.U. heparin and slowly infused into the right ventricle over 10 minutes while monitoring mean pulmonary artery pressure (PAP). Microsphere infusions were repeated until the PAP reached ~60 mmHg, or the arterial P_aO_2 dropped below ~40 mmHg, as measured 30 min after infusion at rest, or when a maximum of 3 gram (~15000) microspheres was infused on one day. In the subsequent four weeks, hemodynamics were weekly assessed, and microsphere infusions were repeated when PAP was <25 mmHg and P_aO2 >70 mmHg, as described above. During the final 5 weeks of follow-up, no microsphere infusions were performed.

The control animals (n=4) were healthy chronically instrumented swine.

CMR protocol

CMR examination was performed on a 1.5T clinical scanner with a dedicated receive-only 32-channel phased-array cardiac surface coil (Discovery MR450, GE Healthcare, Milwaukee, WI, USA). The animals were sedated, and intubated as described above. Anesthesia during imaging was maintained with pentobarbital sodium (6-12 mg/kg/h). Mechanical ventilation and breath-holds were performed

using a mobile ventilator (Carina™, Dräger Medical, Best, The Netherlands). Heart rate and blood pressures were monitored throughout the scan. When necessary, and always in absence of pain reflexes, muscle relaxation was achieved using pancuronium bromide (2–4 mg bolus). The image protocol consisted of 2D balanced Steady-State Free Precession (SSFP) cine imaging, 4D flow, and 2D phase contrast flow measurements. Standard long-axis and short-axis images with full left ventricular (LV) coverage were acquired using retrospectively ECG-gated SSFP cine imaging with breath-holding (FIESTA, GE Healthcare acronym). Typical scan parameters were slice thickness 6.0 mm, slice gap 0 mm, TR/TE 3.4/1.4 ms, flip angle (FA) 75°, field of view (FOV) 320×240 mm, acquired matrix 128×180, and reconstructed to a pixel size of 1.3x1.3 mm. The free-breathing, retrospectively ECG-gated 4D flow acquisition was performed directly after administration of a gadolinium-based contrast agent (Gadovist 1,0 mmol/mL, Bayer, Mijdrecht, The Netherlands, single dose of up to 15 mL). The 4D flow sequence has been described before (4-6), in short the sequence was prescribed in axial plane, including the entire thorax in the field of view. The k-space was filled with variable-density Poisson-disc undersampling with acceleration factors of 1.8×1.8 (phase x slice) and the parallel imaging algorithm used was ESPIRiT. The following imaging parameters were used: matrix 192x160x78, acquired resolution 2.1x1.7x2.8 mm, reconstructed resolution 2.1x1.7x1.4 mm, TR/TE 3.8/1.5 ms, FA 15°, views per segment 4, bandwidth 63kHz, number of reconstructed phases 20 per cardiac cycle, and a velocity encoded value set at 250 cm/s. Scan time ranged between 5.57 and 8.51 minutes. Finally, one-directional through plane 2D phase contrast flow measurements of the aorta (at the level of the aortic valve or just above) and pulmonary artery were performed during an end-expiratory breath-hold. The imaging planes were planned perpendicular to the great vessels. Typical scan parameters were slice thickness 6.0 mm, matrix 256x166, TR/TE 4.0/2.2 ms,

FA 18°, FOV 340x220, velocity encoding value set at 180 cm/s. The invasive flow probe was attached to the amplifier and a flow signal was obtained immediately before and after the 4D flow CMR sequence.

Post-processing and data analysis

To assess left ventricular volumes, endocardial contours were drawn manually on end-diastolic and end-systolic 2D short axis SSFP cine images, and stroke volume and ejection fraction were calculated. No substantial mitral regurgitation was visually noted on CMR in any of the animals, therefore stroke volume (mL/beat) and cardiac output (CO, L/min) of the left ventricle were also compared to invasive measurements. To analyze the 2D phase contrast images a region of interest was manually traced around the aorta and pulmonary valve. Both 2D flow CMR and left ventricular function were analyzed with Medis software (QMass and QFlow analytical software version 8.1, Medis, Leiden, The Netherlands).

The 4D flow data were analyzed using a dedicated cloud-based post-processing software (ArterysInc, San Francisco, CA, USA). Semi-automatic eddy-current correction was applied. (6) Data were visualized, and flow quantification was performed at the level of aortic valve and at the level of the sinotubular junction/proximal part of the ascending aorta below the flow probe. Also the pulmonary flow was determined by measuring in the main pulmonary artery (MPA). For both 2D and 4D flow shunt fractions (Qp/Qs) were calculated.

Digital recording and offline analysis of heart rate (HR) and aorta flow were performed with MatLab (MathWorks, Natick, MA, USA) and have been described in detail elsewhere. (8, 19)Briefly, HR and aorta flow were analyzed offline using a proprietary program written in MatLab. Over at least 10 consecutive seconds, both before and after the 4D flow CMR sequence, CO and SV

were determined from each individual beat and averaged. HR was calculated as the ratio of the number of beats and time. The end-diastolic time point was used to align the (average) phasic flow signals obtained with the different methods.

All measurements were performed independently from each other (2D flow and left ventricular function measurements by NvdV and AH, 4D flow CMR by RC, and invasive flow probe measurements by KS).

Statistics

Statistical analysis was performed with SPSS software version 21 (IBM, New York, US) and Graphpad Prism 4 Project (San Diego, CA, US). Correlation between measurements was evaluated using Spearman's (rho) coefficient for nonparametric data, and agreement was analyzed with Bland-Altman plots. The Spearman rho coefficient was classified as "very weak" for values of 0.00–0.19, "weak" for 0.20–0.39, "moderate" for 0.40–0.59, "strong" for 0.60–0.79 and "very strong" for 0.80–1.0. (1, 4)

Results

A total of nine animals were scanned, but not all animals were included in every method of CO determination: two animals had a malfunctioning invasive flow probe, in all nine animals CO could be determined with 4D flow CMR at the level of the aortic valve, while susceptibility artefacts from the invasive flow probe precluded measurement of CO at the ascending aorta level in two animals. Finally, one animal was excluded due to technical problems for measurement of CO with 2D flow CMR as well as LV functional measurements. Typical examples of the 4D flow CMR images and measurements are shown in Figure 1 and supplemental video's.

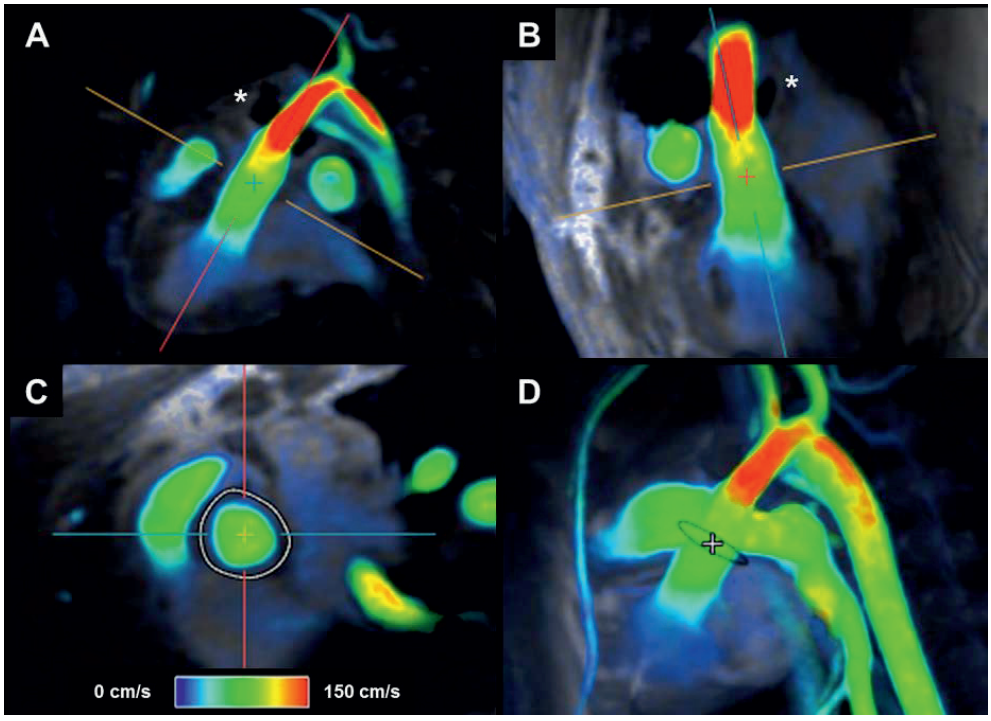

Figure 1. Example of 4D flow CMR images and measurement.

Example of 4D flow CMR with a flow measurement in the ascending aorta. The magnitude images are shown with a color velocity overlay (red: velocity >150 cm/s). (A) 3 chamber view (online supplementary file 1 for movie), (B) coronal view, (C) corresponding short-axis view of the aorta with tracing for flow measurement, and (D) overview of both aortic and pulmonary flow (online supplementary file 2 for movie). (*) susceptibility artefacts from the invasive flow probe around the ascending aorta.

Table 1. Summary of flow measurements with the different methods.

Method		Mean ± SD	n	Spearman's rho*	Bland-Altman	
					Bias	±1.96 SD
Invasive flow probe	Heart rate (beats/min)	98 ± 16	7			
	SV ascending aorta (mL/beat)	62 ± 15	7			
	CO ascending aorta (L/min)	5.0 ± 1.2	7			
4D flow CMR	Heart rate (beats/min)	98 ± 16	9			
	SV aortic valve (mL/beat)	62 ± 14	9	0.86	-8	-23 to 6
	CO aortic valve (L/min)	6.0 ± 1.4	9	0.86	-0.8	-2.1 to 0.5
	SV ascending aorta (mL/beat)	56 ± 17	7	1.00	-7	-20 to 6
	CO ascending aorta (L/min)	5.6 ± 1.5	7	0.90	-0.6	-1.8 to 0.6
	SV MPA (mL/beat)	58 ± 15	9			
	CO MPA (L/beat)	5.6 ± 1.3	9			
	Qp:Qs	0.9 ± 0.1	9			

2D flow CMR	Heart rate aortic valve (beats/min)	99 ± 20	8			
	SV aortic valve (mL/beat)	62 ± 17	8	0.71	-12	-40 to 16
	CO aortic valve (L/min)	5.9 ± 1.4	8	0.67	-1.1	-3.7 to 1.5
	Heart rate MPA (beats/min)	102 ± 24	8			
	SV MPA (mL/beat)	54 ± 21	8	0.60	-3	-32 to 27
	CO MPA (L/min)	5.1 ± 1.5	8	0.81	-0.4	-2.7 to 2.0
	Qp:Qs	0.9 ± 0.3	8	0.10	0.0	-0.6 to 0.5
Left ventricular parameters	Heart rate (beats/min)	103 ± 29	8			
	End-diastolic volume (mL)	138 ± 32	8			
	End-systolic volume (mL)	75 ± 25	8			
	Ejaction fraction (%)	46 ± 9	8			
	SV (mL/beat)	63 ± 16	8	0.94	-12	-28 to 4
	CO (L/min)	6.3 ± 1.4	8	0.77	-1.3	-3.3 to 0.6

*** Invasive flow probe measurements are taken as reference for the aortic flow measurements; 4D flow CMR measurements are taken as reference for the main pulmonary artery and Qp:Qs measurements. MPA=main pulmonary artery; SV=Stroke volume; CO=cardiac output.**

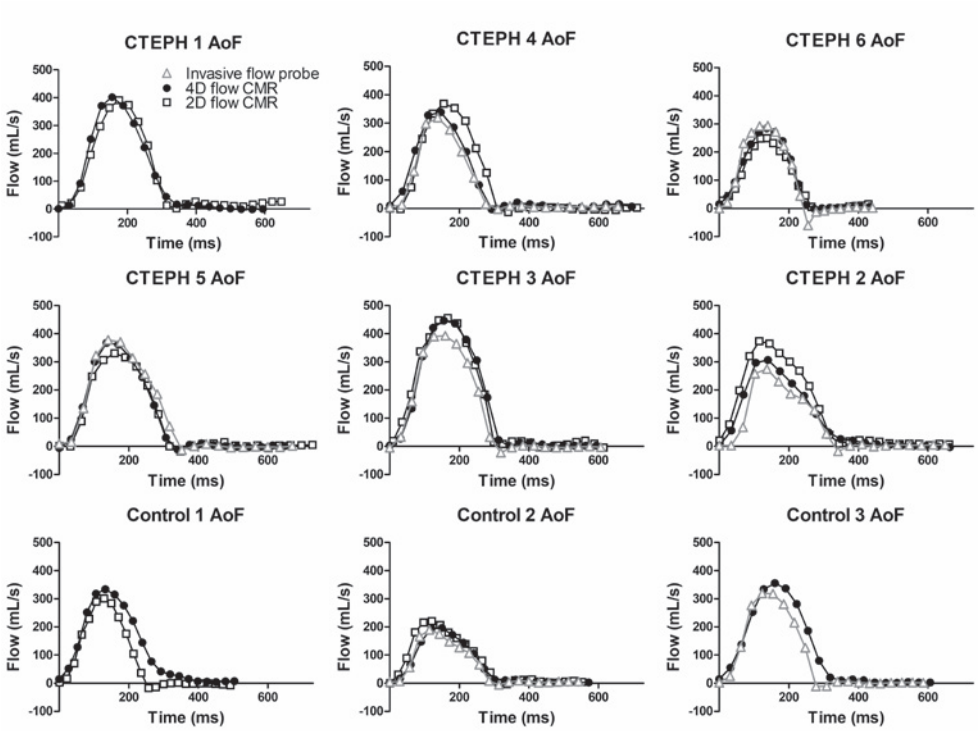

Figure 2. Individual aorta flow curves per heartbeat.

Individual aorta flow curves per heartbeat of the invasive flow probe, 4D flow CMR (measured at level of the aortic valve), and 2D flow CMR superimposed per animal. 2D flow CMR measurements of Control 3 and invasive flow probe measurements of CTEPH 1 and Control 1 are missing due to technical problems. CTEPH animals are ordered on disease severity, CTEPH 1 presented with the most severe PH and CTEPH 6 with the mildest.

The shape of the individual aorta flow patterns measured by all three methods showed good agreement and individual flow curves per animal are depicted in Figure 2. Indeed, the correlation between the CO measured by the invasive flow probe and 4D flow CMR was very strong (Spearman's rho=0.86 at the aortic valve level and 0.90 at the ascending aorta level) (Table 1 and Figure 3). Relative to the invasive flow probe measurements, the flow measured by 4D flow CMR was overestimated by 0.8 L/min at the aortic valve level and by 0.6 L/min at the ascending aorta level (Bland-Altman, Table 1 and Figure 3). The correlation between the invasive flow probe and 2D flow CMR and volumetric LV measurements were strong (2D flow CMR: Spearman's rho=0.67 and volumetric LV measurements: Spearman's rho=0.77). Relative to the invasive flow probe measurements, the flow measured by 2D flow CMR was overestimated by 1.1 L/min and by 1.3 L/min with the LV parameters (Bland-Altman, Table 1 and Figure 2).

The shape of the individual pulmonary flow patterns measured by 4D flow CMR and 2D flow CMR showed good agreement and individual flow curves per animal are depicted in Figure 4. The correlation between the 4D flow CMR and 2D flow CMR MPA CO measurement was very strong (Spearman's rho=0.81) (Table 1). Relative to the 4D flow CMR measurements, the MPA CO measured by 2D flow CMR was underestimated by 0.4 L/min. Although the correlation between MPA and aorta flow at the aortic valve level as measured with 4D flow CMR only tended to be significant (Spearman's rho=0.65, P=0.07), no correlation was found between MPA and aorta flow measured with 2D flow CMR (Spearman's rho=0.40, P=0.33) (Figure 5).

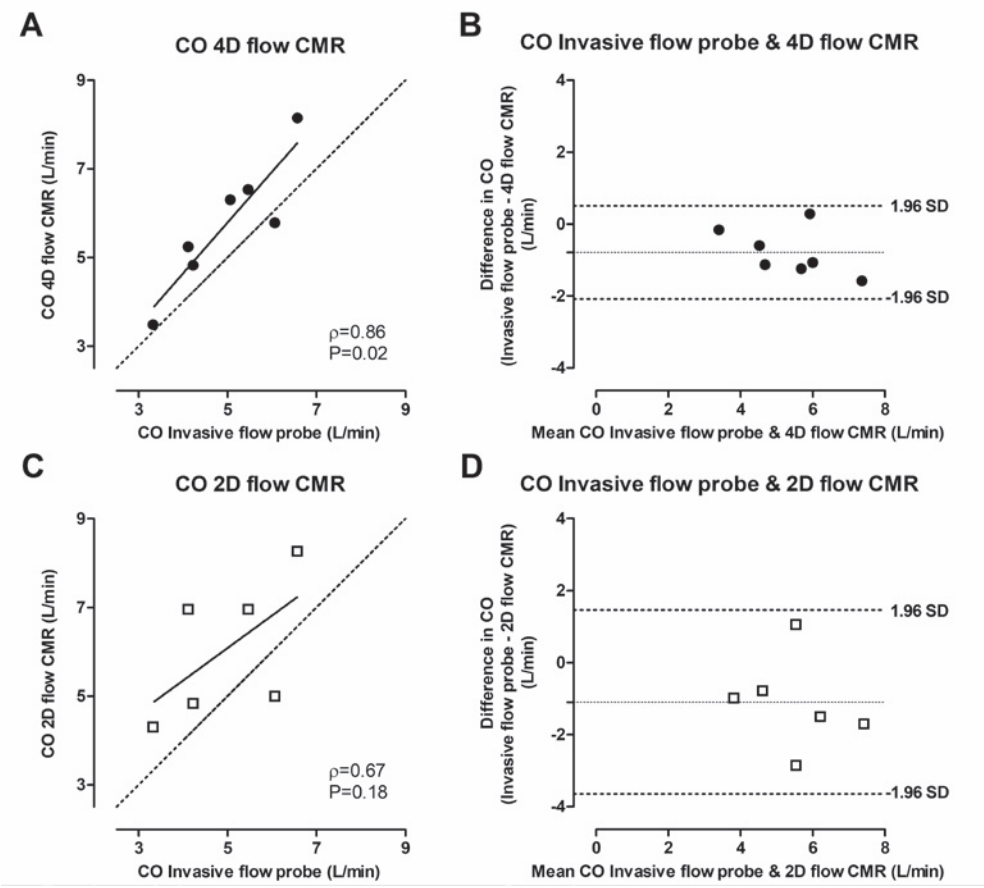

Figure 3. Comparison of cardiac output in the aorta measured by the invasive flow probe, 4D flow and 2D flow CMR.

Correlation between the invasive flow probe, 4D flow CMR (A, n=7), and 2D flow CMR (C, n=6) measurements of the aortic flow. Line of identity is indicated as the dotted line and Spearman's rho (ρ) and P-value are indicated in the legends (A&C). Bland-Altman plots of the cardiac output (CO), with the mean, 1.96 standard deviation (SD) and -1.96 SD lines indicated as the dotted lines. (B) invasive flow probe and 4D flow CMR measurements (n=7), and (D) invasive flow probe and 2D flow CMR measurements (n=6).

To investigate any differences in flow between the CTEPH and Control animals, and investigate any differences in flow through the aorta and pulmonary artery, we superimposed the MPA and aorta flow pattern measured by 4D flow CMR of each animal (Figure 6). In this figure, the CTEPH animals were ordered by disease

severity, in which CTEPH 1 was most affected and CTEPH 6 presented with the mildest PH. Although the MPA and aorta flow were almost perfectly aligned in the control animals while the peak MPA flow appears to be decreased compared to the peak aorta flow in the CTEPH animals, this is not significantly different. In addition, the flow pattern appears to be more elongated in the control animals when compared to the more steep, sharp flow pattern of the CTEPH animals, but this is also not significantly different.

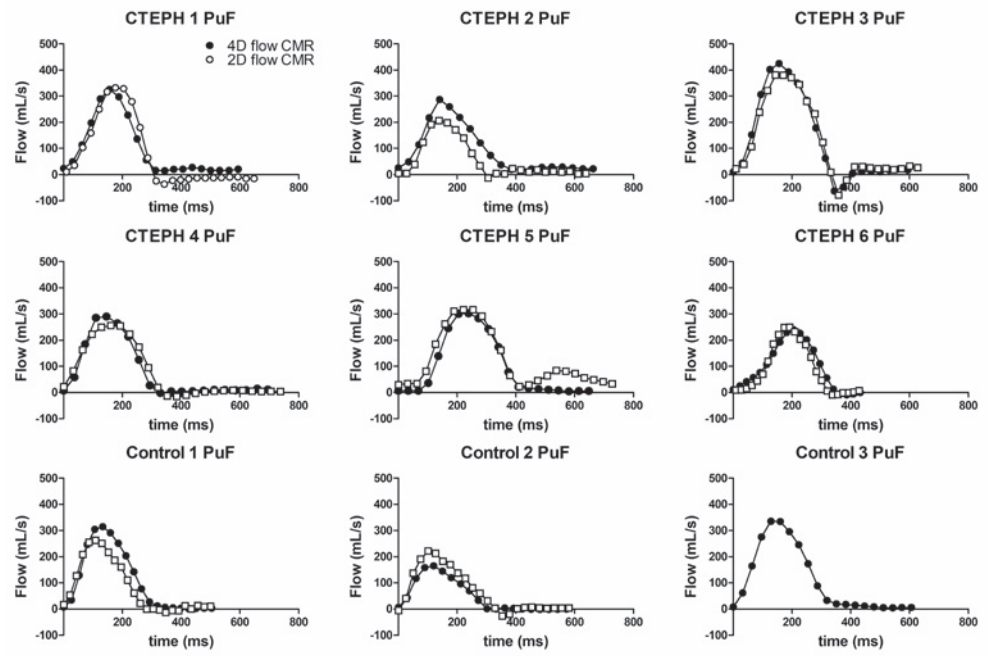

Figure 4. Individual pulmonary artery flow curves per heartbeat.

Individual Pulmonary Flow (PuF) curves per heartbeat of 4D flow and 2D flow CMR superimposed per animal. 2D flow CMR measurements of Control 3 are missing due to technical problems. CTEPH animals are ordered on disease severity, CTEPH 1 presented with the most severe PH and CTEPH 6 with the mildest.

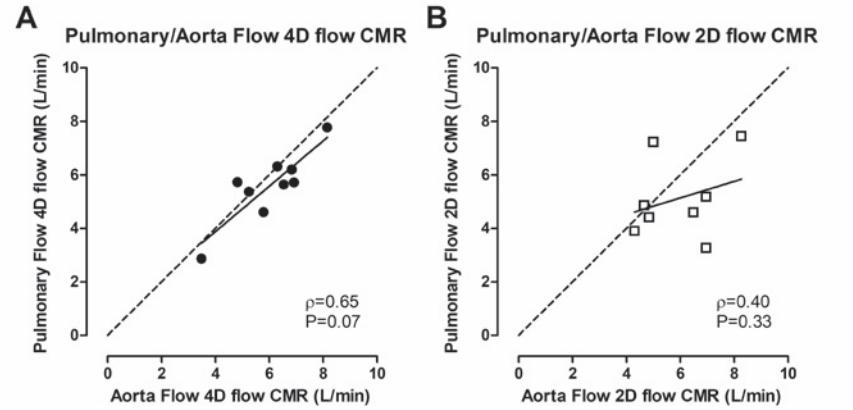

Figure 5. Comparison of pulmonary and aorta flow measured by 4D flow CMR and 2D flow CMR.

Correlation between the aorta and pulmonary measured by 4D flow CMR (A, n=9) and 2D flow CMR (B, n=8). Line of identity is indicated as the dotted line. Spearman's rho (ρ) and P-value are indicated in the legends.

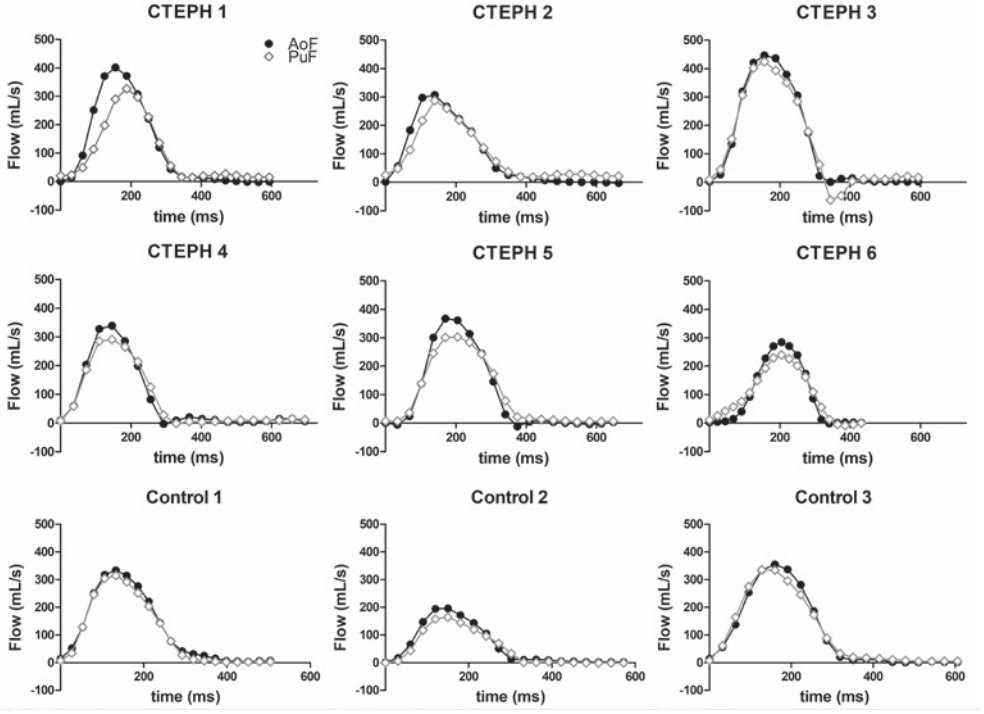

Figure 6 Individual pulmonary artery and aorta flow curves per heart beat superimposed.

Individual flow curves, measured by 4D flow CMR, superimposed per animal. CTEPH animals are ordered on disease severity, CTEPH 1 presented with the most severe PH and CTEPH 6 with the mildest.

Discussion

The main findings of this study were that (1) CO measured by 4D flow CMR showed a very strong correlation with invasively measured aortic flow, although there was an overestimation of the CO by 4D flow CMR of ~15%, (2) the correlation between 2D flow CMR and volumetric LV measurements in relation to invasively measured flow was less strong with a larger overestimation of the flow, and (3) the difference between MPA and aorta flow was much smaller with 4D flow compared to 2D flow CMR.

4D flow CMR is a relatively new technique but increasingly used in clinical practice due to its simplicity. The application of 4D flow CMR in the clinical setting provides many benefits as the technique is patient and operator friendly, less operator dependent and any flow in any plane can be selected retrospectively since the whole field of interest is acquired. (5, 9, 11) The latter is not the case for 2D flow CMR, in which flow measurements are limited to preselected planes. (3, 5, 9) Importantly, 4D flow CMR is in most cases more patient friendly than 2D flow CMR. One important benefit for the patients is that the sequence can be performed without breath holds (free breathing), which is not only more comfortable but will be an advantage in children, decompensated and importantly pulmonary hypertension patients in which breath holds are mostly impossible. (4, 5, 9) In addition, data on flow and anatomic structures can be obtained simultaneously which can shorten the scan time for the patients, especially in patients with a difficult anatomy. (2, 4, 6, 9) However, it is important to note that there are some existing challenges with the 4D flow CMR technique such as long scan time, reliability of respiratory gating and lower resolution. Given the benefits and existing challenges, it is important to assess accuracy of 4D flow CMR measurements. Our data show that indeed, 4D flow CMR measurements correlate

strongly with flow measured with an invasive flow probe, and overestimation of flow with this technique is less than measurements obtained using 2D flow CMR as well as compared to CO determined from volumetric LV measurements.

This is the first study to validate 4D flow CMR against both 2D flow CMR and invasively measured flow within the same animal, at the same time. Thus far, 4D flow CMR has only been validated against 2D flow CMR (6, 12) and ultrasound (5) measurements in humans. Although data are obtained in a relatively small group of animals, and magnetic interference of the metal in the flow probe could not be completely ruled out (two animals were excluded due to artifacts and in the other animals there were no noticeable imaging artifacts), both flow pattern and average flow showed a very strong correlation between invasively measured flow and 4D flow CMR. Although the invasively measured flow is considered the gold standard in validation studies, according to the manufacturer's specifications, this technique has an absolute accuracy of 10%. Both 2D flow CMR and 4D flow CMR overestimated CO as compared to the invasively measured flow by 25% and 16% respectively. When comparing the individual flow patterns between the different techniques (Figure 2) we do not see a consistent difference between the CMR and invasively measured flow, suggesting that there is no systematic bias. Consistent with data obtained in a canine model of acute thromboembolic pulmonary hypertension, 4D flow CMR resulted in slightly lower values of CO as compared to 2D flow CMR measurements (16), suggesting that determination of flow using 4D CMR is slightly more accurate than 2D CMR. The higher accuracy of 4D flow CMR vs 2D flow CMR can also be inferred from the comparison between aorta flow and MPA flow. Also here, there tended to be a correlation of the measurements with 4D flow CMR while no correlation was found with 2D flow CMR.

In conclusion, this study shows that aorta flow and pulmonary flow can be accurately and simultaneously measured by 4D flow CMR. This helps to further validate the quantitative reliability of this technique for implementation of 4D flow CMR in routine clinical practice. Unfortunately, we did not observe any significant distinctions in flow patterns in the CTEPH swine.

Acknowledgements:

This work was supported by the Netherlands Cardiovascular Research Initiative; the Dutch Heart Foundation, the Dutch Federation of University Medical Centers, the Netherlands Organization for Health Research and Development and the Royal Netherlands Academy of Science. CVON (2012-08), PHAEDRA.

References

1. **Bland JM, and Altman DG**. Statistical methods for assessing agreement between two methods of clinical measurement. *Lancet* 1: 307-310, 1986.

2. **Bock J, Töger J, Bidhult S, Markenroth Bloch K, Arvidsson P, Kanski M, Arheden H, Testud F, Greiser A, Heiberg E, and Carlsson M**. Validation and reproducibility of cardiovascular 4D-flow MRI from two vendors using 2×2 parallel imaging acceleration in pulsatile flow phantom and in vivo with and without respiratory gating. *Acta Radiologica* 0: 0284185118784981.

3. **Bollache E, van Ooij P, Powell A, Carr J, Markl M, and Barker AJ**. Comparison of 4D flow and 2D velocity-encoded phase contrast MRI sequences for the evaluation of aortic hemodynamics. *Int J Cardiovasc Imaging* 32: 1529-1541, 2016.

4. **Chelu RG, Horowitz M, Sucha D, Kardys I, Ingremeau D, Vasanawala S, Nieman K, Paul JF, and Hsiao A**. Evaluation of atrial septal defects with 4D flow MRI-multilevel and inter-reader reproducibility for quantification of shunt severity. *MAGMA* 2018.

5. **Chelu RG, van den Bosch AE, van Kranenburg M, Hsiao A, van den Hoven AT, Ouhlous M, Budde RP, Beniest KM, Swart LE, Coenen A, Lubbers MM, Wielopolski PA, Vasanawala SS, Roos-Hesselink JW, and Nieman K**. Qualitative grading of aortic regurgitation: a pilot study comparing CMR 4D flow and echocardiography. *Int J Cardiovasc Imaging* 32: 301-307, 2016.

6. **Chelu RG, Wanambiro KW, Hsiao A, Swart LE, Voogd T, van den Hoven AT, van Kranenburg M, Coenen A, Boccalini S, Wielopolski PA, Vogel MW, Krestin GP, Vasanawala SS, Budde RPJ, Roos-Hesselink JW, and Nieman K**. Cloud-processed 4D CMR flow imaging for pulmonary flow quantification. *Eur J Radiol* 85: 1849-1856, 2016.

7. **De Wijs-Meijler DP, Stam K, van Duin RW, Verzijl A, Reiss IK, Duncker DJ, and Merkus D**. Surgical Placement of Catheters for Long-term Cardiovascular Exercise Testing in Swine. *J Vis Exp* e53772, 2016.

8. **Duncker DJ, Stubenitsky R, and Verdouw PD**. Role of adenosine in the regulation of coronary blood flow in swine at rest and during treadmill exercise. *Am J Physiol* 275: H1663-1672, 1998.

9. **Dyverfeldt P, Bissell M, Barker AJ, Bolger AF, Carlhall CJ, Ebbers T, Francios CJ, Frydrychowicz A, Geiger J, Giese D, Hope MD, Kilner PJ, Kozerke S,**

Myerson S, Neubauer S, Wieben O, and Markl M. 4D flow cardiovascular magnetic resonance consensus statement. *J Cardiovasc Magn Reson* 17: 72, 2015.

10. **Hanneman K, Kino A, Cheng JY, Alley MT, and Vasanawala SS**. Assessment of the precision and reproducibility of ventricular volume, function, and mass measurements with ferumoxytol-enhanced 4D flow MRI. *J Magn Reson Imaging* 44: 383-392, 2016.

11. **Hanneman K, Sivagnanam M, Nguyen ET, Wald R, Greiser A, Crean AM, Ley S, and Wintersperger BJ**. Magnetic resonance assessment of pulmonary (QP) to systemic (QS) flows using 4D phase-contrast imaging: pilot study comparison with standard through-plane 2D phase-contrast imaging. *Acad Radiol* 21: 1002-1008, 2014.

12. **Hsiao A, Alley MT, Massaband P, Herfkens RJ, Chan FP, and Vasanawala SS**. Improved cardiovascular flow quantification with time-resolved volumetric phase-contrast MRI. *Pediatr Radiol* 41: 711-720, 2011.

13. **Hsiao A, Lustig M, Alley MT, Murphy M, Chan FP, Herfkens RJ, and Vasanawala SS**. Rapid pediatric cardiac assessment of flow and ventricular volume with compressed sensing parallel imaging volumetric cine phase-contrast MRI. *AJR Am J Roentgenol* 198: W250-259, 2012.

14. **Hsiao A, Yousaf U, Alley MT, Lustig M, Chan FP, Newman B, and Vasanawala SS**. Improved quantification and mapping of anomalous pulmonary venous flow with four-dimensional phase-contrast MRI and interactive streamline rendering. *J Magn Reson Imaging* 42: 1765-1776, 2015.

15. **Roest AA, Helbing WA, van der Wall EE, and de Roos A**. Postoperative evaluation of congenital heart disease by magnetic resonance imaging. *J Magn Reson Imaging* 10: 656-666, 1999.

16. **Roldan-Alzate A, Frydrychowicz A, Johnson KM, Kellihan H, Chesler NC, Wieben O, and Francois CJ**. Non-invasive assessment of cardiac function and pulmonary vascular resistance in an canine model of acute thromboembolic pulmonary hypertension using 4D flow cardiovascular magnetic resonance. *J Cardiovasc Magn Reson* 16: 23, 2014.

17. **Stam K, van Duin RWB, Uitterdijk A, Cai Z, Duncker DJ, and Merkus D**. Exercise facilitates early recognition of cardiac and vascular remodeling in chronic thromboembolic pulmonary hypertension in swine. *Am J Physiol Heart Circ Physiol* 314: H627-H642, 2018.

18. **Stam K, van Duin RWB, Uitterdijk A, Krabbendam-Peters I, Sorop O, Danser AHJ, Duncker DJ, and Merkus D**. Pulmonary microvascular remodeling in chronic thrombo-embolic pulmonary hypertension. *Am J Physiol Lung Cell Mol Physiol* 2018.

19. **Stubenitsky R, Verdouw PD, and Duncker DJ**. Autonomic control of cardiovascular performance and whole body O2 delivery and utilization in swine during treadmill exercise. *Cardiovasc Res* 39: 459-474, 1998.

20. **Thomson LE, Crowley AL, Heitner JF, Cawley PJ, Weinsaft JW, Kim HW, Parker M, Judd RM, Harrison JK, and Kim RJ**. Direct en face imaging of secundum atrial septal defects by velocity-encoded cardiovascular magnetic resonance in patients evaluated for possible transcatheter closure. *Circ Cardiovasc Imaging* 1: 31-40, 2008.

21. **Uitterdijk A, Springeling T, van Kranenburg M, van Duin RW, Krabbendam-Peters I, Gorsse-Bakker C, Sneep S, van Haeren R, Verrijk R, van Geuns RJ, van der Giessen WJ, Markkula T, Duncker DJ, and van Beusekom HM**. VEGF165A microsphere therapy for myocardial infarction suppresses acute cytokine release and increases microvascular density but does not improve cardiac function. *Am J Physiol Heart Circ Physiol* 309: H396-406, 2015.

22. **Valsangiacomo Buechel ER, Grosse-Wortmann L, Fratz S, Eichhorn J, Sarikouch S, Greil GF, Beerbaum P, Bucciarelli-Ducci C, Bonello B, Sieverding L, Schwitter J, and Helbing WA**. Indications for cardiovascular magnetic resonance in children with congenital and acquired heart disease: an expert consensus paper of the Imaging Working Group of the AEPC and the Cardiovascular Magnetic Resonance Section of the EACVI. *Cardiol Young* 25: 819-838, 2015.

23. **Valverde I, Simpson J, Schaeffter T, and Beerbaum P**. 4D phase-contrast flow cardiovascular magnetic resonance: comprehensive quantification and visualization of flow dynamics in atrial septal defect and partial anomalous pulmonary venous return. *Pediatr Cardiol* 31: 1244-1248, 2010.

24. **Vasanawala SS, Hanneman K, Alley MT, and Hsiao A**. Congenital heart disease assessment with 4D flow MRI. *J Magn Reson Imaging* 42: 870-886, 2015.

Part II

Characterization

Chapter 5

Pulmonary microvascular remodeling in chronic thrombo-embolic pulmonary hypertension

Kelly Stam, Richard W. van Duin, André Uitterdijk, Ilona Krabbendam-Peters, Oana Sorop, AH Jan Danser, Dirk J. Duncker, Daphne Merkus

Am J Physiol Lung Cell Mol Physiol 2018Dec 1; 315(6):L951-L964

Abstract

Rationale: Pulmonary vascular remodeling in pulmonary arterial hypertension involves perturbations in the nitric oxide (NO) and endothelin-1 (ET-1) pathways. However, the implications of pulmonary vascular remodeling and these pathways remain unclear in chronic thrombo-embolic pulmonary hypertension (CTEPH).

Objectives: The objective of the present study was to characterize changes in microvascular morphology and function, focussing on the ET-1 and NO pathways, in a CTEPH swine model.

Methods: Swine were chronically instrumented and received up to 5 pulmonary embolizations by microsphere infusion, while endothelial dysfunction was induced by daily administration of the eNOS inhibitor L-N^{ω}-Nitroarginine methyl ester, until two weeks prior to the end of study. Swine were subjected to exercise and the pulmonary vasculature was investigated by hemodynamic, histological, qPCR and myograph experiments.

Results: In swine with CTEPH, the increased RV-afterload, decreased cardiac index and mild ventilation-perfusion mismatch were exacerbated during exercise. These findings suggest that pulmonary microvascular remodeling was evidenced by increased muscularization which was accompanied by an increased maximal vasoconstriction. Although ET-1-induced vasoconstriction was increased in CTEPH pulmonary small arteries, the ET-1-sensitivity was decreased. Moreover, the contribution of the ET_A receptor to ET-1 vasoconstriction was increased, while the contribution of the ET_B receptor was decreased and the contribution of Rho-Kinase was lost. A reduction in endogenous NO-production was compensated in part by a decreased PDE5-activity resulting in an apparent increased NO-sensitivity in CTEPH pulmonary small arteries.

Conclusions: Pulmonary microvascular remodeling with a reduced activity of PDE5 and Rho-kinase may contribute to the lack of therapeutic efficacy of PDE5-inhibitors and Rho-kinase inhibitors in CTEPH.

Introduction

Chronic thrombo-embolic pulmonary hypertension (CTEPH) is a form of pulmonary hypertension (PH) initiated by thrombo-emboli in the pulmonary vasculature (9). The obstructions in the pulmonary vascular bed cause a direct increase in pulmonary vascular resistance, which results in an increase in pulmonary artery pressure (PAP). CTEPH is defined as a PAP ≥ 25 mmHg at rest persisting for at least six weeks (26). Both the increase in pressure and a redistribution of flow through the unobstructed parts of the pulmonary vasculature have been proposed to contribute to pathological processes including endothelial dysfunction, thrombophilia, inflammation, vasoconstriction and impaired vasodilation (36), eventually resulting in structural pulmonary vascular remodeling of both the obstructed and unobstructed pulmonary vasculature (17, 42). This remodeling encompasses both the pulmonary small arteries as well as the microvasculature.

It is well known that perturbations in the endothelin-1 (ET-1) and the nitric oxide (NO) pathways play an important role in the dysregulation of pulmonary vascular tone as well as in microvascular remodeling in pulmonary arterial hypertension (PAH) (14, 52). Plasma markers of oxidative stress and the endogenous endothelial NO synthase (eNOS) inhibitor asymmetric dimethyl arginine (ADMA) are increased in patients with CTEPH (59). Moreover, circulating ET-1 levels are elevated in patients with CTEPH and correlate with clinical severity of the disease as well as with hemodynamic outcome after pulmonary endarterectomy (47). Nevertheless, therapeutic agents that modulate the NO and the ET-1 pathways, including phosphodiesterase 5 (PDE5)-inhibitors and ET-receptor antagonists, which are the cornerstones of PAH therapy, are not as effective in CTEPH (13, 22, 45). The only approved therapy for CTEPH is the

soluble guanylate cyclase (sGC) stimulator Riociguat (13, 22, 45), suggesting that indeed the NO-pathway is compromised in CTEPH. However, the contribution of alterations in the NO and ET-1 pathways to pulmonary microvascular (dys)function have not been investigated to date in CTEPH.

We recently developed and hemodynamically characterized a swine model of CTEPH, using a combination of repeated micro-embolizations and eNOS-inhibition to mimic endothelial dysfunction (54). In this study, micro-embolizations alone resulted in transient elevations in pulmonary artery pressure but did not induce sustained PH. In contrast, in animals in which repeated micro-embolizations were combined with eNOS-inhibition, PH persisted for several weeks, even after discontinuation of micro-embolization and eNOS-inhibition. In the present study, we characterized changes in pulmonary microvascular morphology and hypothesized that microvascular remodeling is associated with altered regulation of pulmonary microvascular function through the ET-1- and NO-pathways in this CTEPH model.

Methods

Animal studies were performed following the "Guide for the Care and Use of Laboratory Animals" as approved by the Council of the American Physiological Society, and with approval of the Animal Care Committee of the Erasmus University Medical Center (EMC3158, 109-13-09). Twenty-four swine (2-3 months old, 21±1 kg) entered the study. Lungs from seven additional swine were obtained at a local slaughterhouse for in vitro control experiments.

CTEPH induction

Animals were chronically instrumented as previously described (8, 54). In short, swine were sedated with an intramuscular injection (i.m.) of

tiletamine/zolazepam (5 mg/kg), xylazine (2.25 mg/kg) and atropine (1 mg), intubated and ventilated with a mixture of O_2 and N_2 (1:2 v/v) to which 2% (v/v) isoflurane was added to maintain anesthesia (8, 54). Under sterile conditions, the chest was opened via a left thoracotomy in the fourth intercostal space and fluid-filled polyvinylchloride catheters (Braun Medical Inc., Bethlehem, PA, USA) were placed in the right ventricle, pulmonary artery, aorta and left atrium for blood sampling and measurement of pressures. A flow probe (Transonic Systems Inc., Ithaca, NY, USA) was positioned around the ascending aorta for measurement of cardiac output. The catheters were tunneled to the back and animals were allowed to recover for one week, receiving analgesia (0.015 mg/kg buprenorphine i.m. and a slow-release fentanyl patch 12 µg/h for 48 hours) on the day of the surgery and daily intravenous (i.v.) antibiotic prophylaxis (25 mg/kg amoxicillin) for 7 days (8).

Following the recovery week, on the first day, the CTEPH animals (n=11), were given the eNOS-inhibitor L-N^{ω}-Nitroarginine methyl ester (LNAME) (10 mg/kg i.v., Enzo Life Sciences International Inc, NY, USA) as a bolus infusion. On subsequent days, the dose of LNAME was increased by 10 mg/kg per day up to 30 mg/kg i.v., which was maintained until 2 weeks before the end of the study (35, 46, 54). Four days after the start of LNAME administration, microsphere infusions were started. Polyethylene microspheres (diameter 600-710 µm, density 1.13 g/cm^3, 500 mg, corresponding to ~2500 microspheres, Cospheric LLC, Santa Barbara, California, US) were suspended in 50 mL autologous blood with 2500 I.U. heparin and slowly infused into the right ventricle over 10 minutes while monitoring mean pulmonary artery pressure (PAP). Microsphere infusions were repeated until the PAP reached ~60 mmHg, or the arterial P_aO_2 dropped below ~40 mmHg, as measured 30 min after infusion at rest, or when a maximum of 3 gram (~15000) microspheres was infused on one day (54). In the subsequent four

weeks, hemodynamics were weekly assessed, and microsphere infusions were repeated when PAP was <25 mmHg and P_aO2 >70 mmHg, as described above. During the final 5 weeks of follow-up, no microsphere infusions were performed.

Seven sham-operated animals which did not receive LNAME or microspheres served as controls. A third group of six swine did receive LNAME but no microspheres and also served as controls (54). Similar to the CTEPH group, LNAME was discontinued two weeks before the end of the study.

Mortality due to acute cardiopulmonary failure after CTEPH induction occurred in 2 out of 11 animals. In addition, 2 animals were excluded due to catheter failure (1 CTEPH and 1 Control) and 2 animals had to be euthanized following infections (1 CTEPH and 1 Control).

In vivo experiments

Hemodynamic studies were performed nine weeks after surgery. With swine standing quietly on a motor-driven treadmill and during exercise at 4 km/h, cardiac output, PAP, aorta pressure, left atrial pressure and right ventricular pressure, were continuously recorded, and blood samples were taken when hemodynamics had reached a steady-state. Measurements of arterial and mixed venous pO_2, pCO_2, O_2 saturation, pH and lactate were performed immediately with a blood gas analyzer (ABL 800, Radiometer, Denmark) (8, 12). Furthermore, EDTA plasma was stored for measurement of endothelin-1 (ET-1) levels with an enzyme-linked immunoassay (ELISA; Enzo Life Sciences International Inc, NY, USA) and D-Dimer levels with a particle-enhanced, immunoturbidimetric assay (INNOVANCE®, Siemens Healtineers, Erlangen, Duitsland) following the standard protocols.

Euthanasia

After completion of the experiments (week 9), the animals were re-anaesthetized with pentobarbital sodium (6-12 mg/kg/h iv), intubated and ventilated as described before (8, 54). Following sternotomy, the heart was arrested and immediately excised together with the lungs. Parts of one lung were snap frozen in liquid nitrogen for molecular analyses, and one lung lobe was placed in cold Krebs buffer for dissection of pulmonary small arteries for wire-myograph experiments to delineate changes in microvascular function (2, 18, 41, 43). The accessory lobe was obtained for histological analyses.

Quantitative PCR of lung tissue

Lung tissue was excised and immediately snap frozen in liquid nitrogen for the measurement of mRNA levels of prepro-endothelin 1 (PPET-1), endothelin converting enzyme 1 (ECE-1), endothelin receptor A (ET_A), endothelin receptor B (ET_B), endothelial nitric oxide synthase (eNOS), Ras homolog gene family, member A (RhoA), rho-associated, coiled-coil-containing protein kinase 1 (ROCK1), Rho associated coiled-coil containing protein kinase 2 (ROCK2),Platelet endothelial cell adhesion molecule (CD31), vascular cell adhesion molecule 1 (VCAM-1), vascular endothelial cadherin (VE-cadherin, CD144), interleukin-6 (Il-6), interferon-γ, tumor necrosis factor α (TNF-α) and transforming growth factor β1 (TGF-β). Small pieces of lung tissue (<30 mg) were homogenized by adding RLT lysisbuffer (Qiagen, Venlo, The Netherlands) and 2-mercaptoethanol (Sigma-Aldrich, Zwijndrecht, The Netherlands) using a homogenizer (PRO Scientific Inc., Oxford, Connecticut, USA). After a proteinase K (Invitrogen, Breda, The Netherlands) treatment at 55 °C for 10 min, total RNA was isolated using RNeasy Fibrous Tissue Mini Kit (Qiagen, Venlo, The Netherlands). RNA was eluted in RNase-free water and the concentration was determined by using a NanoDrop (NanoDrop1000, Thermo

Fisher Scientific, Bleiswijk, The Netherlands). RNA integrity was confirmed using a Bioanalyzer (2100 Bioanalyzer, Agilent, Santa Clara, California, USA). cDNA was synthesized from 500 ng of total RNA with the SensiFAST cDNA Synthesis Kit (Bioline, London, UK). qPCR (CFX-96, Bio-Rad, Hercules, California, USA) was performed with SensiFAST SYBR & Fluorescein Kit (Bioline, London, UK). Target gene mRNA levels were normalized against β-actin, glyceraldehyde-3-phosphate dehydrogenase (GADPH), and Cyclophilin using the CFX manager software (Bio-Rad, Hercules, California, USA). Relative gene expression data were calculated using the ΔΔCt method. All primer sequences are presented in Table 1.

Myograph studies of isolated pulmonary small arteries

Myograph studies have been extensively described before (43, 54, 60). Unless otherwise mentioned, all chemicals were obtained from Sigma Aldrich, Zwijndrecht, The Netherlands. Pulmonary small arteries (diameter ~300µm) were dissected from the lung and stored overnight in cold, oxygenated (95% O_2/5% CO_2) Krebs bicarbonate solution (composition in mM: 118 NaCl, 4.7 KCl, 2.5 $CaCl_2$, 1.2 $MgSO_4$, 1.2 KH_2PO_4, 25 $NaHCO_3$, and glucose 8.3; pH 7.4). The next day, pulmonary small arteries were cut into segments of ~2 mm length and mounted in microvascular myographs (Danish MyoTechnology) with separated 6-ml organ baths containing Krebs bicarbonate solution aerated with 95% O_2-5% CO_2 and maintained at 37°C. Changes in contractile force were recorded with a Harvard isometric transducer. Following a 30-min stabilization period, the internal diameter was set to a tension equivalent to 0.9 times the estimated diameter at 20 mmHg effective transmural pressure (18, 60). The vessels were subsequently exposed to 30 mM KCl twice. Endothelial integrity was ascertained by measuring the dilation response to 10 nM substance P after preconstriction with 100 nM of the stable thromboxane-A2 analog 9,11-dideoxy-11α,9α

epoxymethanoprostaglandin $F_{2\alpha}$ (U46619). Then, after washout, vessels were subjected to 100 mM KCl to determine maximal vascular contraction. Thereafter, vessels were allowed to equilibrate in fresh Krebs solution for 30 min before different experimental protocols were started. Only one protocol was performed per vessel segment, and each vessel segment within an experimental protocol was obtained from a different animal with a minimum of five per experiment per group.

Following preconstriction with 100 nM U46619, vessel segments were exposed to incremental concentrations of the Rho-kinase inhibitor Y-27632 (10^{-8}-$3{\cdot}10^{-5}$M), the cGMP analogue 8Br-cGMP (10^{-7}-$3{\cdot}10^{-4}$M), the PDE5-inhibitor Sildenafil (10^{-10}-$3{\cdot}10^{-5}$M), the NO-donor sodium nitroprusside (SNP) (10^{-9}-$3{\cdot}10^{-5}$M), or the endothelium dependent-vasodilator Bradykinin (10^{-10}-$3{\cdot}10^{-7}$M), in the absence and presence of 30 minutes pre-incubation with *LNAME*(10^{-4}M).

In pulmonary small artery segments from a subgroup of seven CTEPH animals and eleven Control animals, concentration-response curves to Endothelin-1 (ET-1) were constructed, by subjecting these segments to incremental concentrations of ET-1 (10^{-10}-$3{\cdot}10^{-7}$M) in the absence and presence of the ET_A receptor antagonist BQ123 (10^{-6}M), the ET_B receptor antagonist BQ788 (10^{-8}M), a combination of both BQ123 and BQ788, or the Rho-kinase inhibitor Y-27632 (10^{-5}M) (2, 18, 41).

Histology of the lung tissue

The accessory lobe was flushed with saline, and fixed by bronchial installation of 3.5-4% buffered formaldehyde at a physiological pressure of 18 mmHg (34). Tissues were processed and embedded in paraffin. Sections (4.5 µm) were cut, stained with Resorcin Fuchsin von Gieson (RF) and evaluated by light microscopy

(NDP slide scanner, Hamamatsu Nanozoomer 2.0HT, Hamamatsu Photonics K.K., Japan).

Data analysis and statistics

Digital recording and offline analysis of hemodynamic data were performed as described previously (12, 56). To account for differences in growth between animals, cardiac output was corrected for bodyweight, yielding cardiac index (CI). Total pulmonary vascular resistance index (tPVRi) was calculated as PAP/CI and body oxygen consumption index (BVO_2i) as CI·(arterial-mixed venous oxygen content) i.e. CI·(C_aO_2-$C_{mv}O_2$). Alveolar-arterial oxygen gradient ($AaDO_2$) was calculated as:

$$AaDO_2 = \left(F_iO_2 \cdot (P_{ATM} - pH_2O) - \frac{P_aCO_2}{RER}\right) - P_aO_2$$

With F_IO_2=0.21; P_{ATM}=760 mmHg; pH_20=47 mmHg; RER=0.9 at rest (based on the assumption that pig chow contains predominantly protein and carbohydrates) and 1.15 at 4km/h (27) and P_aCO_2 and P_aO_2 were measured in the blood gases obtained from the animals.

Vascular responses to ET-1 in the myograph experiments were normalized to 100 mM KCl. Vasorelaxation was expressed as the percentage of contraction to U46619.

Morphometric measurements of pulmonary small arteries and microvasculature were performed using NanoZoomer Digital Pathology (NDP) viewer (Hamamatsu Photonics K.K., Japan). To ensure that pulmonary veins were excluded for analysis, vessels within, or in close proximity to the lung septae were not included in the analysis. Only transversely cut vessels (ratio largest/ smallest diameter <1.5) of predetermined diameters (<50, 50-100, 100-300 µm) were

analyzed. All vessels complying with these conditions were analyzed resulting in an average of 68 vessels per animal. Assuming circularity of the vessels, inner and outer radius were calculated as r = perimeter/2*π. Wall-to-lumen ratio was calculated as (outer – inner radius)/inner radius.

Data analysis of the concentration-response curves in the isolated pulmonary small arteries was performed using Prism (version 5.0, Graphpad Software, Inc., La Jolla, CA, USA)and StatView (version 5.0, SAS Institute, Cary, North Carolina, USA). SPSS (version 21.0 IBM, Armonk, NY, USA)was used for statistical analysis of exercise responses and qPCR data.Statistical analysis was performed using a two-way ANOVA for repeated measures or one-way ANOVA when applicable. Statistical significance was accepted when $P \leq 0.05$. Data are presented in box and whisker plots with the whiskers reflecting min to max, median presented as line and means are presented as +.

Results

CTEPH and exercise response in vivo

As the hemodynamic responses over time were not different between the sham-operated animals with and without LNAME, these were pooled into one single Control group. Repeated embolizations combined with LNAME resulted in CTEPH as evidenced by a PAP > 25 mmHg (43±6 mmHg vs 20±1 mmHg in Control, $p<0.001$) as a result of an increased tPVRi (266±56 mmHg L^{-1}minkg vs 119±10 mmHg L^{-1} minkg in Control, $p=0.007$) (Figure 1) (54).

Table 1. Primer sequences used for the qPCR.

	Sequence	
Genes	**Forward**	**Reverse**
IL-6	CTCCAGAAAGAGTATGAGAGC	AGCAGGCCGGCATTTGTGGTG
IFN-γ	GAAGAATTGGAAAGAGGAGAGTGAC	TGCTCCTTTGAATGGCCTGG
TNF-α	TGCACTTCGAGGTTATCGGCC	CCCACTCTGCCATTGGAGCTG
TGF-β	GTGGAAAGCGGCAACCAAAT	CACTGAGGCGAAAACCCTCT
PPET-1	TCATCGGCAGCTGGTGATGGG	GGCTTTCAGCTTGGCGATGTG
ECE-1	TGGGGGACCTTCAGCAACCT	GGGTGTCCTGGAAGTTGTCCTTG
ET_A	ACAGGTACAGAGCAGTTGCC	TCTCGACGCTGTTTCAGGTG
ET_B	CCCCTTCATCTCAGCAGGATT	GCACCAGCAGCATAAGCATG
eNOS	GGACACACGGCTAGAAGAGC	TCCGTTTGGGGCTGAAGATG
CD31	AGTGTACAGTGAAATCCGGAAA	TCTCAGAATGCGGTGTCTCC
VCAM-1	TGTGAAGGGATTAACCAGGCT	CAGTGTCCCCTTCCTTGACG
CD144	AGGGAGAAGAACACTTCCGC	GGGCATCTTGTGTTTCCACC
RhoA	AGGACCAATTCCCGGAGGTA	AGCCAACTCTACCTGCTTTCC
ROCK1	ATCAAACGATATGGCTGGAAG	CCATAGACGGATTGGATTGTTCC
ROCK2	TTCGACCAGTTACACAGACAG	TAAATTCATGTCCCTTGTGGC

IL-6, interleukin-6; IFN-γ, interferon-γ; TNF-α, tumor necrosis factor α; TGF-β, transforming growth factor β1; PPET-1, prepro endothelin 1; ECE-1, endothelin converting enzyme 1; ET_A, endothelin receptor A; ET_B, endothelin receptor B; eNOS, endothelial nitric oxide synthase; CD31,Platelet endothelial cell adhesion molecule; VCAM-1, vascular cell adhesion molecule 1; CD144, vascular endothelial cadherin (VE-cadherin); RhoA, Ras homolog gene family member A; ROCK1, rho-associated, coiled-coil-containing protein kinase 1; ROCK2, Rho associated coiled-coil containing protein kinase 2.

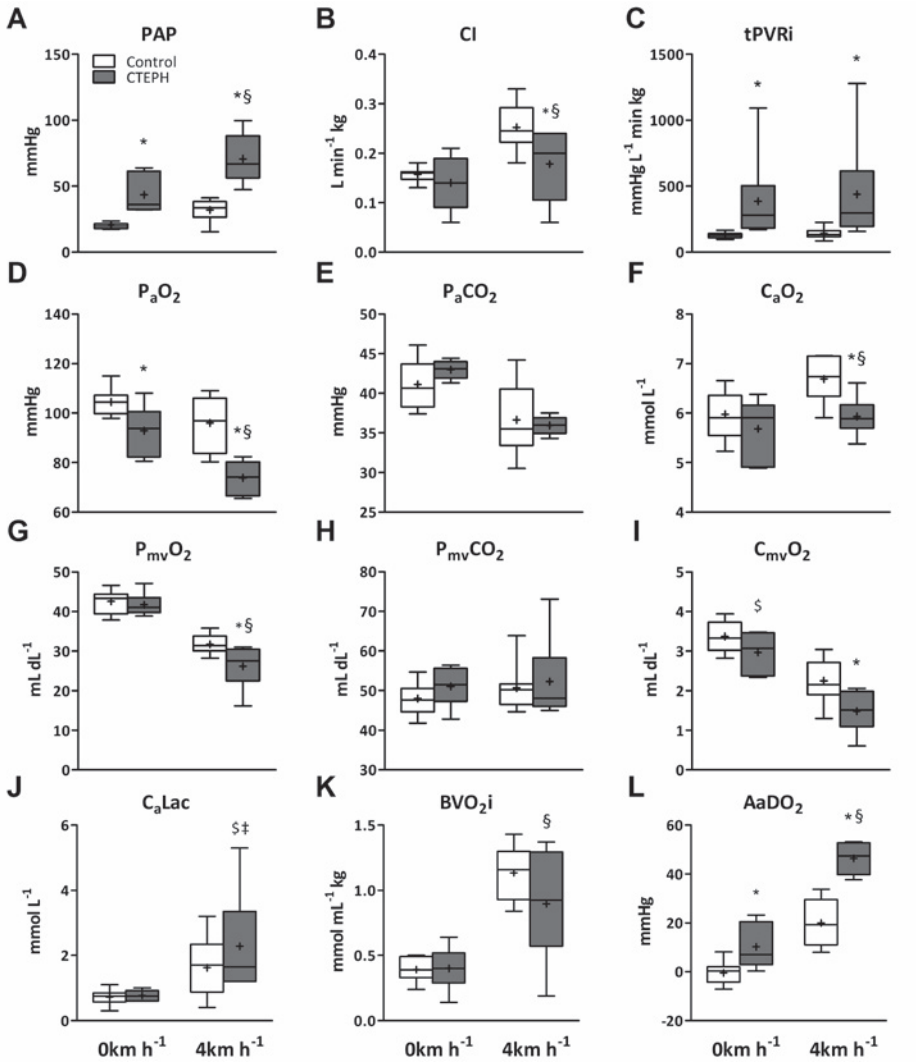

Figure 1. Pulmonary hemodynamics and oxygenation during exercise.

*Effect of exercise after 9 weeks of CTEPH. Shown are data obtained at rest and during maximal exercise at 4 km h^{-1} in Control swine (white boxes, n=10) and CTEPH swine (grey boxes, n=6) A) Mean pulmonary artery pressure (PAP), B) Cardiac Index (CI), C) total pulmonary vascular resistance index (tPVRi), D) arterial oxygen pressure (P_aO_2), E) arterial carbon dioxide pressure (P_aCO_2), F) arterial oxygen content (C_aO_2), G) mixed venous oxygen pressure ($P_{mv}O_2$), H) mixed venous carbon dioxide pressure ($P_{mv}CO_2$), I) mixed venous oxygen content ($C_{mv}O_2$), J) arterial lactate concentration (C_aLac), K) body oxygen consumption index (BVO_2i), L) alveolar-arterial oxygen gradient ($AaDO_2$). Whiskers denote min to max and means are presented as +. * P < 0.05 CTEPH vs Control; $ P ≤ 0.10 CTEPH vs Control; § P ≤ 0.05 Effect of exercise vs Control; ‡ ≤ 0.1 Effect of exercise vs Control.*

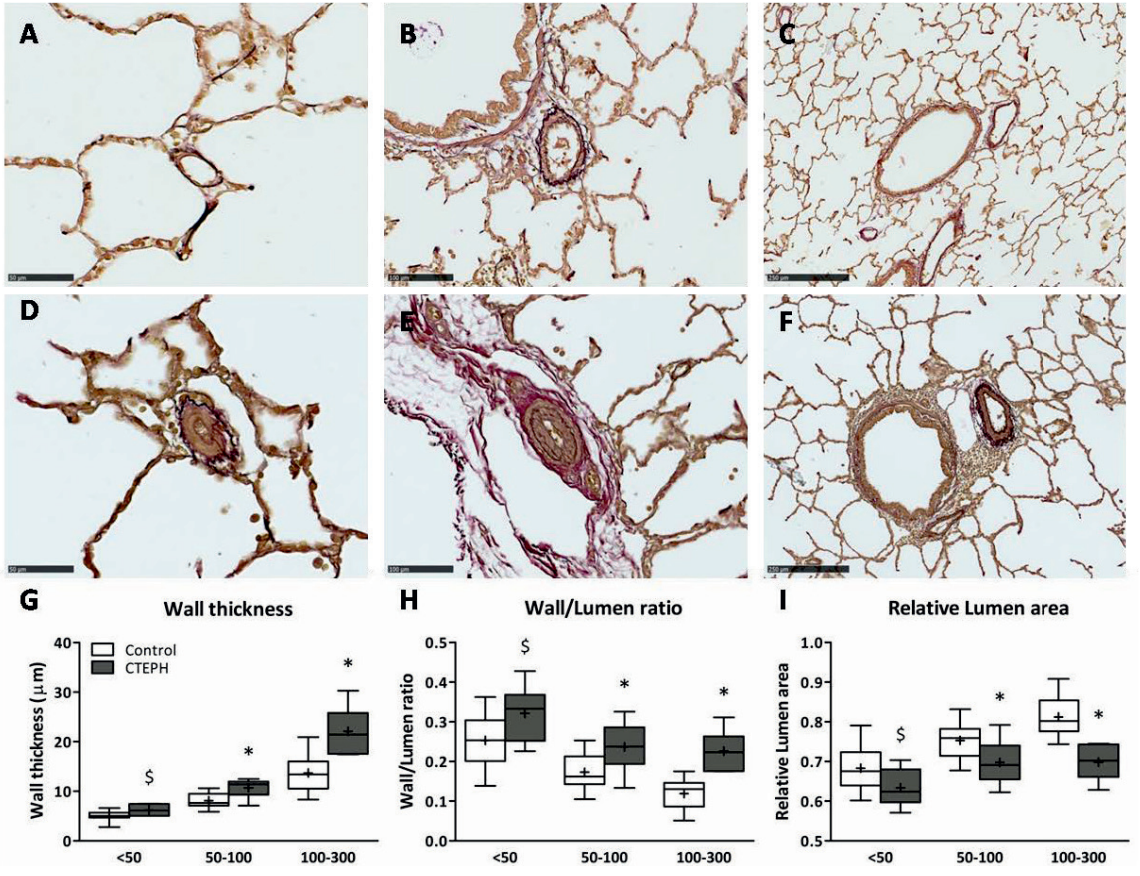

Figure 2. Pulmonary microvascular morphometry.

*Typical examples of a Resorcin Fuchsin von Gieson (RF) staining of distal pulmonary arteries with a diameter of <50 µm (A&D, 40x magnification, bar 50 µm), 50-100 µm (B&E, 20x magnification, bar 100 µm) and 100-300 µm (C&F, 10x magnification, bar 250 µm) from the Control (A-E) and CTEPH (D-F) lungs. Morphometry of these vessels, G) wall thickness, H) wall to lumen ratio and I) relative lumen area. Whiskers denote min to max and means are presented as +. Control n=13, CTEPH n=6. * P < 0.05 CTEPH vs Control, $ P < 0.10 CTEPH vs Control.*

Although the exercise-induced increase in CI was reduced in CTEPH, the higher tPVRi resulted in an exaggerated exercise-induced increase in PAP in CTEPH as compared to Control swine. Ventilation-perfusion (V/Q)-mismatch was suggested by a lower P_aO_2 in CTEPH compared to Control at rest, and the reduction in P_aO_2 was exacerbated during exercise. The lower P_aO_2 and arterial O_2 content (C_aO_2) during exercise were partially due to a reduction in $P_{mv}O_2$ and $C_{mv}O_2$ as a consequence of the diminished exercise-induced increase in CI, and in part due to widening of the $AaDO_2$, but were not accompanied by significant changes in arterial or mixed venous CO_2 (Figure 1). The impaired oxygen uptake in the lungs resulted in an attenuation of the exercise-induced increase in BVO_2i in CTEPH compared to Control, which was accompanied by a trend towards an increase in lactate, particularly during exercise (Figure 1), reflecting a lower anaerobic threshold. Furthermore, CTEPH was not accompanied by increased D-Dimer concentrations, indicating that contribution of endogenous clot formation to CTEPH induction is minimal in this swine model (Figure 3 C).

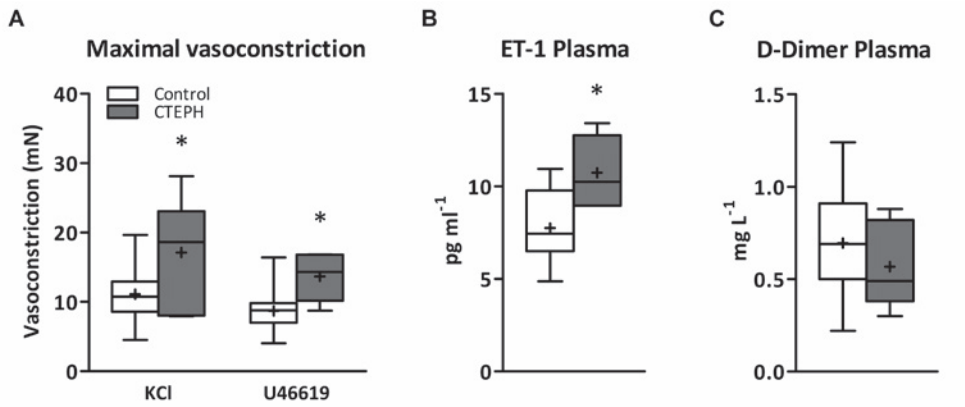

Figure 3. Maximal vasoconstriction of pulmonary small arteries and plasma Endothelin-1 and D-Dimer.

*Maximal vasoconstriction response of CTEPH and Control isolated pulmonary small arteries to KCl (100mM) and U46619 (100nM) (A). Plasma endothelin-1 (B) and plasma D-Dimer levels (C). Whiskers denote min to max and means are presented as +. Control n=12, CTEPH n=6 (A); Control n=11, CTEPH n=5 (B); Control n=11, CTEPH n=6 (C). * P < 0.05 CTEPH vs Control.*

Pulmonary microvascular morphometry

The increase in PAP in CTEPH resulted in pulmonary microvascular remodeling. The pulmonary small arteries of both 50-100 μm and 100-300 μm in lumen diameter showed a higher wall thickness, wall to lumen ratio and lower relative lumen area in CTEPH compared to Control animals (Figure 2). The remodeling of the pulmonary small arteries encompassed predominantly an increased muscularization in the tunica media. In the pulmonary microvasculature (vessel diameter <50 μm), remodeling was also predominantly present in the tunica media. The wall thickness (6.2±0.4 μm vs 5.2±0.3 μm, p=0.08) as well as the wall to lumen ratio (0.32±0.03 vs 0.25±0.02, p<0.06) tended to be higher in CTEPH compared to Control, while the relative lumen area tended to be smaller in the CTEPH compared to the Control microvasculature (0.63±0.02 vs 0.68±0.01, p=0.07) (Figure 2).

The changes in microvascular morphology were not accompanied by an overt inflammatory response, as IFN-γ, TNF-α and TGF-β were unaltered and IL-6 showed only a trend towards an increase in the CTEPH lung tissue (Figure 4 A). Consistent with the unaltered inflammatory state, neither CD31, VCAM-1 or CD144 were altered in the CTEPH swine lung tissue, indicating that vascular integrity was preserved (Figure 4 B).

Pulmonary small artery vasoreactivity in vitro: endothelin pathway

The increased muscularization of the pulmonary small arteries in CTEPH animals as observed histologically, was associated with an increase in pulmonary small artery vasoconstriction to both potassium chloride and the thromboxane analogue U46619 in CTEPH compared to Control vessels (Figure 3 A). The absolute vasoconstriction in response to ET-1 was also augmented (17.7±2.4 mN in CTEPH

vs 12.8±1.4 mN in Control, $p<0.05$). However, when normalized to KCl, the concentration-response curve to ET-1 was shifted to the right, reflecting a reduced sensitivity in CTEPH compared to Control vessels. The reduced sensitivity inversely correlated (R^2=0.49) with the elevated plasma levels of ET-1 in CTEPH animals.

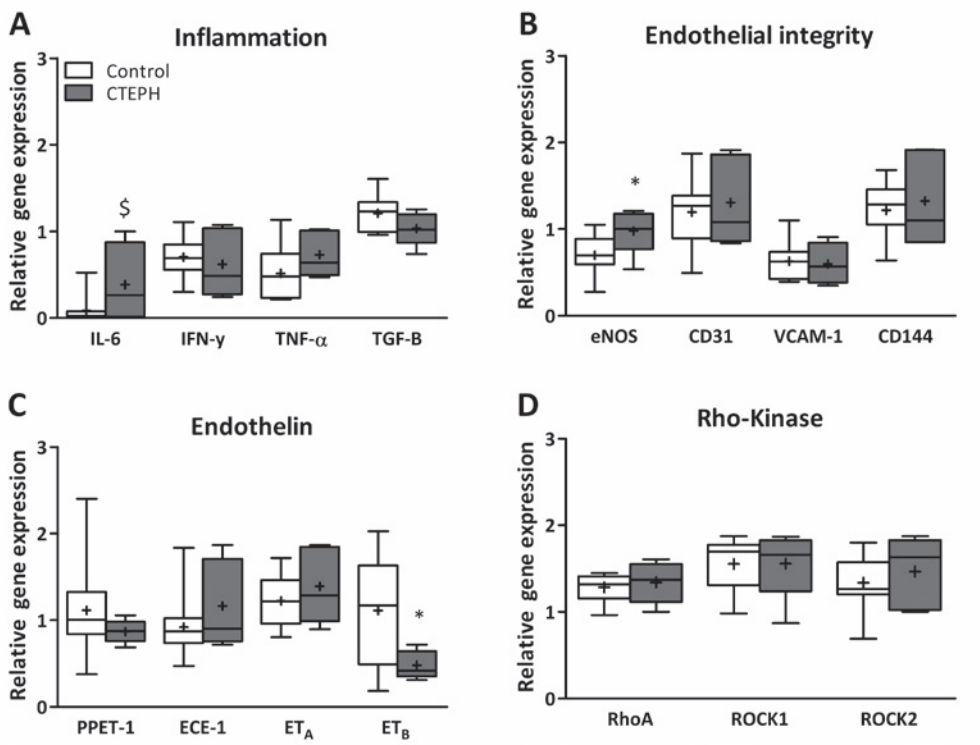

Figure 4. Gene expression in lung tissue.

*Gene expression measured by a quantitativepolymerase chain reaction (qPCR) of interleukin-6 (Il-6), interferon-γ (IFN- γ), tumor necrosis factor α (TNF-α) and transforming growth factor β1 (TGF-β) (A), endothelial nitric oxide synthase (eNOS), Platelet endothelial cell adhesion molecule (CD31), vascular cell adhesion molecule 1 (VCAM-1) and vascular endothelial cadherin (VE-cadherin, CD144)(B), prepro endothelin (PPET-1), endothelin converting enzyme (ECE-1), endothelin receptor A (ET_A) and endothelin receptor B (ET_B) (C), Ras homolog gene family, member A (RhoA), rho-associated, coiled-coil-containing protein kinase 1 (ROCK1), Rho associated coiled-coil containing protein kinase 2 (ROCK2) (D) in Control and CTEPH lung tissue. Whiskers denote min to max and means are presented as +. Control n=13, CTEPH n=5. * P < 0.05 CTEPH vs Control; $ P < 0.10 CTEPH vs Control.*

Consistent with the higher plasma ET-1 levels (Figure 3 B), expression of the ET_B receptor, which is the clearance receptor for ET-1, was reduced, while neither expression of PPET-1 nor that of ECE-1 in lung tissue was different in CTEPH as compared to Control animals (Figure 4 C), suggesting that ET-1 clearance rather than ET-1 production was altered in CTEPH. To investigate the contributions of the ET_A and ET_B receptors to the ET-induced vasoconstriction, concentration response curves to ET-1 were also performed in pulmonary small arteries in the presence of ET_A and ET_B receptor blockers alone as well as their combination. ET_A blockade by BQ123 resulted in an attenuation of ET-1-induced vasoconstriction that appeared relatively more pronounced in CTEPH compared to Control vessels. In contrast, ET_B blockade with BQ788 did not affect the vasoconstrictor response to ET-1 in either Control or CTEPH pulmonary small arteries. The effect of ET_A blockade was maintained in the presence of ET_B blockade (ET_A/ET_B vs ET_B) in both CTEPH and Control vessels, but only in Control vessels combined ET_A/ET_B blockade further attenuated the ET-1-induced vasoconstriction compared to ET_A blockade. In the CTEPH vessels there was no difference between ET_A/ET_B and ET_A blockade, suggesting a reduced contribution of the ET_B receptor and increased contribution of the ET_A receptor to the ET-vasoconstrictor response in the CTEPH pulmonary small arteries (Figure 5 A-C). These observations are consistent with the lower ET_B gene expression in CTEPH lung tissues (Figure 4 C) and higher ET_A/ET_B ratio (2.9±0.1 in CTEPH vs 1.7±0.4 in Control, $p<0.05$).

To further investigate the lower ET-sensitivity in CTEPH pulmonary small arteries, the contribution of Rho-kinase was examined. After pre-constriction to U46619, CTEPH-vessels showed a reduced vasodilator response to Rho-kinase inhibition with Y-27632 compared to Control (Figure 5 D).

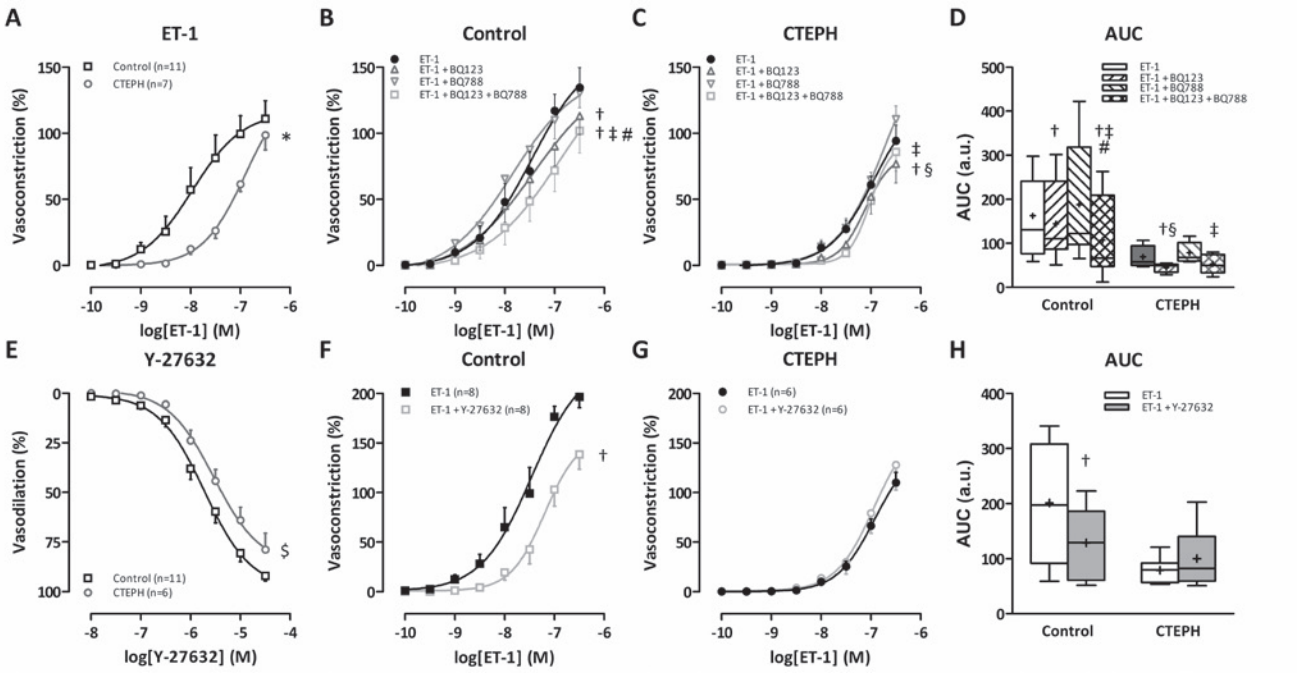

Figure 5. Pulmonary vasoreactivity: Endothelin response.

*Effects of endothelin (ET-1) and with and without ET_A/ET_B blockade (A-C). Area under the curve of the concentration response curves shown in panel B&C (D). Rho-kinase inhibition induced vasodilation after u46619 (E). Effect of Rho-kinase inhibition on ET-1 constriction of pulmonary small arteries (F&G). Area under the curve of the concentration response curves shown in panel F&G (H). BQ123, ET_A blocker; BQ788, ET_B blocker; Y-27632, Rho-kinase inhibitor. Whiskers denote min to max and means are presented as +. In all panels n represents the number of vessels; each vessel was obtained from a different animal, only in panel G 6 vessels were obtained from 5 animals. * P < 0.05 CTEPH vs Control; † P < 0.05 Effect blocker vs ET-1 response; ‡ P < 0.05 Effect blocker vs BQ123 response; # P < 0.05 Effect blocker vs BQ788 response; § P < 0.05 Effect blocker CTEPH vs effect blocker Control; $ P < 0.10 CTEPH vs Control.*

Furthermore, pre-incubation with Y-27632 attenuated ET-1-induced vasoconstriction in the Control arteries while it did not affect the response in arteries from CTEPH animals, so that Rho-kinase inhibition abrogated the difference in ET-1-response between Control and CTEPH. However, Rho-kinase gene expression level was unaltered in CTEPH (Figure 4 D). These findings suggest that reduced Rho-kinase activity, but not gene expression, in CTEPH pulmonary small arteries underlies the decreased ET-1 vasoconstriction in CTEPH compared to Control (Figure 5 E&F).

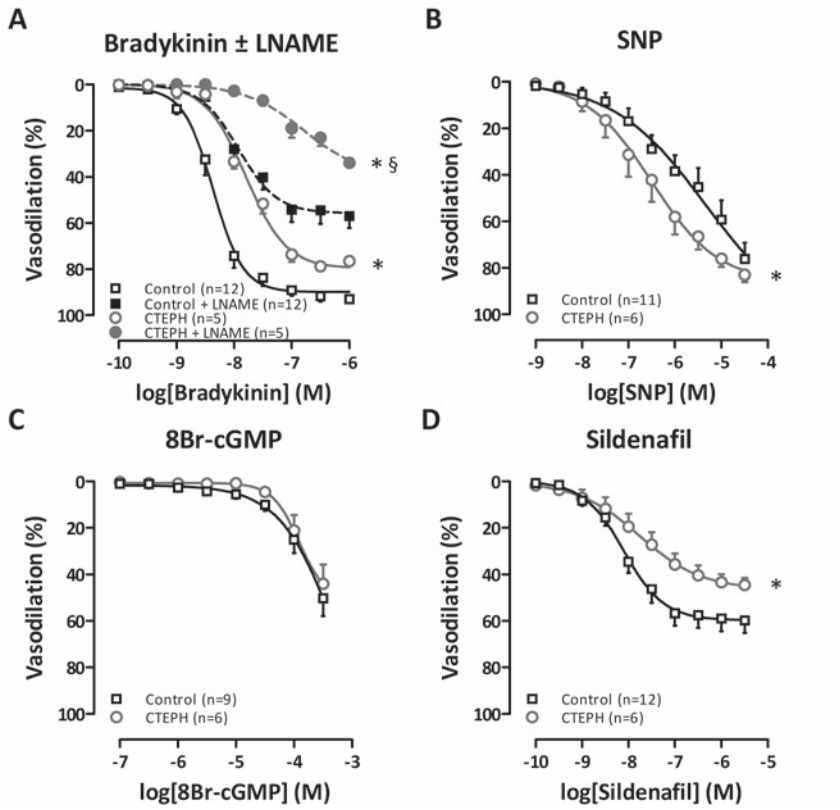

Figure 6. Pulmonary vasoreactivity: NO pathway.

*Effect of Bradykinin with or without eNOS-inhibition (LNAME) (A), the NO-donor sodium nitroprusside (SNP) (B), 8-bromo-cyclic guanosine monophosphate (8Br-cGMP) (C) and phosphodiesterase 5 (PDE5) inhibition (Sildenafil) (D). Control n=12, CTEPH n=5 (A); Control n=11, CTEPH n=6 (B); Control n=9, CTEPH n=6 (C); Control n=12, CTEPH n=6 (D). * P < 0.05 CTEPH vs Control; § Effect blocker CTEPH vs effect blocker Control.*

Pulmonary small artery vasoreactivity in vitro: nitric oxide pathway

The vasodilator response to bradykinin (BK) was reduced in CTEPH as compared to Control pulmonary small arteries (Figure 6), consistent with endothelial dysfunction. Surprisingly however, eNOS gene expression was increased (Figure 4 B), while NOS-inhibition attenuated BK-induced vasodilation to a similar extent in pulmonary small arteries from CTEPH and Control. The NO-donor SNP resulted in vasodilation that was more pronounced in CTEPH compared to Control, indicating that sensitivity to NO was increased. To further assess NO signaling, the responses to the stable cGMP analogue 8Br-cGMP and PDE5-inhibition were investigated. The unaltered response to 8Br-cGMP indicates that protein kinase G (PKG) responsiveness to cGMP was maintained. However, the response to PDE5-inhibition was reduced, suggestive of a reduced PDE5-activity (Figure 6). Altogether, the reduced response to PDE5-inhibition, increased SNP-induced vasodilation and the maintained contribution of NO to BK-induced vasodilation, suggest that loss of endogenous NO production is compensated in part by a decreased PDE5 activity resulting in an increased NO-responsiveness.

Discussion

The main findings of the present study in swine with CTEPH are that *(i)* the exercise-induced increase in PAP was exaggerated while the exercise-induced increase in CI was reduced in CTEPH as compared to Control swine, *(ii)* the mild drop in arterial oxygen content that was already present at rest was exacerbated during exercise, *(iii)* inward microvascular remodeling with increased muscularization was present in the pulmonary microvessels of all sizes, *(iv)* the increased muscularization was accompanied by an increase in maximal vasoconstriction to KCl, ET-1 and U46619, *(v)* although absolute vasoconstriction to ET-1 was increased in CTEPH pulmonary small vessels, the sensitivity to ET-1

was reduced with an increased contribution of the ET_A receptor but decreased contribution of the ET_B receptor and complete loss of the contribution of Rho-kinase to ET-1 vasoconstriction, *(vi)* an apparant reduction in endogenous NO production was compensated in part by a decreased PDE5 activity resulting in an increased NO-sensitivity in CTEPH pulmonary small arteries. These findings will be discussed in detail below.

Exercise intolerance in CTEPH

CTEPH is characterized by exercise intolerance which is principally caused by an exacerbated increase in PAP and thereby in RV afterload during exercise, in combination with a significant V/Q-mismatch in the lungs (4, 6, 7). Our CTEPH swine model recapitulates these characteristics of CTEPH. Thus, PAP was disproportionally increased in CTEPH as compared to Control animals in response to exercise. The increased afterload of the right ventricle limited the exercise-induced increase in CI. In humans with CTEPH, physiological dead space is increased in proportion to the increase in PVR, resulting in a lower P_aO_2, which is accompanied by a reduction in P_aCO_2, as a result of compensatory hyperventilation (38). Similarly, the slightly lower P_aO_2 and higher $AaDO_2$ in CTEPH-swine compared to Control are consistent with a mild V/Q-mismatch and dead space ventilation at rest. Contrary to humans with CTEPH, P_aCO_2 was not significantly affected in our porcine CTEPH-model neither at rest, nor during exercise. This discrepancy in CO_2 response between humans and swine is not readily explained, but may in part be because swine lack collateral ventilation and therefore are less capable of ameliorating intraregional V/Q differences between alveoli as compared to humans (27). Furthermore, as healthy quadrupeds already ventilate and perfuse a major part of their lungs at rest (40), an increase in ventilation with CTEPH cannot further recruit hypoventilated lung areas and

improve V/Q mismatch, and hence their hyperventilatory response may not be capable of reducing P_aCO_2 levels below normal as occurs in humans.

The $AaDO_2$ in CTEPH animals was exacerbated during exercise, which is partially attributable to a lower $P_{mv}O_2$ (31.7±0.7 mmHg in Controls and 26.2±2.2 mmHg in CTEPH) as a consequence of the lower CI, and in part reflects a further worsening of the V/Q mismatch due to the faster passage of blood through the pulmonary capillaries upon the exercise-induced increase in CI (27).

Maximal body oxygen consumption was reduced and arterial lactate concentration was increased by more than 2 mmol/L, indicating that, consistent with patient data (19, 23, 29, 48), the anaerobic threshold was reached in CTEPH but not sham-operated swine during exercise at 4km/h. Particularly the decreased CI (27% lower in CTEPH as compared to Control) and to a lesser extent the decreased C_aO_2 (10% lower as compared to Control), limited the increase in body oxygen delivery during exercise. These findings suggest that exercise intolerance in CTEPH is principally caused by the increased pulmonary vascular resistance, and thereby the afterload of the RV, that limits the exercise induced increase in CI. The V/Q-mismatch that hampers arterial oxygenation also contributes to exercise intolerance, but to a lesser extent. However, the relative contributions of cardiac and pulmonary dysfunction to the exercise intolerance in patients with more severe RV dysfunction remains to be established. Cardiopulmonary exercise testing in CTEPH patients will therefore yield valuable data to help determine the cause(s) of their exercise intolerance (37).

Pulmonary microvascular remodeling

CTEPH occurs in a minority of patients after acute pulmonary embolism. However, also patients that did not experience (or did not notice to) an acute pulmonary

embolism have been reported to develop CTEPH (51). In these patients, it is proposed that CTEPH is the consequence of multiple micro-embolisms (17, 55). Our swine model with repeated micro-embolization procedures is similar to the second group of patients. It is increasingly recognized that, not only proximal obstructions, but also distal remodeling of the unobstructed pulmonary microvasculature contributes to the pathogenesis of CTEPH (17, 42). In accordance with previous studies in humans and animals (5, 11, 42), we observed inward remodeling of both pulmonary small arteries and the pulmonary microvasculature. This remodeling encompassed muscularization and thickening of the vascular wall and resulted in a relative reduction of the vascular lumen (Figure 2 & Figure 8-10). The changes in microvascular morphology were not accompanied by an overt pulmonary inflammatory response at this stage, as only IL-6 showed a trend towards an increase, consistent with the increase in IL-6 in CTEPH patients (49, 57, 58), while IFN- γ, TNF-α and TGF-β were unaltered. Although the existence of pulmonary microvascular remodeling is known since 1993 (42), the consequences of this remodeling for pulmonary microvascular function have not been investigated to date. The present study shows that, consistent with the increased vascular muscularization in CTEPH, the maximal contraction of these vessels was also increased. In addition, microvascular remodeling was accompanied by alterations in two major endothelial signaling pathways, i.e. ET and NO, that are also implicated in development and progression of pulmonary hypertension (3), as will be further discussed below.

Endothelial dysfunction in CTEPH

Endothelial dysfunction was characterized by an imbalance between endothelial production of the vasodilator NO and the vasoconstrictor ET-1 while vascular integrity was intact at this stage. Perturbations in the NO-pathway have been

implicated in the pathogenesis of PH (3, 31, 59). Indeed, we have previously shown that chronic eNOS-inhibition is required to successfully produce stable CTEPH in swine, as microsphere embolizations alone do not result in sustained PH (54). To preclude a direct effect of eNOS-inhibition on both the in vivo and the in vitro measurements, eNOS inhibition was discontinued two weeks before the end of study. Moreover, control animals with and without chronic eNOS-inhibition were included. In accordance with our previous study, which showed no effect of chronic eNOS-inhibition on hemodynamics in control animals (54), in the present study, chronic eNOS-inhibition in control animals had no effect on vasoreactivity, plasma ET-levels and pulmonary gene expression (Figure 7).

In pulmonary small arteries from CTEPH the vasodilator response to BK was reduced as compared to Control. Surprisingly however, eNOS-inhibition attenuated the BK-induced vasodilation to a similar degree in CTEPH and Control, indicating that either NO production was maintained or a decreased NO production was compensated by an increased sensitivity to NO. The increased vasodilation in response to the NO-donor SNP in CTEPH compared to Control is consistent with an increased sensitivity to NO. This increased vasodilator response to NO is in line with vasodilation observed during treatment with inhaled NO in CTEPH patients (1). The response to the stable cGMP analogue 8Br-cGMP was similar in CTEPH compared to Control vessels, indicating that PKG responsiveness to cGMP was preserved in CTEPH.

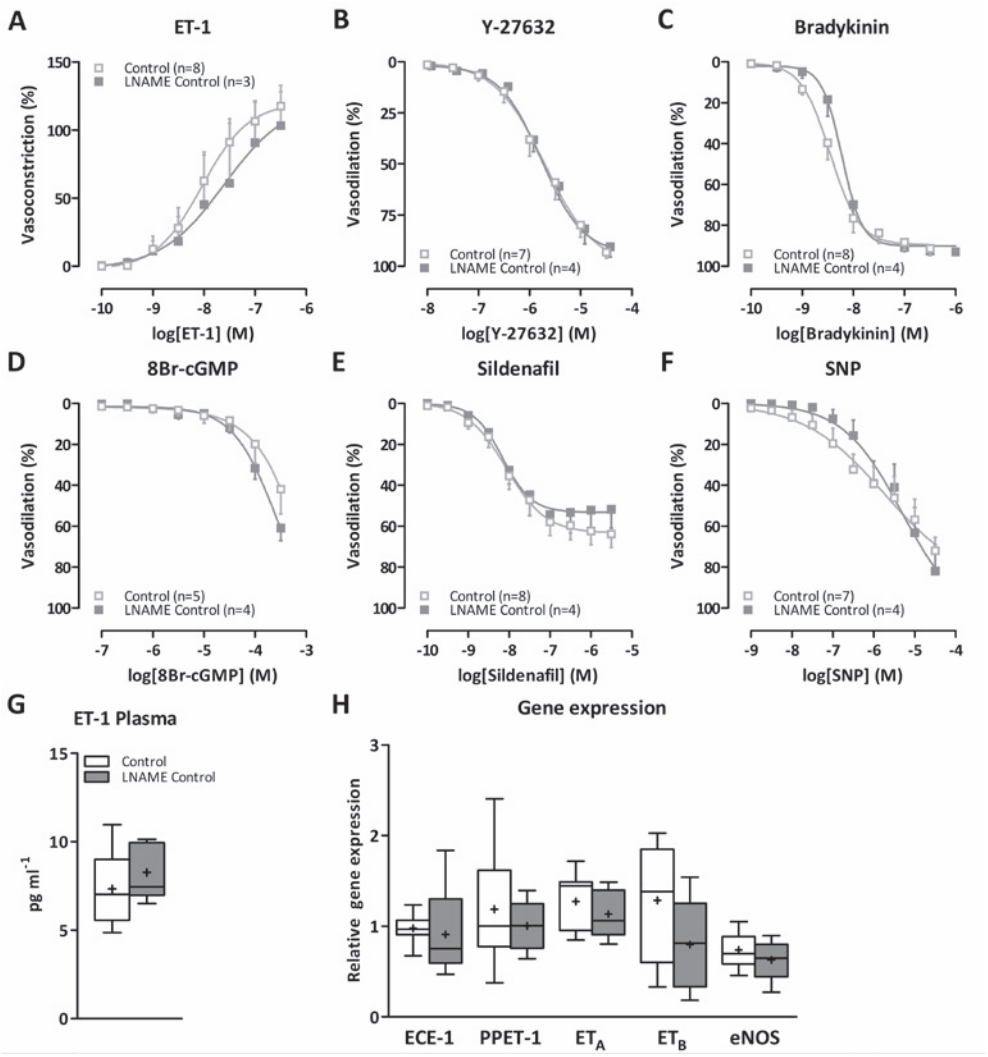

Figure 7. Pulmonary vasoreactivity: Comparison of Control with or without LNAME.

Effect of endothelin (ET-1) (A), Rho-kinase inhibition (Y-27632) (B), Bradykinin (C), 8-bromo-cyclic guanosine monophosphate (8Br-cGMP) (D), phosphodiesterase 5 (PDE5) inhibition (Sildenafil) (E) and the NO-donor sodium nitroprusside (SNP) (F) on the vasoconstriction or vasodilation of pulmonary small arteries, plasma ET-1 levels (G) and gene expression in lung tissue (H) of Control animals with (LNAME Control) and without (Control) LNAME. Whiskers denote min to max and means are presented as +. Control n=8, LNAME Control n=3 (A); Control n=7, LNAME Control n=4 (B&F); Control n=8, LNAME Control n=4 (C&E); Control n=5, LNAME Control n=4 (D); Control n=6, LNAME Control n=5 (G); Control n=9, LNAME Control n=5 (H). No significant differences were observed.

Finally, the response to PDE5-inhibition was reduced in the CTEPH arteries, suggesting that reduced PDE5-activity acted to compensate, in part, for a blunted endogenous NO production, resulting in an increase in NO-sensitivity. The reduced response to Sildenafil provides a potential explanation for the failure of single treatment with Sildenafil as a therapeutic strategy for CTEPH and underscores the importance of intervening more upstream in the NO-pathway either by administering NO (1) or stimulating sGC. Indeed, beneficial therapeutic effects have been reported for Riociguat, a sGC stimulator, which was recently approved for therapeutic use in CTEPH (22, 30, 33, 50).

Endothelin receptor antagonists (ERAs) are an established therapy for PAH (16, 32), but conflicting results of ERA therapy have been reported in CTEPH patients (24, 25, 44). The 40% higher plasma ET-1 in our porcine model is slightly less than the doubling observed in patient studies. However, clinically, our animals represent New York Heart Association (NYHA) class II or III, in which the elevation in ET-1 is less than in patients with NYHA class IV (21, 47). Although plasma ET-1 levels correlate well with clinical severity (21, 47), the contribution of changes in ET signaling to structural and functional changes in the pulmonary microvasculature has not been established. The present study shows that the increase in circulating ET-1 is accompanied by a decreased sensitivity of the pulmonary microvasculature to ET-1, as evidenced by a rightward shift in the ET-1 response in pulmonary small arteries of animals with CTEPH as compared to Control. The relative contribution of the ET_A receptor to the ET-1-induced vasoconstriction was slightly enhanced in pulmonary small arteries from animals with CTEPH as compared to Control. Moreover, ET_B receptor blockade attenuated the contraction to ET-1 in the presence of ET_A receptor blockade but it had no effect in pulmonary small arteries from animals with CTEPH. These data are in accordance with the increased ET_A receptor expression in pulmonary

endarterectomy tissues (53) and in the lungs of swine with CTEPH (39), as well as with the increased ET_A/ET_B ratio observed in the present study. The latter was, however, primarily due to a decrease in ET_B mRNA, which contrasts with another study in a different CTEPH- swine model that shows an increased ET_B mRNA expression in the unobstructed areas of the lungs (39). However as both ET_A and ET_B receptors have also been shown to be present on bronchial smooth muscle (20), a change in mRNA expression may not solely reflect a change in expression in the pulmonary vasculature. These data suggest that CTEPH is accompanied by changes in ET-1 signaling in the pulmonary microvasculature and that the interaction between the ET_A and the ET_B receptor is altered in CTEPH. The loss of ET_B mediated vasoactive effects observed in the present study suggests that dual ERA therapy may not be more effective as compared to ET_A blockade alone. Moreover, in CTEPH the effect of ET-1 is already suppressed by a decreased sensitivity which would explain the observed inefficacy of ERA's.

ET-1 signaling occurs via two pathways, i.e. a calcium-dependent pathway involving phospholipase C (PLC)-mediated activation of myosin-light chain kinase and a calcium-independent pathway involving RhoA-Rho-kinase mediated inactivation of myosin phosphatase (28). Rho-kinase inhibition with Fasudil has been shown to be an effective therapy in some patients with PAH (15), but little is known about this pathway in the pathology of CTEPH. In the present study, Rho-kinase inhibition caused vasodilation of pulmonary small arteries of Control animals, which was blunted in CTEPH as compared to Control. Moreover, ET-1-induced contraction was attenuated by Rho-kinase inhibition in pulmonary small arteries from Control but not CTEPH swine. Although a reduction in Rho-kinase was not present at mRNA level in the CTEPH swine, mRNA levels of lung tissue may not reflect protein levels and/or enzyme activity in the vasculature. The data obtained from the isolated pulmonary small arteries indicate a complete loss of

the Rho-kinase contribution to ET-1-induced vasoconstriction in the CTEPH small arteries, and imply that, ET-1-induced vasoconstriction in CTEPH must therefore be mediated through the PLC-pathway. These results are very different from those obtained in PAH, where the contribution of Rho-kinase was found to be increased (10). Together, these data suggest that microvascular constriction and remodeling occur via different pathways in CTEPH as compared to PAH, and could be interpreted to suggest that the use of Rho-kinase inhibitors to alleviate pulmonary vasoconstriction may be useless in CTEPH patients.

It is however, important to note that the present study investigated the contribution of endothelial dysfunction to the acute regulation of vascular tone, and that these results may not directly apply to the role of endothelial dysfunction in pulmonary microvascular remodeling and long-term effects of therapy. Future studies are thus required to investigate the pulmonary effects of chronic Rho-kinase inhibition in CTEPH.

Altogether, our study shows that alterations in microvascular structure contribute to the increase in pulmonary vascular resistance. These changes in microvascular structure are accompanied by changes in microvascular function that may have therapeutic consequences in that the efficacy of therapeutic agents that are commonly applied in PAH, may not be as effective in CTEPH.

Acknowledgements

The authors would like to acknowledge the expert technical assistance of Annemarie Verzijl and Zongye Cai. We would like to thank Dylan van der Vusse, Brechje de Rapper, Jessica Lange and Paula Krul for their assistance.

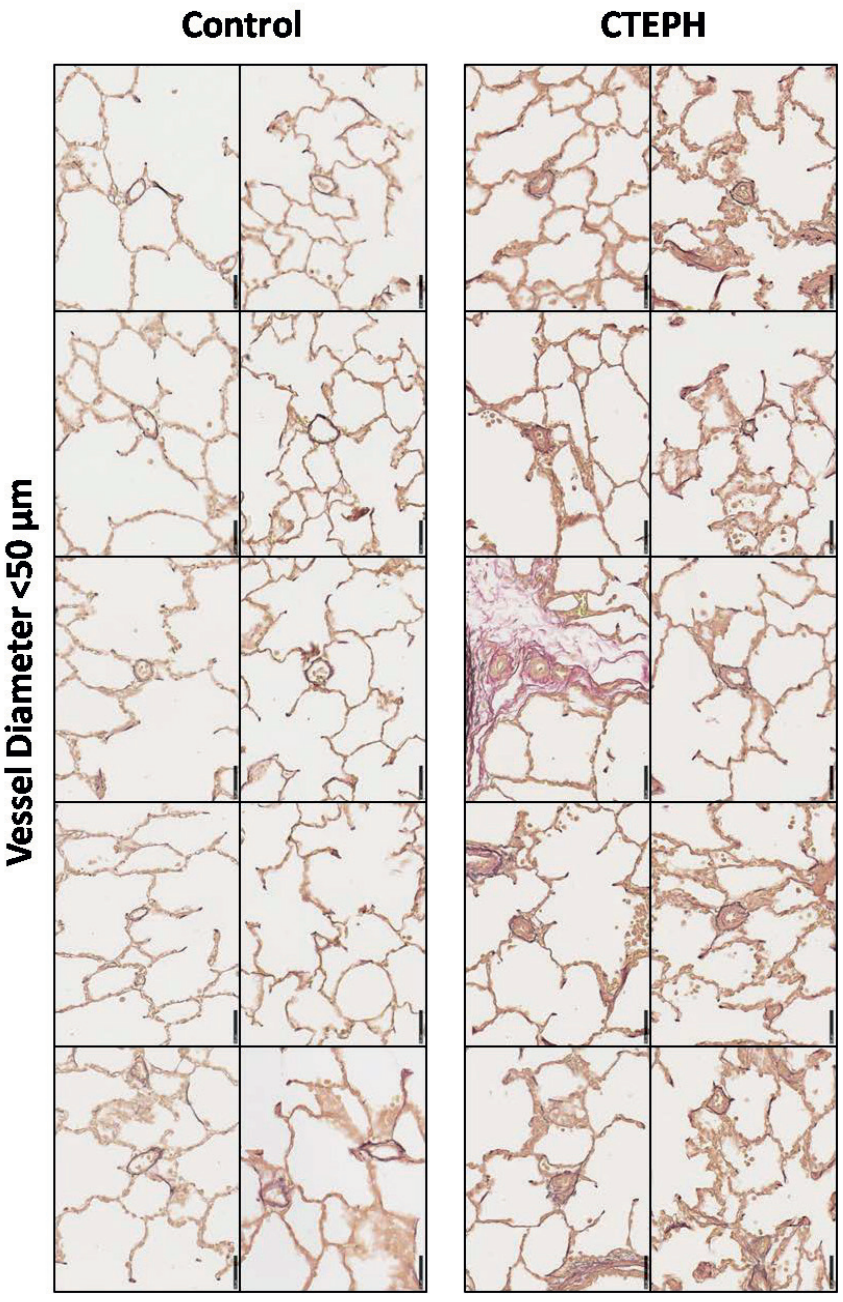

Figure 8. Pulmonary microvascular histology overview, vessel diameter < 50µm.

Pictures of the Resorcin Fuchsin von Gieson (RF) staining of distal pulmonary arteries with a diameter of <50 µm at 40x magnification from the Control (top ten pictures) and CTEPH (bottom ten pictures) lungs. Scale bar is 50 µm.

Figure 9. Pulmonary microvascular histology overview, vessel diameter 51-100µm.
Pictures of the Resorcin Fuchsin von Gieson (RF) staining of distal pulmonary arteries with a diameter of 50-100 µm at 20x magnification from the Control (top ten pictures) and CTEPH (bottom ten pictures) lungs. Scale bar is 100 µm.

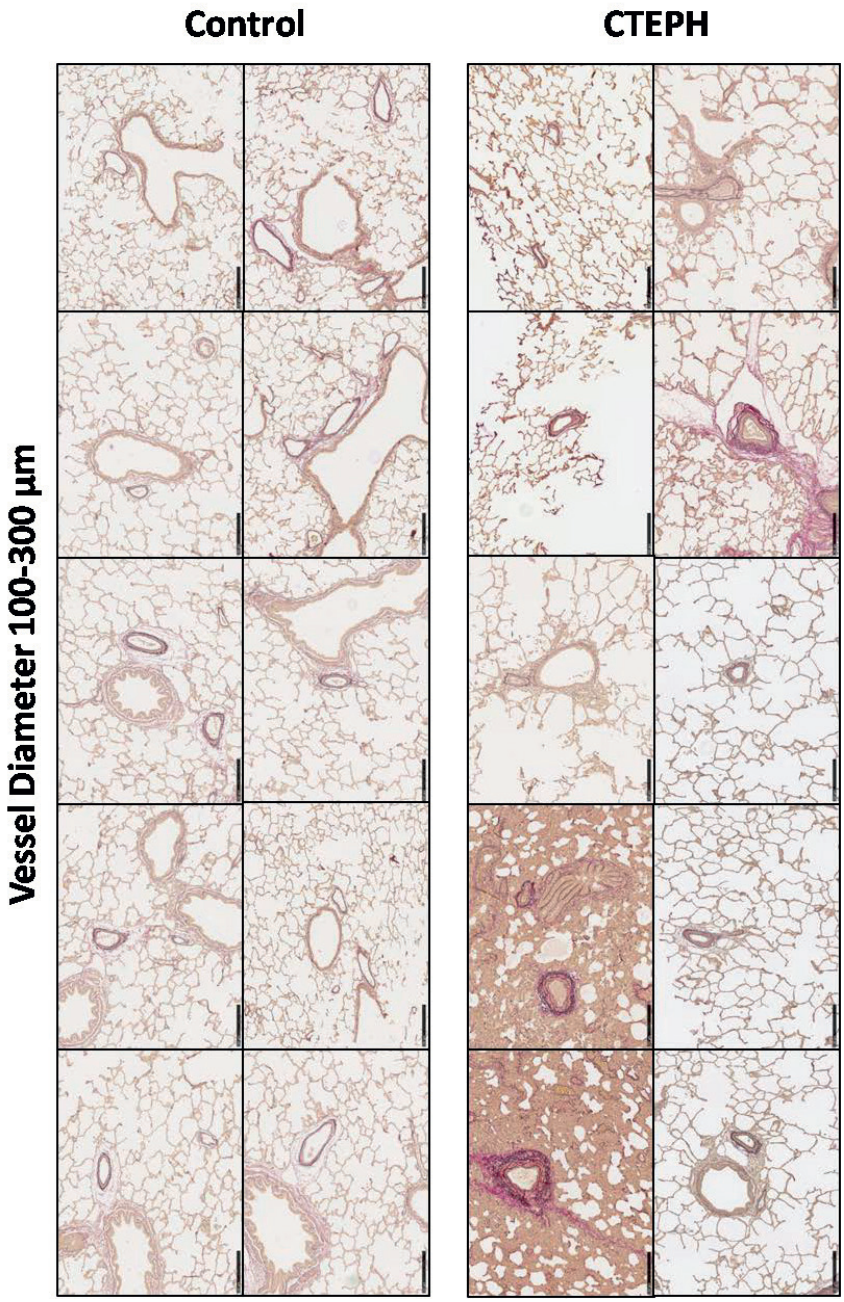

Figure 10. Pulmonary microvascular histology overview, vessel diameter 101-300µm.

Pictures of the Resorcin Fuchsin von Gieson (RF) staining of distal pulmonary arteries with a diameter of 100-300 µm at 10x magnification, from the Control (top ten pictures) and CTEPH (bottom ten pictures) lungs. Scale bar is 250 µm.

References

1. **Abe S, Ishida K, Masuda M, Ueda H, Kohno H, Matsuura K, Tamura Y, Watanabe M, and Matsumiya G**. A prospective, randomized study of inhaled prostacyclin versus nitric oxide in patients with residual pulmonary hypertension after pulmonary endarterectomy. *Gen Thorac Cardiovasc Surg* 65: 153-159, 2017.

2. **Allahdadi KJ, Hannan JL, Tostes RC, and Webb RC**. Endothelin-1 induces contraction of female rat internal pudendal and clitoral arteries through ET(A) receptor and rho-kinase activation. *J Sex Med* 7: 2096-2103, 2010.

3. **Ataya A, Cope J, and Alnuaimat H**. A Review of Targeted Pulmonary Arterial Hypertension-Specific Pharmacotherapy. *J Clin Med* 5: 2016.

4. **Blumberg FC, Arzt M, Lange T, Schroll S, Pfeifer M, and Wensel R**. Impact of right ventricular reserve on exercise capacity and survival in patients with pulmonary hypertension. *Eur J Heart Fail* 15: 771-775, 2013.

5. **Boulate D, Perros F, Dorfmuller P, Arthur-Ataam J, Guihaire J, Lamrani L, Decante B, Humbert M, Eddahibi S, Dartevelle P, Fadel E, and Mercier O**. Pulmonary microvascular lesions regress in reperfused chronic thromboembolic pulmonary hypertension. *J Heart Lung Transplant* 34: 457-467, 2015.

6. **Claessen G, La Gerche A, Dymarkowski S, Claus P, Delcroix M, and Heidbuchel H**. Pulmonary vascular and right ventricular reserve in patients with normalized resting hemodynamics after pulmonary endarterectomy. *J Am Heart Assoc* 4: e001602, 2015.

7. **Claessen G, La Gerche A, Wielandts JY, Bogaert J, Van Cleemput J, Wuyts W, Claus P, Delcroix M, and Heidbuchel H**. Exercise pathophysiology and sildenafil effects in chronic thromboembolic pulmonary hypertension. *Heart* 101: 637-644, 2015.

8. **De Wijs-Meijler DP, Stam K, van Duin RW, Verzijl A, Reiss IK, Duncker DJ, and Merkus D**. Surgical Placement of Catheters for Long-term Cardiovascular Exercise Testing in Swine. *J Vis Exp* e53772, 2016.

9. **Delcroix M, Vonk Noordegraaf A, Fadel E, Lang I, Simonneau G, and Naeije R**. Vascular and right ventricular remodelling in chronic thromboembolic pulmonary hypertension. *Eur Respir J* 41: 224-232, 2013.

10. **Do e Z, Fukumoto Y, Takaki A, Tawara S, Ohashi J, Nakano M, Tada T, Saji K, Sugimura K, Fujita H, Hoshikawa Y, Nawata J, Kondo T, and Shimokawa H**.

Evidence for Rho-kinase activation in patients with pulmonary arterial hypertension. *Circ J* 73: 1731-1739, 2009.

11. **Dorfmuller P, Gunther S, Ghigna MR, Thomas de Montpreville V, Boulate D, Paul JF, Jais X, Decante B, Simonneau G, Dartevelle P, Humbert M, Fadel E, and Mercier O**. Microvascular disease in chronic thromboembolic pulmonary hypertension: a role for pulmonary veins and systemic vasculature. *Eur Respir J* 44: 1275-1288, 2014.

12. **Duncker DJ, Stubenitsky R, and Verdouw PD**. Role of adenosine in the regulation of coronary blood flow in swine at rest and during treadmill exercise. *Am J Physiol* 275: H1663-1672, 1998.

13. **Edward JA, and Mandras S**. An Update on the Management of Chronic Thromboembolic Pulmonary Hypertension. *Curr Probl Cardiol* 42: 7-38, 2017.

14. **Fuji S, Matsushita S, Hyodo K, Osaka M, Sakamoto H, Tanioka K, Miyakawa K, Kubota M, Hiramatsu Y, and Tokunaga C**. Association between endothelial function and micro-vascular remodeling measured by synchrotron radiation pulmonary micro-angiography in pulmonary arterial hypertension. *Gen Thorac Cardiovasc Surg* 64: 597-603, 2016.

15. **Fukumoto Y, Yamada N, Matsubara H, Mizoguchi M, Uchino K, Yao A, Kihara Y, Kawano M, Watanabe H, Takeda Y, Adachi T, Osanai S, Tanabe N, Inoue T, Kubo A, Ota Y, Fukuda K, Nakano T, and Shimokawa H**. Double-blind, placebo-controlled clinical trial with a rho-kinase inhibitor in pulmonary arterial hypertension. *Circ J* 77: 2619-2625, 2013.

16. **Galie N, Humbert M, Vachiery JL, Gibbs S, Lang I, Torbicki A, Simonneau G, Peacock A, Vonk Noordegraaf A, Beghetti M, Ghofrani A, Gomez Sanchez MA, Hansmann G, Klepetko W, Lancellotti P, Matucci M, McDonagh T, Pierard LA, Trindade PT, Zompatori M, Hoeper M, Aboyans V, Vaz Carneiro A, Achenbach S, Agewall S, Allanore Y, Asteggiano R, Paolo Badano L, Albert Barbera J, Bouvaist H, Bueno H, Byrne RA, Carerj S, Castro G, Erol C, Falk V, Funck-Brentano C, Gorenflo M, Granton J, Iung B, Kiely DG, Kirchhof P, Kjellstrom B, Landmesser U, Lekakis J, Lionis C, Lip GY, Orfanos SE, Park MH, Piepoli MF, Ponikowski P, Revel MP, Rigau D, Rosenkranz S, Voller H, and Luis Zamorano J**. 2015 ESC/ERS Guidelines for the diagnosis and treatment of pulmonary hypertension: The Joint Task Force for the Diagnosis and Treatment of Pulmonary Hypertension of the European Society of Cardiology (ESC) and the European Respiratory Society (ERS): Endorsed by: Association for European Paediatric and Congenital Cardiology

(AEPC), International Society for Heart and Lung Transplantation (ISHLT). *Eur Heart J* 37: 67-119, 2016.

17. **Galie N, and Kim NH**. Pulmonary microvascular disease in chronic thromboembolic pulmonary hypertension. *Proc Am Thorac Soc* 3: 571-576, 2006.

18. **Gao Y, Portugal AD, Negash S, Zhou W, Longo LD, and Usha Raj J**. Role of Rho kinases in PKG-mediated relaxation of pulmonary arteries of fetal lambs exposed to chronic high altitude hypoxia. *Am J Physiol Lung Cell Mol Physiol* 292: L678-684, 2007.

19. **Godinas L, Sattler C, Lau EM, Jais X, Taniguchi Y, Jevnikar M, Weatherald J, Sitbon O, Savale L, Montani D, Simonneau G, Humbert M, Laveneziana P, and Garcia G**. Dead-space ventilation is linked to exercise capacity and survival in distal chronic thromboembolic pulmonary hypertension. *J Heart Lung Transplant* 2017.

20. **Goldie RG, D'Aprile AC, Cvetkovski R, Rigby PJ, and Henry PJ**. Influence of regional differences in ETA and ETB receptor subtype proportions on endothelin-1-induced contractions in porcine isolated trachea and bronchus. *Br J Pharmacol* 117: 736-742, 1996.

21. **Guo L, Yang Y, Liu J, Wang L, Li J, Wang Y, Liu Y, Gu S, Gan H, Cai J, Yuan JX, Wang J, and Wang C**. Differentially expressed plasma microRNAs and the potential regulatory function of Let-7b in chronic thromboembolic pulmonary hypertension. *PLoS One* 9: e101055, 2014.

22. **Halank M, Hoeper MM, Ghofrani HA, Meyer FJ, Stahler G, Behr J, Ewert R, Fletcher M, Colorado P, Nikkho S, and Grimminger F**. Riociguat for pulmonary arterial hypertension and chronic thromboembolic pulmonary hypertension: Results from a phase II long-term extension study. *Respir Med* 128: 50-56, 2017.

23. **Held M, Kolb P, Grun M, Jany B, Hubner G, Grgic A, Holl R, Schaefers HJ, and Wilkens H**. Functional Characterization of Patients with Chronic Thromboembolic Disease. *Respiration* 91: 503-509, 2016.

24. **Hirashiki A, Adachi S, Nakano Y, Kamimura Y, Shimokata S, Takeshita K, Murohara T, and Kondo T**. Effects of bosentan on peripheral endothelial function in patients with pulmonary arterial hypertension or chronic thromboembolic pulmonary hypertension. *Pulm Circ* 6: 168-173, 2016.

25. **Hirashiki A, Adachi S, Nakano Y, Kono Y, Shimazu S, Shimizu S, Morimoto R, Okumura T, Takeshita K, Yamada S, Murohara T, and Kondo T**. Cardiopulmonary exercise testing to evaluate the exercise capacity of patients

with inoperable chronic thromboembolic pulmonary hypertension: an endothelin receptor antagonist improves the peak PETCO2. *Life Sci* 118: 397-403, 2014.

26. **Hoeper MM, Bogaard HJ, Condliffe R, Frantz R, Khanna D, Kurzyna M, Langleben D, Manes A, Satoh T, Torres F, Wilkins MR, and Badesch DB**. Definitions and diagnosis of pulmonary hypertension. *J Am Coll Cardiol* 62: D42-50, 2013.

27. **Hopkins SR, Stary CM, Falor E, Wagner H, Wagner PD, and McKirnan MD**. Pulmonary gas exchange during exercise in pigs. *J Appl Physiol (1985)* 86: 93-100, 1999.

28. **Horinouchi T, Terada K, Higashi T, and Miwa S**. Endothelin receptor signaling: new insight into its regulatory mechanisms. *J Pharmacol Sci* 123: 85-101, 2013.

29. **Iwase T, Nagaya N, Ando M, Satoh T, Sakamaki F, Kyotani S, Takaki H, Goto Y, Ohkita Y, Uematsu M, Nakanishi N, and Miyatake K**. Acute and chronic effects of surgical thromboendarterectomy on exercise capacity and ventilatory efficiency in patients with chronic thromboembolic pulmonary hypertension. *Heart* 86: 188-192, 2001.

30. **Koress C, Swan K, and Kadowitz P**. Soluble Guanylate Cyclase Stimulators and Activators: Novel Therapies for Pulmonary Vascular Disease or a Different Method of Increasing cGMP? *Curr Hypertens Rep* 18: 42, 2016.

31. **Kruzliak P, Maruyama J, and Maruyama K**. Role of nitric oxide in pathophysiology and treatment of pulmonary hypertension. *Vitam Horm* 96: 407-424, 2014.

32. **Lau EMT, Giannoulatou E, Celermajer DS, and Humbert M**. Epidemiology and treatment of pulmonary arterial hypertension. *Nat Rev Cardiol* 2017.

33. **Lian TY, Jiang X, and Jing ZC**. Riociguat: a soluble guanylate cyclase stimulator for the treatment of pulmonary hypertension. *Drug Des Devel Ther* 11: 1195-1207, 2017.

34. **Lin YJ, Markham NE, Balasubramaniam V, Tang JR, Maxey A, Kinsella JP, and Abman SH**. Inhaled nitric oxide enhances distal lung growth after exposure to hyperoxia in neonatal rats. *Pediatr Res* 58: 22-29, 2005.

35. **Matsunaga T, Warltier DC, Weihrauch DW, Moniz M, Tessmer J, and Chilian WM**. Ischemia-induced coronary collateral growth is dependent on vascular endothelial growth factor and nitric oxide. *Circulation* 102: 3098-3103, 2000.

36. **Matthews DT, and Hemnes AR**. Current concepts in the pathogenesis of chronic thromboembolic pulmonary hypertension. *Pulm Circ* 6: 145-154, 2016.

37. **McCabe C, Deboeck G, Harvey I, Ross RM, Gopalan D, Screaton N, and Pepke-Zaba J**. Inefficient exercise gas exchange identifies pulmonary hypertension in chronic thromboembolic obstruction following pulmonary embolism. *Thromb Res* 132: 659-665, 2013.

38. **Melot C, and Naeije R**. Pulmonary vascular diseases. *Compr Physiol* 1: 593-619, 2011.

39. **Mercier O, Tivane A, Dorfmuller P, de Perrot M, Raoux F, Decante B, Eddahibi S, Dartevelle P, and Fadel E**. Piglet model of chronic pulmonary hypertension. *Pulm Circ* 3: 908-915, 2013.

40. **Merkus D, de Beer VJ, Houweling B, and Duncker DJ**. Control of pulmonary vascular tone during exercise in health and pulmonary hypertension. *Pharmacol Ther* 119: 242-263, 2008.

41. **Mickley EJ, Gray GA, and Webb DJ**. Activation of endothelin ETA receptors masks the constrictor role of endothelin ETB receptors in rat isolated small mesenteric arteries. *Br J Pharmacol* 120: 1376-1382, 1997.

42. **Moser KM, and Bloor CM**. Pulmonary vascular lesions occurring in patients with chronic major vessel thromboembolic pulmonary hypertension. *Chest* 103: 685-692, 1993.

43. **Mulvany MJ, and Halpern W**. Contractile properties of small arterial resistance vessels in spontaneously hypertensive and normotensive rats. *Circ Res* 41: 19-26, 1977.

44. **Nishikawa-Takahashi M, Ueno S, and Kario K**. Long-term advanced therapy with bosentan improves symptoms and prevents deterioration of inoperable chronic thromboembolic pulmonary hypertension. *Life Sci* 118: 410-413, 2014.

45. **Pepke-Zaba J, Ghofrani HA, and Hoeper MM**. Medical management of chronic thromboembolic pulmonary hypertension. *Eur Respir Rev* 26: 2017.

46. **Rees DD, Palmer RM, Schulz R, Hodson HF, and Moncada S**. Characterization of three inhibitors of endothelial nitric oxide synthase in vitro and in vivo. *Br J Pharmacol* 101: 746-752, 1990.

47. **Reesink HJ, Meijer RC, Lutter R, Boomsma F, Jansen HM, Kloek JJ, and Bresser P**. Hemodynamic and clinical correlates of endothelin-1 in chronic thromboembolic pulmonary hypertension. *Circ J* 70: 1058-1063, 2006.

48. **Richter MJ, Pader P, Gall H, Reichenberger F, Seeger W, Mayer E, Guth S, Kramm T, Grimminger F, Ghofrani HA, and Voswinckel R**. The prognostic relevance of oxygen uptake in inoperable chronic thromboembolic pulmonary hypertension. *Clin Respir J* 2015.

49. **Saleby J, Bouzina H, Lundgren J, and Radegran G**. Angiogenic and inflammatory biomarkers in the differentiation of pulmonary hypertension. *Scand Cardiovasc J* 51: 261-270, 2017.

50. **Simonneau G, D'Armini AM, Ghofrani HA, Grimminger F, Hoeper MM, Jansa P, Kim NH, Wang C, Wilkins MR, Fritsch A, Davie N, Colorado P, and Mayer E**. Riociguat for the treatment of chronic thromboembolic pulmonary hypertension: a long-term extension study (CHEST-2). *Eur Respir J* 45: 1293-1302, 2015.

51. **Simonneau G, Torbicki A, Dorfmuller P, and Kim N**. The pathophysiology of chronic thromboembolic pulmonary hypertension. *Eur Respir Rev* 26: 2017.

52. **Sitbon O, and Gaine S**. Beyond a single pathway: combination therapy in pulmonary arterial hypertension. *Eur Respir Rev* 25: 408-417, 2016.

53. **Southwood M, MacKenzie Ross RV, Kuc RE, Hagan G, Sheares KK, Jenkins DP, Goddard M, Davenport AP, and Pepke-Zaba J**. Endothelin ETA receptors predominate in chronic thromboembolic pulmonary hypertension. *Life Sci* 159: 104-110, 2016.

54. **Stam K, van Duin RWB, Uitterdijk A, Cai Z, Duncker DJ, and Merkus D**. Exercise Facilitates Early Recognition of Cardiac and Vascular Remodeling in Chronic Thrombo-Embolic Pulmonary Hypertension in a Novel CTEPH Swine Model. *Am J Physiol Heart Circ Physiol* ajpheart 00380 02017, 2017.

55. **Stein PD, Goodman LR, Hull RD, Dalen JE, and Matta F**. Diagnosis and management of isolated subsegmental pulmonary embolism: review and assessment of the options. *Clin Appl Thromb Hemost* 18: 20-26, 2012.

56. **Stubenitsky R, Verdouw PD, and Duncker DJ**. Autonomic control of cardiovascular performance and whole body O2 delivery and utilization in swine during treadmill exercise. *Cardiovasc Res* 39: 459-474, 1998.

57. **Xi Q, Liu Z, Liu W, Zhao Z, Luo Q, and Huang Z**. Chronic thromboembolic pulmonary hypertension is not associated with iron overload. *Cardiovasc Pathol* 24: 76-79, 2015.

58. **Zabini D, Heinemann A, Foris V, Nagaraj C, Nierlich P, Balint Z, Kwapiszewska G, Lang IM, Klepetko W, Olschewski H, and Olschewski A**.

Comprehensive analysis of inflammatory markers in chronic thromboembolic pulmonary hypertension patients. *Eur Respir J* 44: 951-962, 2014.

59. **Zhang S, Yang T, Xu X, Wang M, Zhong L, Yang Y, Zhai Z, Xiao F, and Wang C**. Oxidative stress and nitric oxide signaling related biomarkers in patients with pulmonary hypertension: a case control study. *BMC Pulm Med* 15: 50, 2015.

60. **Zhou Z, de Beer VJ, de Wijs-Meijler D, Bender SB, Hoekstra M, Laughlin MH, Duncker DJ, and Merkus D**. Pulmonary vasoconstrictor influence of endothelin in exercising swine depends critically on phosphodiesterase 5 activity. *Am J Physiol Lung Cell Mol Physiol* 306: L442-452, 2014.

Chapter 6

Cardiac Remodeling in a Swine Model of Chronic Thrombo-Embolic Pulmonary Hypertension- Comparison of Right vs Left ventricle

Kelly Stam, Zongye Cai, Nikki van der Velde, Richard van Duin, Esther Lam, Jolanda van der Velden, Alexander Hirsch, Dirk J Duncker, Daphne Merkus

J Physiol 2019 Jun 13

Abstract

Right ventricular (RV) function is the most important determinant of survival and quality of life in patients with chronic thrombo-embolic pulmonary hypertension (CTEPH). This study investigated whether the increased cardiac afterload is associated with 1) cardiac remodeling and hypertrophic signalling, 2) changes in angiogenic factors and capillary density and 3) inflammatory changes associated with oxidative stress and interstitial fibrosis.

CTEPH was induced in eight chronically instrumented swine by chronic NOS inhibition and up to 5-weekly pulmonary embolizations. Nine healthy swine served as control. After nine weeks, RV function was assessed by single beat analysis of RV-pulmonary artery (PA) coupling at rest and during exercise, and by cardiac magnetic resonance imaging. Subsequently, the heart was excised and RV and LV tissues were processed for molecular and histological analyses.

Swine with CTEPH exhibited significant RV hypertrophy in response to the elevated PA pressure. RV-PA coupling was significantly reduced, correlated inversely with pulmonary vascular resistance and did not increase during exercise in CTEPH swine. Expression of genes associated with hypertrophy (BNP), inflammation (TGFβ), oxidative stress (ROCK2, NOX1 and NOX4), apoptosis (BCL2 and Caspase-3) and angiogenesis (VEGFA), were increased in the RV of CTEPH swine and correlated inversely with RV-PA coupling during exercise. In the LV, only significant changes in ROCK2 gene-expression occurred.

In conclusion, RV-remodeling in our CTEPH swine model is associated with increased expression of genes involved in inflammation and oxidative stress, suggesting that these processes contribute to RV remodeling and dysfunction in CTEPH and hence represent potential therapeutic targets.

Introduction

Chronic thrombo-embolic pulmonary hypertension (CTEPH) develops in a subset of patients after acute pulmonary embolism (31, 45). In CTEPH, pulmonary vascular resistance, which is initially elevated due to the obstructions in the larger pulmonary arteries, is further increased by pulmonary microvascular remodeling (31, 45). This increased pulmonary vascular resistance augments afterload of the right ventricle (RV), thereby resulting in RV dilation and RV hypertrophy. RV structural and functional adaptability are important determinants of functional capacity and survival in patients with CTEPH (9, 25, 55). Thus, RV-pulmonary arterial uncoupling is associated with reduced exercise-capacity (9), and patients with RV dilation have a worse prognosis compared to patients with preserved RV function and geometry (2, 20). Furthermore, it has become increasingly recognized that RV dysfunction may also influence the left ventricle (LV), both mechanically, through direct mechanical interaction and changes in LV filling, by inducing interventricular asynchrony (35, 58) as well as through activation of inflammatory pathways, that may be the result of low grade systemic inflammation in combination with neurohumoral activation due to reduced cardiac output (13, 25, 39).

In CTEPH, pulmonary obstructive lesions can be located both proximally and distally. Distal pulmonary lesions have recently been shown to be associated with worse prognosis, in part because distal pulmonary lesions are currently deemed inoperable, and in part because distal pulmonary emboli are associated with worse RV function (20). Furthermore, also in patients with chronic thromboembolic disease, even without overt pulmonary hypertension (PH), RV dysfunction has been observed (38), which is associated with an impaired exercise capacity (9).

It is currently unknown which factor(s) predispose(s) to RV failure. Unlike pulmonary arterial hypertension, which is usually only detected in a very advanced stage of the disease, CTEPH occurs mostly after acute pulmonary embolism, which despite the fact that this first pulmonary embolism may also go unnoticed (Ende-Verhaar *et al*, 2017), may allow earlier intervention in the process of RV remodeling and adaptation,. Mild RV dysfunction is characterized by a deterioration of RV diastolic function (i.e. relaxation), while RV contraction is still preserved (38). The main determinant of cardiac diastolic function is cardiac stiffness, which is negatively influenced by interstitial fibrosis as well as by changes in isoform- expression of the 'cardiac spring protein' titin (41). Furthermore, it has been proposed that the failure of angiogenesis to keep up with RV hypertrophy, resulting in reduced capillary densities and concommittant RV perfusion abnormalities, is a key determinant that discriminates between adaptive RV hypertrophy and RV failure (17).

We have recently developed a swine model, in which a combination of endothelial dysfunction by NOS inhibition with pulmonary embolizations with microspheres of~700 µm in diameter resulted in the development of CTEPH with distal pulmonary microvascular remodeling (47, 48). In CTEPH animals, the increased afterload was accompanied by RV hypertrophy, that resulted in preservation of RV function at rest, but stroke volume (SV) decreased with increasing exercise intensity, suggesting mild RV dysfunction (47).

In the present study, we investigated the changes in RV and LV geometry and morphology in CTEPH as well as concomittant changes in gene expression that may contribute to these changes. Specifically, we studied whether the increased RV afterload is associated with 1) cardiac remodeling and hypertrophic

signalling, 2) changes in angiogenic factors and capillary density and 3) inflammatory changes associated with oxidative stress and interstitial fibrosis.

Methods

Ethical approval

Animal studies were performed following the "Guiding Principles for the Care and Use of Laboratory Animals" as approved by the Council of the American Physiological Society, and with approval of the Animal Care Committee of the Erasmus University Medical Center (EMC3158, 109-13-09). The authors understand the ethical principles under which the Journal of Physiology operates and hereby declare that this work complies with the animal ethics checklist outlined by Grundy (21). Twenty-three crossbred Landrace x Yorkshire swine of either sex obtained from a commercial breeder (3 months old, 22±1 kg) entered the study. Swine were individually housed in the animal facility of the Erasmus University Medical Center, fed twice a day and had free access to drinking water. Our experimental protocol consists of a chronic instrumentation, followed by induction of CTEPH in twelve animals through a combination of NOS-inhibition with L-N^{ω}-Nitroarginine methyl ester (LNAME) and up to five weekly repeated embolizations with microspheres (see below for details). Mortality due to acute cardio-pulmonary failure upon CTEPH induction occurred in two animals. Two animals were excluded due to catheter failure (1 control, 1 CTEPH) whereas 2 animals (1 control, 1 CTEPH) had to be euthanized following repeated infections due to the catheters and were not included. Only animals that completed the protocol are included in the N-numbers as described in the remainder of the manuscript.

Chronic instrumentation

Animals were chronically instrumented as previously described (11, 47). In short, after an overnight fast, swine were sedated with an intramuscular injection (i.m.) of tiletamine/zolazepam (5 mg kg^{-1}), xylazine (2.25 mg kg^{-1}) and atropine (1 mg), intubated and ventilated with a mixture of O_2 and N_2 (1:2 v/v) to which 2% (v/v) isoflurane was added to maintain anesthesia. Under sterile conditions, a left thoracotomy in the fourth intercostal space was performed, the pericardium was opened and fluid-filled polyvinylchloride catheters (Braun Medical Inc., Bethlehem, PA, USA) were placed in the RV, pulmonary artery and aorta for blood pressure measurement. A flow probe (Transonic Systems Inc., Ithaca, NY, USA) was positioned around the ascending aorta for measurement of cardiac output (CO). The catheters were tunneled to the back, the chest was closed, and animals were allowed to recover for one week, receiving analgesia (0.015 mg kg^{-1} buprenorphine i.m. and a slow-release fentanyl patch 12 µg h^{-1} for 48 hours) on the day of the surgery and daily intravenous (i.v.) antibiotic prophylaxis (25 mg kg^{-1} amoxicillin) for 7 days (11).

CTEPH induction

Following the recovery week, CTEPH was successfully induced in eight animals (4 male, 4 female) as described previously (47, 48). In short, on the first day, the animals were given the NOS-inhibitor LNAME (10 mg kg^{-1} i.v., Enzo Life Sciences International Inc, NY, USA) as a bolus infusion. On subsequent days, the dose of LNAME was increased by 10 mg kg^{-1} per day up to 30 mg kg^{-1} i.v., which was maintained until 1 week before the end of the study (36, 42). LNAME exhibits Ki values of 15 nM, 39 nM, and 4.4 µM for nNOS (bovine), eNOS (human), and iNOS (mouse) (4, 18, 19). Four days after the start of LNAME administration, microsphere infusions were started. Polyethylene microspheres (diameter 600-

710 µm, density 1.13 g cm^{-3}, 500 mg, corresponding to ~2500 microspheres, Cospheric LLC, Santa Barbara, California, US) were suspended in 50 mL autologous blood with 2500 I.U. heparin and slowly infused into the RV while monitoring mean pulmonary artery pressure (mPAP). Microsphere infusions were repeated until the mPAP reached ~60 mmHg, or the arterial P_aO_2 dropped below ~40 mmHg, as measured at rest 30 min after infusion, or when a maximum of 3 g (~15000) microspheres was infused on one day based on the assumption that the porcine lungs contain approximately 25000 small arteries of this diameter. In the subsequent four weeks, hemodynamics were assessed weekly, and microsphere infusions were repeated when mPAP was <25 mmHg and P_aO2 >70 mmHg, as described above. During the final 5 weeks of follow-up, no microsphere infusions were performed while LNAME administration was discontinued one week before sacrifice (47, 48).

Seven sham-operated animals (3 male, 4 female), which did not receive LNAME or microspheres, and two additional healthy animals (2 female), that were not operated, served as controls.

In vivo experiments

Hemodynamic studies. Hemodynamic studies were performed ten weeks after surgery. With swine standing quietly on a motor-driven treadmill and during exercise at 4 km/h, CO, PAP, aorta pressure (AoP), and right ventricular pressure (RVP) were continuously recorded (11, 15).

Digital recording and offline analysis of hemodynamic data were performed as described previously (15, 49). To account for differences in growth between animals, CO was corrected for body weight, yielding cardiac index (CI). Stroke volume index (SVi) was calculated as CI/heart rate. Total pulmonary vascular resistance index (tPVRi) and systemic vascular resistance index (SVRi)

were calculated as mPAP/CI and mAoP/CI respectively. RV function was measured by single beat analysis of RV-pulmonary artery (PA) coupling as described previously (3), using the median value of at least 10 consecutive beats, assuming that end-systolic PAP equals mPAP (3, 5). For calculation of Ees, a sine wave was fitted to the isovolumetric contraction and relaxation phases of RV contraction. The top of the sine wave has previously been shown to be a good approximation of Pmax, derived from isovolumetric contraction. Ees was subsequently calculated as (Pmax-mPAP)/SVi. Ea was calculated as mPAP/SVi. RV-PA coupling was assessed as the ratio of Ees and Ea (Figure 1).

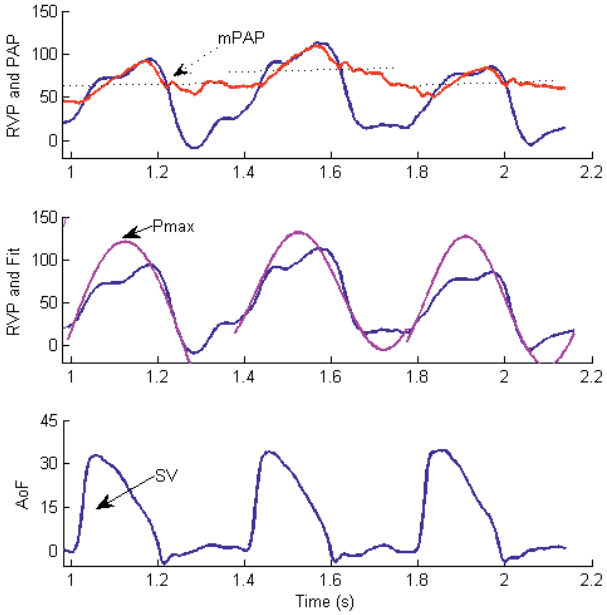

Figure 2. Typical example of RV-PA coupling analysis.

Typical example of RV-PA coupling analysis showing hemodynamic signals (three beats) and their derivatives. Pmax was determined as the maximal value from a sine-fit of Right ventricular pressure (RVP), Pes was estimated to equal mean pulmonary artery pressure (mPAP), whereas stroke volume (SV) was calculated as the time-integral of aorta flow (AoF).

Cardiovascular magnetic resonance imaging. After completion of the hemodynamic experiments, a cardiovascular magnetic resonance (CMR)

examination was performed on a 1.5T clinical scanner with a dedicated 32-channel phased-array cardiac surface coil (Discovery MR450, GE Healthcare, Milwaukee, WI, US) in 5 Control (2 male, 3 female) and 6 CTEPH (4 male, 2 female) animals. For this purpose, animals were sedated and intubated as described above. During imaging, anesthesia was maintained with pentobarbital sodium (6-12 mg kg^{-1} h^{-1} i.v.).Mechanical ventilation and breath-holds were performed using a mobile ventilator (Carina™, Dräger Medical, Best, The Netherlands). When necessary, and always in absence of pain reflexes, muscle relaxation was temporarily achieved using pancuronium bromide (2–4 mg i.v. bolus). The imaging protocol consisted of retrospectively ECG-gated balanced Steady-State Free Precession cine imaging with breath-holding (FIESTA, GE Medical System). Standard long-axis and short axis images with full LV and RV coverage were obtained. Typical scan parameters were slice thickness 6.0 mm, slice gap 0 mm, TR/TE 3.4/1.4 msec, flip angle 75°, field of view 320×240 mm, acquired matrix 180×128, and reconstructed matrix 256×256. To assess dimensions, function and mass of both ventricles, LV and RV epi- and endocardial contours were drawn manually on end-diastolic and end-systolic short axis cine images. Volumes and masses were measured, and stroke volumes and ejection fractions (EF) calculated. All volumes were indexed for bodyweight. QMassMR analytical software (version 8.1, Medis BV, Leiden) was used for analysis.

Euthanasia

After completion of the in vivo experiments, with animals intubated and under deep anesthesia (pentobarbital sodium, 6-12 mg kg^{-1} h^{-1} i.v.), a sternotomy was performed, ventricular fibrillation was induced using a 9 V battery, and the heart was immediately excised. To assess relative RV hypertrophy, the heart was sectioned into RV free wall and LV (including septum), and weighed. RV

hypertrophy was assessed using the Fulton index (RV/LV). Parts of the LV anterior wall and RV were snap frozen in liquid nitrogen within 10 minutes after excision for molecular analyses and fixated in formaldehyde for histological analysis.

Histology

LV and RV tissues were fixated in 3.5-4% buffered formaldehyde for a minimum of 24 hours, and embedded in paraffin wax. Subsequently, 5µm sections were cut, and stained with 1) Gomori to assess cardiomyocyte cross-section area (CSA), 2) Lectin to assess capillary density, and 3) Picrosirius red (PSR) to assess collagen content (46). The stained sections were scanned using a Hamamatsu NDP scanner (Hamamatsu Nanozoomer 2.0 HT, Hamamatsu Photonics K.K., Hamamatsu City, Japan). Morphometric measurements of CSA and capillary density (expressed as number of capillaries per mm^2 and per cardiomyocyte) were performed using Clemex Vision Professional Edition (Clemex Technologies inc. Corporate Headquarters, Quebec, Canada), while collagen content was analyzed using BioPixiQ (Gothenburg, Sweden) as previously described (46).

Real time quantitative PCR

Total RNA was extracted from snap frozen LV and RV tissues with the RNeasy Fibrous Tissue Mini Kit (Qiagen, Venlo, The Netherlands) as previously described (47). RNA integrity was confirmed by Bioanalyzer (2100 Bioanalyzer, Agilent, Santa Clara, California, USA). cDNA was synthesized from 500 ng of total RNA with SensiFAST cDNA Synthesis Kit (Bioline, London, UK). RT-qPCR (CFX-96, Bio-Rad, Hercules, California, USA) was performed with SensiFAST SYBR & Fluorescein Kit (Bioline, London, UK). Target genes mRNA expression levels were normalized against β-actin, glyceraldehyde-3-phosphate dehydrogenase (GADPH) and cyclophilin using the ΔΔCt method with the gene study function in CFX manager

software (Bio-Rad, Hercules, California, USA). All primer sequences are presented in Table 1.

Titin isoform composition

Titin isoform protein composition (i.e. presence of the stiff N2B and compliant N2BA isoforms) was analyzed as previously described (46). In short, snap frozen LV and RV tissues were weighed and pulverized in liquid nitrogen using a mortar and pestle. Cardiac tissue powder was solubilized in 8 mol L^{-1} urea buffer with dithiothreitol and 50% glycerol solution with protease inhibitors (4× Leupeptin, E-64, and phenylmethanesulfonyl fluoride). Equal dilutions were calculated based on myosin heavy chain (MHC) content and homogenate samples were loaded on custom-made 1% agarose gels. Gels were stained with SYPRO Ruby. Samples were measured in triplicate. Only samples with ≦20% degradation were used. Titin isoforms N2B and N2BA were normalized to total titin amount, and the N2B/N2BA ratio was calculated.

Statistical analysis

SPSS (version 21.0 IBM, Armonk, NY, USA) was used for the statistical analysis. Statistical analysis was performed with a mixed-model ANOVA with exercise as a repeated measure and CTEPH as a between group comparison, and exercise*CTEPH as interaction term for the analysis of heamodynamics. ANOVA with CTEPH as a factor was performed for the MRI data, histology and gene-expression. Bonferroni post-hoc testing was performed when appropriate. The correlation coefficient $r^2$was calculated for the relations between two continuous variables. Statistical significance was accepted when $P<0.05$. Data are presented in box and whisker plots with the whiskers reflecting min to max and median presented as line.

Table 1. Primer sequences used for the qPCR.

	Sequence	
Genes	**Forward**	**Reverse**
β-actin	TCCCTGGAGAAGAGCTACGA	AGCACCGTGTTGGCGTAGAG
Cyclophilin	AGACAGCAGAAAACTTCCGTG	AAGATGCCAGGACCCGTATG
GAPDH	GCTCATTTCCTCGTACGAC	GAGGGCCTCTCTCCTC
α -SMA	GGACCCTGTGAAGCACCAG	GGGCAACACGAAGCTCATTG
β-MHC	AGATGAACGAGCATCGGAGC	TACTGTTCCCGAAGCAGGTCAG
ANP	TGAACCCAGCCCAGAGAGAT	CAGTCCACTCTGTGCTCCAA
BNP	CAAGTCCTCCGGGGAATACG	TACCTCCTGAGCACATTGCAG
SERCA2a	GACAATGGCGCTGTCTGTTC	ATCGGTACATGCCGAGAACG
PLN	TTCCAGCTAAACACCGATAAGA	AGGCAGCCTTGGCTGTTTAT
BCL2	GATAACGGAGGCTGGGATGC	TTATGGCCCAGATAGGCACC
BCLXL	TGAGTCGGATCGCAACTTGG	GCTAGAGTCATGCCCGTCAG
Casp3	GCTGCAAATCTCAGGGAGAC	CATGGCTTAGAAGCACGCAA
eNOS	GGACACACGGCTAGAAGAGC	TCCGTTTGGGGCTGAAGATG
VEGFA	ACTGAGGAGTTCAACATCGCC	CATTTACACGTCTGCGGATCTT
HIF1α	TTTACTCATCCGTGCGACCA	AGCTCCGCTGTGTATTTTGC
HIF2α	GTCGAAGATCAGCACACGGA	CACCGCTCCTGAGACTCTTC
IL-6	CTCCAGAAAGAGTATGAGAGC	AGCAGGCCGGCATTTGTGGTG
TNF-α	TGCACTTCGAGGTTATCGGCC	CCCACTCTGCCATTGGAGCTG
IFN-γ	GAAGAATTGGAAAGAGGAGAGTGAC	TGCTCCTTTGAATGGCCTGG
TGF-β1	GTGGAAAGCGGCAACCAAAT	CACTGAGGCGAAAACCCTCT
BMPR2	GGATGCTGACAGGAGATCGT	CTGGCGGTTTGCAAAGGAAA
PAI-1	TGAATGAGAGCGGCACGGTG	TTGTGCCGCACCACGAACAG

Id-1	GGAGTTGGAGCTGAACTCGG	GCGATCGTCCGCTGGAACAC
NOX1	CCATTCATATTCGAGCAGCAGG	AACATCCTCACTGACAGTGCC
NOX2	TTGGCGATCTCAGCAGAAGG	GAGGTCAGGGTGAAAGGGTG
NOX4	GCAGACTTACTCTGTGTGTTG	CCATCTGTCTGACTGAGGTAC
PCNA	GAACCTCACCAGCATGTCCAA	TAGTGCCAAGGTGTCTGCAT
RhoA	AGGGAGAAGAACACTTCCGC	GGGCATCTTGTGTTTCCACC
ROCK1	AGGACCAATTCCCGGAGGTA	AGCCAACTCTACCTGCTTTCC
ROCK2	ATCAAACGATATGGCTGGAAG	CCATAGACGGATTGGATTGTTCC
MMP2	AGGACATCAGCGGTAAGACC	GGTAGAGGTAGACCAGCGGA
MMP9	TCGACGTGAAGACGCAGAAG	ACCTGATTCACCTCGTTCCG
TIMP1	GATCTATGCTGCTGGCTGTGA	GTCTGTCCACAAGCAGTGAGT
TIMP2	TTGCAATGCAGACGTAGTGA	GCCTTTCCTGCGATGAGGT
TIMP3	ACGCCTTCTGCAACTCTGAC	AGCCTCGGTACATCTTCATCT
Col1	AGACATCCCACCAGTCACCT	TCACGTCATCGCACAACACA
Col2	CTTGAGACTCAGCCACCCAG	CCGAATGCAGGTTTCACCAG
Col3	AATCATGCCCTACTGGTGGC	CGGGTCCAACTTCACCCTTA

GAPDH, glyceraldehyde-3-phosphate dehydrogenase;α-SMA, α-smooth muscle actin; β-MHC, β-myosin heavy chain; ANP, atrial natriuretic peptide; BNP, brain natriuretic peptide; SERCA2a, Sarcoplasmic/endoplasmic reticulum Ca(2+)ATPase 2a; PLN, phospholamban; BCL2, B-cell lymphoma 2; BCLXL, B-cell lymphoma-extra large; Casp3, caspase 3; eNOS, endothelial nitric oxide synthase; VEGFA, vascular endothelial growth factor-A; HIF1α, hypoxia inducible factor 1α; HIF2α, hypoxia inducible factor 2α;IL-6, interleukin-6; TNF-α, tumor necrosis factor α; IFN-γ, interferon-γ; TGF-β1, transforming growth factor β1; BMPR2, bone morphogenetic protein receptor 2; PAI-1, Plasminogen activator inhibitor-1; Id-1, inhibitor of DNA binding; NOX1, NADPH oxidase 1; NOX2, NADPH oxidase 2; NOX4, NADPH oxidase 4; PCNA, Proliferating cell nuclear antigen; RhoA, Ras homolog gene family member A; ROCK1, rho-associated, coiled-coil-containing protein kinase 1; ROCK2, Rho associated coiled-coil containing protein kinase 2; MMP2, matrix metalloproteinase-2; MMP9, matrix metalloproteinase-9; TIMP1, tissue inhibitor of metalloproteinases 1; TIMP2, tissue inhibitor of metalloproteinases 2; TIMP3, tissue inhibitor of metalloproteinases 3; Col1, collagen type 1; Col2, collagen type 2; Col3, collagen type 3.

Results

Cardiac hypertrophy and function

CTEPH resulted in an increased RV afterload, as evidenced by an increase in mPAP, tPVRi and Ea (Figure 2). This sustained increase in afterload resulted an increase in RV-BNP expression (Table 3), suggestive of increased RV wall stress. Indeed, trends towards RV dilation (P=0.15) and decreased EF (P=0.08) as measured with CMR were observed (Figure 3). However, end-systolic elastance (Ees), an index of RV contractility, was higher in CTEPH while RV dP/dt_{max} and RV dP/dt_{min} were unchanged (Figure 2). Although RV-PA coupling was reduced, CI was maintained in CTEPH (Figure 2). Furthermore, neither heart rate, mAoP (Table 2), LV volume, LVEF (Figure 3) nor LV-BNP expression (Table 3) were altered.

Exercise resulted in increases in mPAP and Ea that were larger in CTEPH as compared to Control while the exercise induced increase in CI was blunted. Moreover, although Ees increased in both CTEPH and Control animals, Ees was no longer different between groups. Hence, RV-PA coupling, which increased with exercise in the Control swine did not change significantly during exercise in CTEPH animals (Figure 2). In fact, RV-PA coupling worsened with exercise in 4 out of 6 CTEPH animals, and correlated inversely with tPVRi (Figure 4). Moreover, the CTEPH animal with the worst RV function was uncapable of performing exercise at 4 km/h due to RV failure, evidenced by a significant reduction in mAoP during exercise (animal not included in figure). Altogether, these data are consistent with RV dysfunction that is still compensated at rest but that is excacerbated during exercise.

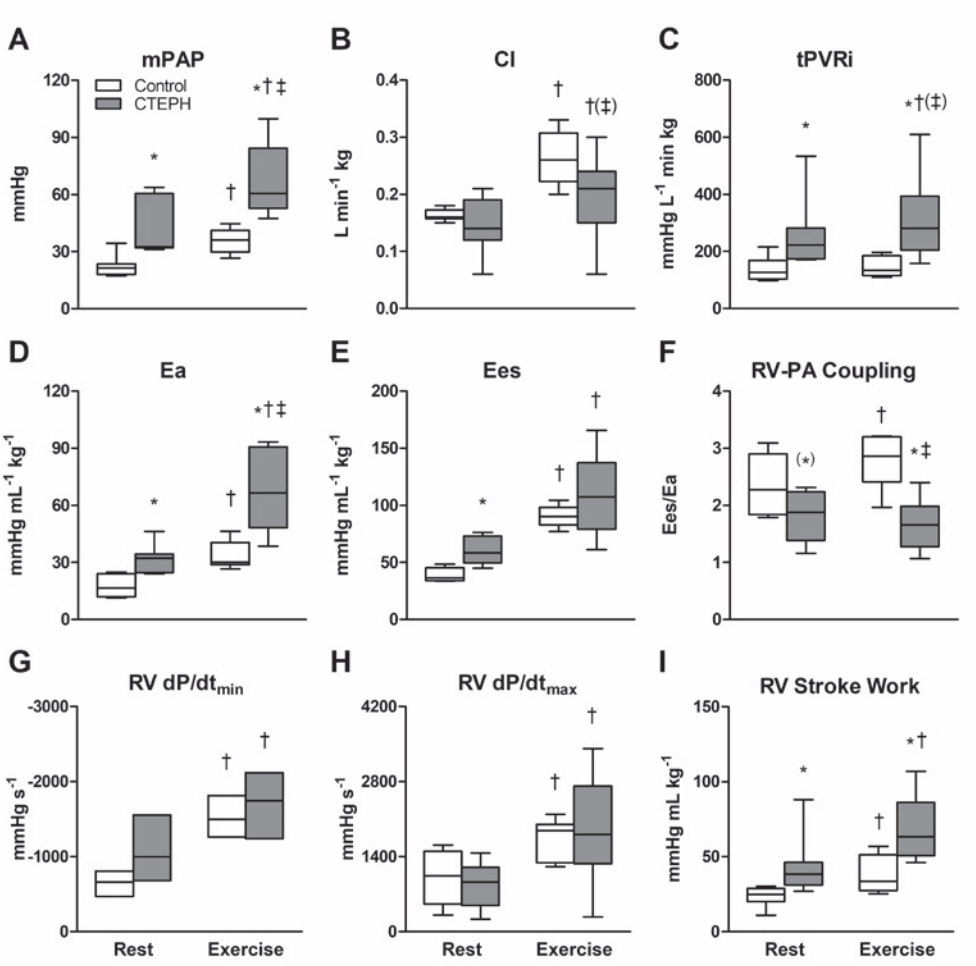

Figure 3. Hemodynamics at rest and during exercise after 9 weeks of CTEPH.

*Shown are data obtained at rest and during maximal exercise at 4 km h-1 in Control swine (n=7) and CTEPH swine (n=7). A) Mean pulmonary artery pressure (mPAP), B) Cardiac index (CI), C) total pulmonary vascular resistance index (tPVRi), D) Arterial elastance (Ea), E) End-systolic elastance (Ees), F) RV-PA coupling (Ees/Ea), G) maximum rate of fall of RV pressure (RV dP/dtmin), H) maximum rate of rise of RV pressure (RV dP/dtmax), I) Stroke work at rest and during exercise. Whiskers denote min to max and median is presented by the line. * P < 0.05, (*) P <0.1 CTEPH vs corresponding Control; † P< 0.05, (†) P<0.1 Exercise vs corresponding rest; ‡ P<0.05, (‡) P < 0.1 Exercise*CTEPH, i.e. effect of exercise on variable is different in CTEPH from Control.*

Table 2. Systemic hemodynamics at rest and during exercise.

		Control				CTEPH			
BW	**Instrumentation**	20	±	1		23	±	1	
	End of Study	61	±	2		62	±	3	
HR	**Rest**	136	±	21		131	±	4	
	Exercise	235	±	15	†	211	±	8	†‡
Svi	**Rest**	1.28	±	0.09		1.17	±	0.17	
	Exercise	1.07	±	0.09	†	0.99	±	0.13	
mAoP	**Rest**	91	±	4		100	±	4	
	Exercise	96	±	4	(†)	116	±	4	*†(‡)
SVRi	**Rest**	561	±	24		839	±	205	
	Exercise	384	±	25	†	752	±	252	

*Bodyweight (BW) and systemic hemodynamic data at rest and during exercise. Heart rate (HR); stroke volume index (SVi); mean aorta pressure (mAoP); systemic vascular resistance index (SVRi). Data are mean ± SEM. Control N=7, CTEPH N=7. * P < 0.05 CTEPH vs corresponding Control; † P< 0.05, (†) P<0.1 Exercise vs corresponding rest; ‡ P<0.05, (‡) P < 0.1 Exercise*CTEPH i.e. effect of exercise on variable is different in CTEPH from Control.*

As previously reported (47), the increased RV afterload resulted in RV hypertrophy, as evidenced by an increased RV/BW and Fulton index (Figure 5), as well as an increased RV cardiomyocyte CSA in CTEPH (Figure 6). RV cardiomyocte CSA of CTEPH animals resembled those of LV cardiomyocytes. LV cardiomyocytes were similar in size in LV of CTEPH as compared to Control animals (Figure 6), consistent with the maintained LVW/BW in CTEPH compared to Control swine (Figure 5). Expression of SERCA2a, its inhibitor phospholamban (PLN), and their ratio did not change in the RV (Table 3). However, there was a shift in RV titin isoform expression from the stiff N2B, to the more compliant N2BA isoform (Figure 6). The pro-apoptotic gene Caspase-3 was upregulated in the RV, while the anti-apoptotic gene BCL2 was also upregulated in the RV of CTEPH animals (Table 3). Expression of BCL2 correlated modestly and inversely with RV-PA coupling during exercise (Figure 7), but not with resting RV-PA

coupling (r^2= 0.08, not shown). In the LV, none of the genes involved in cardiac hypertrophy and apoptosis were significantly affected in the CTEPH animals.

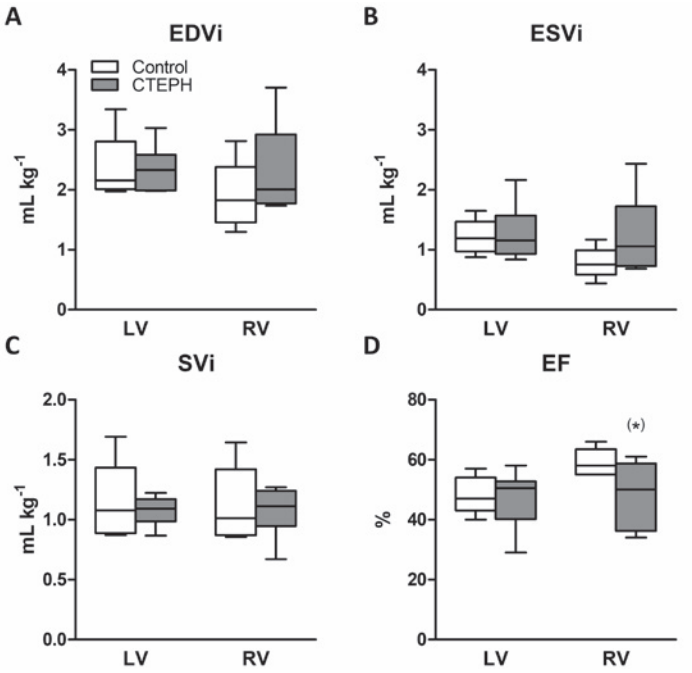

Figure 3.

Right (RV) and left (LV) ventricular dimensions and function measured by cardiovascular magnetic resonance (CMR) imaging. A) end-diastolic volume index (EDVi), B) end-systolic volume index (ESVi), C) stroke volume index (SVi), and D) ejection fraction (EF). Whiskers denote min to max and median is presented by the line. *Control N=5, CTEPH N=6. (*) P < 0.1 CTEPH vs Control.*

Angiogenesis

We observed an increase in capillary density in the RV of swine with CTEPH as compared to Control (Figure 6), that correlated with the increased stroke work (Figure 6) and was consistent with the trend towards the increased VEGFA expression (Table 3). Moreover, VEGFA expression correlated inversely with RV-PA coupling during exercise (Figure 7) but not with resting RV-PA coupling (r^2=0.34, not shown). In contrast, no changes in capillary density or VEGFA expression were observed in the LV.

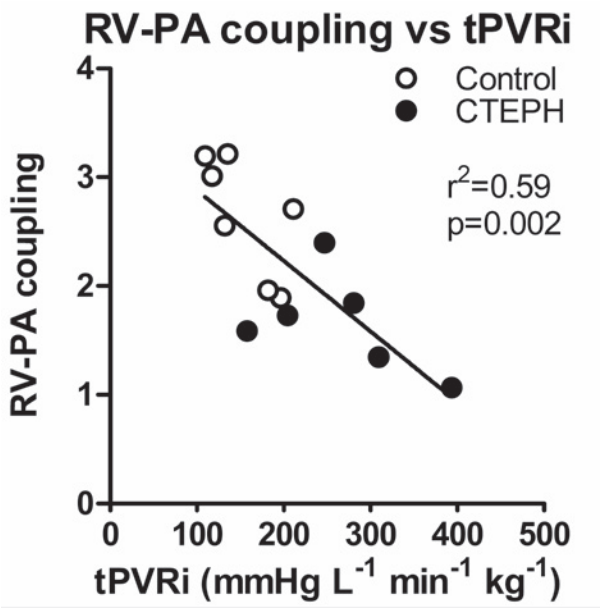

Figure 4.

Correlation between total pulmonary vascular resistance (tPVRi) and RV-PA coupling during maximal exercise at 4 km h^{-1} in Control swine (n=7) and CTEPH swine (n=6). P-value denotes significance of slope from zero.

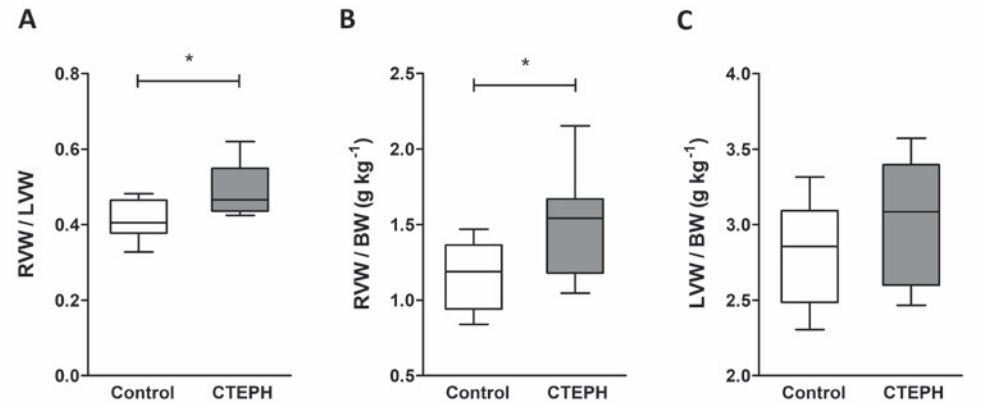

Figure 5.

*Cardiac hypertrophy. A) The Fulton index calculated as the ratio of Right ventricular weight (RVW) and left ventricular weight (LVW) and B) RVW over bodyweight (BW) were increased at sacrifice in CTEPH swine while C) LVW over BW was similar in CTEPH and Control swine. Whiskers denote min to max and median is presented by the line. Control N=9, CTEPH N=8. * P < 0.05 CTEPH vs Control.*

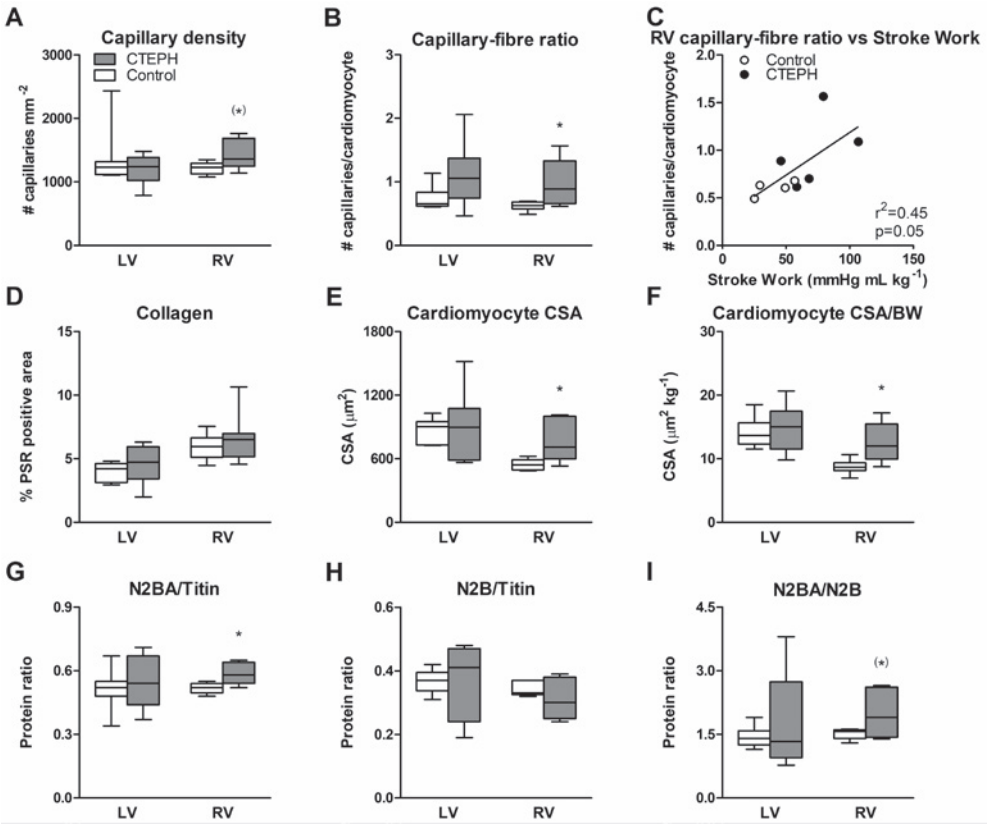

Figure 6.

*Histological analyses in Control and CTEPH animals of both the left ventricle (LV) and right ventricle (RV). A) Capillary density per mm^2 (lectin staining), B) capillary-fibre ratio, C) correlation between stroke work during maximal exercise at 4 km h^{-1} and RV capillary-fibre ratio, D) Interstitial fibrosis (picrosirius red (PSR) staining), E) cardiomyocyte size, F) cardiomyocyte size normalized for bodyweight (Gomori staining, cross sectional area (CSA)).Myofilament composition in terms of the two different titin isoforms G) N2BA (N2BA/Titin) and H) N2B (N2B/Titin) and I) their ratio. Whiskers denote min to max and median is presented by the line. Control N=8, CTEPH N=6. * P < 0.05 CTEPH vs Control (*)P < 0.1 CTEPH vs Control.*

Inflammation, oxidative stress, and interstitial fibrosis

Although expression of the immune-modulatory genes TNF-α, IL-6, IFN-γ was not altered in the RV, TGF-β1 gene expression tended to be higher in the RV of CTEPH

Table 3. Relative gene expression in Control and CTEPH left and right ventricle tissue.

		LV					RV				
		Control	n	CTEPH	n	p-value	Control	n	CTEPH	n	p-value
Hypertrophy & Contractility	**α-SMA**	0.36 ± 0.03	9	0.39 ± 0.08	6	0.72	0.17 ± 0.04	9	0.45 ± 0.23	5	0.14
	β-MHC	1.06 ± 0.08	9	0.94 ± 0.14	6	0.43	1.02 ± 0.07	9	1.10 ± 0.10	5	0.50
	ANP	0.34 ± 0.07	8	0.29 ± 0.07	6	0.65	0.81 ± 0.18	9	0.45 ± 0.14	5	0.20
	BNP	0.11 ± 0.03	9	0.22 ± 0.07	6	0.12	0.12 ± 0.06	9	0.90 ± 0.23	5	***0.001***
	SERCA2a	1.05 ± 0.09	9	1.08 ± 0.12	6	0.88	0.77 ± 0.10	9	0.78 ± 0.25	5	0.97
	PLN	1.40 ± 0.07	9	1.28 ± 0.10	6	0.30	1.32 ± 0.13	9	1.26 ± 0.12	5	0.76
	PLN/ SERCA2a	1.39 ± 0.12	9	1.21 ± 0.06	6	0.25	1.87 ± 0.19	9	1.95 ± 0.29	5	0.81
Apoptosis	**BCL2**	0.57 ± 0.04	9	0.72 ± 0.09	6	*0.10*	0.86 ± 0.06	9	1.16 ± 0.12	5	***0.03***
	BCLXL	0.74 ± 0.08	9	0.62 ± 0.15	6	0.48	1.07 ± 0.10	9	0.87 ± 0.13	5	0.26
	Casp3	0.74 ± 0.06	9	0.70 ± 0.06	6	0.64	0.88 ± 0.05	9	1.22 ± 0.16	5	***0.03***
Endothelial function & Angiogenesis	**eNOS**	0.94 ± 0.06	9	0.87 ± 0.13	6	0.61	0.77 ± 0.05	9	0.81 ± 0.06	5	0.56
	VEGFA	1.16 ± 0.12	9	1.36 ± 0.14	6	0.31	0.93 ± 0.09	9	1.25 ± 0.14	5	*0.07*
	HIF1α	1.19 ± 0.03	9	1.14 ± 0.12	6	0.61	1.14 ± 0.04	9	1.06 ± 0.05	5	0.20
	HIF2α	1.00 ± 0.02	9	0.91 ± 0.11	6	0.35	1.20 ± 0.10	9	1.16 ± 0.12	5	0.81
Inflammation	**IL-6**	0.24 ± 0.06	9	0.90 ± 0.57	6	0.19	0.09 ± 0.04	9	0.31 ± 0.25	5	0.26
	TNF-α	0.22 ± 0.06	9	0.31 ± 0.11	6	0.46	0.27 ± 0.04	9	0.35 ± 0.12	5	0.40
	IFN-γ	0.84 ± 0.20	9	0.48 ± 0.13	6	0.20	0.44 ± 0.09	9	0.31 ± 0.06	5	0.33
TGF-β & BMP	**TGF-β1**	0.80 ± 0.05	9	0.79 ± 0.04	6	0.92	0.81 ± 0.02	9	0.91 ± 0.06	5	*0.08*
	BMPR2	0.92 ± 0.09	9	0.79 ± 0.09	6	0.35	1.04 ± 0.05	9	1.15 ± 0.06	5	0.22

	PAI-1	0.38	±	0.05	9	0.46	±	0.09	6	0.42	0.23	±	0.08	9	0.48	±	0.14	5	*0.10*
	Id-1	0.49	±	0.05	9	0.47	±	0.12	6	0.92	0.61	±	0.09	9	0.75	±	0.20	5	0.50
Oxidative stress	**NOX1**	1.11	±	0.26	9	1.33	±	0.42	6	0.64	0.71	±	0.13	9	1.20	±	0.17	5	***0.04***
	NOX2	0.45	±	0.04	9	0.61	±	0.09	6	*0.08*	0.63	±	0.09	9	0.68	±	0.11	5	0.70
	NOX4	0.97	±	0.08	9	1.13	±	0.09	6	0.24	0.70	±	0.06	9	1.03	±	0.15	5	***0.03***
	PCNA	0.95	±	0.07	9	0.82	±	0.07	6	0.25	1.04	±	0.09	9	1.10	±	0.22	5	0.79
	RhoA	1.13	±	0.22	9	1.13	±	0.03	6	0.72	1.12	±	0.04	9	1.05	±	0.06	5	0.36
	ROCK1	1.23	±	0.05	9	1.22	±	0.04	6	0.91	1.06	±	0.06	9	1.11	±	0.11	5	0.62
	ROCK2	0.76	±	0.05	9	0.93	±	0.06	6	***0.05***	0.61	±	0.04	9	0.95	±	0.11	5	***0.004***
Extracellular matrix & Fibrosis	**MMP2**	1.30	±	0.18	6	1.65	±	0.49	4	0.46	0.89	±	0.13	9	0.72	±	0.05	5	0.38
	MMP9	0.89	±	0.23	9	1.27	±	0.49	6	0.45	0.61	±	0.16	8	0.58	±	0.06	4	0.89
	TIMP1	0.65	±	0.11	9	0.65	±	0.11	6	0.75	0.69	±	0.14	9	0.78	±	0.13	5	0.69
	TIMP1/MMP9	1.13	±	0.25	9	0.90	±	0.28	6	0.56	1.79	±	0.40	8	1.49	±	0.43	4	0.65
	TIMP2	1.03	±	0.10	9	1.24	±	0.22	6	0.35	0.89	±	0.12	9	0.95	±	0.08	5	0.74
	TIMP2/MMP2	0.90	±	0.12	6	0.84	±	0.05	4	0.69	1.04	±	0.05	9	1.35	±	0.12	5	***0.02***
	TIMP3	1.27	±	0.08	9	1.08	±	0.06	6	0.12	0.79	±	0.05	9	0.76	±	0.08	5	0.75
	Col1	0.94	±	0.14	9	1.11	±	0.50	6	0.70	0.56	±	0.16	9	0.44	±	0.17	5	0.63
	Col2	0.85	±	0.15	9	1.12	±	0.49	6	0.54	0.65	±	0.15	9	0.46	±	0.15	5	0.42
	Col3	0.95	±	0.14	9	1.13	±	0.50	6	0.70	0.73	±	0.16	9	0.43	±	0.12	5	0.24
	Col1/3	0.99	±	0.05	9	0.98	±	0.03	6	0.88	0.75	±	0.06	9	0.95	±	0.09	5	*0.09*

Relative gene expression of right and left ventricle tissue obtained from Control and CTEPH swine. For abbreviations, see Table 1. Data are mean ± SEM. Bold & Italics P<0.05, Italics P<0.10.

swine, while BMPRII was not altered (Table 3). Consistent with a perturbation in the TGF-β – BMP balance, PAI also tended to be increased, while Id-1 did not change (Table 3). This shift in the TGF-β – BMP balance was accompanied by increased expression of ROCK2, NOX-1 and NOX-4 in the RV (Table 3), indicative of an increase in oxidative stress. Expression of ROCK2, NOX-1 and NOX-4 correlated inversely with RV-PA coupling during exercise (Figure 7), but not with resting RV-PA coupling (r^2= 0.29, 0.01 and 0.16 for ROCK2, NOX1 and NOX4, respectively).

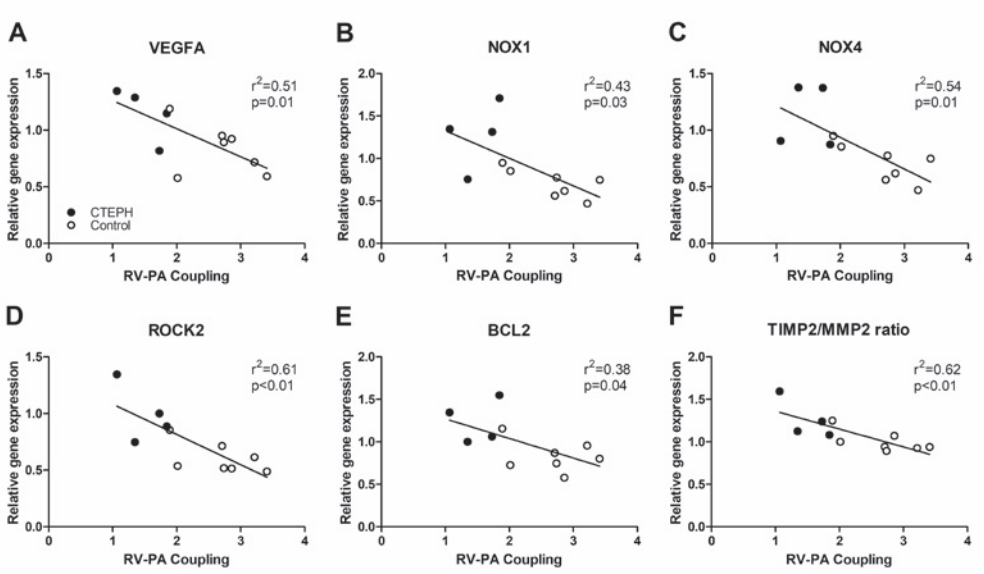

Figure 7.

Correlation of the RV-PA coupling during exercise with expression of A) vascular endothelial growth factor A (VEGFA) , B) NADPH oxidase 1 (NOX1), C) NADPH oxidase 4 (NOX4), D) Rho-associated protein kinase 2 (ROCK2), E) B-cell lymphoma 2 (BCL2), F) ratio of tissue inhibitor of metalloproteinases 2 (TIMP2) over matrix metalloproteinase-2 (MMP2) in the RV. Control N=7, CTEPH N=4. P-value denotes significance of slope from zero.

These changes in gene expression of pro-inflammatory genes and genes promoting oxidative stress did not result in overt changes in interstitial fibrosis, as collagen content was similar in the RV of CTEPH versus Control swine (Figure 6). Yet, although no change in interstitial fibrosis was observed, there was a trend

towards a shift in expression of Col3 to the stiffer Col1 isoform, that was accompanied by an increase in the ratio of TIMP2/MMP2 (Table 3) that correlated inversely with RV-PA coupling (Figure 7), suggesting reduced ECM turnover in the diseased RV.

With the exception of an increase in ROCK2 and a trend towards an increase in NOX2 expression, no changes in genes involved in inflammation, oxidative stress and fibrosis were observed in the LV (Table 3), which is consistent with the absence of changes in LV myocardial interstitial collagen content.

Discussion

The present study investigated functional, histological and molecular changes in the RV and LV in swine with CTEPH. The main findings were that CTEPH resulted in 1) RV hypertrophy, both at the global and the myocyte level, 2) mild RV dysfunction as evidenced by decreased RV-PA coupling and elevated BNP expression, with trends towards an increased RV EDVi and a lower EF, 3) further decrease in RV-PA coupling during exercise that correlated with an increase in ROCK2, NOX1, NOX4 expression, 4) increased VEGFA expression that was accompanied by an increased capillary density in the RV. Finally, CTEPH did not result in changes in LV structure or function, and was associated with minor changes in LV gene expression in our swine model.

Animal model

CTEPH was induced in juvenile swine by first inducing endothelial dysfunction through chronic NOS-inhibition, followed by up to 5 repeated embolizations with microspheres. We previously showed that this combination was required as neither NOS-inhibition nor embolization alone were sufficient to induce chronically elevated pulmonary artery pressures, while the combination of

NOS-inhibition and embolization resulted in a progressive increase in tPVRi that continued to increase after the last embolization and was accompanied by pulmonary microvascular remodeling (47, 48). The required induction of endothelial dysfunction may be the result of the younger age of our animals, as endothelial NO-production decreases with age (32, 40). Also in humans, endothelial dysfunction is often present both in patients with acute pulmonary embolism as well as with CTEPH and correlates with disease severity (8, 29, 43). In humans, CTEPH prevalence is higher in females (30), but male patients typically have a worse prognosis (7). In the present study, male and female swine were used as we have previously shown that there are subtle differences in regulation of pulmonary vascular tone (10, 12), and hence it is possible that sex also affects development of CTEPH and subsequent RV remodeling in our animals. Unfortunately, the small group size precludes statistical assessment of the effect of sex. However, in supplemental figure 1-4 individual data are shown and different symbols are used for male and female swine.

RV-function and remodeling

RV afterload increases during development and progression of pulmonary hypertension. To cope with the increased afterload, the RV undergoes structural and functional changes to augment contractility, and there is evidence that this RV structural and functional adaptability are important determinants of functional capacity and survival in patients with CTEPH (9, 25, 55). The effects of CTEPH on cardiac structure, function and gene expression were therefore examined in our porcine model. CTEPH resulted in an increase in RV cardiomyocyte size and global RV hypertrophy, that was accompanied by activation of both pro- and anti-apoptotic gene expression (increases in Caspase-3 and BCL2 respectively). Although these data suggest that apoptosis is likely altered in the remodeled RV,

apoptosis is determined by enzyme activity rather than expression. Future experiments examining activity of enzymes involved in apoptosis and TUNEL staining should be performed to elucidate whether the increased mRNA expression is indeed translated to alterations in apoptosis.

Consistent with our previous study in which RV dimensions were assessed using echocardiography in awake swine (47), CTEPH resulted in trends towards RV dilation and a reduced RVEF. In the present study, RV resting function was still preserved, as evidenced by a maintained CI, but BNP expression was increased, suggestive of an increased wall stress (52). These findings are consistent with observations in another porcine CTEPH model, in which CTEPH is induced by ligation of the left pulmonary artery, in combination with embolization of the proximal segmental arteries with glue (22-24). In that model, RV dilation (24) and RV myocyte hypertrophy (22) were also accompanied by an increased BNP expression (22, 24), that correlated inversely with stroke volume and positively with global RV hypertrophy (22). Furthermore, RV-PA coupling, an index of how well the RV can cope with the increased afterload, was reduced in that study and a correlation was found between reduced coupling and a reduced SV reserve with dobutamine (24). Similarly, in the present study, severity of CTEPH reflected in the tPVRi, correlated inversely with RV-PA coupling during exercise. Importantly, recent studies in patients with CTEPH show that RV-PA coupling correlates with exercise capacity (9), which in turn is a strong prognosticator (2).

It is increasingly recognized that not only RV systolic function, but also RV diastolic function correlates with prognosis in patients with pulmonary arterial hypertension (PAH) (53). Indeed, in pigs with type II PH, abnormalities in RV-PA coupling were accompanied by diastolic dysfunction (1). Diastolic RV chamber stiffness is determined by myocyte stiffness as well as interstitial collagen. In a rat

model of pulmonary artery banding, mild RV dysfunction was accompanied by an increase in myocyte stiffness, whereas interstitial fibrosis was only observed in the presence of severe RV dysfunction (41). In these rats, the increased myocyte stiffness was accompanied by a paradoxical increase in the more compliant titin N2BA isoform, possibly to blunt a further increase in myocyte stiffness. Consistent with these findings the mild RV dysfunction in our swine with CTEPH was accompanied by an increase in titin N2BA, while no changes in myocardial collagen content were observed histologically. Furthermore, no changes in Col1 and Col3 expression were observed, although there was a change in the ratio between Col1 and Col3 indicating a relatively higher expression of the stiff Col1 isoform. These data are also consistent with the isoform shift observed by Rain et al (41), and may have contributed to a stiffer RV.

The transition from RV dysfunction to overt RV failure is associated with inflammation and activation of the immune response (14, 16, 50). Although expression of genes involved in immune modulation (TNF-α, IL-6, IFN-γ) was not altered, expression of TGF-β1 tended to be increased. Activation of the TGF-β pathway was further confirmed by the increase in expression of its downstream target PAI-1. Both activation of the TGF-β pathway and increased circulating levels of endothelin, as we previously showed to be present in our porcine CTEPH model (48), can result in activation of the Rho-kinase pathway (44, 54, 59). Indeed, ROCK2 expression was upregulated in CTEPH swine and showed a strong inverse correlation with RV-PA coupling. ROCK2 activation is involved in cardiac hypertrophy and oxidative stress, and plays a deleterious role in RV-remodeling (28, 51). ROCK2 phosphorylates protein phosphatase 1 (PP1), which regulates both myofilament sensitivity to Ca^{2+} as well as Ca^{2+}-handling (26). Hence, although neither SERCA2a nor phospholamban gene expression were changed in the present study, it is possible that post-translational modifications in their

phosphorylation status contributed to altered Ca^{2+} handling. Indeed, it has been suggested that changes in Ca^{2+}-handling may play a role in the development of RV dysfunction as diastolic dysfunction in swine with type II PH was associated with reduced SERCA2a-expression (1). Future studies in our CTEPH model are required to further investigate the post-translational modifications in contractile and Ca^{2+}-handling proteins.

Another key factor that distinguishes adaptive RV remodeling from RV failure is myocardial angiogenesis (17). Angiogenesis allows RV perfusion to be enhanced commensurate with the increase in RV mass. Indeed, many studies have shown that RV failure is accompanied by a reduction in capillary density, whereas capillary density is preserved or even increased in adaptive RV remodeling (for an overview of angiogenesis in the RV in a variety of animal models with PH see (17)). Although chronic administration of LNAME could significantly reduce myocardial angiogenesis (37) and limit myocardial perfusion, capillary density was actually increased in the RV of CTEPH swine and correlated with stroke work during exercise. These data are in accordance with recent data in another porcine CTEPH model (33), and suggests a state of adaptive RV remodeling with sufficient myocardial perfusion and oxygenation under resting conditions. Nevertheless, VEGFA-expression was higher in swine with CTEPH (Loisel *et al*., 2019, present study) and correlated with RV-PA coupling during exercise, suggesting that, even though expression of HIF-1α and HIF-2α was unchanged, there was still a need for additional perfusion during stress. Indeed, myocardial perfusion reserve has been shown to be reduced in humans with CTEPH and PAH (56, 57). Furthermore, myocardial perfusion reserve correlated inversely with mPAP and RV work in these studies, suggesting that flow reserve is recruited as a result of the increased work (57) and maximal flow may be limited due to increased extravascular compression (56).

ROCK2 is not only expressed in the myocardium but also in the vasculature, where its expression correlates with oxidative stress and NOX-expression (6). NOX1, NOX2 and NOX4 were upregulated in the right coronary artery of swine with pulmonary artery banding, which was accompanied by oxidative stress and endothelial dysfunction, despite maintained eNOS expression (34). The upregulation of NOX1 and NOX4, and the unaltered eNOS expression in the RV of CTEPH swine, as observed in the present study, are consistent with these data, although we did not determine the exact intramyocardial location of their expression. Furthermore, the upregulation of NOX4 is also consistent with recent data from patients with PAH, in which circulating NOX4 was increased (27). Finally, the correlation of NOX1 and NOX4 with RV-PA coupling suggest that oxidative stress in the myocardium may contribute to worsening of RV-function.

Conclusion and clinical implications

In swine with CTEPH, the increased afterload resulted in RV hypertrophy, that contributed to a maintained resting RV function, although a trend towards RV dilation and reduced RVEF was observed with CMR. Consistent with data obtained in CTEPH-patients without overt RV failure (25), neither LV function nor LV gene expression (perhaps with exception of ROCK2, NOX2 and BCL2) were altered.

CTEPH is different from PAH in that patients often experience an acute thrombo-embolic event prior to development of the disease. This form of PH therefore has the potential for follow-up and earlier therapeutic interventions. Exercise unmasked mild RV dysfunction as evidenced by reduced RV-PA coupling, which may facilitate early diagnosis of patients at risk for developing persistent RV failure. The present study shows that this mild RV dysfunction correlates with changes in expression of genes involved in oxidative stress, apoptosis and angiogenesis. These changes in gene expression suggest activation of an

inflammatory response in the RV, promoting oxidative stress. Given that ROCK2 shows a strong correlation with RV dysfunction and has been shown to play a detrimental role in inflammation, oxidative stress, interstitial fibrosis, cardiac hypertrophy and impaired myocardial perfusion, ROCK2 inhibition may provide a viable target for early therapeutic intervention.

Acknowledgements

The authors would like to acknowledge the expert technical assistance of Piotr Wielopolski, Esther van de Kamp, Annemarie Verzijl and Ruud Zaremba. We would like to thank Dylan van der Vusse, Brechje de Rapper and Paula Krul for their assistance.

References

1. **Aguero J, Ishikawa K, Hadri L, Santos-Gallego C, Fish K, Hammoudi N, Chaanine A, Torquato S, Naim C, Ibanez B, Pereda D, Garcia-Alvarez A, Fuster V, Sengupta PP, Leopold JA, and Hajjar RJ**. Characterization of right ventricular remodeling and failure in a chronic pulmonary hypertension model. *Am J Physiol Heart Circ Physiol* 307: H1204-1215, 2014.

2. **Blumberg FC, Arzt M, Lange T, Schroll S, Pfeifer M, and Wensel R**. Impact of right ventricular reserve on exercise capacity and survival in patients with pulmonary hypertension. *Eur J Heart Fail* 15: 771-775, 2013.

3. **Brimioulle S, Wauthy P, Ewalenko P, Rondelet B, Vermeulen F, Kerbaul F, and Naeije R**. Single-beat estimation of right ventricular end-systolic pressure-volume relationship. *Am J Physiol Heart Circ Physiol* 284: H1625-1630, 2003.

4. **Buckner CK, Saban R, Castleman WL, and Will JA**. Analysis of leukotriene receptor antagonists on isolated human intralobar airways. *Ann N Y Acad Sci* 524: 181-186, 1988.

5. **Chemla D, Hebert JL, Coirault C, Salmeron S, Zamani K, and Lecarpentier Y**. Matching dicrotic notch and mean pulmonary artery pressures: implications for effective arterial elastance. *Am J Physiol* 271: H1287-1295, 1996.

6. **Chen IC, Tan MS, Wu BN, Chai CY, Yeh JL, Chou SH, Chen IJ, and Dai ZK**. Statins ameliorate pulmonary hypertension secondary to left ventricular dysfunction through the Rho-kinase pathway and NADPH oxidase. *Pediatr Pulmonol* 52: 443-457, 2017.

7. **Chen TX, Pudasaini B, Guo J, Gong SG, Jiang R, Wang L, Zhao QH, Wu WH, Yuan P, and Liu JM**. Sex-specific cardiopulmonary exercise testing indices to estimate the severity of inoperable chronic thromboembolic pulmonary hypertension. *Int J Chron Obstruct Pulmon Dis* 13: 385-397, 2018.

8. **Chibana H, Tahara N, Itaya N, Ishimatsu T, Sasaki M, Sasaki M, Nakayoshi T, Ohtsuka M, Yokoyama S, Sasaki KI, Ueno T, and Fukumoto Y**. Pulmonary artery dysfunction in chronic thromboembolic pulmonary hypertension. *Int J Cardiol Heart Vasc* 17: 30-32, 2017.

9. **Claeys M, Claessen G, La Gerche A, Petit T, Belge C, Meyns B, Bogaert J, Willems R, Claus P, and Delcroix M**. Impaired Cardiac Reserve and Abnormal Vascular Load Limit Exercise Capacity in Chronic Thromboembolic Disease. *JACC Cardiovasc Imaging* 2018.

10. **de Beer VJ, de Graaff HJ, Hoekstra M, Duncker DJ, and Merkus D**. Integrated control of pulmonary vascular tone by endothelin and angiotensin II in exercising swine depends on gender. *Am J Physiol Heart Circ Physiol* 298: H1976-1985, 2010.

11. **De Wijs-Meijler DP, Stam K, van Duin RW, Verzijl A, Reiss IK, Duncker DJ, and Merkus D**. Surgical Placement of Catheters for Long-term Cardiovascular Exercise Testing in Swine. *J Vis Exp* e53772, 2016.

12. **de Wijs-Meijler DPM, Danser AHJ, Reiss IKM, Duncker DJ, and Merkus D**. Sex differences in pulmonary vascular control: focus on the nitric oxide pathway. *Physiol Rep* 5: 2017.

13. **Dell'Italia LJ**. The forgotten left ventricle in right ventricular pressure overload. *J Am Coll Cardiol* 57: 929-930, 2011.

14. **Dewachter L, and Dewachter C**. Inflammation in Right Ventricular Failure: Does It Matter? *Front Physiol* 9: 1056, 2018.

15. **Duncker DJ, Stubenitsky R, and Verdouw PD**. Role of adenosine in the regulation of coronary blood flow in swine at rest and during treadmill exercise. *Am J Physiol* 275: H1663-1672, 1998.

16. **Frangogiannis NG**. Fibroblasts and the extracellular matrix in right ventricular disease. *Cardiovasc Res* 113: 1453-1464, 2017.

17. **Frump AL, Bonnet S, de Jesus Perez VA, and Lahm T**. Emerging role of angiogenesis in adaptive and maladaptive right ventricular remodeling in pulmonary hypertension. *Am J Physiol Lung Cell Mol Physiol* 314: L443-L460, 2018.

18. **Furfine ES, Harmon MF, Paith JE, and Garvey EP**. Selective inhibition of constitutive nitric oxide synthase by L-NG-nitroarginine. *Biochemistry* 32: 8512-8517, 1993.

19. **Garvey EP, Tuttle JV, Covington K, Merrill BM, Wood ER, Baylis SA, and Charles IG**. Purification and characterization of the constitutive nitric oxide synthase from human placenta. *Arch Biochem Biophys* 311: 235-241, 1994.

20. **Grosse A, Grosse C, and Lang I**. Evaluation of the CT imaging findings in patients newly diagnosed with chronic thromboembolic pulmonary hypertension. *PLoS One* 13: e0201468, 2018.

21. **Grundy D**. Principles and standards for reporting animal experiments in The Journal of Physiology and Experimental Physiology. *J Physiol* 593: 2547-2549, 2015.

22. **Guihaire J, Haddad F, Boulate D, Capderou A, Decante B, Flecher E, Eddahibi S, Dorfmuller P, Herve P, Humbert M, Verhoye JP, Dartevelle P, Mercier O, and Fadel E**. Right ventricular plasticity in a porcine model of chronic pressure overload. *J Heart Lung Transplant* 33: 194-202, 2014.

23. **Guihaire J, Haddad F, Boulate D, Decante B, Denault AY, Wu J, Herve P, Humbert M, Dartevelle P, Verhoye JP, Mercier O, and Fadel E**. Non-invasive indices of right ventricular function are markers of ventricular-arterial coupling rather than ventricular contractility: insights from a porcine model of chronic pressure overload. *Eur Heart J Cardiovasc Imaging* 14: 1140-1149, 2013.

24. **Guihaire J, Haddad F, Noly PE, Boulate D, Decante B, Dartevelle P, Humbert M, Verhoye JP, Mercier O, and Fadel E**. Right ventricular reserve in a piglet model of chronic pulmonary hypertension. *Eur Respir J* 45: 709-717, 2015.

25. **Hardziyenka M, Campian ME, Reesink HJ, Surie S, Bouma BJ, Groenink M, Klemens CA, Beekman L, Remme CA, Bresser P, and Tan HL**. Right ventricular failure following chronic pressure overload is associated with reduction in left ventricular mass: evidence for atrophic remodeling. *J Am Coll Cardiol* 57: 921-928, 2011.

26. **Hartmann S, Ridley AJ, and Lutz S**. The Function of Rho-Associated Kinases ROCK1 and ROCK2 in the Pathogenesis of Cardiovascular Disease. *Front Pharmacol* 6: 276, 2015.

27. **He J, Li X, Luo H, Li T, Zhao L, Qi Q, Liu Y, and Yu Z**. Galectin-3 mediates the pulmonary arterial hypertension-induced right ventricular remodeling through interacting with NADPH oxidase 4. *J Am Soc Hypertens* 11: 275-289 e272, 2017.

28. **Ikeda S, Satoh K, Kikuchi N, Miyata S, Suzuki K, Omura J, Shimizu T, Kobayashi K, Kobayashi K, Fukumoto Y, Sakata Y, and Shimokawa H**. Crucial role of rho-kinase in pressure overload-induced right ventricular hypertrophy and dysfunction in mice. *Arterioscler Thromb Vasc Biol* 34: 1260-1271, 2014.

29. **In E, Deveci F, and Kaman D**. Assessment of heat shock proteins and endothelial dysfunction in acute pulmonary embolism. *Blood Coagul Fibrinolysis* 27: 378-383, 2016.

30. **Kirson NY, Birnbaum HG, Ivanova JI, Waldman T, Joish V, and Williamson T**. Prevalence of pulmonary arterial hypertension and chronic thromboembolic pulmonary hypertension in the United States. *Curr Med Res Opin* 27: 1763-1768, 2011.

31. **Lang IM, Dorfmuller P, and Vonk Noordegraaf A**. The Pathobiology of Chronic Thromboembolic Pulmonary Hypertension. *Ann Am Thorac Soc* 13 Suppl 3: S215-221, 2016.

32. **Liu SF, Hislop AA, Haworth SG, and Barnes PJ**. Developmental changes in endothelium-dependent pulmonary vasodilatation in pigs. *Br J Pharmacol* 106: 324-330, 1992.

33. **Loisel F, Provost B, Guihaire J, Boulate D, Arouche N, Amsallem M, Arthur-Ataam J, Decante B, Dorfmuller P, Fadel E, Uzan G, and Mercier O**. Autologous endothelial progenitor cell therapy improves right ventricular function in a model of chronic thromboembolic pulmonary hypertension. *J Thorac Cardiovasc Surg* 157: 655-666 e657, 2019.

34. **Lu X, Dang CQ, Guo X, Molloi S, Wassall CD, Kemple MD, and Kassab GS**. Elevated oxidative stress and endothelial dysfunction in right coronary artery of right ventricular hypertrophy. *J Appl Physiol (1985)* 110: 1674-1681, 2011.

35. **Marcus JT, Gan CT, Zwanenburg JJ, Boonstra A, Allaart CP, Gotte MJ, and Vonk-Noordegraaf A**. Interventricular mechanical asynchrony in pulmonary arterial hypertension: left-to-right delay in peak shortening is related to right ventricular overload and left ventricular underfilling. *J Am Coll Cardiol* 51: 750-757, 2008.

36. **Matsunaga T, Warltier DC, Weihrauch DW, Moniz M, Tessmer J, and Chilian WM**. Ischemia-induced coronary collateral growth is dependent on vascular endothelial growth factor and nitric oxide. *Circulation* 102: 3098-3103, 2000.

37. **Matsunaga T, Weihrauch DW, Moniz MC, Tessmer J, Warltier DC, and Chilian WM**. Angiostatin inhibits coronary angiogenesis during impaired production of nitric oxide. *Circulation* 105: 2185-2191, 2002.

38. **McCabe C, White PA, Hoole SP, Axell RG, Priest AN, Gopalan D, Taboada D, MacKenzie Ross R, Morrell NW, Shapiro LM, and Pepke-Zaba J**. Right ventricular dysfunction in chronic thromboembolic obstruction of the pulmonary artery: a pressure-volume study using the conductance catheter. *J Appl Physiol (1985)* 116: 355-363, 2014.

39. **Naeije R, and Badagliacca R**. The overloaded right heart and ventricular interdependence. *Cardiovasc Res* 113: 1474-1485, 2017.

40. **Parker TA, le Cras TD, Kinsella JP, and Abman SH**. Developmental changes in endothelial nitric oxide synthase expression and activity in ovine fetal lung. *Am J Physiol Lung Cell Mol Physiol* 278: L202-208, 2000.

41. **Rain S, Andersen S, Najafi A, Gammelgaard Schultz J, da Silva Goncalves Bos D, Handoko ML, Bogaard HJ, Vonk-Noordegraaf A, Andersen A, van der Velden J, Ottenheijm CA, and de Man FS**. Right Ventricular Myocardial Stiffness in Experimental Pulmonary Arterial Hypertension: Relative Contribution of Fibrosis and Myofibril Stiffness. *Circ Heart Fail* 9: 2016.

42. **Rees DD, Palmer RM, Schulz R, Hodson HF, and Moncada S**. Characterization of three inhibitors of endothelial nitric oxide synthase in vitro and in vivo. *Br J Pharmacol* 101: 746-752, 1990.

43. **Reesink HJ, Meijer RC, Lutter R, Boomsma F, Jansen HM, Kloek JJ, and Bresser P**. Hemodynamic and clinical correlates of endothelin-1 in chronic thromboembolic pulmonary hypertension. *Circ J* 70: 1058-1063, 2006.

44. **Shimizu T, and Liao JK**. Rho Kinases and Cardiac Remodeling. *Circ J* 80: 1491-1498, 2016.

45. **Simonneau G, Torbicki A, Dorfmuller P, and Kim N**. The pathophysiology of chronic thromboembolic pulmonary hypertension. *Eur Respir Rev* 26: 2017.

46. **Sorop O, Heinonen I, van Kranenburg M, van de Wouw J, de Beer VJ, Nguyen ITN, Octavia Y, van Duin RWB, Stam K, van Geuns RJ, Wielopolski PA, Krestin GP, van den Meiracker AH, Verjans R, van Bilsen M, Danser AHJ, Paulus WJ, Cheng C, Linke WA, Joles JA, Verhaar MC, van der Velden J, Merkus D, and Duncker DJ**. Multiple common comorbidities produce left ventricular diastolic dysfunction associated with coronary microvascular dysfunction, oxidative stress, and myocardial stiffening. *Cardiovasc Res* 114: 954-964, 2018.

47. **Stam K, van Duin RWB, Uitterdijk A, Cai Z, Duncker DJ, and Merkus D**. Exercise facilitates early recognition of cardiac and vascular remodeling in chronic thromboembolic pulmonary hypertension in swine. *Am J Physiol Heart Circ Physiol* 314: H627-H642, 2018.

48. **Stam K, van Duin RWB, Uitterdijk A, Krabbendam-Peters I, Sorop O, Danser AHJ, Duncker DJ, and Merkus D**. Pulmonary microvascular remodeling in chronic thrombo-embolic pulmonary hypertension. *Am J Physiol Lung Cell Mol Physiol* 2018.

49. **Stubenitsky R, Verdouw PD, and Duncker DJ**. Autonomic control of cardiovascular performance and whole body O2 delivery and utilization in swine during treadmill exercise. *Cardiovasc Res* 39: 459-474, 1998.

50. **Sun XQ, Abbate A, and Bogaard HJ**. Role of cardiac inflammation in right ventricular failure. *Cardiovasc Res* 113: 1441-1452, 2017.

51. **Sunamura S, Satoh K, Kurosawa R, Ohtsuki T, Kikuchi N, Elias-Al-Mamun M, Shimizu T, Ikeda S, Suzuki K, Satoh T, Omura J, Nogi M, Numano K, Siddique MAH, Miyata S, Miura M, and Shimokawa H**. Different roles of myocardial ROCK1 and ROCK2 in cardiac dysfunction and postcapillary pulmonary hypertension in mice. *Proc Natl Acad Sci U S A* 115: E7129-E7138, 2018.

52. **Torbicki A, and Fijałkowska A**. Role of cardiac biomarkers in assessment of RV function and prognosis in chronic pulmonary hypertension. *European Heart Journal Supplements* 9: H41-H47, 2007.

53. **Trip P, Rain S, Handoko ML, van der Bruggen C, Bogaard HJ, Marcus JT, Boonstra A, Westerhof N, Vonk-Noordegraaf A, and de Man FS**. Clinical relevance of right ventricular diastolic stiffness in pulmonary hypertension. *Eur Respir J* 45: 1603-1612, 2015.

54. **Tsai SH, Lu G, Xu X, Ren Y, Hein TW, and Kuo L**. Enhanced endothelin-1/Rho-kinase signalling and coronary microvascular dysfunction in hypertensive myocardial hypertrophy. *Cardiovasc Res* 113: 1329-1337, 2017.

55. **van de Veerdonk MC, Bogaard HJ, and Voelkel NF**. The right ventricle and pulmonary hypertension. *Heart Fail Rev* 21: 259-271, 2016.

56. **van Wolferen SA, Marcus JT, Westerhof N, Spreeuwenberg MD, Marques KM, Bronzwaer JG, Henkens IR, Gan CT, Boonstra A, Postmus PE, and Vonk-Noordegraaf A**. Right coronary artery flow impairment in patients with pulmonary hypertension. *Eur Heart J* 29: 120-127, 2008.

57. **Vogel-Claussen J, Skrok J, Shehata ML, Singh S, Sibley CT, Boyce DM, Lechtzin N, Girgis RE, Mathai SC, Goldstein TA, Zheng J, Lima JA, Bluemke DA, and Hassoun PM**. Right and left ventricular myocardial perfusion reserves correlate with right ventricular function and pulmonary hemodynamics in patients with pulmonary arterial hypertension. *Radiology* 258: 119-127, 2011.

58. **Vonk Noordegraaf A, Westerhof BE, and Westerhof N**. The Relationship Between the Right Ventricle and its Load in Pulmonary Hypertension. *J Am Coll Cardiol* 69: 236-243, 2017.

59. **Zeidan A, Gan XT, Thomas A, and Karmazyn M**. Prevention of RhoA activation and cofilin-mediated actin polymerization mediates the antihypertrophic effect of adenosine receptor agonists in angiotensin II- and endothelin-1-treated cardiomyocytes. *Mol Cell Biochem* 385: 239-248, 2014.

Chapter 7

Summary and General discussion

Chronic thromboembolic pulmonary hypertension (CTEPH) develops in about 3-4% of patients after acute pulmonary embolism (PE), although the disease is probably highly underdiagnosed. CTEPH is associated with a poor quality life, high mortality and although pulmonary endarterectomy and balloon angioplasty may initially provide symptom relief by removing the proximal obstructions, there is no curative treatment for the pulmonary microvasculopathy. Furthermore, it is unclear why only a subpopulation of patients develops chronic pulmonary hypertension after an acute PE, and what the underlying mechanism(s) are for this transition from acute to chronic pulmonary disease. There are some risk factors such as genetics, ineffective endogenous fibrinolysis, hypercoagulability, deficient angiogenesis, inflammation and platelet endothelial cell adhesion molecule-1 deficiency linked and hypothesized to play a role in the development of CTEPH (53, 82).

In this thesis, we proposed that (pulmonary) endothelial dysfunction is a key mechanism in the transition from acute PE to development of CTEPH. With a dysfunctional endothelium, emboli cannot be properly resolved and the remodeling of the pulmonary vasculature, both functional as structural, cannot be prevented. A healthy pulmonary endothelium is characterized by production of nitric oxide (NO) and prostacyclin, while production of endothelin (ET) is kept low and circulating ET is largely cleared in the lungs. Pulmonary endothelial dysfunction and/or high pulmonary pressure are associated with perturbations in the prostacyclin, nitric oxide (NO) and endothelin (ET) pathways. These perturbations lead to pulmonary vascular vasoconstriction and, together with the high blood pressure, contribute to muscularization of the pulmonary vessels. Both vasoconstriction and muscularization of the pulmonary vessels cause an increase in vascular resistance, increasing the right ventricular afterload. The RV responds to this chronic increase in afterload by an initially adaptive response,

encompassing cardiomyocyte hypertrophy to increase contractile capacity, fibrosis to prevent cardiomyocyte overstretch and maintain RV shape for optimal function and angiogenesis to maintain blood supply to the thickened ventricular wall. However, eventually there is an inflammatory response and maladaptive (increased diastolic stiffness) fibrosis. However, although these adaptations are initially enabling the RV to cope with the increased afterload, they are eventually not sufficient, and can even be contributing to RV dysfunction/failure (5, 77, 82).

The aim of the current thesis was to develop a CTEPH swine model in which both the emboli and the endothelial dysfunction are simulated in order to establish the role of pulmonary endothelial (dys)function in the development and progression of CTEPH and characterize (molecular) pathways involved in cardiac remodeling with the emphasis on hypertrophy, contractility, inflammation, oxidative stress, apoptosis and angiogenesis. In addition, we investigated the effects of acute exercise and the possibilities of exercise as a stress test for early detection in this CTEPH model.

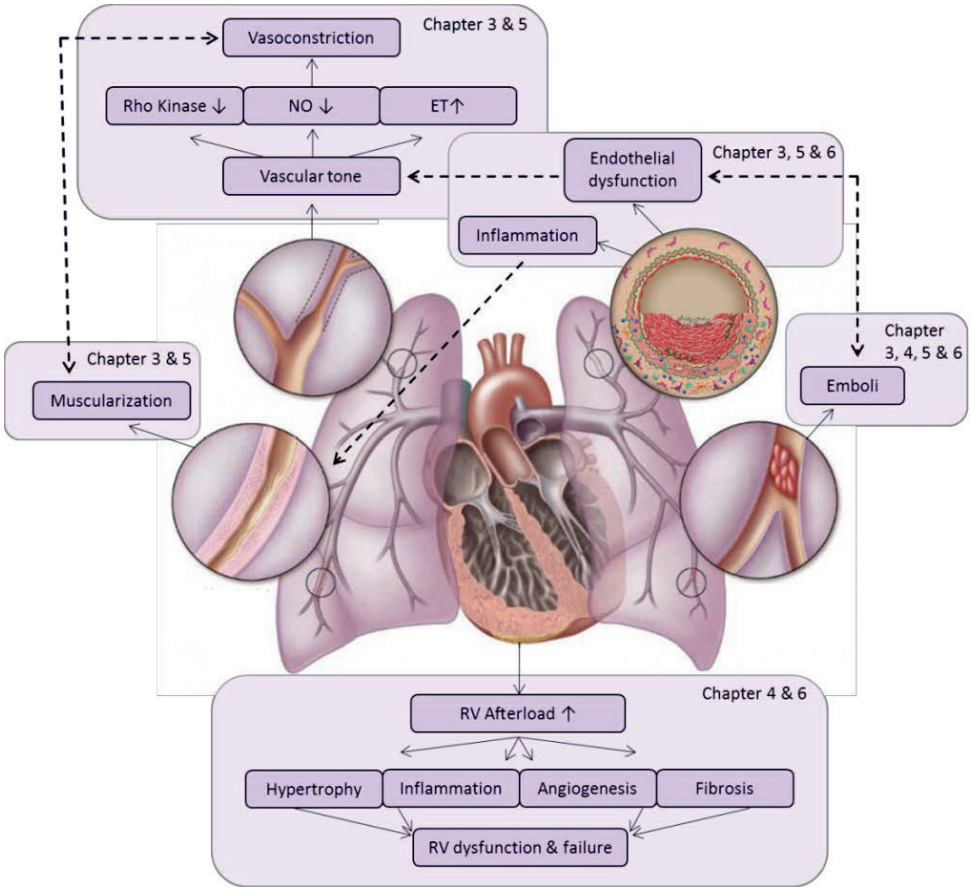

Figure 1. Pathophysiology of CTEPH.

The key pathways involved in the pathophysiology of CTEPH. CTEPH is a pulmonary and cardiac disease. The pulmonary changes are characterized by vascular obstructions due to emboli, vascular muscularization, vasoconstriction and endothelial dysfunction and inflammation which all interfere with each other. The cardiac changes are caused by the increased afterload and characterized by hypertrophy, inflammation, angiogenesis and fibrosis and lead to RV dysfunction and failure. NO, nitric oxide; ET, endothelin; RV, right ventricle (adapted from(94)).

Characterization of a new CTEPH swine model

Applicability, interpretation and limitations of chronically instrumenting swine

The use of chronically instrumented animals allows serial assessment of cardiopulmonary function either during development of disease or evaluation of treatment, thereby increasing statistical power and limiting the number of animals required for a study. In addition, chronic instrumentation of swine allow for awake monitoring of changes in regulation of the cardiopulmonary system during exercise testing. Therefore, we presented this chronic instrumentation of swine in **Chapter 2**, and explained its implications in cardiopulmonary monitoring and stress testing.

A potential drawback is that, when commercially available swine breeds such as Yorkshire, Landrace, Large White etc, are used for chronic instrumentation, adult swine are very large and may therefore be difficult to handle. Therefore, juvenile swine are often used. The heart and pulmonary endothelium of juvenile swine are still very adaptable to stress and damage. An alternative is the use of adult miniature swine, such as Yucatan or Göttingen swine, of which the adult weight is 40 - 60 kg (8). Several swine models of cardiopulmonary disease, such as and pulmonary hypertension are available (56, 66) or being developed and could be combined, and thereby significantly improved, with chronic instrumentation.

Induction of CTEPH requires both repeated embolizations and endothelial dysfunction

In order to combine the strengths and circumvent the shortcomings of the previous large animal models (2, 10, 24, 27, 29, 46, 57, 60, 61, 67, 68, 74, 75, 78, 88, 95, 100) (see Table 1 of Chapter 3) we developed and characterized a new

CTEPH swine model in **Chapter 3.** CTEPH induction required both repeated embolizations by means of microsphere infusion via the inserted RV catheter, and endothelial dysfunction by means of eNOS inhibition, as either intervention alone did not result in sustained CTEPH. In this model we could monitor hemodynamics and perform echocardiography and exercise testing, all in the awake state.

During the embolization procedures, microspheres were slowly injected into the RV, assuming that microspheres flow to perfused, non-embolized vessels to ensure full coverage of the pulmonary vasculature. A total of approximately 36000 microspheres with a diameter of ~700 µm were infused per animal. When compared to the number of branches of the corresponding size present in the pulmonary vascular bed, it is likely that 60% of the pulmonary small arteries were obstructed. Since it has been suggested that 40-60% of the lung vasculature needs to be obstructed for CTEPH to develop (7, 18), the infused microspheres should be sufficient to induce CTEPH in the swine. Nevertheless, as we show in **Chapter 3**, with microspheres alone, no sustained CTEPH developed.

In addition however, CTEPH occurs only in a minority of patients after acute pulmonary embolism while also patients that did not (notice to) experience an acute pulmonary embolism have been reported to develop CTEPH (82). In these patients, it is proposed that CTEPH is the consequence of multiple micro-embolisms (23, 85). Since CTEPH patients present with dysfunctional endothelium as evidenced by alterations in coagulation, inflammation, angiogenesis and vasoregulation (4, 54, 69, 82, 83), this could be the second hit present in the group of patients that develop CTEPH. We therefore induced endothelial dysfunction as a second hit by inhibiting eNOS by chronic LNAME administration in our swine model to produce sustained CTEPH in **Chapter 3, 4, 5 and 6**. Nitric oxide is an important endothelium-derived anti-coagulatory, anti-inflammatory,

pro-angiogenic, vasodilator which are all factors leading to progression of CTEPH. We observed in our animal model that endothelial dysfunction in combination with multiple microsphere infusions resulted in a sustained increase in PAP and tPVRi. This increase in PAP above 25mmHg for a prolonged period of time after embolizations and in the awake state is evidence for successful induction of chronic PH (2, 29, 46, 57, 60, 67, 68, 75, 78, 95, 100). Our findings are in accordance with a recent study in rats, that show that sustained CTEPH developed when combining embolizations with endothelial dysfunction produced by VEGF-inhibition (63) which also signals through the NO pathway. Importantly, in the studies presented in this thesis, CTEPH persisted when eNOS inhibition was discontinued, which implies that vascular remodeling and endothelial dysfunction developed as a consequence of high blood pressure and increased vascular shear stress in our swine.

Characterization of pulmonary remodeling in CTEPH swine

It is well established that secondary to pulmonary embolism, worsening of PH results from progressive microvascular remodeling of the non-obstructed distal pulmonary small arteries (23, 41, 59). Indeed, we also observed microvascular remodeling as evidenced by an increased wall thickness of the non-obstructed pulmonary small arteries and exaggerated vasoconstriction to both KCl and the thromboxane analogue U46619. Although the exact time-course of microvascular remodeling may not be exactly determined from our data, as the increase in resistance due to embolizations cannot be distinguished from the increase in resistance due to microvascular remodeling during the embolization period, pulmonary vascular resistance continued to increase after cessation of the embolization procedures, which is consistent with remodeling of the distal vasculature. Even after cessation of the eNOS inhibitor, which may also have

contributed by increasing microvascular tone, the high pulmonary pressure and resistance persisted.

Pulmonary microvascular remodeling

In accordance with previous studies in humans and animals (10, 17, 59), we observed in **Chapter 5** inward remodeling of both pulmonary small arteries and the pulmonary microvasculature. This remodeling encompassed muscularization and thickening of the vascular wall and resulted in a relative reduction of the vascular lumen which would be contributing to a worsening of PH by further increasing the PAP. The changes in microvascular morphology in our CTEPH swine were not accompanied by an overt pulmonary inflammatory response at the disease stage, as only IL-6 showed a trend towards an increase, while this increase in IL-6 was consistent with the increase in CTEPH patients (76, 96, 97). However, since we measured inflammation on gene expression level, further investigations such as on the protein level could reveal even more specifics. Although the existence of pulmonary microvascular remodeling in CTEPH is known since 1993 (59), the consequences of this remodeling for pulmonary microvascular function had not been investigated. In contrast to the lack of evidence of overt inflammation in our model of CTEPH, microvascular remodeling was accompanied by alterations in two major endothelial signaling pathways, i.e. ET and NO, that are also implicated in development and progression of pulmonary hypertension (6), and will be further discussed below.

Pulmonary vascular endothelium

Perturbations in the NO-pathway have been implicated in the pathogenesis of PH (6, 48, 99). Indeed, we observed that chronic eNOS-inhibition is required as a second hit, in addition to embolizations, to successfully produce stable CTEPH in

swine, as repeated microsphere embolization alone does not result in sustained PH (**Chapter 3**). We investigated the endothelial dysfunction in our CTEPH animals in **Chapter 5**, which was characterized by an imbalance between endothelial production of the vasodilator NO and the vasoconstrictor ET-1, while vascular integrity was intact.

We observed in **Chapter 5** that, in accordance with inhaled NO treatment in patients (1), NO sensitivity was increased in pulmonary small arteries from CTEPH animals. This increase in NO sensitivity was evidenced by an enhanced vasodilatory response to the NO-donor SNP, reduced vasodilator response to bradykinin although there was a similar attenuation of BK-induced vasodilation by eNOS-inhibition. The increased NO sensitivity was therefore most likely caused by a decrease in NO production, although we did not directly measure NO plasma levels. In addition, the response to PDE5-inhibition with Sildenafil was reduced in the CTEPH arteries, suggesting that reduced PDE5-activity acted to compensate, in part, for a blunted endogenous NO production, resulting in an apparently increased NO-sensitivity. Such reduced response to PDE5-inhibition provides a potential explanation for the failure of single treatment with PDE5-inhibition as a therapeutic strategy for CTEPH and underscores the importance of intervening more upstream in the NO-pathway either by administering NO (1) or stimulating/activating sGC. Indeed, beneficial therapeutic effects have been reported for Riociguat, a sGC stimulator, which was recently approved for therapeutic use in CTEPH (31, 47, 50, 81).

Consistent with endothelial dysfunction, we observed a 40% higher plasma ET-1 in our porcine model in **Chapter 5**. Clinically, it has been shown that plasma ET-1 levels correlate well with clinical severity (30, 71), and that patients with NYHA class IV show a doubling of circulating ET (30, 71). Hence the 40%

elevation in circulating ET-levels are consistent with the clinical phenotype of our animals representing NYHA class II or III. As ET can induce vasoconstriction and vascular remodeling, we investigated the contribution of changes in ET signaling to functional changes in the pulmonary microvasculature. In **Chapter 5** we show that the increase in circulating ET-1 is accompanied by a decreased sensitivity of the pulmonary microvasculature to ET-1. Endothelin receptor antagonists (ERAs) are an established therapy in PAH (22, 49), but conflicting results of ERA therapy have been reported in CTEPH patients (39, 40, 64). For example, the randomized, double-blind, placebo-controlled BENEFIT study, which investigated dual ERA therapy with Bosentan, showed no statistically significant effects of Bosentan in CTEPH patients (45). In **Chapter 5** we observed an increased ET_A, decreased ET_B contribution to ET-1 vasoconstriction and increased ET_A/ET_B gene expression ratio which are in accordance with the increased ET_A receptor expression in human pulmonary endarterectomy tissues (84) and in the lungs of swine with CTEPH (57). These data suggest that CTEPH is accompanied by changes in ET-1 signaling in the pulmonary microvasculature and that the interaction between the ET_A and the ET_B receptor is altered in CTEPH. The loss of ET_B mediated vasoactive effects observed in **Chapter 5** suggests that specific ET_A blockade alone would be more therapeutically efficacious. Moreover, in CTEPH the effect of ET-1 is already suppressed by a decreased sensitivity which could explain inefficacy of ERA therapy. Although the AMBER studies, which investigated the ET_A specific ERA Ambrisentan was terminated early (ClinicalTrials.gov NCT02021292, NCT02060721), there are ongoing studies to ET_A specific ERA's such as Macitentan (MERIT) which is an ERA with high specificity for ET_A(25), which is consistent with our data that ET_A blockade alone would be more therapeutically efficient than dual ERA therapy.

ET-1 signaling occurs via two pathways, i.e. a calcium-dependent pathway involving phospholipase C (PLC)-mediated activation of myosin-light chain kinase and a calcium-independent pathway involving RhoA-Rho-kinase mediated inactivation of myosin phosphatase (42). Rho-kinase inhibition with Fasudil has been shown to be an effective therapy in some patients with PAH (21), but little is known about this pathway in the pathology of CTEPH. As we show in **Chapter 5**, the data obtained from the isolated pulmonary small arteries indicate a complete loss of the Rho-kinase contribution to ET-1-induced vasoconstriction in the CTEPH small arteries, and imply that, ET-1-induced vasoconstriction in CTEPH must therefore be mediated through the PLC-pathway. Although a reduction in Rho-kinase was not present at mRNA level in the CTEPH swine, mRNA levels of lung tissue may not reflect protein levels and/or enzyme activity in the vasculature. These results are very different from those obtained in PAH, where the contribution of Rho-kinase was found to be increased (16). Together, these data suggest that microvascular constriction and remodeling occur via different pathways in CTEPH as compared to PAH, and suggest that the use of Rho-kinase inhibitors to alleviate pulmonary vasoconstriction and remodeling may not be efficacious in CTEPH patients.

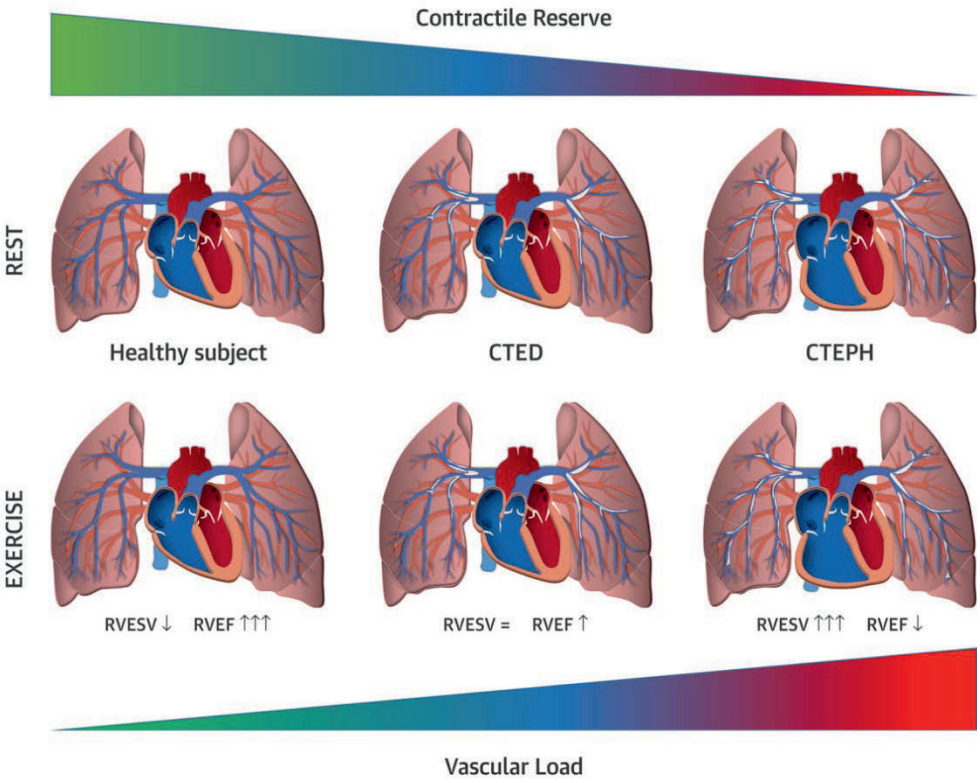

Figure 2. Cardiac remodeling in CTEPH at rest and during exercise.

Cardiac remodeling in CTEPH, and the effects of exercise on the heart. CTED, chronic thrombo-embolic disease; CTEPH, chronic thrombo-embolic pulmonary hypertension; RVESV, right ventricular end-systolic volume; RVEF, right ventricular ejection fraction. Reprinted and adapted from (14), with permission from Elsevier.

Characterization of cardiac remodeling in CTEPH swine

Cardiac dimensions and function

It has been shown that RV structural and functional adaptability are important determinants of functional capacity and survival in patients with CTEPH (14, 32, 91). The RV afterload increases during development and progression of PH. To cope with this increased afterload, the RV exhibits structural and functional changes to augment contractility (Figure 2). The effects of CTEPH on cardiac structure, function and gene expression were therefore examined in our porcine model in **Chapter 3 and 6**. We observed a trend towards RV dilation and a reduced RV ejection fraction both by echocardiography (**Chapter 3**) and by cardiac magnetic resonance imaging (**Chapter 6**). In addition, the CTEPH animals presented with an increase in RV cardiomyocyte size and global RV hypertrophy, that was accompanied by activation of both pro- and antiapoptotic gene expression (increases in Caspase-3 and BCL2 respectively). RV resting function was preserved in our animals, but BNP expression was increased, suggestive of an increased wall stress. Our findings are consistent with observations in another porcine CTEPH model, in which CTEPH is induced by ligation of the left pulmonary artery, in combination with embolization of the proximal segmental arteries with glue (27-29). In that model, RV dilation (29) and RV myocyte hypertrophy (27) were also accompanied by an increased BNP expression (27, 29), that correlated inversely with stroke volume and positively with global RV hypertrophy (27). In addition, we aimed to identify differences and/or correlations between CTEPH severity and PA flow patterns with the promosing new 4D flow CMR technique in **Chapter 4**. It appeared from the 4D CMR flow measurements that the pulmonary acceleration time was prolonged in the animals with the most severe CTEPH, although this was not statistically significant (Figure 3).

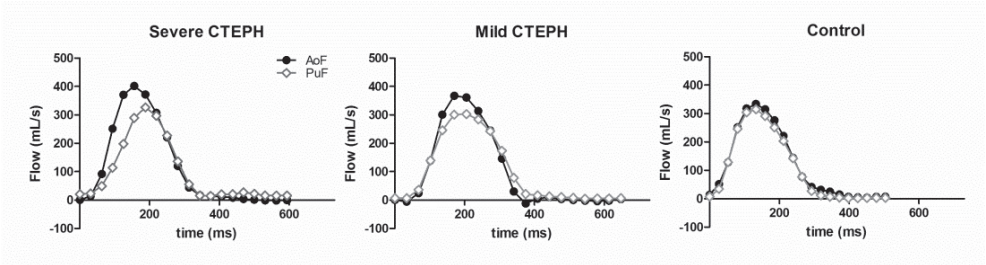

Figure 3. Pulmonary and aorta flow measured with 4D CMR
Pulmonary and aorta flow patterns of swine with severe, mild or no CTEPH in which the acceleration time appears to be prolonged in the most severe CTEPH animal.

It is increasingly recognized that not only RV systolic function, but also RV diastolic function correlates with prognosis in patients with PAH (89). Indeed, in pigs with type II pulmonary hypertension, changes in RV-PA coupling were accompanied by diastolic dysfunction (3). Diastolic stiffness is determined by passive myocyte stiffness as well as interstitial fibrosis. Consistent with the findings in a rat model of pulmonary artery banding (70), the mild RV dysfunction in our CTEPH swine was accompanied by an increase in the stiff titin isoform N2BA but not with changes in myocardial fibrosis as measured histologically. Furthermore, there was a change in the ratio between Col1 and Col3 in the RV, suggesting relatively more expression of the stiff Col1 isoform. These data, investigated in **Chapter 6,** are also consistent with the isoform shift observed by Rain et al (70), and may have contributed to a stiffer RV. Although neither SERCA nor phospholamban gene expression were changed in our CTEPH swine, it is possible that changes in their phosphorylation may play a role in altered Ca^{2+} handling, which is in turn implied to play a role in the development of RV dysfunction (3). Hence, future studies should investigate contractile function of individual cardiomyocytes as well as expression and phosphorylation of the contractile and calcium handling proteins SERCA, phospholamban, smooth muscle actin, titin, troponin kinase-A and -C and troponins.

Cardiac inflammation, oxidative stress, apoptosis and angiogenesis

A key factor that distinguishes compensated RV remodeling from RV failure is adequate myocardial perfusion (20). Angiogenesis allows the RV perfusion to be enhanced commensurate with the increase in RV mass. Indeed, many studies show that RV failure is accompanied by a reduction in capillary density, whereas capillary density is preserved or even increased in adaptive RV remodeling (20). Furthermore, myocardial perfusion reserve has been shown to be reduced in humans with both CTEPH and PAH (92, 93). As presented in **Chapter 6**, capillary density was increased in our CTEPH swine, in accordance with another porcine CTEPH model (51), which is beneficial for myocardial perfusion and oxygenation, and suggests a state of adaptive RV remodeling. Nevertheless, VEGFA-expression was higher in swine with CTEPH, suggesting that there was still a need for additional perfusion, although we did not actually measure myocardial perfusion in these animals. Hence, future studies should address the myocardial perfusion and coronary flow reserve in different stages of RV (mal) adaptation.

The transition from compensated RV remodeling to RV failure is also associated with inflammation and activation of the immune response (15, 19, 86). Although the RV expression of genes involved in immune modulation (TNF-α, IL-6, IFN-γ) was not altered, expression of TGF-β was increased in our CTEPH swine (**Chapter 6)**. Activation of the TGF-β pathway is increasingly recognized to play a pivotal role in de development in PH (65, 73)and was further confirmed in our animals by the increase in expression of its downstream target PAI-1. Both activation of the TGF-β pathway and increased circulating levels of endothelin can result in activation of the Rho-kinase pathway (80, 90, 98). Indeed, ROCK2 expression was upregulated in the RV of CTEPH swine. Importantly, ROCK2 activation is involved in cardiac hypertrophy, oxidative stress, angiogenesis,

apoptosis and fibrosis and therefore may present a major deleterious factor in RV-remodeling (33, 43, 87) (Figure 3), particularly given the observation that ROCK2 phosphorylates protein phosphatase 1 (PP1), which regulates both myofilament sensitivity to Ca^{2+} as well as Ca^{2+} handling (33).

ROCK2 is not only expressed in the myocardium but also in the vasculature, where its expression correlates with oxidative stress and NOX-expression (11). NOX1, NOX2 and NOX4 were upregulated in the right coronary artery of swine with pulmonary artery banding, which was accompanied by oxidative stress and endothelial dysfunction, despite unaltered eNOS expression (52). The upregulation of NOX1 and NOX4, and the unaltered eNOS expression in the RV of our CTEPH swine are consistent with these data, although we did not determine the exact location of their expression (**Chapter 6**). Furthermore, the upregulation of NOX4 is consistent with recent data from patients with PAH, in which circulating NOX4 was increased (35). Finally, the negative correlation of NOX1 and NOX4 with RV-PA coupling, as observed in **Chapter 6**, suggests that oxidative stress in the myocardium contributes to worsening of RV-function.

Hence, although therapeutic Rho-kinase inhibition may not be beneficial for the pulmonary vascular tone and remodeling, it may prevent adverse cardiac remodeling.

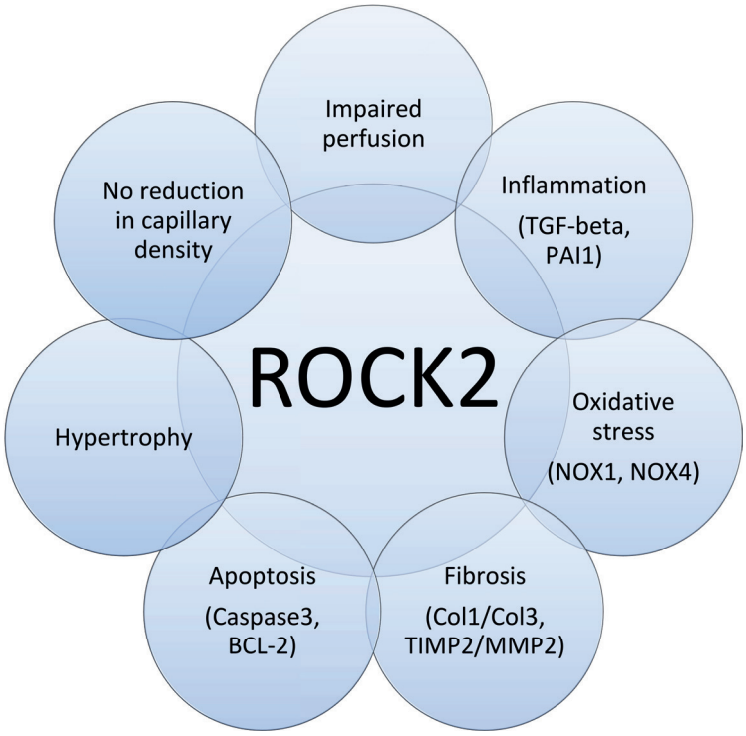

Figure 4. ROCK2 involvement in RV remodeling.
ROCK2 is associated with the mentioned factors and plays a major deleterious role in RV-remodeling. Between parentheses are the genes that are altered in our CTEPH swine.

Cardiopulmonary stress testing

Exercise testing after pulmonary embolism is predictive of development of PH and/or patient outcome in established CTEPH (34, 36, 37, 72). We presented in **Chapter 3, 5 and 6** that CTEPH is characterized by exercise intolerance (Figure 4). This impaired exercise capacity is principally caused by an exacerbated increase in PAP and pulmonary vascular resistance during exercise, that further increases RV afterload and the V/Q-mismatch in the lungs (9, 12, 13).

In humans with CTEPH, physiological dead space is increased in proportion to the increase in PVR, resulting in a lower P_aO_2, which is accompanied

by a reduction in P_aCO_2, as a result of compensatory hyperventilation (55). Similarly, the slightly lower P_aO_2 in our CTEPH swine is consistent with a mild V/Q-mismatch and dead space ventilation at rest. However, contrary to humans with CTEPH, P_aCO_2 was not significantly affected in our porcine CTEPH-model neither at rest, nor during exercise. This discrepancy in CO_2 response may in part be due to the observation that swine lack collateral ventilation and therefore are less capable of ameliorating intraregional V/Q differences between alveoli as compared to humans. Furthermore, as healthy quadrupeds already ventilate and perfuse their entire lungs at rest (58), an increase in ventilation with CTEPH cannot further recruit hypoventilated lung areas and improve V/Q mismatch, and hence their hyperventilatory response may not be capable of reducing P_aCO_2 levels below normal as occurs in humans. The lower $P_{mv}O_2$ observed in CTEPH is partly a consequence of the lower P_aO_2 due to the V/Q mismatch, and in part reflects the decreased blood flow due to a lower CI, forcing the body to extract more oxygen.

In accordance with the studies of Claessen et al. 2015 in CTEPH patients (12, 13), we observed in our CTEPH swine that the right ventricle was not able to cope with this increased afterload evidenced by the limited exercise-induced increase in stroke volume and CI (Figure 2). Furthermore, RV-PA coupling, an index of how well the RV can cope with the increased afterload, is reduced in CTEPH and a correlation was found between reduced coupling and a reduced SV reserve with dobutamine in swine (29). Similarly, in **Chapter 6**, severity of CTEPH indicated by the PVR, correlated inversely with RV-PA coupling. Importantly, recent studies in patients with CTEPH show that RV-PA coupling correlates with exercise capacity (14), which in turn is a strong predictor of outcome (9).

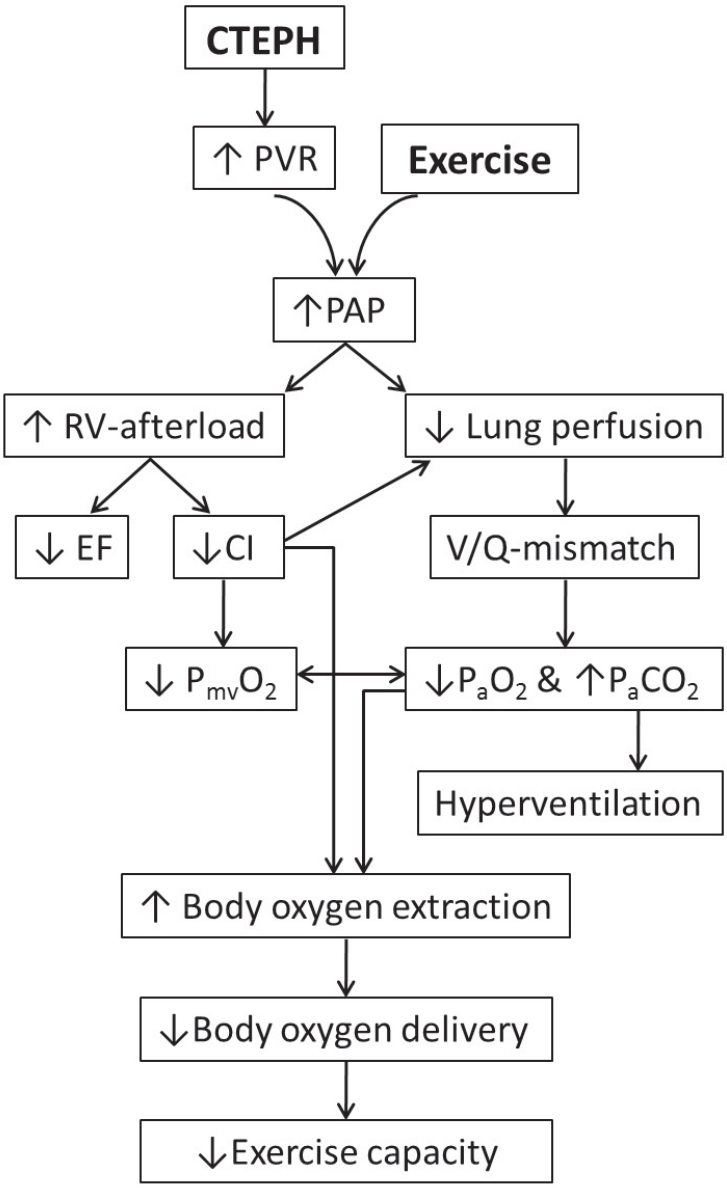

Figure 5. Effects of exercise in CTEPH.

The pathway after exercise that eventually leads to a decrease in exercise capacity in CTEPH. PAP, pulmonary artery pressure; PVR, pulmonary vascular resistance; RV, right ventricle; V/Q-mismatch, ventilation/perfusion-mismatch; $P_{mv}O_2$, mixed venous oxygen pressure; P_aO_2, arterial oxygen pressure; P_aCO_2, arterial carbon dioxide pressure.

During exercise, maximal body oxygen consumption was reduced and arterial lactate concentration was increased by more than 2 mmol/L, indicating that, consistent with patient data (26, 38, 44, 72), the anaerobic threshold was reached in CTEPH swine during exercise at 4 km/h. Particularly the decreased CI (27%) and to a lesser extent the decreased C_aO_2 (10%), limited the increase in body oxygen delivery during exercise. These findings in **Chapter 5** suggest that exercise intolerance in CTEPH is principally caused by the increased pulmonary vascular resistance, and thereby the afterload of the RV, that limits the exercise induced increase in CI. The V/Q-mismatch that hampers arterial oxygenation also contributes to exercise intolerance, but to a lesser extent. However, the relative contributions of cardiac and pulmonary dysfunction to the exercise intolerance in patients with more severe RV dysfunction remains to be established.

Methodological limitations

In the clinic, CTEPH occurs as a result of thrombo-emboli with different sizes which are not adequately resolved in the pulmonary vasculature. In the swine model described and characterized in this thesis, CTEPH is induced by artificial non-degradable microspheres with a diameter of ~700 µm. The absence of endogenous emboli in our studies could have altered the inflammatory response and vascular remodeling. In addition, the hypercoagulable state and/or inadequate endogenous fibrinolysis, often observed in CTEPH patients, are not present in our animal model.

Future perspectives

Although we show in **Chapter 3** that the double-hit model is necessary to induce CTEPH in the relatively young Yorkshire x Landrace swine, recent studies suggest that microsphere infusion only is enough to induce PH in Göttinger

Minipigs (unpublished work from our laboratory) and beagles (61). These findings suggest an influence of age on pulmonary vascular function, resulting in a biological "second hit" to induce CTEPH (62). Chronic instrumentation of these minipigs according to the methods as described in **Chapter 2**, will allow for prolonged serial assessment of cardiopulmonary function in more adult CTEPH swine.

Our CTEPH animal model can be further utilized to investigate disease development for possible discovery of potential early diagnostic markers to facilitate early detection of disease in patients, and interventions that interfere with microvascular remodeling to get more insight in the pathways involved in this remodeling and get more specific targeted therapy for inoperable CTEPH patients or patients with residual PH after surgery. In addition, this swine model may also be used to delineate sex-differences that are known to exist in development, progression and possibly interventions of CTEPH (79) and shed more light on the importance and implications of cardiopulmonary exercise testing in CTEPH patients. Secondary to diagnostic cardiopulmonary exercise testing, therapeutic long term exercise training can be performed in the CTEPH swine model presented in this thesis.

Finally, it is important to note that we investigated the contribution of endothelial dysfunction to the acute regulation of vascular tone, and that, although vasoconstriction likely contributes to the elevated pulmonary vascular resistance in CTEPH, microvascular remodeling is also an important contributor. Although vasoconstriction and vascular remodeling in part share the same signaling pathways, and endothelial dysfunction plays a key role in both, the acute response to blockade of vasoactive pathways may not be identical to chronic blockade of such pathways, which may also impact vascular remodeling. Hence,

long-term effects of therapy, with future studies investigating chronic administration of therapeutic agents, for example the effects of chronic Rho-kinase inhibition, activation of the prostacyclin pathway, ET_A antagonists and sGC stimulation in CTEPH, are required to study the impact of these agents on (pulmonary) vascular as well as cardiac remodeling in CTEPH. Some of these agents are indeed currently being investigated in clinical trials (ClinicalTrials.gov NCT03689244, NCT01416636, NCT03809650, NCT03273257, NCT02634203, NCT00910429). Importantly, both acute and chronic administration of these agents could be studied in our CTEPH animal model since real time monitoring during administration or after long term administration is possible in awake animals. In addition, the effects of acute or chronic therapy such as ERA's, phosphodiesterase inhibitors, NO donors, sGC stimulators or Rho-kinase inhibitors on acute exercise can be obtained in our CTEPH swine.

References

1. **Abe S, Ishida K, Masuda M, Ueda H, Kohno H, Matsuura K, Tamura Y, Watanabe M, and Matsumiya G**. A prospective, randomized study of inhaled prostacyclin versus nitric oxide in patients with residual pulmonary hypertension after pulmonary endarterectomy. *Gen Thorac Cardiovasc Surg* 65: 153-159, 2017.

2. **Aguero J, Ishikawa K, Fish KM, Hammoudi N, Hadri L, Garcia-Alvarez A, Ibanez B, Fuster V, Hajjar RJ, and Leopold JA**. Combination proximal pulmonary artery coiling and distal embolization induces chronic elevations in pulmonary artery pressure in Swine. *PLoS One* 10: e0124526, 2015.

3. **Aguero J, Ishikawa K, Hadri L, Santos-Gallego C, Fish K, Hammoudi N, Chaanine A, Torquato S, Naim C, Ibanez B, Pereda D, Garcia-Alvarez A, Fuster V, Sengupta PP, Leopold JA, and Hajjar RJ**. Characterization of right ventricular remodeling and failure in a chronic pulmonary hypertension model. *American journal of physiology Heart and circulatory physiology* 307: H1204-1215, 2014.

4. **Alias S, Redwan B, Panzenbock A, Winter MP, Schubert U, Voswinckel R, Frey MK, Jakowitsch J, Alimohammadi A, Hobohm L, Mangold A, Bergmeister H, Sibilia M, Wagner EF, Mayer E, Klepetko W, Holzenbein TJ, Preissner KT, and Lang IM**. Defective angiogenesis delays thrombus resolution: a potential pathogenetic mechanism underlying chronic thromboembolic pulmonary hypertension. *Arterioscler Thromb Vasc Biol* 34: 810-819, 2014.

5. **Andersen S, Nielsen-Kudsk JE, Vonk Noordegraaf A, and de Man FS**. Right Ventricular Fibrosis. *Circulation* 139: 269-285, 2019.

6. **Ataya A, Cope J, and Alnuaimat H**. A Review of Targeted Pulmonary Arterial Hypertension-Specific Pharmacotherapy. *J Clin Med* 5: 2016.

7. **Azarian R, Wartski M, Collignon MA, Parent F, Herve P, Sors H, and Simonneau G**. Lung perfusion scans and hemodynamics in acute and chronic pulmonary embolism. *J Nucl Med* 38: 980-983, 1997.

8. **Bender SB, van Houwelingen MJ, Merkus D, Duncker DJ, and Laughlin MH**. Quantitative analysis of exercise-induced enhancement of early- and late-systolic retrograde coronary blood flow. *Journal of applied physiology* 108: 507-514, 2010.

9. **Blumberg FC, Arzt M, Lange T, Schroll S, Pfeifer M, and Wensel R**. Impact of right ventricular reserve on exercise capacity and survival in patients with pulmonary hypertension. *Eur J Heart Fail* 15: 771-775, 2013.

10. **Boulate D, Perros F, Dorfmuller P, Arthur-Ataam J, Guihaire J, Lamrani L, Decante B, Humbert M, Eddahibi S, Dartevelle P, Fadel E, and Mercier O**. Pulmonary microvascular lesions regress in reperfused chronic thromboembolic pulmonary hypertension. *J Heart Lung Transplant* 34: 457-467, 2015.

11. **Chen IC, Tan MS, Wu BN, Chai CY, Yeh JL, Chou SH, Chen IJ, and Dai ZK**. Statins ameliorate pulmonary hypertension secondary to left ventricular dysfunction through the Rho-kinase pathway and NADPH oxidase. *Pediatr Pulmonol* 52: 443-457, 2017.

12. **Claessen G, La Gerche A, Dymarkowski S, Claus P, Delcroix M, and Heidbuchel H**. Pulmonary vascular and right ventricular reserve in patients with normalized resting hemodynamics after pulmonary endarterectomy. *J Am Heart Assoc* 4: e001602, 2015.

13. **Claessen G, La Gerche A, Wielandts JY, Bogaert J, Van Cleemput J, Wuyts W, Claus P, Delcroix M, and Heidbuchel H**. Exercise pathophysiology and sildenafil effects in chronic thromboembolic pulmonary hypertension. *Heart* 101: 637-644, 2015.

14. **Claeys M, Claessen G, La Gerche A, Petit T, Belge C, Meyns B, Bogaert J, Willems R, Claus P, and Delcroix M**. Impaired Cardiac Reserve and Abnormal Vascular Load Limit Exercise Capacity in Chronic Thromboembolic Disease. *JACC Cardiovasc Imaging* 2018.

15. **Dewachter L, and Dewachter C**. Inflammation in Right Ventricular Failure: Does It Matter? *Front Physiol* 9: 1056, 2018.

16. **Do e Z, Fukumoto Y, Takaki A, Tawara S, Ohashi J, Nakano M, Tada T, Saji K, Sugimura K, Fujita H, Hoshikawa Y, Nawata J, Kondo T, and Shimokawa H**. Evidence for Rho-kinase activation in patients with pulmonary arterial hypertension. *Circ J* 73: 1731-1739, 2009.

17. **Dorfmuller P, Gunther S, Ghigna MR, Thomas de Montpreville V, Boulate D, Paul JF, Jais X, Decante B, Simonneau G, Dartevelle P, Humbert M, Fadel E, and Mercier O**. Microvascular disease in chronic thromboembolic pulmonary hypertension: a role for pulmonary veins and systemic vasculature. *Eur Respir J* 44: 1275-1288, 2014.

18. **Fedullo PF, Auger WR, Kerr KM, and Rubin LJ**. Chronic thromboembolic pulmonary hypertension. *N Engl J Med* 345: 1465-1472, 2001.

19. **Frangogiannis NG**. Fibroblasts and the extracellular matrix in right ventricular disease. *Cardiovasc Res* 113: 1453-1464, 2017.

20. **Frump AL, Bonnet S, de Jesus Perez VA, and Lahm T**. Emerging role of angiogenesis in adaptive and maladaptive right ventricular remodeling in pulmonary hypertension. *Am J Physiol Lung Cell Mol Physiol* 314: L443-L460, 2018.
21. **Fukumoto Y, Yamada N, Matsubara H, Mizoguchi M, Uchino K, Yao A, Kihara Y, Kawano M, Watanabe H, Takeda Y, Adachi T, Osanai S, Tanabe N, Inoue T, Kubo A, Ota Y, Fukuda K, Nakano T, and Shimokawa H**. Double-blind, placebo-controlled clinical trial with a rho-kinase inhibitor in pulmonary arterial hypertension. *Circ J* 77: 2619-2625, 2013.
22. **Galie N, Humbert M, Vachiery JL, Gibbs S, Lang I, Torbicki A, Simonneau G, Peacock A, Vonk Noordegraaf A, Beghetti M, Ghofrani A, Gomez Sanchez MA, Hansmann G, Klepetko W, Lancellotti P, Matucci M, McDonagh T, Pierard LA, Trindade PT, Zompatori M, Hoeper M, Aboyans V, Vaz Carneiro A, Achenbach S, Agewall S, Allanore Y, Asteggiano R, Paolo Badano L, Albert Barbera J, Bouvaist H, Bueno H, Byrne RA, Carerj S, Castro G, Erol C, Falk V, Funck-Brentano C, Gorenflo M, Granton J, Iung B, Kiely DG, Kirchhof P, Kjellstrom B, Landmesser U, Lekakis J, Lionis C, Lip GY, Orfanos SE, Park MH, Piepoli MF, Ponikowski P, Revel MP, Rigau D, Rosenkranz S, Voller H, and Luis Zamorano J**. 2015 ESC/ERS Guidelines for the diagnosis and treatment of pulmonary hypertension: The Joint Task Force for the Diagnosis and Treatment of Pulmonary Hypertension of the European Society of Cardiology (ESC) and the European Respiratory Society (ERS): Endorsed by: Association for European Paediatric and Congenital Cardiology (AEPC), International Society for Heart and Lung Transplantation (ISHLT). *Eur Heart J* 37: 67-119, 2016.
23. **Galie N, and Kim NH**. Pulmonary microvascular disease in chronic thromboembolic pulmonary hypertension. *Proc Am Thorac Soc* 3: 571-576, 2006.
24. **Garcia-Alvarez A, Fernandez-Friera L, Garcia-Ruiz JM, Nuno-Ayala M, Pereda D, Fernandez-Jimenez R, Guzman G, Sanchez-Quintana D, Alberich-Bayarri A, Pastor-Escuredo D, Sanz-Rosa D, Garcia-Prieto J, Gonzalez-Mirelis JG, Pizarro G, Jimenez-Borreguero LJ, Fuster V, Sanz J, and Ibanez B**. Noninvasive monitoring of serial changes in pulmonary vascular resistance and acute vasodilator testing using cardiac magnetic resonance. *J Am Coll Cardiol* 62: 1621-1631, 2013.
25. **Ghofrani HA, Simonneau G, D'Armini AM, Fedullo P, Howard LS, Jais X, Jenkins DP, Jing ZC, Madani MM, Martin N, Mayer E, Papadakis K, Richard D, Kim NH, and investigators Ms**. Macitentan for the treatment of inoperable

chronic thromboembolic pulmonary hypertension (MERIT-1): results from the multicentre, phase 2, randomised, double-blind, placebo-controlled study. *Lancet Respir Med* 5: 785-794, 2017.

26. **Godinas L, Sattler C, Lau EM, Jais X, Taniguchi Y, Jevnikar M, Weatherald J, Sitbon O, Savale L, Montani D, Simonneau G, Humbert M, Laveneziana P, and Garcia G**. Dead-space ventilation is linked to exercise capacity and survival in distal chronic thromboembolic pulmonary hypertension. *J Heart Lung Transplant* 2017.

27. **Guihaire J, Haddad F, Boulate D, Capderou A, Decante B, Flecher E, Eddahibi S, Dorfmuller P, Herve P, Humbert M, Verhoye JP, Dartevelle P, Mercier O, and Fadel E**. Right ventricular plasticity in a porcine model of chronic pressure overload. *J Heart Lung Transplant* 33: 194-202, 2014.

28. **Guihaire J, Haddad F, Boulate D, Decante B, Denault AY, Wu J, Herve P, Humbert M, Dartevelle P, Verhoye JP, Mercier O, and Fadel E**. Non-invasive indices of right ventricular function are markers of ventricular-arterial coupling rather than ventricular contractility: insights from a porcine model of chronic pressure overload. *Eur Heart J Cardiovasc Imaging* 14: 1140-1149, 2013.

29. **Guihaire J, Haddad F, Noly PE, Boulate D, Decante B, Dartevelle P, Humbert M, Verhoye JP, Mercier O, and Fadel E**. Right ventricular reserve in a piglet model of chronic pulmonary hypertension. *Eur Respir J* 45: 709-717, 2015.

30. **Guo L, Yang Y, Liu J, Wang L, Li J, Wang Y, Liu Y, Gu S, Gan H, Cai J, Yuan JX, Wang J, and Wang C**. Differentially expressed plasma microRNAs and the potential regulatory function of Let-7b in chronic thromboembolic pulmonary hypertension. *PLoS One* 9: e101055, 2014.

31. **Halank M, Hoeper MM, Ghofrani HA, Meyer FJ, Stahler G, Behr J, Ewert R, Fletcher M, Colorado P, Nikkho S, and Grimminger F**. Riociguat for pulmonary arterial hypertension and chronic thromboembolic pulmonary hypertension: Results from a phase II long-term extension study. *Respir Med* 128: 50-56, 2017.

32. **Hardziyenka M, Campian ME, Reesink HJ, Surie S, Bouma BJ, Groenink M, Klemens CA, Beekman L, Remme CA, Bresser P, and Tan HL**. Right ventricular failure following chronic pressure overload is associated with reduction in left ventricular mass: evidence for atrophic remodeling. *J Am Coll Cardiol* 57: 921-928, 2011.

33. **Hartmann S, Ridley AJ, and Lutz S**. The Function of Rho-Associated Kinases ROCK1 and ROCK2 in the Pathogenesis of Cardiovascular Disease. *Front Pharmacol* 6: 276, 2015.

34. **Hasler ED, Muller-Mottet S, Furian M, Saxer S, Huber LC, Maggiorini M, Speich R, Bloch KE, and Ulrich S**. Pressure-Flow During Exercise Catheterization Predicts Survival in Pulmonary Hypertension. *Chest* 150: 57-67, 2016.

35. **He J, Li X, Luo H, Li T, Zhao L, Qi Q, Liu Y, and Yu Z**. Galectin-3 mediates the pulmonary arterial hypertension-induced right ventricular remodeling through interacting with NADPH oxidase 4. *J Am Soc Hypertens* 11: 275-289 e272, 2017.

36. **Held M, Grun M, Holl R, Hubner G, Kaiser R, Karl S, Kolb M, Schafers HJ, Wilkens H, and Jany B**. Cardiopulmonary exercise testing to detect chronic thromboembolic pulmonary hypertension in patients with normal echocardiography. *Respiration* 87: 379-387, 2014.

37. **Held M, Hesse A, Gott F, Holl R, Hubner G, Kolb P, Langen HJ, Romen T, Walter F, Schafers HJ, Wilkens H, and Jany B**. A symptom-related monitoring program following pulmonary embolism for the early detection of CTEPH: a prospective observational registry study. *BMC Pulm Med* 14: 141, 2014.

38. **Held M, Kolb P, Grun M, Jany B, Hubner G, Grgic A, Holl R, Schaefers HJ, and Wilkens H**. Functional Characterization of Patients with Chronic Thromboembolic Disease. *Respiration* 91: 503-509, 2016.

39. **Hirashiki A, Adachi S, Nakano Y, Kamimura Y, Shimokata S, Takeshita K, Murohara T, and Kondo T**. Effects of bosentan on peripheral endothelial function in patients with pulmonary arterial hypertension or chronic thromboembolic pulmonary hypertension. *Pulm Circ* 6: 168-173, 2016.

40. **Hirashiki A, Adachi S, Nakano Y, Kono Y, Shimazu S, Shimizu S, Morimoto R, Okumura T, Takeshita K, Yamada S, Murohara T, and Kondo T**. Cardiopulmonary exercise testing to evaluate the exercise capacity of patients with inoperable chronic thromboembolic pulmonary hypertension: an endothelin receptor antagonist improves the peak PETCO2. *Life Sci* 118: 397-403, 2014.

41. **Hoeper MM, Mayer E, Simonneau G, and Rubin LJ**. Chronic thromboembolic pulmonary hypertension. *Circulation* 113: 2011-2020, 2006.

42. **Horinouchi T, Terada K, Higashi T, and Miwa S**. Endothelin receptor signaling: new insight into its regulatory mechanisms. *J Pharmacol Sci* 123: 85-101, 2013.

43. **Ikeda S, Satoh K, Kikuchi N, Miyata S, Suzuki K, Omura J, Shimizu T, Kobayashi K, Kobayashi K, Fukumoto Y, Sakata Y, and Shimokawa H**. Crucial role of rho-kinase in pressure overload-induced right ventricular hypertrophy and dysfunction in mice. *Arterioscler Thromb Vasc Biol* 34: 1260-1271, 2014.

44. **Iwase T, Nagaya N, Ando M, Satoh T, Sakamaki F, Kyotani S, Takaki H, Goto Y, Ohkita Y, Uematsu M, Nakanishi N, and Miyatake K**. Acute and chronic effects of surgical thromboendarterectomy on exercise capacity and ventilatory efficiency in patients with chronic thromboembolic pulmonary hypertension. *Heart* 86: 188-192, 2001.

45. **Jais X, D'Armini AM, Jansa P, Torbicki A, Delcroix M, Ghofrani HA, Hoeper MM, Lang IM, Mayer E, Pepke-Zaba J, Perchenet L, Morganti A, Simonneau G, Rubin LJ, and Bosentan Effects in iNopErable Forms of chronIc Thromboembolic pulmonary hypertension Study G**. Bosentan for treatment of inoperable chronic thromboembolic pulmonary hypertension: BENEFiT (Bosentan Effects in iNopErable Forms of chronIc Thromboembolic pulmonary hypertension), a randomized, placebo-controlled trial. *J Am Coll Cardiol* 52: 2127-2134, 2008.

46. **Kim H, Yung GL, Marsh JJ, Konopka RG, Pedersen CA, Chiles PG, Morris TA, and Channick RN**. Endothelin mediates pulmonary vascular remodelling in a canine model of chronic embolic pulmonary hypertension. *Eur Respir J* 15: 640-648, 2000.

47. **Koress C, Swan K, and Kadowitz P**. Soluble Guanylate Cyclase Stimulators and Activators: Novel Therapies for Pulmonary Vascular Disease or a Different Method of Increasing cGMP? *Curr Hypertens Rep* 18: 42, 2016.

48. **Kruzliak P, Maruyama J, and Maruyama K**. Role of nitric oxide in pathophysiology and treatment of pulmonary hypertension. *Vitam Horm* 96: 407-424, 2014.

49. **Lau EMT, Giannoulatou E, Celermajer DS, and Humbert M**. Epidemiology and treatment of pulmonary arterial hypertension. *Nat Rev Cardiol* 2017.

50. **Lian TY, Jiang X, and Jing ZC**. Riociguat: a soluble guanylate cyclase stimulator for the treatment of pulmonary hypertension. *Drug Des Devel Ther* 11: 1195-1207, 2017.

51. **Loisel F, Provost B, Guihaire J, Boulate D, Arouche N, Amsallem M, Arthur-Ataam J, Decante B, Dorfmuller P, Fadel E, Uzan G, and Mercier O**. Autologous endothelial progenitor cell therapy improves right ventricular function

in a model of chronic thromboembolic pulmonary hypertension. *The Journal of thoracic and cardiovascular surgery* 157: 655-666 e657, 2019.

52. **Lu X, Dang CQ, Guo X, Molloi S, Wassall CD, Kemple MD, and Kassab GS**. Elevated oxidative stress and endothelial dysfunction in right coronary artery of right ventricular hypertrophy. *Journal of applied physiology* 110: 1674-1681, 2011.

53. **Mahmud E, Madani MM, Kim NH, Poch D, Ang L, Behnamfar O, Patel MP, and Auger WR**. Chronic Thromboembolic Pulmonary Hypertension: Evolving Therapeutic Approaches for Operable and Inoperable Disease. *J Am Coll Cardiol* 71: 2468-2486, 2018.

54. **Matthews DT, and Hemnes AR**. Current concepts in the pathogenesis of chronic thromboembolic pulmonary hypertension. *Pulm Circ* 6: 145-154, 2016.

55. **Melot C, and Naeije R**. Pulmonary vascular diseases. *Comprehensive Physiology* 1: 593-619, 2011.

56. **Mercier O, Sage E, Izziki M, Humbert M, Dartevelle P, Eddahibi S, and Fadel E**. Endothelin A receptor blockade improves regression of flow-induced pulmonary vasculopathy in piglets. *The Journal of thoracic and cardiovascular surgery* 140: 677-683, 2010.

57. **Mercier O, Tivane A, Dorfmuller P, de Perrot M, Raoux F, Decante B, Eddahibi S, Dartevelle P, and Fadel E**. Piglet model of chronic pulmonary hypertension. *Pulm Circ* 3: 908-915, 2013.

58. **Merkus D, de Beer VJ, Houweling B, and Duncker DJ**. Control of pulmonary vascular tone during exercise in health and pulmonary hypertension. *Pharmacol Ther* 119: 242-263, 2008.

59. **Moser KM, and Bloor CM**. Pulmonary vascular lesions occurring in patients with chronic major vessel thromboembolic pulmonary hypertension. *Chest* 103: 685-692, 1993.

60. **Moser KM, Cantor JP, Olman M, Villespin I, Graif JL, Konopka R, Marsh JJ, and Pedersen C**. Chronic pulmonary thromboembolism in dogs treated with tranexamic acid. *Circulation* 83: 1371-1379, 1991.

61. **Mulchrone A, Kellihan HB, Forouzan O, Hacker TA, Bates ML, Francois CJ, and Chesler NC**. A Large Animal Model of Right Ventricular Failure due to Chronic Thromboembolic Pulmonary Hypertension: A Focus on Function. *Front Cardiovasc Med* 5: 189, 2018.

62. **Navarro S, and Driscoll B**. Regeneration of the Aging Lung: A Mini-Review. *Gerontology* 63: 270-280, 2017.

63. **Neto-Neves EM, Brown MB, Zaretskaia MV, Rezania S, Goodwill AG, McCarthy BP, Persohn SA, Territo PR, and Kline JA**. Chronic Embolic Pulmonary Hypertension Caused by Pulmonary Embolism and Vascular Endothelial Growth Factor Inhibition. *Am J Pathol* 187: 700-712, 2017.

64. **Nishikawa-Takahashi M, Ueno S, and Kario K**. Long-term advanced therapy with bosentan improves symptoms and prevents deterioration of inoperable chronic thromboembolic pulmonary hypertension. *Life Sci* 118: 410-413, 2014.

65. **Opitz I, and Kirschner MB**. Molecular Research in Chronic Thromboembolic Pulmonary Hypertension. *Int J Mol Sci* 20: 2019.

66. **Pereda D, Garcia-Alvarez A, Sanchez-Quintana D, Nuno M, Fernandez-Friera L, Fernandez-Jimenez R, Garcia-Ruiz JM, Sandoval E, Aguero J, Castella M, Hajjar RJ, Fuster V, and Ibanez B**. Swine model of chronic postcapillary pulmonary hypertension with right ventricular remodeling: long-term characterization by cardiac catheterization, magnetic resonance, and pathology. *Journal of cardiovascular translational research* 7: 494-506, 2014.

67. **Perkett EA, Brigham KL, and Meyrick B**. Continuous air embolization into sheep causes sustained pulmonary hypertension and increased pulmonary vasoreactivity. *Am J Pathol* 132: 444-454, 1988.

68. **Pohlmann JR, Akay B, Camboni D, Koch KL, Mervak BM, and Cook KE**. A low mortality model of chronic pulmonary hypertension in sheep. *J Surg Res* 175: 44-48, 2012.

69. **Quarck R, Wynants M, Ronisz A, Sepulveda MR, Wuytack F, Van Raemdonck D, Meyns B, and Delcroix M**. Characterization of proximal pulmonary arterial cells from chronic thromboembolic pulmonary hypertension patients. *Respir Res* 13: 27, 2012.

70. **Rain S, Andersen S, Najafi A, Gammelgaard Schultz J, da Silva Goncalves Bos D, Handoko ML, Bogaard HJ, Vonk-Noordegraaf A, Andersen A, van der Velden J, Ottenheijm CA, and de Man FS**. Right Ventricular Myocardial Stiffness in Experimental Pulmonary Arterial Hypertension: Relative Contribution of Fibrosis and Myofibril Stiffness. *Circ Heart Fail* 9: 2016.

71. **Reesink HJ, Meijer RC, Lutter R, Boomsma F, Jansen HM, Kloek JJ, and Bresser P**. Hemodynamic and clinical correlates of endothelin-1 in chronic thromboembolic pulmonary hypertension. *Circ J* 70: 1058-1063, 2006.

72. **Richter MJ, Pader P, Gall H, Reichenberger F, Seeger W, Mayer E, Guth S, Kramm T, Grimminger F, Ghofrani HA, and Voswinckel R**. The prognostic relevance of oxygen uptake in inoperable chronic thromboembolic pulmonary hypertension. *Clin Respir J* 2015.

73. **Rol N, Kurakula KB, Happe C, Bogaard HJ, and Goumans MJ**. TGF-beta and BMPR2 Signaling in PAH: Two Black Sheep in One Family. *Int J Mol Sci* 19: 2018.

74. **Rothman A, Wiencek RG, Davidson S, Evans WN, Restrepo H, Sarukhanov V, and Mann D**. Challenges in the development of chronic pulmonary hypertension models in large animals. *Pulm Circ* 7: 156-166, 2017.

75. **Sage E, Mercier O, Herve P, Tu L, Dartevelle P, Eddahibi S, and Fadel E**. Right lung ischemia induces contralateral pulmonary vasculopathy in an animal model. *The Journal of thoracic and cardiovascular surgery* 143: 967-973, 2012.

76. **Saleby J, Bouzina H, Lundgren J, and Radegran G**. Angiogenic and inflammatory biomarkers in the differentiation of pulmonary hypertension. *Scand Cardiovasc J* 51: 261-270, 2017.

77. **Schmitt-Opitz I, and Ulrich S**. Chronic thromboembolic pulmonary hypertension. *Swiss Med Wkly* 148: w14702, 2018.

78. **Shelub I, van Grondelle A, McCullough R, Hofmeister S, and Reeves JT**. A model of embolic chronic pulmonary hypertension in the dog. *J Appl Physiol Respir Environ Exerc Physiol* 56: 810-815, 1984.

79. **Shigeta A, Tanabe N, Shimizu H, Hoshino S, Maruoka M, Sakao S, Tada Y, Kasahara Y, Takiguchi Y, Tatsumi K, Masuda M, and Kuriyama T**. Gender differences in chronic thromboembolic pulmonary hypertension in Japan. *Circ J* 72: 2069-2074, 2008.

80. **Shimizu T, and Liao JK**. Rho Kinases and Cardiac Remodeling. *Circ J* 80: 1491-1498, 2016.

81. **Simonneau G, D'Armini AM, Ghofrani HA, Grimminger F, Hoeper MM, Jansa P, Kim NH, Wang C, Wilkins MR, Fritsch A, Davie N, Colorado P, and Mayer E**. Riociguat for the treatment of chronic thromboembolic pulmonary hypertension: a long-term extension study (CHEST-2). *Eur Respir J* 45: 1293-1302, 2015.

82. **Simonneau G, Torbicki A, Dorfmuller P, and Kim N**. The pathophysiology of chronic thromboembolic pulmonary hypertension. *Eur Respir Rev* 26: 2017.

83. **Skoro-Sajer N, Mittermayer F, Panzenboeck A, Bonderman D, Sadushi R, Hitsch R, Jakowitsch J, Klepetko W, Kneussl MP, Wolzt M, and Lang IM**.

Asymmetric dimethylarginine is increased in chronic thromboembolic pulmonary hypertension. *Am J Respir Crit Care Med* 176: 1154-1160, 2007.

84. **Southwood M, MacKenzie Ross RV, Kuc RE, Hagan G, Sheares KK, Jenkins DP, Goddard M, Davenport AP, and Pepke-Zaba J**. Endothelin ETA receptors predominate in chronic thromboembolic pulmonary hypertension. *Life Sci* 159: 104-110, 2016.

85. **Stein PD, Goodman LR, Hull RD, Dalen JE, and Matta F**. Diagnosis and management of isolated subsegmental pulmonary embolism: review and assessment of the options. *Clin Appl Thromb Hemost* 18: 20-26, 2012.

86. **Sun XQ, Abbate A, and Bogaard HJ**. Role of cardiac inflammation in right ventricular failure. *Cardiovasc Res* 113: 1441-1452, 2017.

87. **Sunamura S, Satoh K, Kurosawa R, Ohtsuki T, Kikuchi N, Elias-Al-Mamun M, Shimizu T, Ikeda S, Suzuki K, Satoh T, Omura J, Nogi M, Numano K, Siddique MAH, Miyata S, Miura M, and Shimokawa H**. Different roles of myocardial ROCK1 and ROCK2 in cardiac dysfunction and postcapillary pulmonary hypertension in mice. *Proc Natl Acad Sci U S A* 115: E7129-E7138, 2018.

88. **Tang CX, Yang GF, Schoepf UJ, Han ZH, Qi L, Zhao YE, Wu J, Zhou CS, Zhu H, Stubenrauch AC, Mangold S, Zhang LJ, and Lu GM**. Chronic thromboembolic pulmonary hypertension: Comparison of dual-energy computed tomography and single photon emission computed tomography in canines. *Eur J Radiol* 85: 498-506, 2016.

89. **Trip P, Rain S, Handoko ML, van der Bruggen C, Bogaard HJ, Marcus JT, Boonstra A, Westerhof N, Vonk-Noordegraaf A, and de Man FS**. Clinical relevance of right ventricular diastolic stiffness in pulmonary hypertension. *Eur Respir J* 45: 1603-1612, 2015.

90. **Tsai SH, Lu G, Xu X, Ren Y, Hein TW, and Kuo L**. Enhanced endothelin-1/Rho-kinase signalling and coronary microvascular dysfunction in hypertensive myocardial hypertrophy. *Cardiovasc Res* 113: 1329-1337, 2017.

91. **van de Veerdonk MC, Bogaard HJ, and Voelkel NF**. The right ventricle and pulmonary hypertension. *Heart Fail Rev* 21: 259-271, 2016.

92. **van Wolferen SA, Marcus JT, Westerhof N, Spreeuwenberg MD, Marques KM, Bronzwaer JG, Henkens IR, Gan CT, Boonstra A, Postmus PE, and Vonk-Noordegraaf A**. Right coronary artery flow impairment in patients with pulmonary hypertension. *Eur Heart J* 29: 120-127, 2008.

93. **Vogel-Claussen J, Skrok J, Shehata ML, Singh S, Sibley CT, Boyce DM, Lechtzin N, Girgis RE, Mathai SC, Goldstein TA, Zheng J, Lima JA, Bluemke DA, and Hassoun PM**. Right and left ventricular myocardial perfusion reserves correlate with right ventricular function and pulmonary hemodynamics in patients with pulmonary arterial hypertension. *Radiology* 258: 119-127, 2011.

94. **Webpage**. https://respiratoryupdates.files.wordpress.com/2015/09/pathophysiology-of-pulmonary-arterial-hypertension-650x438.jpg. [01-03, 2019].

95. **Weimann J, Zink W, Schnabel PA, Jakob H, Gebhard MM, Martin E, and Motsch J**. Selective vasodilation by nitric oxide inhalation during sustained pulmonary hypertension following recurrent microembolism in pigs. *J Crit Care* 14: 133-140, 1999.

96. **Xi Q, Liu Z, Liu W, Zhao Z, Luo Q, and Huang Z**. Chronic thromboembolic pulmonary hypertension is not associated with iron overload. *Cardiovasc Pathol* 24: 76-79, 2015.

97. **Zabini D, Heinemann A, Foris V, Nagaraj C, Nierlich P, Balint Z, Kwapiszewska G, Lang IM, Klepetko W, Olschewski H, and Olschewski A**. Comprehensive analysis of inflammatory markers in chronic thromboembolic pulmonary hypertension patients. *Eur Respir J* 44: 951-962, 2014.

98. **Zeidan A, Gan XT, Thomas A, and Karmazyn M**. Prevention of RhoA activation and cofilin-mediated actin polymerization mediates the antihypertrophic effect of adenosine receptor agonists in angiotensin II- and endothelin-1-treated cardiomyocytes. *Mol Cell Biochem* 385: 239-248, 2014.

99. **Zhang S, Yang T, Xu X, Wang M, Zhong L, Yang Y, Zhai Z, Xiao F, and Wang C**. Oxidative stress and nitric oxide signaling related biomarkers in patients with pulmonary hypertension: a case control study. *BMC Pulm Med* 15: 50, 2015.

100. **Zhou X, Wang D, Castro CY, Hawkins H, Lynch JE, Liu X, and Zwischenberger JB**. A pulmonary hypertension model induced by continuous pulmonary air embolization. *J Surg Res* 170: e11-16, 2011.

Chapter 8

Nederlandse samenvatting

Het hart en de longen behoren tot de meest belangrijke organen van het menselijk lichaam. Ze zijn essentieel in de toevoer van zuurstof en voedingsstoffen en afvoer van koolstofdioxide en andere afvalstoffen van en naar organen. Aandoeningen aan het hart en de longen zorgen dan ook voor zowel een sterk verminderde kwaliteit van leven als een verkorte levensverwachting.

Het hart en bloedvatenstelsel is verdeeld in twee circulaties. De systeem circulatie welke aangestuurd wordt door de linker harthelft, deze pompt zuurstofrijk bloed met voedingsstoffen naar de organen en zorgt ervoor dat zuurstofarm bloed met afvalstoffen van de organen afgevoerd wordt. De pulmonaal circulatie wordt juist aangestuurd door de rechter harthelft en deze pompt het teruggekomen zuurstof arme bloed door de longvaten waar koolstofdioxide wordt afgegeven aan, en zuurstof wordt opgenomen uit de longblaasjes, zodat dit zuurstofrijke bloed vervolgens weer via de systemische circulatie naar de organen getransporteerd kan worden.

Wanneer er een te hoge bloeddruk in pulmonaal circulatie optreedt, >25mmHg in de longslagader (PAP, pulmonary artery pressure), spreekt men van pulmonale hypertensie (PH). Patiënten met PH hebben erg vervelende maar algemene symptomen zoals kortademigheid, ernstige ongewone moeheid, flauwvallen, hartkloppingen en een verminderde inspanningscapaciteit. Doordat de symptomen zo algemeen zijn wordt de ziekte vaak pas in een laat stadium gediagnosticeerd, wat een negatieve invloed heeft op de prognose.

PH is een verzamelnaam van chronische aandoeningen met verschillende oorzaken waarbij de bloeddruk in de pulmonaal circulatie te hoog is. Een van deze oorzaken zijn longemboliën. Deze vorm van pulmonale hypertensie wordt dan ook wel chronische thrombo-embolische pulmonale hypertensie (CTEPH) genoemd.

Omdat de ziekte nog incompleet begrepen wordt, therapeutische interventies gelimiteerd zijn en er nog geen genezende medicaties zijn goedgekeurd voor CTEPH, ontrafelen we enkele mechanismen achter deze ziekte in dit proefschrift. Om dit te kunnen doen hebben we een groot CTEPH proefdiermodel ontwikkeld waarbij we chronische katheters in en rondom het hart hebben geplaatst waardoor we de bloeddrukken, hartminuutvolume en zuurstofopname in de dieren serieel, wakker en zelf tijdens inspanning kunnen meten (**Hoofdstuk 2**). CTEPH wordt geïnduceerd in deze varkens middels een double-hit, namelijk door 1) pulmonale vaatdysfunctie te induceren middels chronische administratie van de endotheliaal stikstofoxide-synthase remmer L-NAME en 2) herhaaldelijke embolisaties van de longvaten met microsferen, aangezien beide als enkele toediening niet resulteerde in PH (**Hoofdstuk 3**).

Alhoewel CTEPH in eerste instantie veroorzaakt wordt door obstructies in het longvaatbed door embolieën, is algemeen bekend dat secundair verergering van PH het gevolg is van progressieve microvasculaire remodellering van de niet-geblokkeerde distale pulmonale kleine slagaders. Wij zien dan ook in **Hoofstuk 5** dat, in onze CTEPH varkens, de wand van deze distale pulmonale kleine slagaders en microvasculatuur verdikt en sterk gemusculariseerd is wat leidt tot een vernauwing van het lumen waar het bloed door stroomt. Deze muscularisatie in combinatie met lumen vernauwing zorgt voor een nog hogere vaatweerstand wat op zijn beurt de PAP nog verder verhoogt. Daarnaast zijn twee grote spelers in de endotheel regulatie van pulmonale vaattonus, namelijk vasodilator stikstofoxide (NO) en de vasoconstrictor endotheline (ET), ook uit balans waardoor de pulmonale vaten nog meer samentrekken en de PAP nog verder verhoogd (**Hoofdstuk 5**). Dit bij elkaar zorgt ervoor dat de longen in een vicieuze cirkel terechtkomen waarbij een hoge bloeddruk zorgt voor remodellering van de vaten en verdere endotheel dysfunctie wat op zijn beurt weer een hogere bloeddruk

veroorzaakt. In **Hoofdstuk 5** hebben laten zien wat er precies mis gaat in het signaleringspad van NO en ET in het CTEPH longvaatbed, waardoor we een stap dichter zijn bij het ontrafelen van de mechanismen en wordt het duidelijker welke nieuwe therapieën effectief zullen zijn in de behandeling van CTEPH.

Naast veranderingen in het pulmonale vaatbed zijn er ook verandering in het hart, voornamelijk het rechter ventrikel (RV), ten gevolge van de hoge weerstand (afterload) waar het rechter ventrikel tegen moet pompen. Het is bewezen dat het aanpassingsvermogen van het RV een belangrijke determinant is voor de functionele capaciteit en levensverwachting van de patiënt met CTEPH. In **Hoofdstuk 3 en 6** laten we zien dat er een trend is dat het RV dilateert in combinatie met een verminderde ejectie fractie (fractie uitgepompt bloed) ten gevolge van CTEPH. Daarnaast laten we zien dat het CTEPH RV, om te compenseren voor de verhoogde afterload, is verdikt op zowel macroscopisch als microscopisch niveau. De snelheid waarmee de bloedstroom in de longslagader vanuit het RV stroomt, gemeten met de nieuwe 4D flow CMR techniek, **Hoofdstuk 4**, leek ook lager in de dieren met de meest ernstige CTEPH, alhoewel dit niet statistisch significant was. Dit kan veroorzaakt zijn door een stijver RV, omdat we in **Hoofdstuk 6** hebben laten zien dat er een verandering was in het RV weefsel richting de stijvere collageen isoform.

In **Hoofdstuk 6** hebben we ook laten zien dat er een aantal genexpressies veranderd zijn in het RV weefsel van de CTEPH dieren. Een van de belangrijkste hierin is ROCK2, dat een rol speelt in hypertrofie, apoptose, fibrose, inflammatie en oxidatieve stress. Dit zijn allemaal factoren waardoor het RV op negatieve wijze remodelleert en uiteindelijk niet meer naar behoren zal functioneren. Deze bevindingen suggereren dat therapie gericht op ROCK2 inhibitie de nadelige RV remodellering tegen kan gaan.

Ondanks dat de patiënten met CTEPH in het dagelijks leven last hebben van een verminderde inspanningscapaciteit, zijn inspanningstesten een goede voorspeller voor zowel de kans op CTEPH na een acute longembolie als de prognose van de CTEPH patiënt. In **Hoofdstuk 3, 5 en 6** hebben we laten zien dat ook in ons varkensmodel, CTEPH gekarakteriseerd wordt door inspanningsintolerantie. Deze verminderde inspanningscapaciteit wordt voornamelijk veroorzaakt door een sterk verhoogde toename in PAP en pulmonale vasculaire weerstand tijdens inspanning, wat ervoor zorgt dat de RV afterload nog meer toeneemt en de ventilatie/perfusie mismatch in de longen ook alleen maar groter wordt. De bevindingen in **Hoofdstuk 5** laten zien dat de inspanningsintolerantie in CTEPH voornamelijk veroorzaakt wordt door een toename in RV afterload, en daarbij een gelimiteerde toename in RV functie tijdens inspanning, en in een kleinere mate wordt veroorzaakt door de ventilatie/perfusie mismatch in de longen waardoor de arteriële oxygenatie belemmert wordt.

Concluderend, het onderzoek in dit proefschrift schijnt meer licht op de onderliggende mechanismen welke zorgen voor de aanpassingen van het pulmonale vaatbed en het hart. De bevindingen laten zien dat specifiek onderzoek binnen globale signaleringspaden zoals NO, ET en Rho-kinase erg belangrijk zijn voor de ontwikkeling van effectievere behandelingen voor CTEPH. Daarnaast laten we het belang van inspanningstesten, voornamelijk in een vroeg stadium voor snellere diagnose, bij PH zien. Alles tezamen is er in dit proefschrift veel kennis vergaard over de pathofysiologie van CTEPH dankzij een nieuw ontwikkeld diermodel, alhoewel er nog veel vervolg onderzoek uitgevoerd moet worden voordat uiteindelijk de ideale genezende therapie bij de patiënt zal belanden.

List of publications

PhD portfolio

About the author

List of publications

1. **Stam K**, Cai Z, van der Velde N, van Duin RWB, Lam E, Van der Velden J, Hirsch A, Duncker DJ, Merkus D. Cardiac Remodeling in a Swine Model of Chronic Thrombo-Embolic Pulmonary Hypertension- Comparison of Right vs Left ventricle. J Physiol 2019

2. **Stam K**, Chelu RG, van der Velde N, van Duin R, Wielopolski P, Nieman K, Merkus D, Hirsch A. Validation of 4D flow CMR against simultaneous invasive hemodynamic measurements: a swine study. Int J Cardiovasc Imaging 2019.

3. **Stam K**, van Duin RWB, Uitterdijk A, Krabbendam-Peters I, Sorop O, Danser AHJ, Duncker DJ, Merkus D. Pulmonary microvascular remodeling in chronic thrombo-embolic pulmonary hypertension. Am J Physiol Lung Cell Mol Physiol 2018.

4. van Duin RWB, **Stam K**, Cai Z, Uitterdijk A, Garcia-Alvarez A, Ibanez B, Danser AHJ, Reiss IKM, Duncker DJ, Merkus D. Transition from post-capillary pulmonary hypertension to combined pre- and post-capillary pulmonary hypertension in swine: a key role for endothelin. J Physiol 2018.

5. **Stam K**, van Duin RWB, Uitterdijk A, Cai Z, Duncker DJ, Merkus D. Exercise facilitates early recognition of cardiac and vascular remodeling in chronic thromboembolic pulmonary hypertension in swine. Am J Physiol Heart Circ Physiol 2018;314(3):H627-H642.

6. Sorop O, Heinonen I, van Kranenburg M, van de Wouw J, de Beer VJ, Nguyen TN, Octavia Y, van Duin RWB, **Stam K**, van Geuns RJ, Wielopolski PA, Krestin GP, van den Meiracker AH, Verjans R, van Bilsen M, Danser AHJ, Paulus WJ, Cheng C, Linke WA, Joles JA, Verhaar MC, van der Velden J, Merkus D, Duncker DJ. Multiple common co-morbidities produce left ventricular diastolic dysfunction associated with coronary microvascular dysfunction, oxidative stress and myocardial stiffening. Cardiovasc Res 2018.

7. Hulshof HG, van Dijk AP, George KP, Merkus D, **Stam K**, van Duin RW, van Tertholen K, Hopman MTE, Haddad F, Thijssen DHJ, Oxborough DL. Echocardiographic-Derived Strain-Area Loop of the Right Ventricle is Related to Pulmonary Vascular Resistance in Pulmonary Arterial Hypertension. JACC Cardiovasc Imaging 2017;10(10 Pt B):1286-1288.

8. Joureau B, de Winter JM, **Stam K**, Granzier H, Ottenheijm CA. Muscle weakness in respiratory and peripheral skeletal muscles in a mouse model for nebulin-based nemaline myopathy. Neuromuscul Disord 2017;27(1):83-89.

9. **Stam K**, De Wijs-Meijler DP, van Duin RW, Verzijl A, Reiss IK, Duncker DJ, Merkus D. Surgical Placement of Catheters for Long-term Cardiovascular Exercise Testing in Swine. J Vis Exp 2016(108):e53772.

10. Witjas-Paalberends ER, Piroddi N, **Stam K**, van Dijk SJ, Oliviera VS, Ferrara C, Scellini B, Hazebroek M, ten Cate FJ, van Slegtenhorst M, dos Remedios C, Niessen HW, Tesi C, Stienen GJ, Heymans S, Michels M, Poggesi C, van der Velden J. Mutations in MYH7 reduce the force generating capacity of sarcomeres in human familial hypertrophic cardiomyopathy. Cardiovasc Res 2013;99(3):432-41.

PhD portfolio

Name PhD student:	Kelly Stam
ErasmusMC department:	Experimental Cardiology
PhD Period:	2013-2019
Promotors:	Prof. Dr. D.J. Duncker
	Prof. Dr. D. Merkus

1. PhD training	**Year**	**ECTS**
General academic skills		
Laboratory animal science (AMC)	2013	3
MRI safety course	2014	0.1
In-depth courses (e.g. Research school, Medical Training)		
NHS course “Cardiac Function and Adaptation)	2014	2
COEUR courses	2014-2015	4.5
Presentations		
COEUR PhD day	2014-2015	1.6
Thalys meeting	2015	1.1
Dutch physiology days	2015-2016	2.2
International conferences		
LICR TGF-beta meeting	2014	0.9
Microcirculation and Vascular Biology meeting *(Poster)*	2014	0.7
NVF Papendal Symposium	2014	1
FCVB Florence *(Poster)*	2016	1.3
Experimental Biology *(Poster)*	2017	1.9
Translational congress " Better together” *(Poster)*	2017-2018	1.2
ErasmusMC Pulmonary hypertension Symposium	2018	0.3
Seminars and workshops		
COEUR PhD day	2016	0.4
COEUR seminars	2013-2017	3.2
Other		
PHAEDRA Summer School *(Organization 2015)*	2014-2017	3.5

2. Teaching activities	**Year**	**ECTS**
Lecturing		
Student education endothelial cells & PH type 4	2015-2017	1
Supervising and teaching		
Internship Biology & medical laboratory research *(Brechje de Rapper, Dylan van de Vusse, Paula Krul, Esther Lam)*	2013-2018	5
Total		**34.9**